ISSN 0915-6364

NATIONAL INSTITUTE FOR FUSION SCIENCE

Cross Sections and Rate Coefficients for Electron-Impact Ionization of Hydrocarbon Molecules

R.K. Janev, J.G. Wang, I. Murakami and T. Kato

(Received - Sep. 27, 2001)

NIFS-DATA-68 Oct. 2001

RESEARCH REPORT
NIFS-DATA Series

TOKI, JAPAN

Cross Sections and Rate Coefficients for Electron-Impact Ionization of Hydrocarbon Molecules

R. K. Janev[1,2], J. G. Wang[3], I. Murakami[1], T. Kato[1]

[1] *National Institute for Fusion Science, Oroshi-cho, Toki, Gifu 509-5292, Japan*

[2] *Macedonian Academy of Sciences and Arts, P.O.Box 428, 91000 Skopje, Macedonia*

[3] *Department of Physics and Astronomy, University of Georgia, Athens, GA 30605, USA*

September 26, 2001

Abstract

A critical assessment of available experimental and theoretical cross sections for electron-impact direct and dissociative ionization of hydrocarbon molecules, C_xH_y ($x = 1 - 3, 1 \leq y \leq 2x + 2$), has been carried out. Recommended cross sections are suggested in the energy range from threshold to 10 keV for those reaction channels for which more than one set of data were found in the literatures. For the molecules for which no cross section information was found available, the cross sections for the dominant ionization channels were derived on the basis semi-empirical cross section relationships. The recommended and derived cross sections are represented by analytic fit functions, the coefficients of which are provided. The rate coefficients for all the ionization channels have been calculated in the temperature range from 1 eV to 1 keV. The cross sections and rate coefficients for all studied ionization channels are presented in graphical form as well.

Keywords: Electron-impact ionization; hydrocarbon molecules; dissociative ionization; cross sections; rate coefficients

1 Introduction

Carbon-based materials (graphite, carbon-carbon composites) are currently being used in most of the operating magnetic fusion devises as plasma facing materials because of their low radiation power capacity and the capability to withstand high heat fluxes. They have also been included as one of the plasma facing materials in the divertor design of International Thermonuclear Experimental Reactor (ITER) [1]. The interaction of hydrogenic plasma with carbon materials, however, results in copious production of hydrocarbon molecules C_xH_y (chemical erosion) [2], which enter the plasma as molecular impurities. The composition of hydrocarbon erosion fluxes depends on the energy of bombarding hydrogenic particles and surface temperature of carbon materials. At higher particle impact energies (30-500 eV), lighter hydrocarbons (CH_3, CH_4, C_2H_2) are dominant, while with decreasing the impact energy towards 1-20 eV, the heavier hydrocarbons (C_2H_4, C_2H_6, C_3H_4, C_3H_6, C_3H_8) become increasingly more present in the erosion fluxes, and dominant at hyperthermal energies ($\lesssim$1 eV) [3]. The present-day tokamaks tend to operate with divertor plasma temperatures below $\sim$ 5 eV, supporting the conditions for release of heavier hydrocarbons. When present in the plasma, the hydrocarbon molecules become subject of a multitude of collision processes with plasma electrons and protons [4]. Most of these processes (e.g. electron-impact excitation, ionization, and recombination) lead to dissociation of interacting molecule to two or more fragments and, as a result, to production of hydrocarbon molecules (or molecular ions) initially not present in the erosion fluxes. Therefore, the collisional kinetics of hydrocarbon molecules in a low-temperature divertor plasma includes all the members of CH_y, C_2H_y and C_3H_y families of hydrocarbon molecules for an initial erosion flux containing (at least some fraction of) CH_4, C_2H_6 and C_3H_8.

The most important electron-impact processes of C_xH_y molecules are excitation (only dissociative channels exist!) and ionization (both direct and dissociative channels). The $C_xH_y^+$ ions from the C_xH_y ionization are subject to further dissociative excitation and ionization, and to dissociative recombination. The only important proton-impact process of C_xH_y is the charge exchange.

The collision processes of hydrocarbon molecules have been studied in the past only for a limited number of C_xH_y species. The available cross section information on these processes has been compiled periodically [5-10], with a critical data assessment being given only for the charge exchange processes [10]. In Ref.[5] only the cross sections for the processes involving the CH_y ($1 \leq y \leq 4$) molecules were given. Refs. [6-8] are focussed on the electron-impact processes, while most of the cross sections in Ref.[9] have been derived on the basis of certain (not always correct) physical arguments.

In the present report we give an assessment of the available cross sections for the ionization processes of C_xH_y ($x = 1-3;\ 1 \leq y \leq 2x+2$) by electron impact

$$e + C_xH_y \rightarrow e + C_xH_y^+ + e \qquad (1a)$$

$$\rightarrow e + (C_{x-x'}H_{y-y'})^+ + [C_{x'}H_{y'}] + e \qquad (1b)$$

where (1a) represents the direct ionization channel, and (1b) represents the dissociative channels ($1 \leq x' < x; 1 \leq y' \leq y$). The square bracket [ ] in (1b) indicates that some of the H atoms in $H_{y'}$ may not be bound on $C_{x'}$ (e.g. in the channels $C_{x'}H_{y'-1}$ + H, $C_{x'}H_{y'-3} + H_2$ + H, etc.). The number of dissociative ionization channels rapidly increases with the increase of x and y; for C_3H_8 it may become larger than 40 for energies above $\sim$ 50 eV. In the experimental studies, only the "gross" ionization (or ion-production) channels, represented by the product ions $(C_{x-x'}H_{y-y'})^+$, can be identified (and their cross sections measured). The channels, within a given "gross" ionization channel, associated with the various fragmentations of the neutral complex $[C_{x'}H_{y'}]$, remain unidentified. Only for the simplest C_xH_y molecules, the neutral fragmentation channels $[C_{x'}H_{y'}]$ can be determined unambiguously.

The purpose of the present work is to provide a complete (or as complete as possible) cross section database for the processes (1) for use in the modeling of hydrocarbon (and carbon) transport in fusion divertor plasmas. Since the available experimental and theoretical data are limited to a relatively small number of members of the C_xH_y ($x = 1-3$) families of molecules, we have to adopt some strategies for deriving the cross sections for those molecules and reaction channels for which cross section data are not available in the literature. These strategies are based mainly on the cross section scaling laws contained in the simple theoretical models (such as the Bethe-Born approximation for the high-energy cross section behaviour), or derived semi-empirically in the present work, or elsewhere. These strategies are described in the next section. For the cases where more than one set of cross section measurements exist, the determination of the cross section, recommended for use in modeling and other applications, was based on a careful analysis of experimental uncertainties of the data.

The scope of the present work is limited only to the integral cross sections of reactions (1) (and the reaction rate coefficients derived from them). The differential characteristics of processes (1), such as energy and angular distributions of reaction products, which are important for the Monte-Carlo-based transport modeling codes, are not included in the present report. The available information on these quantities for the considered reactions is too scarce. Excluded from the scope of the present report is also the information about the internal energy of reaction products. In most of the dissociative channels of considered reactions, the molecular products are likely to be vibrationally excited and neutral H atoms electronically excited. However, the information on the internal states of the reaction products is virtually absent in the literature. The cross sections presented in this report assume that the C_xH_y molecule in the entry channel is in its ground vibrational state (as in the experiment). The electron-impact ionization processes with vibrationally excited C_xH_y molecules may have considerably different cross sections with respect to those with ground-state C_xH_y molecules. This difference may have serious consequences in the application of present database in modeling codes.

The organization of the report is as follows. In the next section we give an overview of the literature sources used in the data assessment and discuss the general properties of total and partial (channel specific) ionization cross sections, including some scaling relationships. In Sections 3 to 5 we present the results of data assessment, together with the recommended cross sections, for the total and partial ionization cross sections for the CH_y, C_2H_y and C_3H_y families of molecules, respectively. In Section 6 we present the analytic fit functions for the recommended cross sections, with the values of fitting coefficients being given in Appendix 1. In Section 7 we describe the calculations of reaction rate coefficients calculated on the basis of recommended cross sections. In Section 8 we give some concluding remarks. In Appendix 2, we give the graphs of the recommended cross sections and rate coefficients for all the reactions considered in the energy / temperature range from 1 eV to 1 keV.

2 General Properties of Total and Partial Ionization Cross Sections

2.1 Review of Cross Section Data Sources

Most of the experimental electron-impact ionization cross section measurements for the hydrocarbon molecules under consideration in the present work have been performed for the saturated hydrocarbons CH_4, C_2H_6 and C_3H_8. The main part of these measurements relates to the total cross sections. The other members of the CH_y, C_2H_y and C_3H_y families of hydrocarbons have been much less investigated, especially in the case of C_3H_y. For some molecules, such as C_2H, C_2H_3, C_2H_5, C_3H – C_3H_5, and C_3H_7, no experimental cross section measurements have been performed as yet. The experimental difficulties in the work with hydrocarbons partly lie in the fact that most of these species are radicals.

The theoretical studies of electron-impact ionization of hydrocarbon molecules are also difficult because of their complex electronic structure and large number of dissociation channels. Accurate quantum-mechanical cross section calculations for the electron-impact ionization of these molecules, with due inclusion of dissociation channels, have still not been carried out.

The literature data sources which were taken as a basis for our data analysis and assessment in the present report are given in Table 1. Not included in this table are references from the same authors, the cross section data in which have been superseded by the data in the reference cited in Table 1. Also excluded from the table are references to the pioneering work of Brüche [34] and Tozer [35] on CH_4, the data of which have been superseded by the more recent measurements, but we have included the classical work of Tate and Smith [30] on C_2H_2, since it complements the results of more recent references in the threshold region. In Table 1 are also included references on the results of theoretical calculations of total ionization cross section using the binary-encounter-Bethe (BEB) model [21,36] and the classical Deutsch-Märk model [37]. Only in the cases where no experimental data were found in the literature (such as C_2H_3 and C_3H_4), the results of these models were taken into consideration in deriving the total cross section. The physical basis of both BEB and D-M models remain unclear, particularly for the heavier hydrocarbons where the dissociative ionization channels dominate the total cross section.

2.2 Total Cross Sections

The total cross sections are measured either directly (by a system of parallel plate ion collectors), or indirectly, by measuring first the relative partial cross sections (using mass spectrum analysis) and normalizing their sum to an absolute cross section value from another measurement at a certain energy. In Table 1, these two ways of determining the total ionization cross section are indicated by (b) and (a), respectively. The total ionization cross sections for all C_xH_y molecules show a typical behaviour in the entire energy region (from threshold up to ~ 10 keV), and all attain their maximum value in the energy range around 80 eV. Below, we discuss the behaviour of total ionization cross sections at the high and intermediate energies, separately, with the purpose to reveal their general properties (scaling relationships). In the threshold region (~ 10-15 eV), all ionization cross sections show a sharp increase.

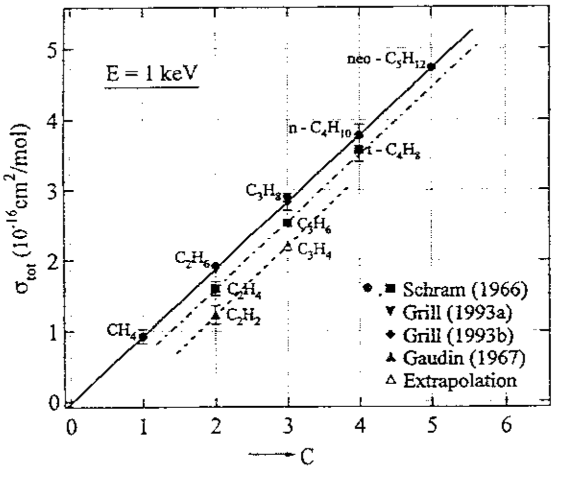

Figure 1: Dependence of total electron-impact ionization cross section for a number of C_xH_y molecules on the number of C atoms in C_xH_y for the collision energy $E = 1$ keV.

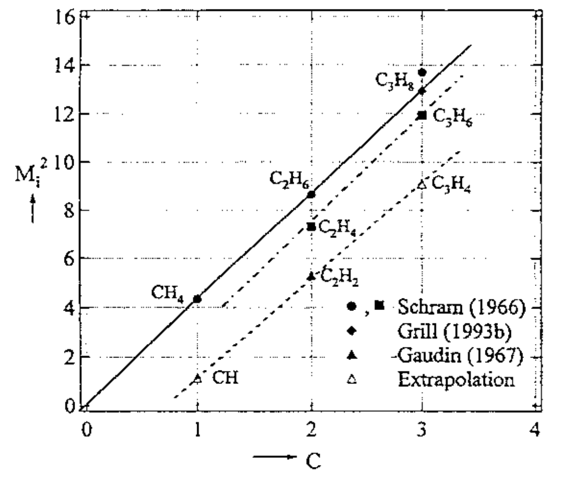

Figure 2: Dependence of the quantity M_i^2 in Eq.(2) for some C_xH_y molecules on the number of C atoms in C_xH_y.

2.2.1 High-Energy Cross Section Behaviour and Scalings

The high-energy (above a few hundreds eV) behaviour of the total ionization cross sections for a large number of hydrocarbon molecules was analyzed by Schram *et al.* [18] in terms of Bethe-Born theory for ionization. The Bethe-Born ionization cross section has the well known form

$$\sigma_i = \frac{4\pi a_o^2 Ry}{E} M_i^2 \ln(C_i E) \qquad (2)$$

where E is the collision energy, a_0 is the Bohr radius of atomic hydrogen, Ry is the Rydberg constant ($\simeq 13.6$ eV), M_i^2 is the collision strength for electron transition to continuum and C_i is some constant. By analyzing the cross section behaviour in the energy range $0.6 - 12$ keV of 18 hydrocarbon molecules C_xH_y (with 11 of them having $x \geq 4$), Schram *et al.* [18] have observed a liner dependence of σ_i on the number x of C atoms in C_xH_y molecules for a given impact energy. This is illustrated in Fig. 1 for $E = 1$ eV, where, besides the data of Schram *et al.*, some more recent data of other authors are also shown. From the linearity of $\sigma_i(C_xH_y)$ with x for the series C_xH_{2x+2} and C_xH_{2x}, Schram *et al.* were able to derive an "additivity rule" for the total cross sections of C_xH_y, assigning to each of the C-H and C-C (σ and π type) bonds in C_xH_y a specific "partial" cross section. From their cross section data they have derived the constants M_i^2 and C_i in Eq.(2) for the considered C_xH_y molecules and found that M_i^2 also linearly increase with x (see Fig. 2). From the observed linear dependence of M_i^2 with x for the C_xH_{2x+x} and C_xH_{2x} series of hydrocarbons they concluded that the additivity rule also applies to M_i^2 and obtained the values $M_i^2(C-H) = 1.07$, $M_i^2(C-C)_\sigma = 2.5$ and $M_i^2(C-C)_\pi = 0.4$ for the C-H, (C-C)$_\sigma$ and (C-C)$_\pi$ bonds in C_xH_y, respectively. The values of M_i^2 for the hydrocarbon molecules C_xH_y with $x \leq 3$, calculated by the additivity rule using the above values for $M_i^2(C-H)$ and $M_i^2(C-C)_\sigma$, are given in Table 2. This table also contains M_i^2 values derived from the available experimental data. The calculated and experimental values for M_i^2 are consistent with each other within about 8% (on average). Schram *et al.* have also derived the values of constant C_i in Eq.(2) from the energy behaviour of their cross sections. For the hydrocarbon molecules with $x \leq 3$, C_i varies between 0.071 and 0.107, with an average value of 0.089. Since the total cross section σ_i is not sensitive to the accurate value of C_i, by taking $C_i \simeq 0.089$ and the values of M_i^2 given in Table 2, one can calculate the total ionization cross sections for C_xH_y molecules by using Eq.(2) in the energy region above ~ 300 eV with an accuracy of 15-30%, or better.

We note that the C_3H_6 molecule appears in two isomeric forms: as propene and cyclopropan. The total ionization cross sections for these two isomers, measured in Refs.[18] and [20], differ by less than 8% [20] (5% in Ref.[18]), which is within the experimental uncertainties. The D-M model calculations [32] could not confirm the existence of this difference. The cross section and M_i^2 values shown in Figs. 1 and 2 refer to those of propene. Throughout this work we shall use only the cross sections for propene, for consistency. The molecules C_3H_7 and C_3H_5 also appear in two isomeric forms, while C_3H_4 has even three isomers. The isomers of a given C_3H_y molecules have somewhat different ionization potentials and in our analyses we shall be using the smallest of them.

We should also like to note that the linearity of σ_{tot}

and M_i^2 in Figs. 1 and 2 on the number of carbon atoms in C_xH_y is strictly observed only within the series C_xH_{2x+2}, C_xH_{2x} and C_xH_{2x-2}. For the total cross sections, this features is observed down to $E \simeq$40-50 eV, as demonstrated in the next sub-section.

2.2.2 Cross Section Behaviour at Intermediate and Low Energies

There is no simple theoretical model which can describe the total ionization cross section behaviour for hydrocarbon molecules at the intermediate and low energies (except for the strict threshold region where the Wannier law should be valid). However, the experimental cross sections show certain regularities, both with respect to their energy behaviour and with respect to the number of C and H atoms in the molecule, which allow to derive certain empirical scaling relationships. For instance, the maxima of measured total ionization cross sections for all hydrocarbon molecules (from CH to C_3H_8) lie around 80 eV (±10 eV) and are very broad. For C_2H_y and C_3H_y, the cross section dependence in this energy region on the number of hydrogen atoms in the molecule is very weak. This is illustrated in Fig. 3, where the total cross section values for E = 80 eV from the most accurate measurements are shown (filled symbols). The sum of the cross sections for CH_y^+ and CH_{y-1}^+ production in $e + CH_y$ collisions shows a linear dependence on y (first remarked in Ref.[14]). The experimental total cross sections for C_2H_2, C_2H_4, and C_2H_6 also show a linear dependence on the number of H atoms. Furthermore, the linear dependence of total cross section on the number of C atoms within the series C_xH_{2x+2} and C_xH_{2x}, demonstrated in Fig. 1 for E = 1 keV, is also observed on Fig. 3 for E = 80 eV. Combining these regularities one can safely determine the unknown total ionization cross sections for some C_xH_y molecules, such as CH and C_3H_4, for E = 80 eV. The linear dependence of the total cross sections for C_2H_y and C_3H_y can be related to the polarizability α_{pol} of these molecules, as pointed out in Refs.[39-40]. The relation between $\sigma_{tot}(C_xH_y)$ and $\alpha_{pol}(C_xH_y)$ is

$$\sigma_{tot}(C_xH_y) \sim [\alpha_{pol}(C_xH_y)]^{1/2}. \qquad (3)$$

The cross section values for $C_{2,3}H_y$ calculated from Eq.(3) and normalized to the experimental cross section for C_xH_{2x+2} are shown in Fig. 3 by dotted lines. The values for α_{pol} were taken from Ref.[9] (and Ref.[41], for C_3H_8) and are given in Table 3. As seen from Fig. 3, the scaling (3) is not valid for CH_y, but for C_2H_y and C_3H_y it gives results very close to those experimentally observed (for C_2H_2, C_2H_4 and C_3H_6), or predicted by the experimentally determined linear dependence of σ_{tot} on H (shown on Fig. 3 by open symbols). The cross section value for C_3H_6 (propene) was taken from Ref.[18], but corrected by a factor of 0.935 which was obtained from the ratio of the data of Ref.[18] and Ref.[20] at E = 600 eV. The crossed square for C_3H_4 is the result of calculations with the D-M model [33], while one for C_3H_6 is the D-M model result from Ref.[32]. It is worth noting that the partial cross sections for CH_y^+ production from the $e + CH_y$ ionization also show a (very weak) linear dependence on y [14] (also shown in Fig. 3).

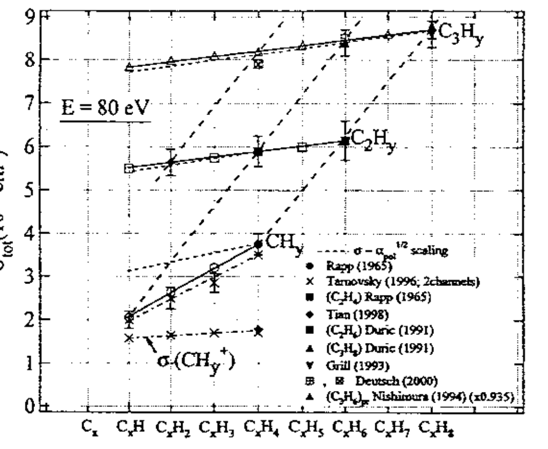

Figure 3: Total electron-impact ionization cross sections for C_xH_y at E = 80 eV. Full symbols: experimental data; open symbols: inter- and extrapolated values. Dotted lines: $\alpha_{pol}^{1/2}$ scaling. $\sigma_{tot}(CH_y^+)$ from Ref.[14] is also shown.

The linearity of σ_{tot} with the number of C and H atoms in C_xH_y remains also for energies below and above 80 eV. Figs. 4 and 5 illustrate the behaviour of total ionization cross section for E = 200 eV and E = 50 eV, respectively. In Fig. 4 also the cross sections of C_2H_2, C_2H_4, and C_2H_6 for E = 1000 eV are shown to demonstrate the linearity of σ_{tot} with x even at the high energies. (The linearity of σ_{tot} with x was shown in Fig. 1 for E = 1000 eV.) The point of Nishimura (1994) [20] for C_2H_4 was corrected by a factor equal to the ratio of the cross sections of Ref.[20] and Ref.[17] at E = 145 eV. The linear dependence of σ_{tot} with the number of H atoms in C_xH_y persists also for energies below 50 eV (as shown for the C_2H_y molecules for E = 40 eV in Fig. 4), but for energies below 30 eV the deviations from this linearity start to become large.

Figures 3-5 show that one can safely derive the value of the total cross section at a given energy $E \gtrsim$40 eV for a C_xH_y molecule with unknown cross section on the basis of the existing cross sections for other molecules in the isocarbon (x =constant) series, or from the $y = 2x + 2 - k$, $k = 0, 1, 2, \cdots$ series (CH_2 and CH_3 make an exception from this second rule; see Fig. 5).

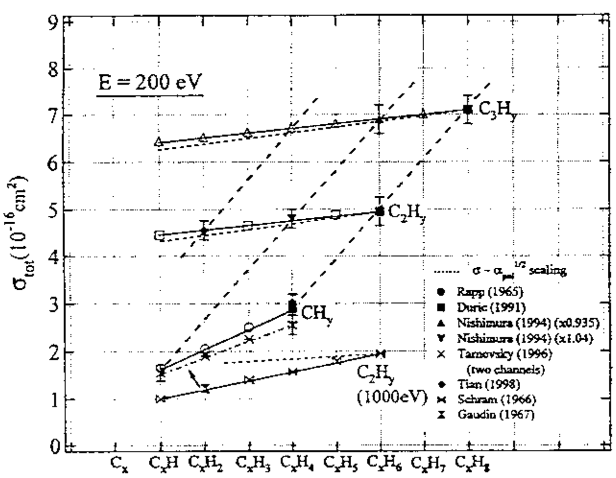

Figure 4: Same as in Fig.3, but for $E = 200$ eV. The data $\sigma_{tot}(C_2H_y)$ at $E = 1000$ eV are also shown.

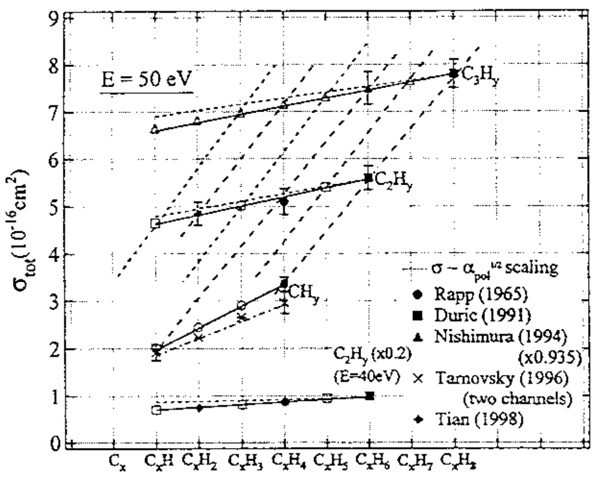

Figure 5: Same as in Fig.3, but for $E = 50$ eV. The data $\sigma_{tot}(C_2H_y)$ at $E = 40$ eV are also shown.

The linearities of σ_{tot} with the number of C and H atoms in C_xH_y molecule, observed in Figs. 3-5, are a consequence of the empirical "additivity rule" for the integrated continuum dipole oscillator strengths, M_i^2, mentioned in the previous sub-section. Figs. 3-5 suggest that this rule applies down to collision energies about $30 - 40$ eV. Figures 3-5 also show that the scaling of σ_{tot} for C_2H_y and C_3H_y with α_{pol} works well (to within 2-4 %) in the energy range from 40 eV to 200 eV, but it starts to fail with increasing the energy (see Fig. 4, the C_2H_y curve for 1000 eV).

In the energy region below ~ 30 eV, the total ionization cross section of C_xH_y molecules decreases rapidly towards its threshold, lying typically in the range 9-13 eV.

2.3 Partial Cross Sections

The partial cross sections in this Report refer to both "gross" ionization (or to specific ion-production) channels, in which the neutral fragmentation is not specified (or unknown), and to channels with well defined product composition. As discussed in the Introduction, the ion-production channels may include many dissociative channels with different composition of dissociation products. Only in the cases of simpler C_xH_y molecules the "gross" ionization channels can be easily related to the proper ionization channels (or are identical with them). In the experiments, only the partial cross sections for ion-production channels can be measured. In most of the applications, however, (e.g. particle transport in fusion divertors), the composition of neutral products from dissociative ionization is essential to fully describe the collisional kinetics. The determination of the neutral fragmentation channels within a given "gross" ionization (ion-production) channel will be discussed in Sections 3-5 in more detail. In this subsection we shall concentrate on the general properties of partial cross sections of ion production channels.

As Table 1 shows, the ion production partial cross sections have been measured only for a limited number of C_xH_y molecules: CH_y, $y = 1 - 4$, C_2H_2, C_2H_6 and C_3H_8. There have been also relative measurements of the different ion fractions in the total ion current from electron impact ionization of C_2H_2, C_2H_4 and C_2H_6 for two collision energies, $E = 75$ eV and $E = 3.5$ MeV [26]. The analysis of available information allows nevertheless to derive certain conclusions about the general properties of ion-production partial cross sections, and on that basis to predict the values of corresponding cross sections for the molecules for which no such measurements have been performed. We shall focus our attention on the ion-production channels, the cross sections of which constitute individually not less than 5-10% of the total ionization cross section in the entire energy range in which the measurements have been performed.

In Fig. 6 we show the ratios of partial cross sections for production of the ions CH_y^+, CH_{y-1}^+ and CH_{y-2}^+ in e + CH_y collisions and the corresponding total cross section for the collision energy $E = 80$ eV. The experimental data were taken from Straub *et al.*[15] for CH_4, and from Tarnovsky *et al.*[14] for CH_3, CH_2 and CH. (The measurements of Ref.[14] were done for CD_y, but comparison of the CD_4 data with those for CH_4 shows that there is no isotope effect in the cross section values.) The values of these ratios for CH_4, calculated from the partial and total cross section of Ref.[16] are identical (or very close) to the values from Ref.[15]. The considered three ion-production channels for CH_4 contribute with about 92% to the total cross section at $E = 80$ eV, while the chan-

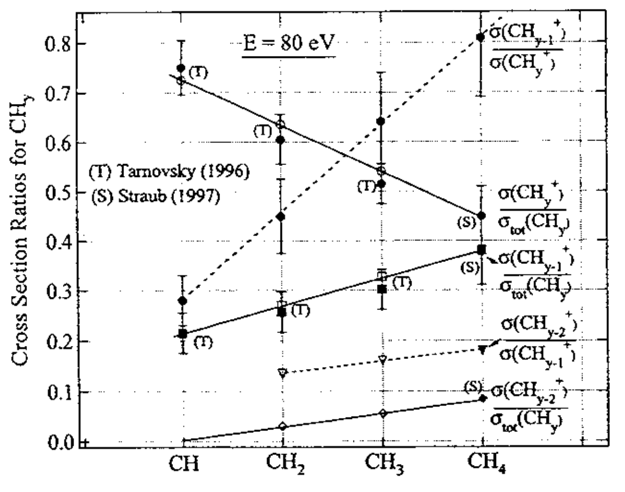

Figure 6: Cross section ratios at $E = 80$ eV for different ionization channels for CH_y molecules with respect to total ionization and mutually . Full symbols: experimental data; open symbols: inter- or extrapolations.

nels for CH^+ and C^+ ion production from CH, contribute with about 96% to the total cross section at this energy. For the ratios $\sigma(CH_y^+)/\sigma_{tot}(CH_y)$ and $\sigma(CH_{y-1}^+)/\sigma_{tot}(CH_y)$ we have experimental values for all the monocarbon $CH_y (y = 1-4)$ molecules. Within their experimental uncertainties, the values of these ratios show a linear dependence on the number of H-atoms in the CH_y molecule. This linear dependence is, of course, translated into a linear dependence of the mutual ratio of these two partial cross sections (also shown in Fig. 6). The observed linear dependences on y of CH_y^+ and CH_{y-1}^+ fractions in the total cross section suggest that a similar linear dependence can be expected also for the ratio $\sigma(CH_{y-2}^+)/\sigma_{tot}(CH_y)$. Since for CH $\sigma(CH_{y-2}^+)$ does not exist, one can formally assign a zero value for the ratio $\sigma(CH_{y-2}^+)/\sigma_{tot}(CH_y)$ for this molecule. The straight line joining this point with the known experimental value of this ratio for CH_4, would determine the upper limit of the values for this ratio for CH_2 and CH_3. The lowest limit for the value $\sigma(CH_{y-2}^+)/\sigma_{tot}(CH_y)$ for CH_2 would be zero, which would give the lower limit for the value of this ratio for the CH_3 molecule, if its linear dependence is assumed. This would introduce an uncertainty in the determination of cross section $\sigma(CH_{3-2}^+)$ of about 25%. However, there is no physical basis to assume that the partial cross section $\sigma(CH_{2-2}^+) \equiv \sigma(C^+)$ should be zero at $E = 80$ eV, i.e. well above the thermochemical thresholds, $E_{th} \simeq 14.6$ eV and $E_{th} \simeq 19.2$ eV for the reactions $e + CH_2 \to C^+ + H_2 + 2e$ and $e + CH_2 \to C^+ + 2H + 2e$ (for the values of E_{th}, see Section 3.1). Therefore, the determination of the linear dependence for the ratio $\sigma(CH_{y-2}^+)/\sigma_{tot}(CH_y)$ on the basis of $\sigma(CH_{y-2}) = 0$ for CH looks much more natural. Moreover, with the values of $\sigma(CH_{y-2}^+)/\sigma_{tot}(CH_y)$ determined this way, the linearity of the ratio $\sigma(CH_{y-2}^+)/\sigma_{tot}(CH_y)$ is also obtained, consistent with the similar linearity of the $\sigma(CH_{y-1}^+)/\sigma_{tot}(CH_y)$ ratio (see Fig. 6). It should be noted that the accuracy of the presented method, based on the observed (and expected) linearity of the fractional contributions of partial ion-production cross sections to the total ionization cross section, cannot obviously exceed the accuracy of experimentally measured partial cross sections (or their ratios relative to the total cross section). For dominant ion-production channels, that accuracy in the most carefully performed experiments amounts 8-10%, while for the weak channels: it increases up to 12-15%, or more. (See e.g. Refs.[12]-[16], [25], [31]).

A general criterion in the derivation of the unknown (but also for checking the measured) partial ion-production cross sections is that the sum of their fractional contributions to the total ionization cross section should be equal to one. For instance, for the CH molecule, the fractional contribution of $\sigma(CH^+)$ and $\sigma(CH_{1-1}^+) \equiv \sigma(C^+)$ cross section to $\sigma_{tot}(CH)$ in Fig. 6 sum up to 0.94, meaning that the fractional contribution of the $\sigma(H^+)$ cross section (for the channel $e + CH \to H^+ + C + 2e$) equals to 0.06 at this energy. Similarly, in the case of CH_2, the fractional contribution of the $\sigma(H^+)$ partial cross section to the total ionization is 0.07, according to the values from Fig. 6 for the fractional contributions of other three ion-production channels.

It is worth noting in Fig. 6 that the contribution of parent ionization (the CH_y^+ channel) decreases with increasing the number of H atoms in CH_y, while the contributions of CH_{y-1}^+ and CH_{y-2}^+ channels increase with increasing y.

The results of a similar analysis for the C_2H_y families of hydrocarbons are shown in Fig. 7 for $E = 80$ eV. The experimental data for the rates $\sigma(C_2H_{y-k}^+)/\sigma_{tot}(C_2H_6)$, $k = 0-4$, are available only for C_2H_2, C_2H_4 and C_2H_6. The channels shown in this figure are the dominant ion-production channels not only for $E = 80$ eV, but also for energies up to the MeV region [26]. The linear dependence of cross section ratios on y is observed for all considered ion-production channels, except for the $C_2H_{y-1}^+$ ion channel, where this dependence is broken in two parts, at the C_2H_4 – member of C_2H_y family. This change of the slope of linear behaviour reflects the fact that with increasing the number of H atoms in C_2H_y over $y = 4$, the release of H_2 (or 2H) from C_2H_y becomes a more favorable relaxation process than the release of only one H-atom. The change of the slope of linearity for the $C_2H_{y-3}^+$ channel may be due to a similar phenomenon, but may also be an artefact of the uncertainties in measured relative ion fractions in Ref.[26]. It is worth noting that

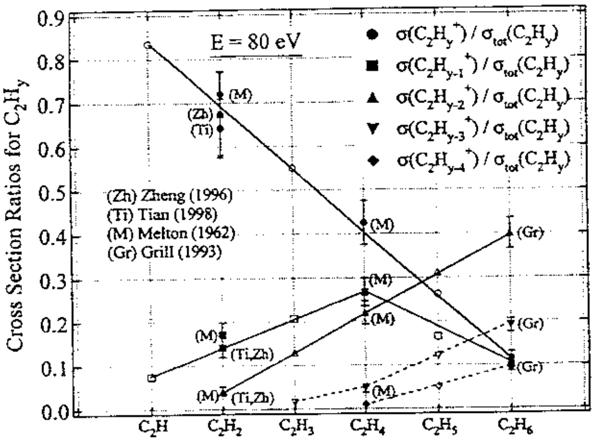

Figure 7: Same as in Fig.6, but for C_2H_y molecules. (See text.).

the contribution of parent ionization ($C_2H_y^+$ channel) to the total ionization decreases with increasing y much faster than in the case of CH_y family of hydrocarbons.

A similar analysis of the behaviour of fractional contributions of partial ion-production cross sections to the total ionization cross sections in the C_3H_y family of hydrocarbons is not possible since these contributions are known only for the C_3H_8 molecule [31]. However, by using the observed linearities of fractional contributions in the CH_y and C_2H_y systems, extrapolations to the C_3H_y system are still possible. This will be discussed in detail in Section 5.

In Table 4 we give the values of the fractional contributions to the total cross section for the dominant ion-production channels in $e + C_3H_8$ collisions at the energy $E = 100$ eV. This table shows that the dominant channels in the electron impact ionization of C_3H_8 at $E = 100$ eV are not the dissociative channels associated with hydrogen atoms (or molecule(s)) release but those which are associated with the breakage of one $(C-C)_\sigma$ bond. The channels for production of $C_2H_y^+$ (y=1-5) ions contribute with 58% to the total ionization cross section. The $\sigma(C_xH_{y-2}^+)$ cross section, which was the dominant one in $e + C_2H_6$ collisions at $E = 80$ eV with a contribution of 40% to the total cross section, in the case of C_3H_8 contributes only 1.5% to the total cross section.

An important question is whether the relative contributions of partial ion-production cross sections to the total ionization cross section vary with the energy, i.e. whether the analysis resulting in Figs. 6 and 7, has to be repeated for each energy (or a sufficient large number of energy points) in order to infer the values of partial ion-production cross sections for the molecules of CH_y and C_2H_y families for which such data are not experimentally available.

For the ion fractions resulting from C_2H_2, C_2H_4 and C_2H_6 upon electron impact with energies of 75 eV and 3.5 MeV, Melton [26] found that they are practically the same (within the experimental uncertainties) for these two energies. In Tables 5-7, we give the relative contributions of dominant ion-production channels to the total cross sections of CH_4, C_2H_6 and C_3H_8, respectively, in the energy range from 20 eV to 2000 eV (for CH_4) and 900 eV (for C_2H_6 and C_3H_8). The tables show that indeed, the variation of relative contributions of dominant ion-production channels to the total ionization cross section with the collision energy is fairly weak (with the exception of the values at $E = 20$ eV for some channels). For the most dominant channels (such as CH_4^+ and CH_3^+ from CH_4, $C_2H_4^+$ and $C_2H_3^+$ from C_2H_6, and $C_2H_5^+$, $C_2H_4^+$ and $C_2H_3^+$ from C_3H_8), the deviation of the values of relative contributions from their average value in the interval 20-1000 eV is within 10%. For the weaker channels, this deviation can increase up to 15-20%. In both cases, however, the observed deviations from the average values of the relative contributions in this energy range are close to the experimental uncertainties of corresponding partial ionization cross sections. In deriving the cross sections for the ion-production channels of $e + C_xH_y (x = 1, 2)$ collision systems for which no experimental data were found in the literature we have used the experimental values of fractional contributions for the investigated systems at a number of collision energies (i.e. tables like Table 6 for C_2H_2, C_2H_4 and C_2H_6, for instance), and only for the weaker channels we have used the average values of fractional contributions.

In the next three sections we shall discuss the cross sections for specific channels in electron impact ionization of molecules in the CH_y, C_2H_y and C_3H_y hydrocarbon families, respectively. Discussions of the corresponding total cross sections will be given as well.

3 Cross Sections for $e + CH_y$ Collision Systems

3.1 Total and Partial Cross Sections for CH_4

3.1.1 Total Cross Section

Direct absolute total ionization cross section measurements for the $e + CH_4$ system have been done in Refs.[17]-[20], covering the energy range from threshold ($\simeq 12.63$ eV) up to 12 keV. The data of Refs.[17], [19], available in the energy range below 1000 eV, and of Ref.[18], available in the energy range from 0.6 to 12 keV, agree in the overlapping energy range to within 5% ($\leq 10\%$ in the threshold region) and are considered as the most accurate ones. The data of Ref.[20] have somewhat higher uncertainty. The most accurate

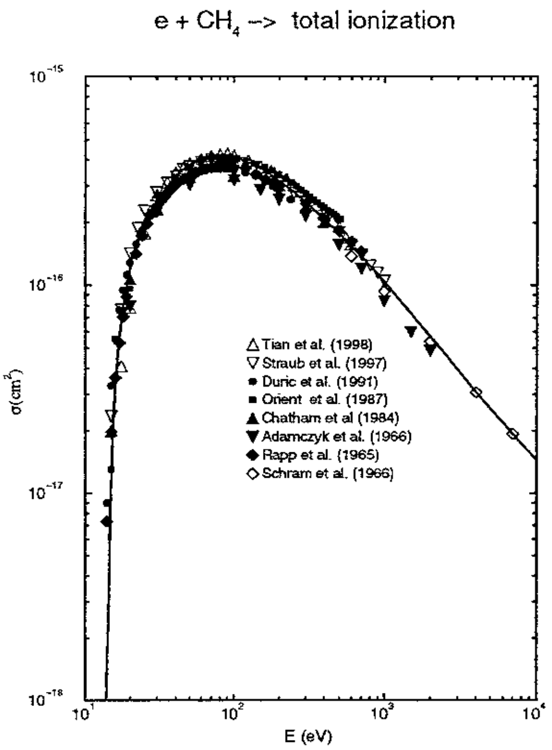

Figure 8: Total electron-impact ionization cross section for CH_4. Symbols: experimental data. Solid line: least-square fit of selected sets of data (see text).

partial ion-production cross section measurements of Refs.[15] and [16], (uncertainty of 8-10%), also agree with the absolute measurements of Refs.[17] and [19] in the overlapping energy ranges.

In Fig. 8, the experimental total cross sections data for CH_4 from these and some other references are shown. The solid line in this figure is a least-square fit of the data, excluding those of Refs.[11] and [13] in their high-energy parts, where their uncertainties appear to be larger. The fitted cross section represents the data with an r.m.s. of 3%.

3.1.2 Partial Cross Sections

The ion-production partial cross sections for CH_4 have been measured in Refs.[11]-[16]. The accuracy of the data from the most recent experiments (Refs.[15] and [16]) is in the range 8-10% and these data will be taken as a basis for the recommended cross sections. In Ref.[14] not all ion-production channels from the $e + CH_4$ collision were considered, while the data of Ref.[13] contain larger (~ 20-25%) uncertainties. The dominant ionization channels for the $e + CH_4$ collision system are given in Table 8, together with the ionization potential I_p for CH_4 and the threshold energies (appearance potentials A_p) for the specific reaction channels. The values for I_p and A_p were taken from Ref.[42]. In this table also shown are the appearance potentials obtained from the thermochemical tables [43], and those obtained in Ref.[12]. The values of Ref.[42] are considered to be the most accurate ones. They are close to those calculated from the thermochemical tables. The channels shown in Table 8 are the most important ones. Other channels with more complex neutral fragmentation have higher appearance potentials and their cross sections are expected to be much smaller. For instance the CH_2^+ product may be accompanied not only with the H_2 product, but also with 2H products. The thermochemical threshold for this channel is about 20 eV, and its cross section in the energy region around its maximum (~ 80 eV) is expected to be by a factor about five smaller than the cross section for the $CH_2^+ + H_2$ channel. With decreasing the energy this difference should increase, particularly in the threshold region for the $CH_2^+ + 2H$ channel (20-30 eV) where the cross section $\sigma(CH_2^+ + 2H)$ should rapidly decrease towards zero with decreasing the energy towards threshold. Similar arguments apply also for the other (neglected) neutral fragmentation channels within the C^+, H_2^+ and H^+ ion-production channels, since the value of thermochemical threshold increases with increasing the number of fragmented products.

The experimental cross sections for the ionization channels shown in Table 8 are given in Figs. 9-15. The solid lines in these figures are the least-square fits of the data of Refs.[15] and [16], extended appropriately towards the threshold and high energies by taking also into account the data from Refs.[11-14]. The extensions of the solid lines in the keV energy region were controlled by two criteria: (i) preservation of the Bethe-Born behaviour of the cross section from the 0.6-1 keV range in the region $E > 1$ keV, and (ii) the sum of the partial cross section should reproduce the total ionization for CH_4, which is known experimentally up to 12 keV.

It should be noted that there is a rather strong correlation between the magnitude of ionization channel cross section and the value of channel appearance potential. This correlation is particularly pronounced for the weaker channels. For instance, for the H^+-, C^+- and H_2^+- ion-production channels, the thermochemical reaction thresholds are 18.11, 19.46, and 20.27 eV, respectively, (see Table 8), and Figs. 13-15 show that the cross sections for these channels strongly decrease with increasing the threshold energy. The energy threshold for the H^+ ion-production channel is also smaller than that for CH^+ ion-production channel, which makes $\sigma(H^+)$ larger than $\sigma(CH^+)$ (compare Figs. 12 and 14). The reason for this is the inverse dependence of the break-up reaction on the threshold energy, which is also reflected in the classical picture of ionization process. However, the observed inverse dependence of σ on E_{th} for the weak dissociative channels

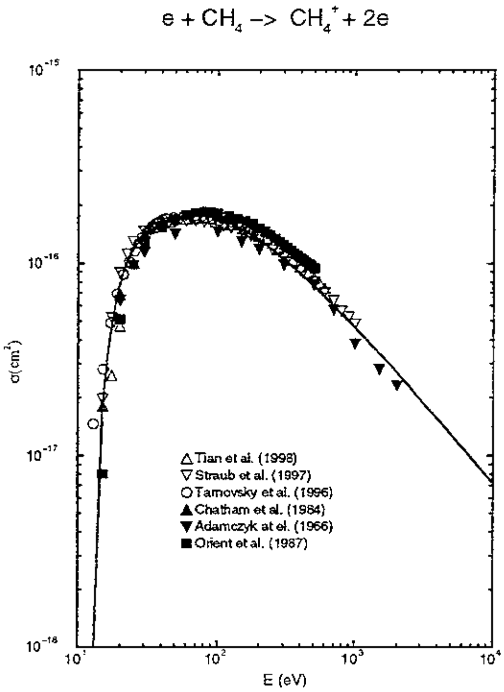

Figure 9: Partial cross section for parent (non-dissociative) ionization of CH_4. Symbols: experimental data. Solid curve: least-square fit of selected data (see text).

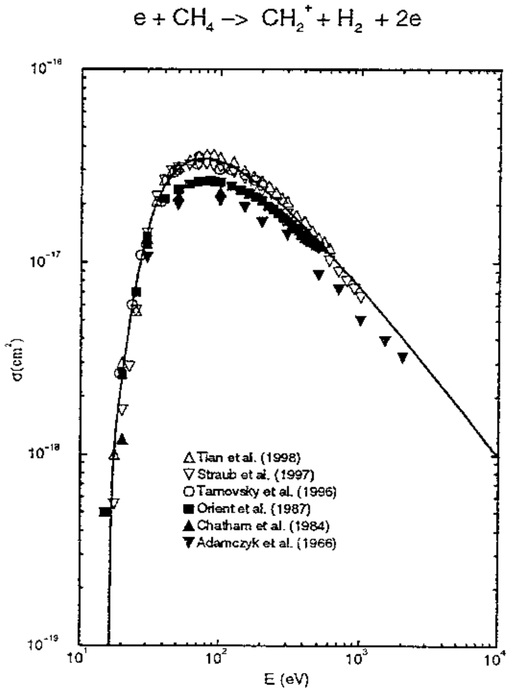

Figure 11: Same as in Fig.9, but for the CH_2^+ + H_2 dissociative channel (see text).

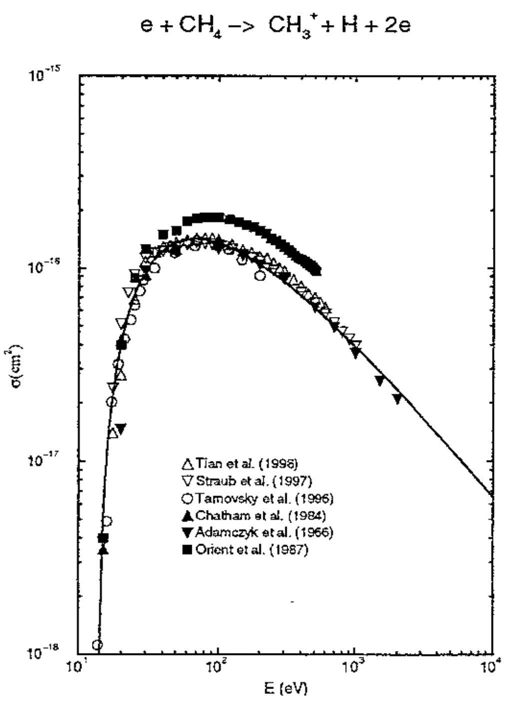

Figure 10: Same as in Fig.9, but for the CH_3^+ + H dissociative channel.

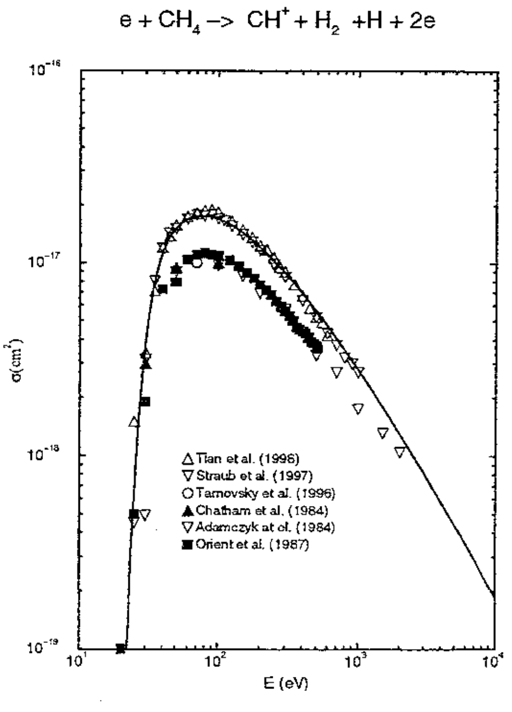

Figure 12: Same as in Fig.9, but for the $CH^+ + H_2 + H$ dissociative channel.

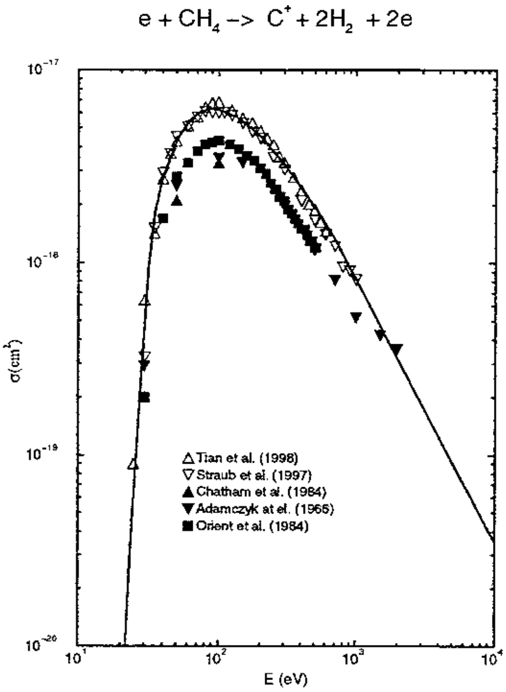

Figure 13: Same as in Fig.9, but for the $C^+ + 2H_2$ dissociative channel.

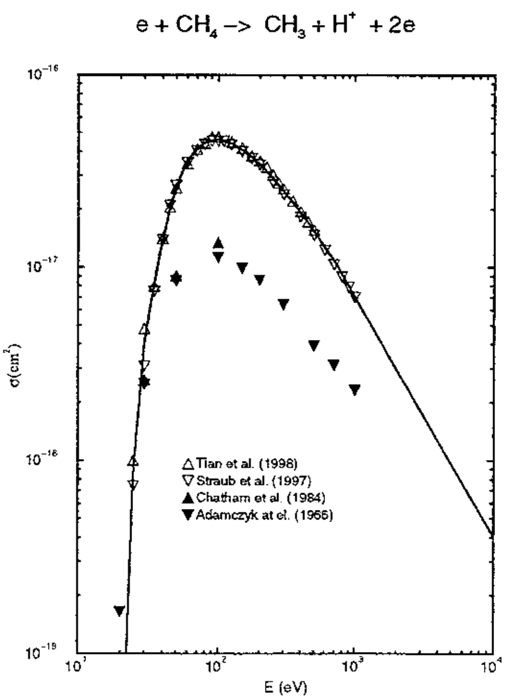

Figure 14: Same as in Fig.9, but for the $CH_3 + H^+$ dissociative channel.

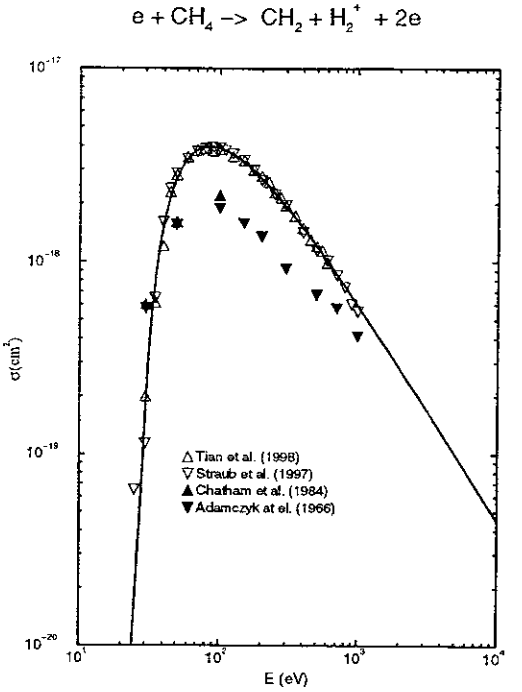

Figure 15: Same as in Fig.9, but for the $CH_2 + H_2^+$ dissociative channel.

is much stronger than E_{th}^{-1}.

3.2 Total and Partial Cross Sections for CH_3

The total cross section for the methyl radical CH_3 has not been measured directly. In Refs.[14] and [22] the cross sections for the two dominant ion-production channels (parent ionization and $CH_2^+ + H$ dissociative ionization) were measured, while in Ref.[23] only the parent ionization cross section was measured. (The D-isotopic version of this molecule was used.) The claimed accuracies are $\pm 15 - 18\%$ in Ref.[14] and $\pm 30\%$ in Ref.[22]. The ion-production channels for the $e + CH_3$ collision system are given in Table 9, together with the values of their threshold energies (calculated from thermochemical tables, [44, 45]). Only the dominant neutral fragmentation channels are shown in this table.

The cross sections for the first two channels of Table 9 are shown in Figs. 16 and 17. The available experimental data, both for the parent ionization and $CH_2^+ + H$ dissociation channel, agree well with each other. The solid lines on these figures are least-square fits of the data for $E \leq 200$ eV. The high energy parts of the cross sections represented by the solid lines were obtained from the ratios $\sigma(CH_3^+)/\sigma_{tot}(CH_3)$ and $\sigma(CH_2^+)/\sigma_{tot}(CH_3)$ for $E = 200$ eV, assuming that they remain the same also for $E > 200$ eV. The value of $\sigma_{tot}(CH_3)$ was taken from the BEB calculations [21] at

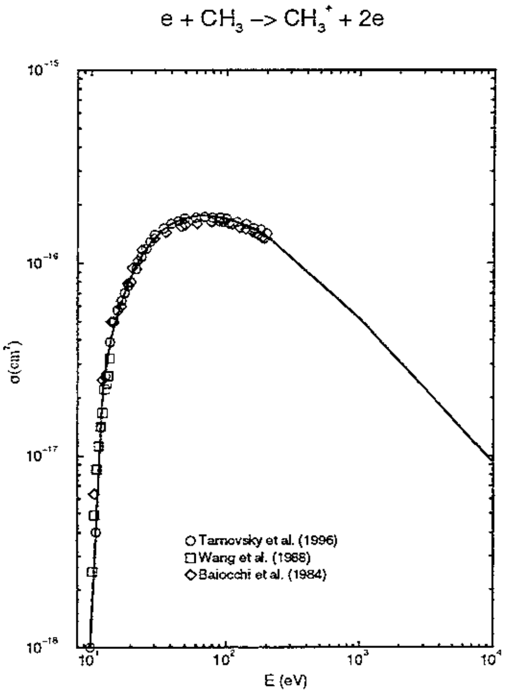

Figure 16: Partial cross section for parent (non-dissociative) ionization of CH_3. Symbols: experimental data. Solid curve: least-square fit of the data, extended to high energies by using scaling relationships (see text).

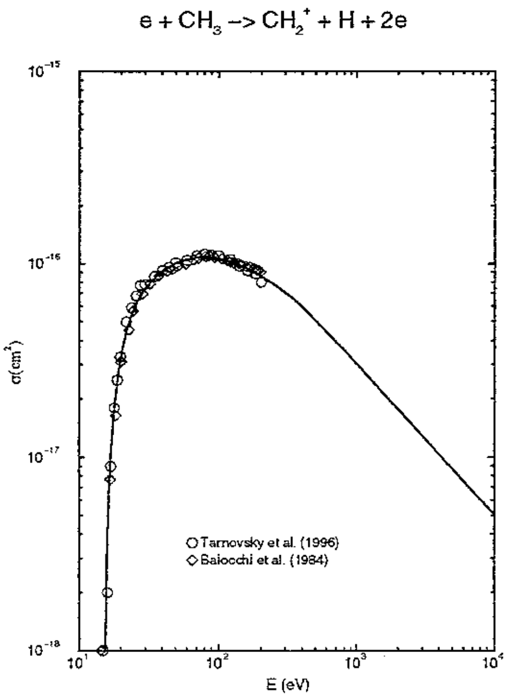

Figure 17: Same as in Fig.16, but for the $CH_2^+ + H$ dissociative channel.

$E = 500$ eV and $E = 1000$ eV. The value of $\sigma_{tot}(CH_3)$ at 1000 eV was increased from 0.83×10^{-16}cm^2 to 0.9×10^{-16}cm^2 to preserve the linearity of $\sigma_{tot}(CH_y)$ BEB cross sections [21, 24] with respect to y at this energy. The other values of $\sigma(CH_3^+)$ and $\sigma(CH_2^+)$ in the energy region above 200 eV were obtained by interpolation, using the Bethe-Born character of cross section behaviour. The unknown cross section $\sigma(CH^+)$ for the $CH^+ + H_2$ channel was obtained in the energy region below 200 eV by using the linear y-dependence of $\sigma_{tot}(CH_y)$ for the energies 40, 80, 200 eV (the last two of them shown in Figs. 3 and 4) and the ratio $\sigma(CH^+)/\sigma_{tot}(CH_3)$. The values of this ratio were found to be very close to each other, and for $E = 80$ eV it is shown in Fig. 6 (the $\sigma(CH_{y-2}^+)/\sigma_{tot}(CH_y)$ line). By using the value of this ratio at $E = 200$ eV also for the high energies, and, as before, by using the BEB values of $\sigma_{tot}(CH_3)$ at $E = 500$ and 1000 eV, the cross section $\sigma(CH^+)$ was determined in the entire energy range by an interpolation / extrapolation procedure (based on the Bethe-Born cross section behaviour at high energies and its steep decrease towards the threshold at energies below $\sim$ 30 eV). The cross section $\sigma(CH^+)$ derived in this way is shown in Fig. 18. We note that the sum of the partial cross sections $\sigma(CH_3^+)$, $\sigma(CH_2^+)$ and $\sigma(CH^+)$ constitutes 94.4% of the total ionization cross section of $\sigma_{tot}(CH_3)$ in the energy region when all three channels are open. The remaining 5.6% of the total cross section is distributed among the last three ion-production channels in Table 9. From the point of view of many gas- (or plasma-) kinetics applications, one can safely neglect these three channels in the kinetics. If nevertheless one would like to include these channels in the kinetics, then, in absence of any clear criteria to determine their cross section from the existing ones, one can use the closeness of the appearance potentials for the H^+, C^+ and H_2^+ channels for the $e + CH_4$ and $e + CH_3$ systems (see Tables 8 and 9) and the remaining 5.6% of the total cross section $\sigma_{tot}(CH_3)$ distribute among the H^+, C^+ and H_2^+ channels in the same proportion as the cross sections for the analogous ion-production channels in the $e + CH_4$ system. This procedure, which cannot be rigorously justified, would give

$$\sigma(H^+) = 0.039\sigma_{tot}(CH_3), \quad (4a)$$

$$\sigma(C^+) = 0.012\sigma_{tot}(CH_3), \quad (4b)$$

$$\sigma(H_2^+) = 0.005\sigma_{tot}(CH_3). \quad (4c)$$

The largest of these cross sections, $\sigma(H^+)$, is shown in Fig. 19, after its appropriate adjustment in the threshold region (i.e. below 30 eV).

The total cross section obtained by summing the partial cross sections for the channels CH_3^+, $CH_2^+ + H$ and $CH^+ + H_2$, and accounting for the remaining in Table 9 via Eq.(4), is given in Fig. 20.

We note that the total ionization cross section for

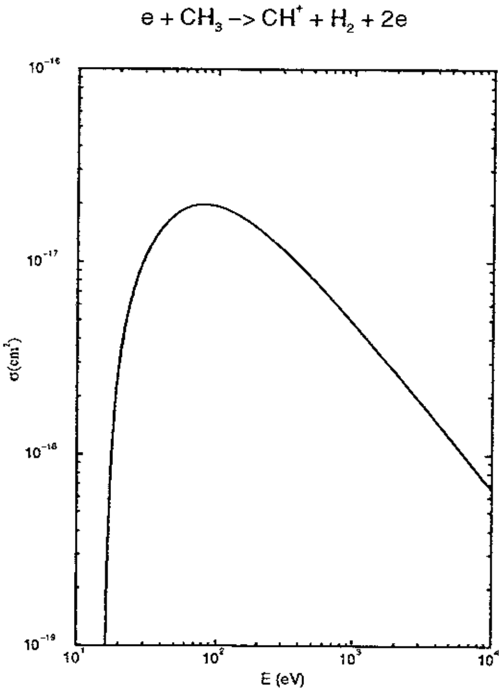

Figure 18: Partial cross section for the $CH^+ + H_2$ dissociative channel of CH_3 derived from scaling relationships (see text).

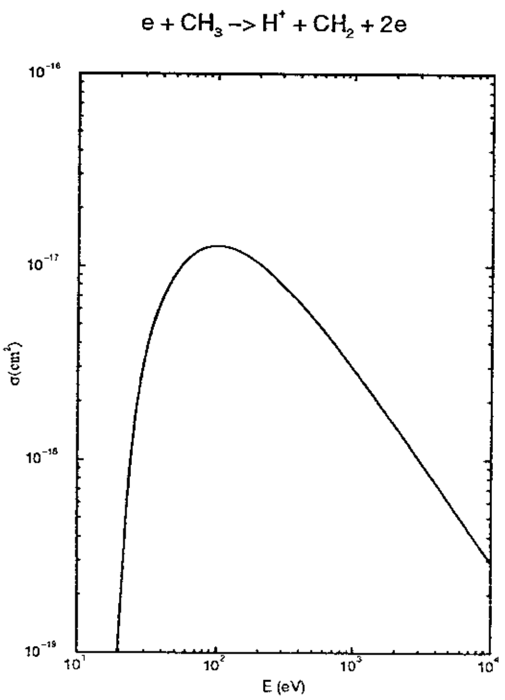

Figure 19: Same as in Fig.18, but for the $CH_2 + H^+$ dissociative channel.

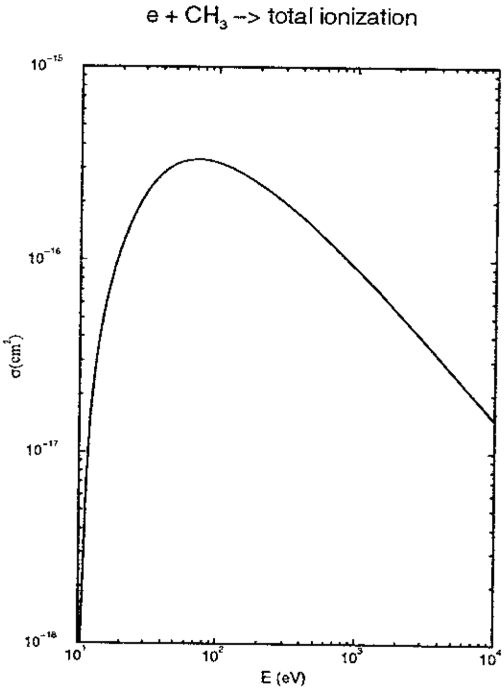

Figure 20: Total electron-impact ionization cross section for CH_3.

CH_3, calculated by the Bethe-Born formula, Eq.(2), with the value of $M_i^2 = 3.21$ (from Table 2) and $C_i = 0.09$, at the energies $E = 500$ and 1000 eV differs from the values in Fig. 20 (or the BEB cross section values) at these energies by 12% and 16%, respectively.

3.3 Total and Partial Cross Sections for CH_2 and CH

The partial cross sections for the CH_2^+ and CH^+ ion-production in e+CH_2 (in fact e+CD_2) collision systems were measured in Refs.[14] and [22], while for the CH^+ and C^+ channels in e+CH (e+CD) system such measurements have been performed only in Ref.[14] so far. These channels may account, according to the authors of these references, up to about ~ 90% (for CH_2) and even more (for CH) of the total cross section. In Table 10 we give the list of other possible channels in these collision systems (with the list for CH being exhaustive). The ionization and appearance potentials for the listed channels are also given in the table (taken from Refs.[44, 45]). The measurements were done in the energy range from the threshold to 200 eV, and the claimed data accuracy is ±15 − 18% in Ref.[14] and ±30% in Ref.[22]. No direct total ionization cross section measurements have been performed so far for these radicals.

The cross sections for the CH_2^+ and $CH^+ + H$ channels are given in Figs. 21 and 22, respectively. The solid curves represent least-square fits of the data of Ref.[14],

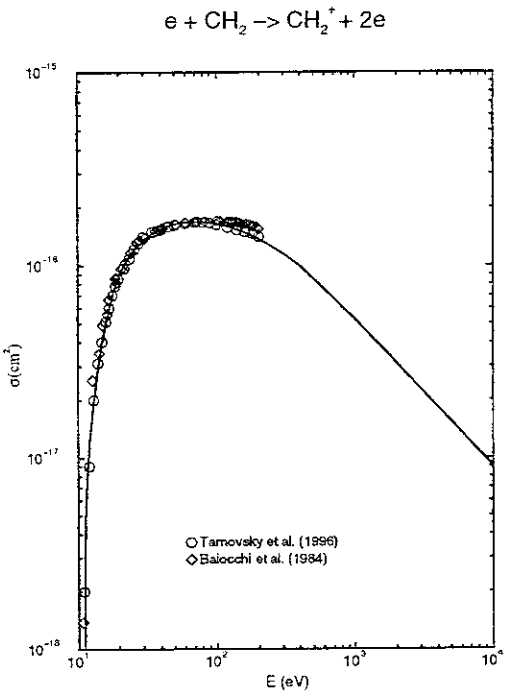

Figure 21: Partial cross section for parent (non-dissociative) ionization of CH_2. Symbols: experimental data. Solid curve: least-square fit of the data, extended to high energies by using scaling relationships (see text).

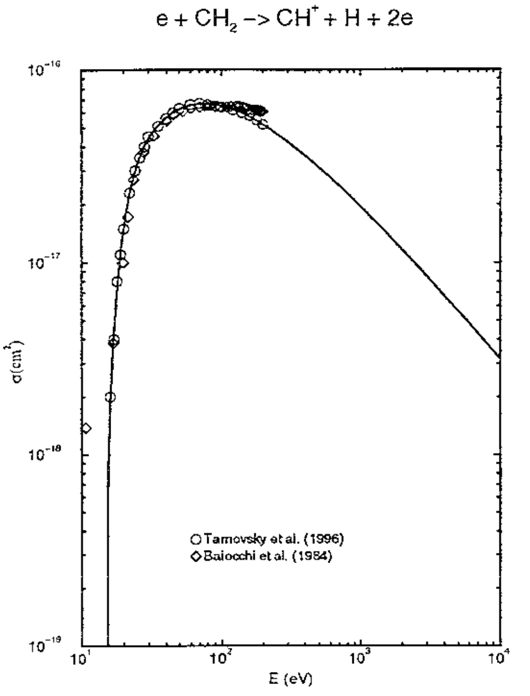

Figure 22: Same as in Fig.21, but for the CH^+ + H dissociative channel.

extended in the energy region above 200 eV by a procedure similar to that described in Section 3.2 for the analogous channel cross sections for CH_3. The cross section for the channel $C^+ + H_2$ was determined from the ratio $\sigma(CH^+_{y-2})/\sigma(CH_2)$, shown in Fig. 6 for the energy E=80 eV, and the similar linear dependences of this ratio for other energies. The partial cross section for this channel is given in Fig. 23.

The sum of partial cross sections for the first three channels in Table 10 accounts for 93.2% of the total ionization cross section for CH_2. The remaining 6.8% of $\sigma_{tot}(CH_2)$ are distributed between the $H^+ + CH$ and $H_2^+ + C$ channels with slight preference for the $H^+ +$ CH channel due to its smaller threshold energy. These two channels can be neglected in the collision kinetics, but if one decides to include them, a plausible way to express the slight dominance of $H^+ + CH$ over the $H_2^+ + C$ channel is to assign them the following cross sections

$$\sigma(H^+) = 0.038\sigma_{tot}(CH_2), \quad (5a)$$

$$\sigma(H_2^+) = 0.03\sigma_{tot}(CH_2), \quad (5b)$$

in the energy region above $\sim$ 50 eV. For $E \lesssim 50$ eV, an adjustment should be made to account for the different thresholds of H^+ and H_2^+ channels from that for CH_2. The total ionization cross section for CH_2 molecule, ob-

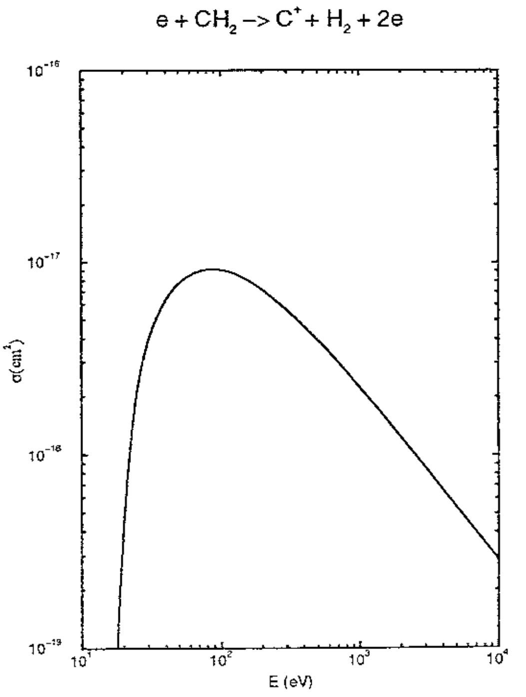

Figure 23: Partial cross section for $C^+ + H_2$ dissociative channel of CH_2 derived from scaling relationships (see text).

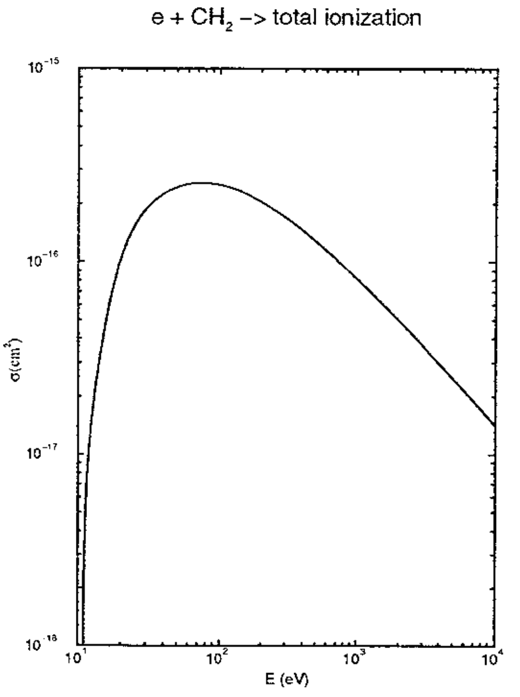

Figure 24: Total electron-impact ionization cross section for CH_2.

tained by summing the partial cross sections $\sigma(CH_2^+)$, $\sigma(CH^+)$ and $\sigma(C^+)$, and including the contributions from $\sigma(H^+)$ and $\sigma(H_2^+)$ via the relations (5), is given in Fig. 24.

For the e + CH collision system there are only three ionization channels possible (see Table 10), and the cross section for the CH^+ and C^+ + H channels are available up to the energy of 200 eV [14]. The energy threshold for the third, $H^+ + C$, channel is much higher than for the first two, and its cross section should be, correspondingly, much smaller than for the first two. In Ref.[14], the H^+ ion signal was not recorded, and the authors claimed that the maximum value of this cross section (in the region 80 ± 10 eV) was smaller than 0.1×10^{-16}cm^2. The value of $\sigma(H^+)$ cross section is obviously equal to the difference of the total cross section and the sum of measured $\sigma(CH^+)$ and $\sigma(C^+)$ cross sections at a given energy. For determining $\sigma(H^+)$ we can use the linearity of total cross sections for $\sigma(C_3H_6)$ (propene) and $\sigma(C_2H_4)$ for a given energy (see Figs. 3-6), the value of $\sigma(H^+)$ being given by the intersection of the line connecting $\sigma(C_3H_6)$ and $\sigma(C_2H_4)$ with the vertical line which defines the position of CH on the C_xH_y axis of $\sigma_{tot}(C_xH_y) - C_xH_y$ plane (see Figs. 3-6). The total ionization cross section σ_{tot}(CH), found by this procedure for E=50, 80, and 200 eV, equals 1.98×10^{-16}cm^2, 2.06×10^{-16}cm^2 and 1.58×10^{-16}cm^2, respectively. Since the total ionization cross sections for C_2H_4 and C_3H_6 are known up to 12 keV [18, 20], the cross section σ_{tot}(CH) can be determined by this procedure up to that energy as well. For instance, using the data of Ref.[18] for E = 1000 eV, one can derive by this procedure (within the experimental uncertainty of the data) the value of 0.55×10^{-16}cm^2 for σ_{tot}(CH). The cross section $\sigma_{tot}(H^+)$, obtained as difference between σ_{tot}(CH) and the sum of $\sigma(CH^+)$ and $\sigma(C^+)$ from Ref.[14], for E = 50, 80 and 200 eV has the values 4.0×10^{-18}cm^2, 4.2×10^{-18}cm^2 and 3.2×10^{-18}cm^2, respectively, which constitutes 2% of the total cross section. For these three energies the ratios $\sigma(CH^+)/\sigma_{tot}(CH)$ and $\sigma(C^+)/\sigma_{tot}(CH)$ are almost constant, with values of 0.76 and 0.22, respectively. According to the discussions in Section 2.3, these ratios should not change appreciably for energies above 200 eV and can be used to derive the cross sections $\sigma(CH^+)$ and $\sigma(C^+)$ in the high-energy region on the basis of known σ_{tot}(CH). The cross sections $\sigma(CH^+)$ and $\sigma(C^+)$ are shown in Figs. 25 and 26, respectively, where their values above 200 eV were determined in the above described way. We should note that the total contribution of $\sigma(CH^+)$ and $\sigma(C^+)$ to σ_{tot}(CH) remains the same (98%) for all energies above 50 eV, and approximately the same for E < 50 eV, so that the cross section $\sigma(H^+)$ can be written

$$\sigma(H^+) = 0.02\sigma_{tot}(CH), \tag{6}$$

with an appropriate adjustment in the threshold region due to the difference of threshold energies for $\sigma(H^+)$ and σ_{tot}(CH). The total cross section σ_{tot}(CH) is shown in Fig. 27.

4 Cross Sections for $e + C_2H_y$ Collision Systems

4.1 Total and Partial Cross Sections for C_2H_6

4.1.1 Total Cross Section

Direct absolute measurements of total electron-impact ionization cross section for C_2H_6 were performed in Refs.[18-20] which together span the energy region up to 12 keV. The data of Refs.[18] and [19] are consistent with each other (when shown on a Platzman plot), while the data of Ref.[20] tend to be somewhat higher than those of Refs.[18, 19]. The partial cross sections for a large number of channels from e+ C_2H_6 ionization were measured in Refs.[12, 25]. With proper normalization (e.g. the sum of partial cross sections in Ref.[25] was normalized on the value of $\sigma_{tot}(C_2H_6)$ at E = 100 eV of Ref.[19]) the sum of these cross sections should also give a total cross sections with an accuracy commensurate with the accuracy of dominant partial cross sections. In Ref.[25] the claimed accuracy of dominant partial cross sections is ±15%, while in Ref.[12] it is 20%. The total cross sections from Refs.[18], [19], [12],

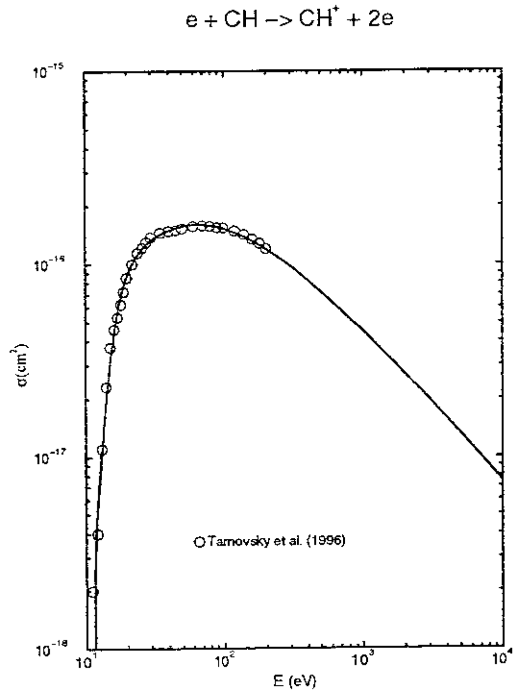

Figure 25: Partial cross section for parent (non-dissociative) ionization of CH. Symbols: experimental data. Solid curve: least-square fit of the data, extended to high energies by using scaling relationships (see text).

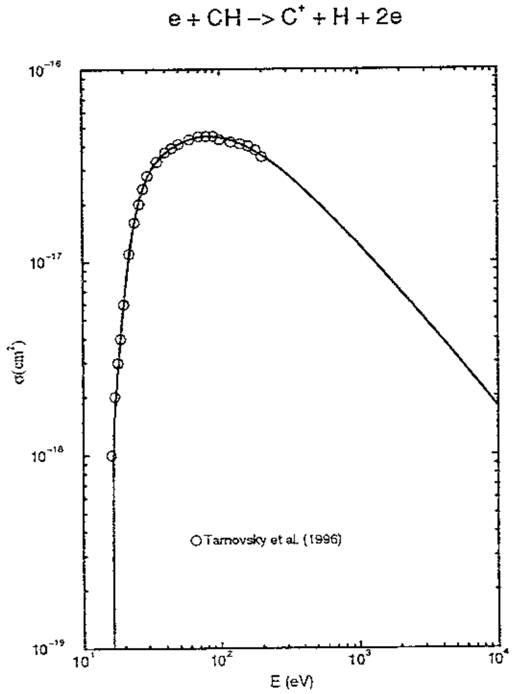

Figure 26: Same as in Fig.25, but for the C^+ + H dissociative channel.

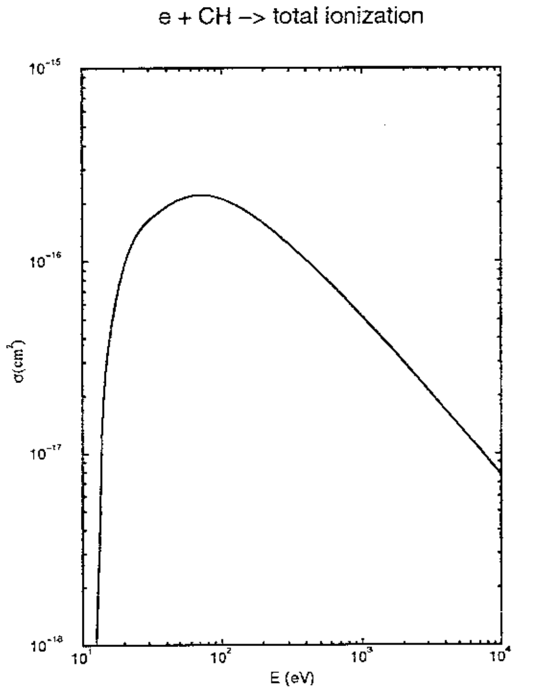

Figure 27: Total electron-impact ionization cross section for CH.

and [25] are shown in Fig. 28. The solid line in this figure is a fit of the data.

4.1.2 Partial Cross Sections

The main ion-production channels with their dominant neutral fragmentation modes for the e + C_2H_6 collision system are shown in Table 11. The threshold energies for these channels are also given in the table. The values for E_{th} of Ref.[46] are considered as the most accurate. The thermochemical dissociation limits for the listed channels are also given in the table [43]. In the experiments on e + C_2H_6 ionization, all channels in Table 11 were observed, and their cross sections measured [25, 26], except for the $CH_4^+ + CH_2$, $H^+ + C_2H_5$ and $H_2^+ + C_2H_4$ channels. (In Ref.[12] the doubly charged ion-production channels were not observed.) Note that some of the ionization channels produce hydrogen atoms in highly excited states [43].

In Figs. 29-37 are shown the experimental data from Refs.[12] and [25] for the channels with peak cross sections above 1.0×10^{-17}cm^2. As discussed earlier (Section 2.3), the dominant contribution to the total cross section give the channels $C_2H_4^+ + H_2$ and $C_2H_3^+ + H_2 + H$ (about 60% of $\sigma_{tot}(C_2H_6)$, see Table 6), while the contribution of the parent ionization channel $C_2H_6^+$ accounts for only about 10% of $\sigma_{tot}(C_2H_6)$, as is the contribution of the $C_2H_2^+$ channel (see Table 6). The data of Refs.[12] and [25] agree well for the dominant channels, but disagree for the weak channels (see Figs. 29-

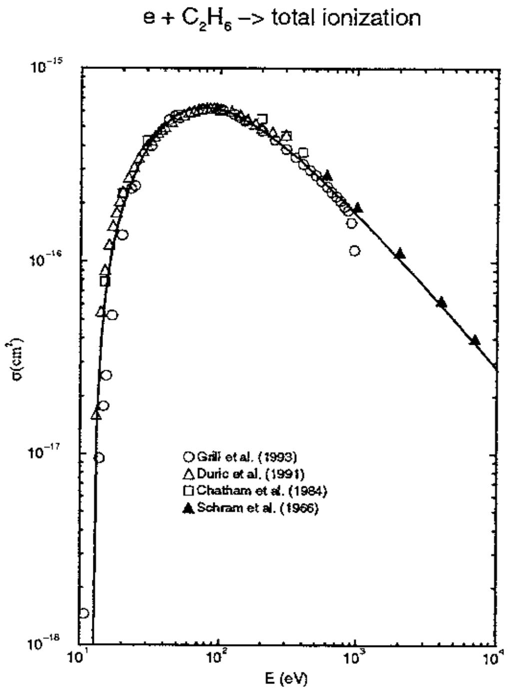

Figure 28: Fig.28. Total electron-impact ionization cross section for C_2H_6. Symbols: experimental data. Solid curve: least-square fit of the data (see text).

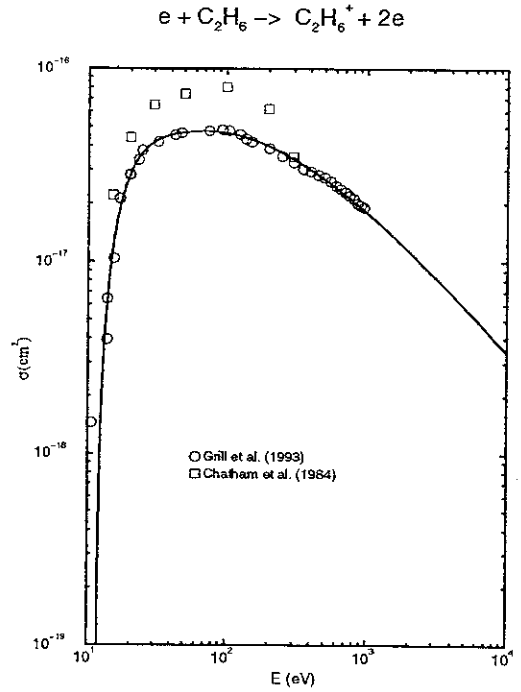

Figure 29: Partial cross section for parent (non-dissociative) ionization of C_2H_6. Symbols: experimental data. Solid curve: least-square fit of the data of Grill *et al.* [25], extended to higher energies by using scaling relationships (see text).

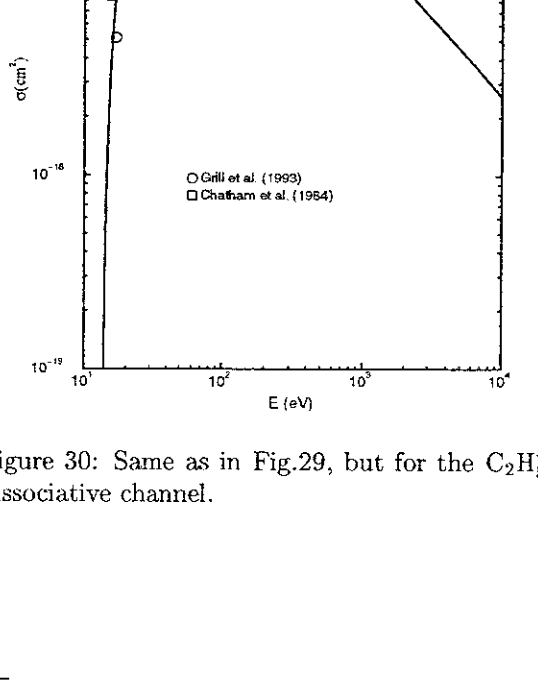

Figure 30: Same as in Fig.29, but for the $C_2H_5^+ + H$ dissociative channel.

37). The accuracy of more recent data of Ref.[25] is higher than the accuracy of Ref.[12], and the solid curves on Figs. 29-37 were obtained by fitting only the data of Ref.[25]. The extension of these fits into the energy region above 900 eV was done by using the ratios of these cross sections and $\sigma_{tot}(C_2H_6)$ at $E = 900$ eV from Table 6, which should stay approximately the same at high energies (see Section 2.3). The cross sections of the weak channels C_2H^+, CH_2^+ and CH^+ show a Bethe-Born type energy behaviour already at energies of 300-400 eV and their extension in the energy region above 900 eV was straightforward.

The large number of available dissociation channels in the complex C_2H_6 molecule has a consequence that the main portion of the total cross section (say 95%) is distributed among a larger number of channels than, for instance, for the case of e+CH_4 collision system. At the energy of 100 eV, one needs to include all the (nine) channels whose cross sections are shown in Figs. 29-37 in order to obtain 95% of $\sigma_{tot}(C_2H_6)$ at that energy.

We note that the weak CH^+ ion-production channel contains two neutral fragmentation channels with equal (or almost equal) thresholds (see Table 11). The partition of CH^+ ion-production cross section between these two channels can be taken by assigning equal contribution to each of them to $\sigma(CH^+)$.

We also note that the $C_2H_4^+$ ion-production channel apart from the neutral fragmentation channel $C_2H_4^+$ +

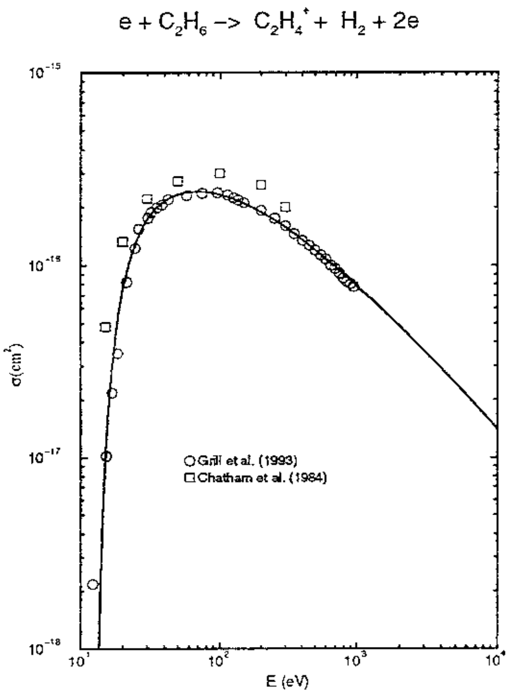

Figure 31: Same as in Fig.29, but for the $C_2H_4^+ + H_2$ dissociative channel (see text).

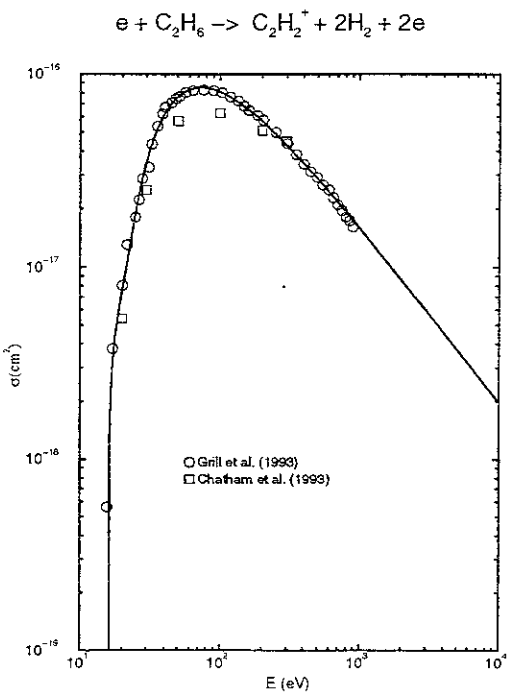

Figure 33: Same as in Fig.29, but for the $C_2H_2^+ + 2H_2$ dissociative channel.

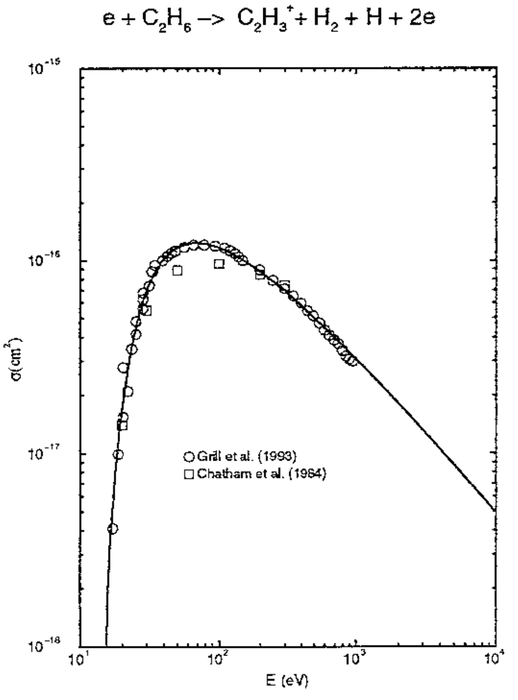

Figure 32: Same as in Fig.29, but for the $C_2H_3^+ + H_2 + H$ dissociative channel.

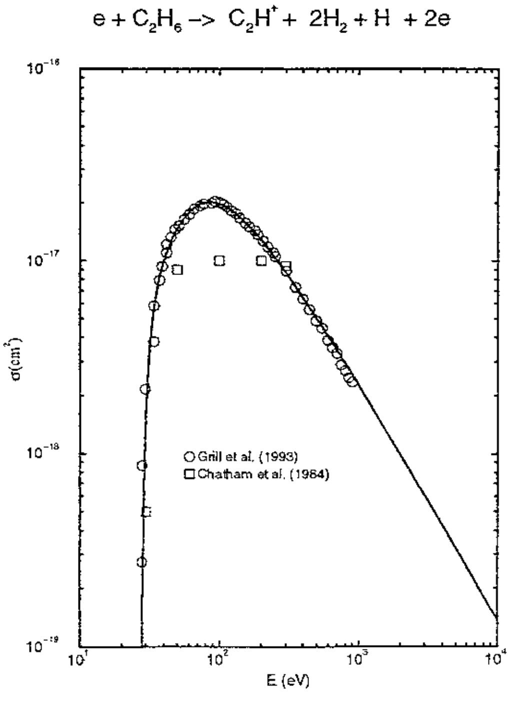

Figure 34: Same as in Fig.29, but for the $C_2H^+ + 2H_2 + H$ dissociative channel.

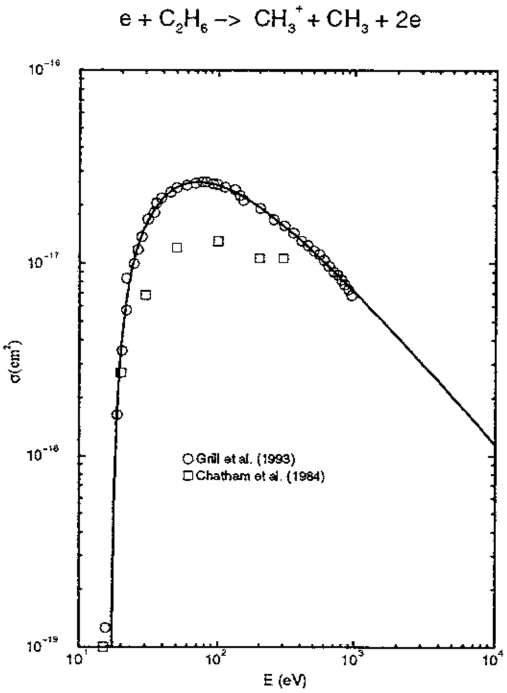

Figure 35: Same as in Fig.29, but for the CH_3^+ + CH_3 dissociative channel.

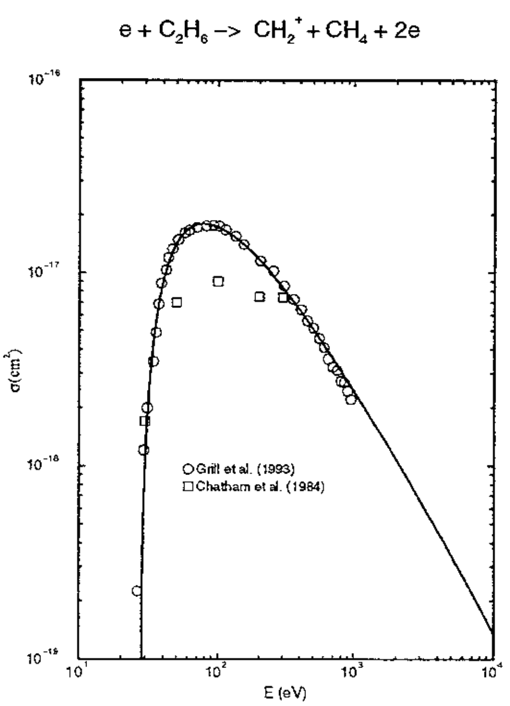

Figure 36: Same as in Fig.29, but for the CH_2^+ + CH_4 dissociative channel.

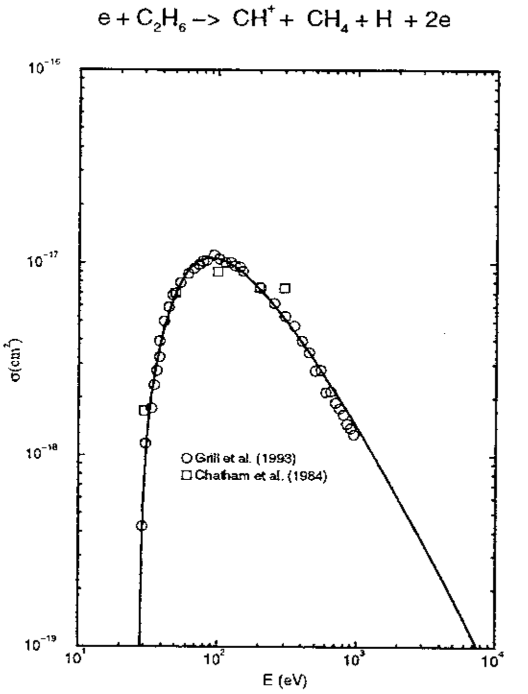

Figure 37: Same as in Fig.29, but for the $CH^+ + CH_4 +$ H dissociative channel.

H_2 may contain also the channel CH_4^+ + 2H. The thermochemical appearance potential for this channel is 16.45 eV and is not shown in Table 11. The cross section shown in Fig. 31 is in fact the $C_2H_4^+$ ion-production cross section and includes also the contribution from the 2H fragmentation channel. Analysis of the dependence of the partial cross sections on the threshold energy indicates that the contribution of 2H fragmentation channel to $\sigma(C_2H_4^+)$ may not exceed 15%.

4.2 Total and Partial Cross Sections for C_2H_5

There have been no experimental measurements or theoretical calculations of the total and partial cross sections for the C_2H_5 radical (see Table 1). These cross sections can nevertheless be derived using the scaling relationships discussed in Sections 2.2 and 2.3. Using Figs. 3-5 for the scaling of total cross sections of C_xH_y molecules for the energies 50, 80, and 200 eV (for C_2H_y also for E = 40 and 1000 eV, see Figs. 4 and 5), and using additional similar diagrams for energies below 40 eV and above 200 eV, one can find the values of $\sigma_{tot}(C_2H_5)$ up to 12 keV (the upper most energy in Ref.[18] for the total cross sections of C_2H_4 and C_2H_6 which are needed for the linear interpolation of the value of $\sigma_{tot}(C_2H_5)$). The cross section $\sigma_{tot}(C_2H_5)$ obtained by this procedure (keeping also in mind the value 8.25 eV of the ionization threshold) is shown in

Fig. 38. We note that the value of Bethe-Born cross section, Eq.(2), calculated with $M_i^2(C_2H_5) = 7.85$ from Table 2, and the average C_i value for all the hydrocarbons of 0.089, differs at $E = 1000$ eV by $\sim$ 6% from the one obtained by the scaling procedure.

The ion-production channels with the dominant neutral fragments for the e + C_2H_5 collision system are shown in Table 12, together with the ionization potential for the parent ionization channel and the appearance potentials for the dissociative channels. The latter were calculated from the thermochemical tables [44, 45]. The $C_2H_3^+$ + 2H channel has a thermochemical threshold of 15.65 eV (compared to the threshold 11.20 eV for the $C_2H_3^+ + H_2$ channel) and is not included in the table. (Its contribution to the $\sigma(C_2H_3^+)$ ion-production cross section will be discussed at the end of this subsection).

The cross sections of ion-production channels were obtained on the basis of $\sigma_{tot}(C_2H_5)$ and the ratios $\sigma(C_2H_{5-k})/\sigma_{tot}(C_2H_5)$, $k = 0, 1, 2, 3, 4$, shown in Fig. 7 for the energy $E = 80$ eV. In accordance with the conclusions of Section 2.3, we have taken that these ratios remain valid for all energies above $\sim$ 40 eV. For $E \lesssim 40$ eV, these ratios may somewhat overestimate the cross section. However, for the channels with high energy thresholds (~15-20 eV) this energy range is relatively small, and even a direct extrapolation of the cross section towards the threshold may not result in large errors. The parent ionization cross section $\sigma(C_2H_5^+)$ obtained by this procedure is shown in Fig. 38, while the cross sections for the $C_2H_4^+$, $C_2H_3^+$, $C_2H_2^+$ and C_2H^+ ion-production channels are shown in Fig. 39. We note that the sum of the above five partial cross sections accounts for 93% of the total cross section. The remaining 7% of $\sigma_{tot}(C_2H_5)$ is distributed among the other channels listed in Table 12. The fractional contributions of the remaining CH_3^+, CH_2^+, CH^+, C^+ and C_2^+ ion-production channels were determined by interpolation of the known values of the contributions of these channels in the e+C_2H_6 (from Ref.[25]) and e+C_2H_4 (from Ref.[26]) systems at the energy $E = 75$ eV. The resulting cross sections of these ion-production channels in the e + C_2H_5 system are (for $E \gtrsim 40$ eV)

$$\sigma(CH_3^+) = 0.028\sigma_{tot}(C_2H_5), \quad (7a)$$
$$\sigma(CH_2^+) = 0.021\sigma_{tot}(C_2H_5), \quad (7b)$$
$$\sigma(CH^+) = 0.012\sigma_{tot}(C_2H_5), \quad (7c)$$
$$\sigma(C^+) = 0.006\sigma_{tot}(C_2H_5), \quad (7d)$$
$$\sigma(C_2^+) = 0.003\sigma_{tot}(C_2H_5). \quad (7e)$$

For $E < 40$ eV, the values of these cross sections can be determined by direct extrapolation towards their (relatively large) thresholds. The small $\sigma(C^+)$ cross section is equally shared between the CH_4 + H and $CH_3 + H_2$ neutral fragmentation channels (which have almost identical thresholds).

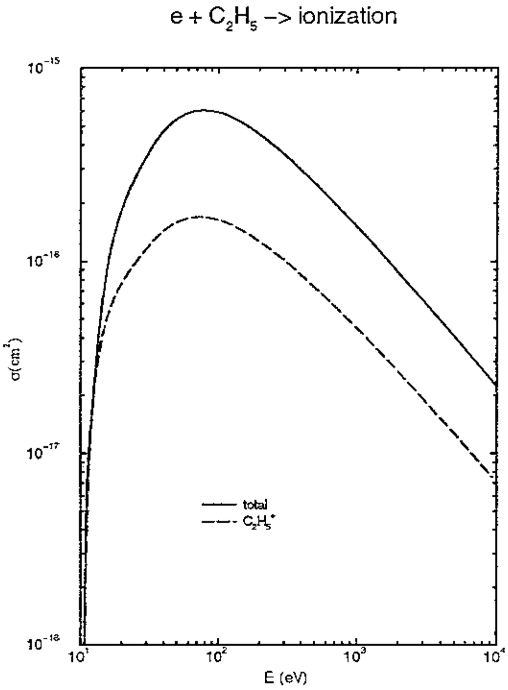

Figure 38: Total and parent (non-dissociative) ionization cross sections for C_2H_5 (see text).

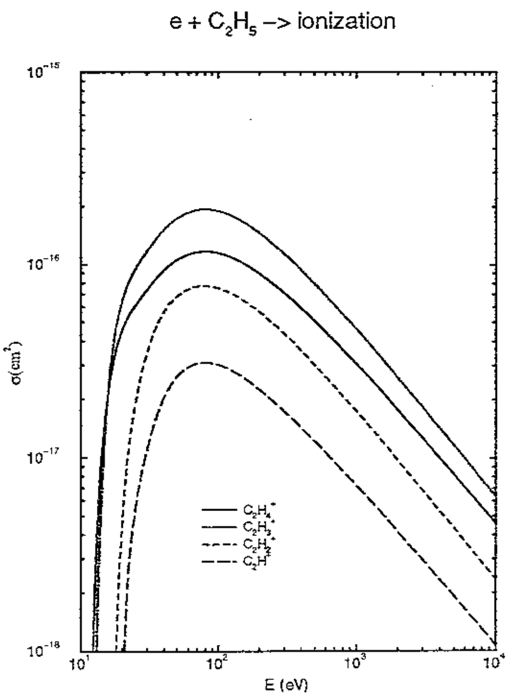

Figure 39: Partial cross sections for $C_2H_{5-k}^+$, $k = 1, 2, 3, 4$, ion-production channels of C_2H_5 (see text).

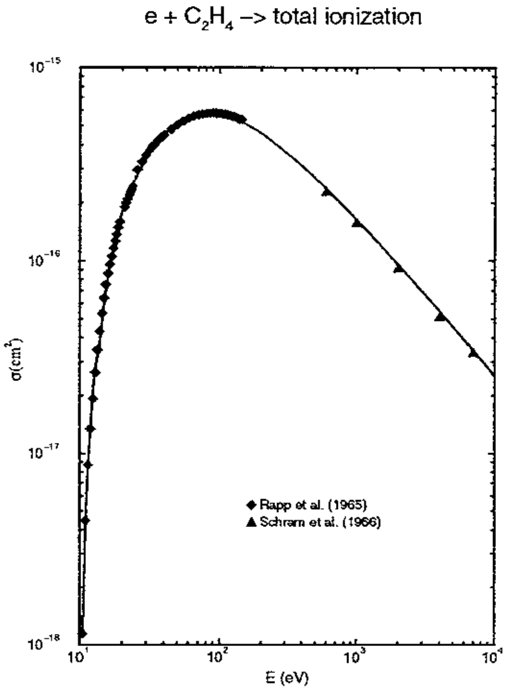

Figure 40: Total electron-impact ionization cross section for C_2H_4. Symbols: experimental data. Solid curve: least-square fit of the data.

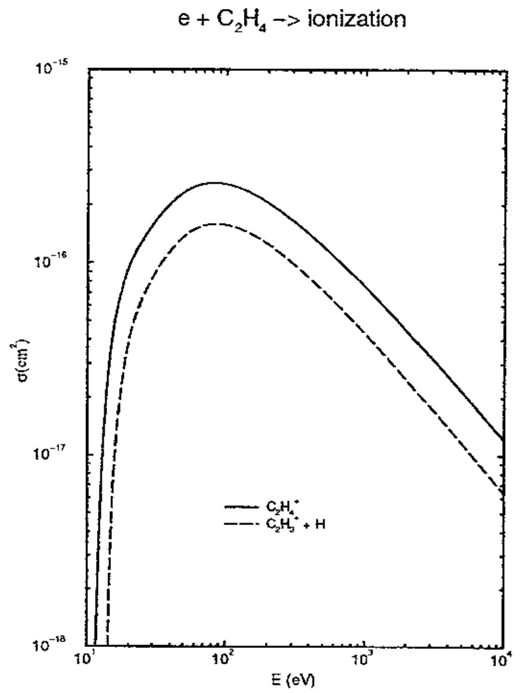

Figure 41: Partial cross sections for the parent, $C_2H_4^+$, and dissociative $C_2H_3^+ + H$ ionization channels of C_2H_4 molecule (see text).

As we have mentioned at the beginning of this subsection, the ion-production cross section $\sigma(C_2H_3^+)$ contains some contribution also from the $C_2H_3^+ + 2H$ neutral fragmentation channel. An analysis of the correlation of threshold energy and the maximum cross section value indicates that the contribution of $C_2H_3^+ + 2H$ channel to $\sigma(C_2H_3^+)$ may not exceed 20%.

4.3 Total and Partial Cross Sections for C_2H_4

The total ionization cross section in $e + C_2H_4$ collision has been measured in Refs.[17, 18, 20] in the combined energy range from threshold to 12 keV. The data of Ref.[17], (available up to 145 eV), are considered to be accurate within 10% and better, while those of Ref.[18] (available in the rage 0.6 - 12 keV) have a similar accuracy. The data of Ref.[20] seem to have, generally speaking, higher uncertainties than those in Refs.[17, 18], but in the range 200-600 eV they give a relatively smooth connection of the data of Refs[17, 18]. The total ionization cross section for C_2H_4 can, thus, be considered as well established in the energy range up to 12 keV. The experimental cross section data are given in Fig. 40. The solid curve through the data represents their least-square fit.

Partial cross section measurements for this collision system have not been performed as yet, except for the relative measurements of the fractions of ten different ions resulting from the ionization process in the total number of ions for two electron-impact energies, 75 eV and 3.5 MeV [26]. Using the fact that these fractions do not change appreciably with the energy (as shown in Ref.[26]), one can derive the partial cross sections for ion-production channels on the basis of known total cross section.

The ionization channels for $e + C_2H_4$ system are shown in Table 13 together with the ionization potential for C_2H_4 and the appearance potentials for the dissociative channels (calculated from the thermochemical tables [44, 45]).

The partial cross sections for the ion-production channels $C_2H_{4-k}^+$, $k = 0, 1, 2, 3, 4$ were derived from the values of $\sigma_{tot}(C_2H_4)$ and the ratios $\sigma(C_2H_{4-k}^+)/\sigma_{tot}(C_2H_4)$. For the energy $E = 80$ eV, these ratios are shown in Fig. 7, and we assume that their values remain the same in the entire energy region above 40 eV. Below 40 eV, these ratios may vary with the energy, but the cross sections here can easily be extrapolated towards their zero-value at the reaction threshold. The cross sections for the channels $C_2H_4^+$ and $C_2H_3^+ + H$ are shown in Fig. 41, while for the channels $C_2H_2^+ + H_2/2H$, $C_2H^+ + H_2 + H$ and $C_2^+ + 2H_2$ they are shown in Fig. 42. The cross section $\sigma(C_2H_2^+)$ contains the contributions from the H_2 and 2H neutral fragmentation channels in the proportion 81% (for H_2) and 19% (for 2H). The considered five ionization

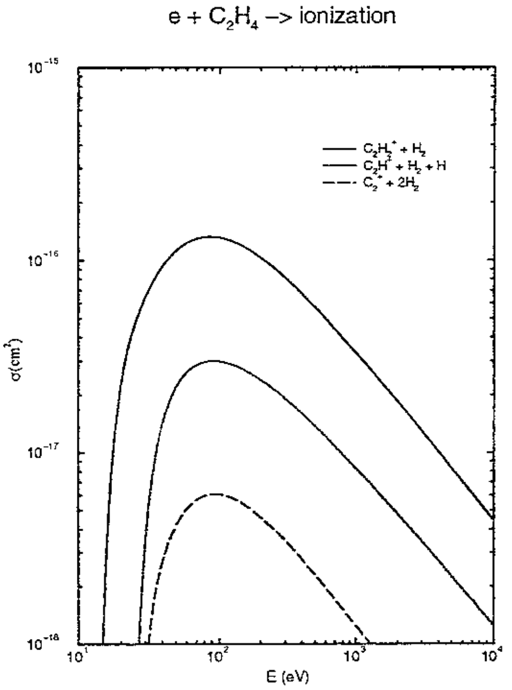

Figure 42: Partial cross sections for the $C_2H_2^+ + H_2$, $C_2H^+ + H_2 + H$ and $C_2^+ + 2H_2$ dissociative channels of C_2H_4 (see text).

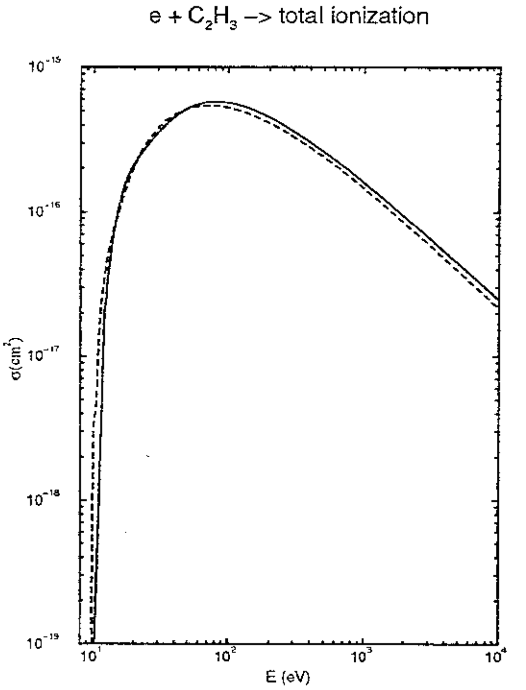

Figure 43: Total electron-impact ionization cross section for C_2H_3 (see text). Dashed line: BEB cross section.

channels account for 96% of the total ionization cross section $\sigma(C_2H_4)$. The remaining 4% of $\sigma_{tot}(C_2H_4)$ are distributed among the last four channels in Table 13. Taking the fractional contributions for these channels from Ref.[26] for $E = 75$ eV, and assuming their validity in the energy region (well) above the corresponding thresholds, the partial cross sections for these channels can be written as

$$\sigma(CH_3^+) = 0.0172\sigma_{tot}(C_2H_4), \tag{8a}$$

$$\sigma(CH_2^+) = 0.0163\sigma_{tot}(C_2H_4), \tag{8b}$$

$$\sigma(CH^+) = 0.0074\sigma_{tot}(C_2H_4), \tag{8c}$$

$$\sigma(C^+) = 0.0040\sigma_{tot}(C_2H_4). \tag{8d}$$

These fractional contributions are consistent with the linear extrapolation of the corresponding values for the C_2H_6 molecules [13] to the C_2H_4 case. The small cross section $\sigma(C^+)$ is shared approximately equally between the two neutral fragmentation channels, $CH_3 + H$ and $CH_2 + H_2$ (see the close values of the appearance potentials for these two channels in Table 13.) The cross sections (8) have to be adjusted in the energy region below ~30-40 eV to account for the vicinity of the threshold.

4.4 Total and Partial Cross Sections for C_2H_3

There are no experimental investigation on the electron-impact ionization of C_2H_3 radical reported so far. There exist only BEB-model calculations of the total ionization cross section for this molecule performed recently [27]. Since for the cases of C_2H_2 and C_2H_4 the BEB model underestimates the total ionization cross section for 22% and 15%, respectively, in the energy region around the cross section maximum, E =70-90 eV, (compare for C_2H_2 the BEB data from Ref.[24] and the most recent experimental data of Ref.[16], and for C_2H_4 the BEB result of Ref.[21] and the experimental data of Ref.[17]), we decided to derive the total cross section for C_2H_3 from the scaling properties of total cross sections for C_xH_y molecules (see Section 2.2). Using the data points for $\sigma_{tot}(C_2H_3)$ from Figs. 3-5 for the energies $E = 40$, 50, 80, 200 and 1000 eV, and deriving such data from similar diagrams for other energies (up to 2000 eV, the highest energy for which $\sigma_{tot}(C_2H_2)$ data are available [28]). The $\sigma_{tot}(C_2H_3)$ cross section obtained by this procedure is shown in Fig. 43. The BEB cross section [27] is also shown in this figure for comparison. The two cross sections agree to within 2-8% in the entire energy region. It should be noted that the Born-Bethe cross section, Eq.(2), with $M_i^2 = 5.71$ from Table 2, gives values for $\sigma_{tot}(C_2H_3)$ which differ by not more than 15% from BEB results for $E \geq 500$ eV.

The ion-production channels in the e+C_2H_3 collision system, with indication of dominant neutral fragmentation(s), are given in Table 14. Also given in this table is the ionization potential of C_2H_3 and the ap-

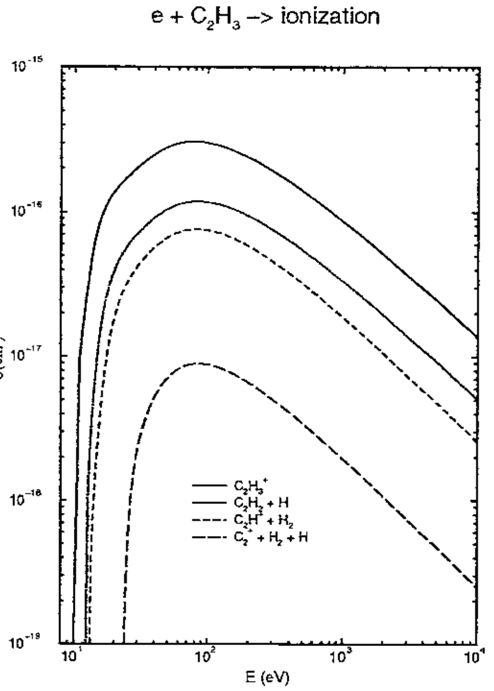

Figure 44: Partial cross sections for the parent and dissociative ion-production channels $C_2H_{3-k}^+$, $k = 0, 1, 2, 3$ of C_2H_3 (see text).

pearance potentials of the dissociative ionization channels (calculated from the thermochemical tables [44, 45]). The cross sections for the ion-production channels $C_2H_3^+$, $C_2H_2^+$, C_2H^+ and C_2^+ were derived from $\sigma_{tot}(C_2H_3)$ and the ratios $\sigma(C_2H_{3-k}^+)/\sigma_{tot}(C_2H_3)$, $k = 0, 1, 2, 3$ shown for $E = 80$ eV in Fig. 7, and assuming that these ratios remain the same at energies above ~ 40 eV. For $E < 40$ eV, the cross sections were extrapolated towards the corresponding channel thresholds.

The ion-production cross sections $\sigma(C_2H_{3-k}^+)$, $k = 0, 1, 2, 3$, are shown in Fig. 44. The cross section $\sigma(C_2H^+)$ contains two neutral fragmentation channels, $C_2H^+ + H_2$ and $C_2H^+ + 2H$, with significantly different thresholds (see Table 14). An analysis of the correlation of the channel cross sections and their thresholds gives that $C_2H^+ + H_2$ channel contributes to $\sigma(C_2H^+)$ with 90%, while the contribution of $C_2H^+ + 2H$ channel in $\sigma(C_2H^+)$ is 10%.

The above four ion-production channels contribute to the total ionization cross section $\sigma_{tot}(C_2H_3)$ by 90% (in the energy region when all channels are open). The contribution of the remaining four channels from Table 14 to $\sigma_{tot}(C_2H_3)$ can be determined by interpolation between the contributions of the corresponding ion-production channels to the total cross sections of C_2H_4 (data from Ref.[26]) and C_2H_2 (averaged data from Refs.[16] and [26]) at $E = 75$ eV. Assuming that these relative contributions remain the same at the energies above 40 eV, the corresponding partial cross sections in this energy region can be represented as

$$\sigma(CH_2^+) = 0.007\sigma_{tot}(C_2H_3), \tag{9a}$$

$$\sigma(CH^+) = 0.030\sigma_{tot}(C_2H_3), \tag{9b}$$

$$\sigma(C^+) = 0.022\sigma_{tot}(C_2H_3), \tag{9c}$$

$$\sigma(H^+) = 0.026\sigma_{tot}(C_2H_3). \tag{9d}$$

For energies below ~ 40 eV, the cross sections can be obtained by direct extrapolation towards the corresponding thresholds. The value $\sigma(CH_2^+)/\sigma_{tot}(C_2H_3)$ agress with the extrapolation of $\sigma(CH_2^+)/\sigma_{tot}(C_2H_6)$ from Ref.[13] to the C_2H_3 molecule case. It should be noted, however, that there are significant (20-30%) uncertainties in the (9b, c, d) ratios. The unaccounted for 1.5% of the total cross section can be attributed to doubly charged ion-production channels, not listed in Table 14.

4.5 Total and Partial Cross Sections for C_2H_2

As early as in 1932, Tate and Smith [30] measured the efficiency for production of ions resulting from the $e + C_2H_2$ collision in the energy range from ~ 15 eV to 500 eV. These data can be converted into total ionization cross section [29]. Other direct total cross sections for C_2H_2 have not been performed. Partial cross sections for six ionization channels in $e + C_2H_2$ collision have been measured in Ref.[16] (up to $E = 600$ eV), Ref.[29] (up to $E = 800$ eV) and for seven channels in Ref.[28] (up to $E = 2000$ eV). The relative ion fractions in the total number of ions resulting from the $e + C_2H_2$ collision were also measured in Ref.[26] for two energies (75 eV and 3.5 MeV). The most accurate of these measurements are those of Ref.[16] with an accuracy of 10% for the dominant channels and 15% for the weak channels. The claimed accuracy of the cross section measurements in Ref.[29] is $\pm 13\%$, while that in Ref.[28] seems to be higher (the claimed one is 15%).

The total cross sections from these references are shown in Fig. 45. The solid curve in this figure represent the fit of the data of Ref.[16], combined in the threshold region with those of Ref.[30]. For energies above 600 eV, the cross section (represented by the solid curve) was derived by using the scaling relationships from Section 2.2. The BEB cross section [24] lies below the data of Refs.[16] and [29], and for $E \geq 100$ eV goes through the data of Ref.[28].

The main ionization channels in the $e + C_2H_2$ collision are shown in Table 15. The C_2H_2 ionization potential and the appearance potentials for the dissociative ionization channels (from Ref.[46]) are also given in the table. The values of appearance potentials, calculated from thermochemical tables (Refs.[44, 45]) are also shown.

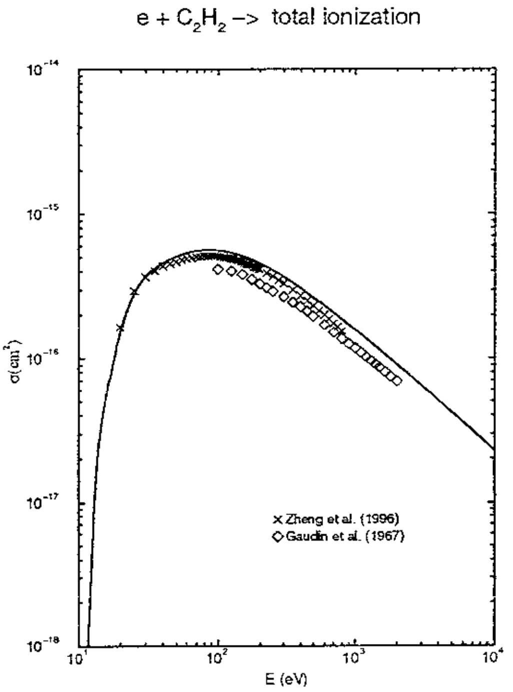

Figure 45: Total electron-impact ionization cross section for C_2H_2. Symbols: experimental data. Solid curve: least-square fit of selected sets of data (see text).

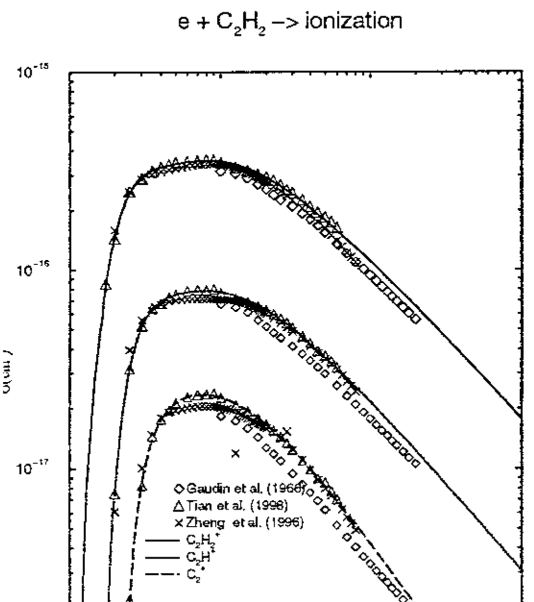

Figure 46: Partial cross sections for the parent and dissociative ion-production channels $C_2H_{2-k}^+$, $k = 0, 1, 2$ of C_2H_2. Symbols: experimental data. Solid curves: least-square-fits of selected sets of data (see text).

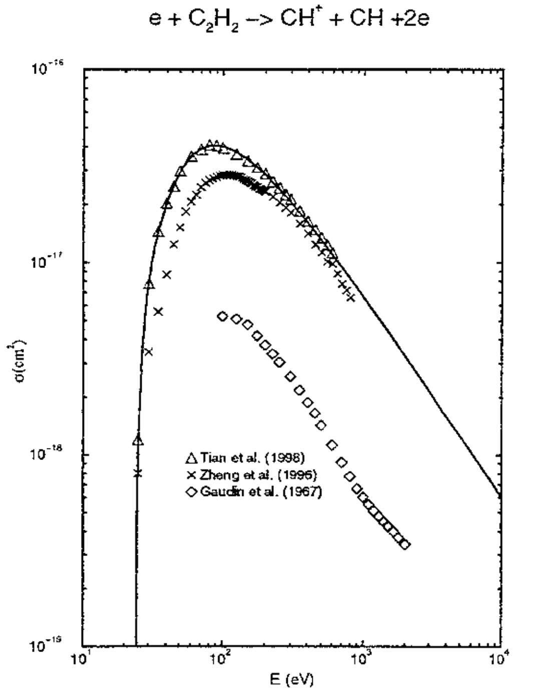

Figure 47: Same as in Fig.46, but for the CH^+ + CH dissociative channel.

The cross sections for $C_2H_2^+$, C_2H^+ and C_2^+ ion-production channels are shown in Fig. 46. The solid curves in this figure are fits of the data from Refs.[16] and [29], with preference given to the data of Ref.[16]. They are extended at higher energies by using the average ratio $\sigma(C_2H_{2-k}^+)/\sigma_{tot}(C_2H_2)$ of the data from Ref.[16] (for E =400-600 eV) and assuming that it remains the same in the high energy region. For the other three ion-production channels the cross sections are given in Figs. 47-49. The solid lines in these figures have the same meaning as in the previous figure, and in the high energy region have been determined in a similar way.

The partition of the C_2^+ ion-production cross section between the H_2 and 2H neutral fragmentation channels remains somewhat unclear despite the indication of experimental thresholds that the two-body neutral fragmentation channel could be favoured in this system. A similar remark can be made also for the CH / C + H and CH_2/CH + H neutral fragmentation channels associated with the CH^+ and C^+ ion-production channels.

4.6 Total and Partial Cross Sections for C_2H

There have been no total or partial ionization cross section measurements or calculations for the e + C_2H collision system. The total cross section for C_2H can be derived using the scaling relations discussed in Section

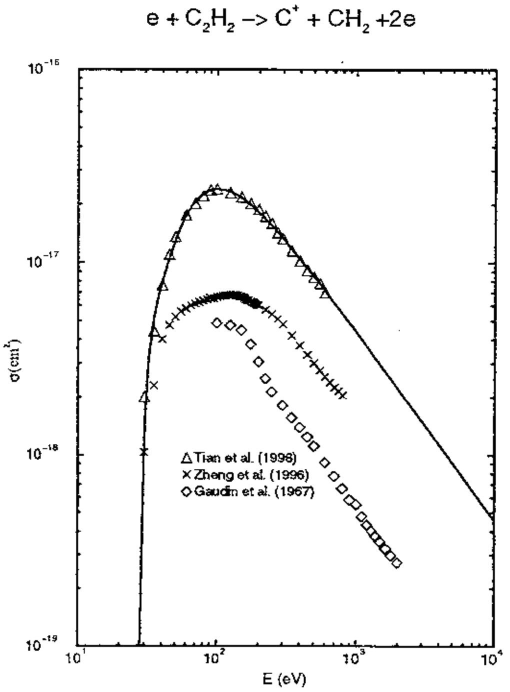

Figure 48: Same as in Fig.46, but for the $C^+ + CH_2$ dissociative channel.

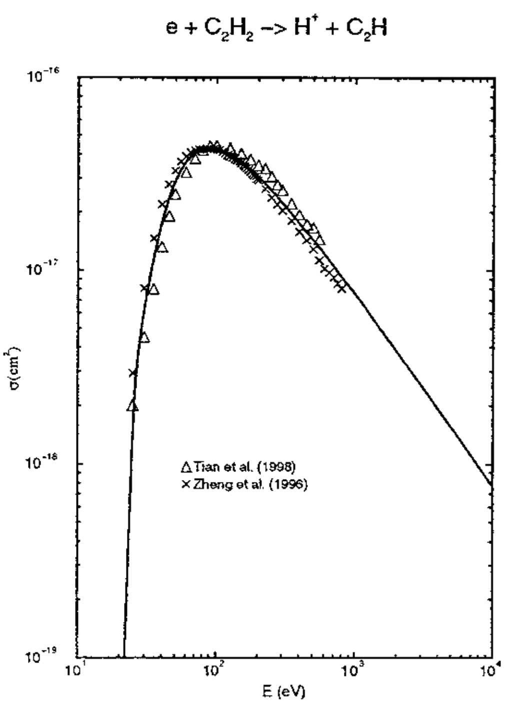

Figure 49: Same as in Fig.46, but for the $H^+ + C_2H$ dissociative channel.

2.2 (cf. Figs. 3-5). The partial cross sections for the C_2H^+ and C_2^+ ion production channels can be derived from the scaling relations discussed in Section 2.3 (cf. Fig. 7). These procedures were explained in detail in the previous sub-sections.

In Table 16 the ionization channels for the e + C_2H system are given, together with the ionization potential for C_2H and the appearance potentials for the dissociative channels [44, 45]. The total and parent ionization cross sections are shown in Fig. 50, while the C_2^+ ion-production cross section is shown in Fig. 51. The C_2H^+ and C_2^+ ionization cross sections contribute jointly about 91% to the total cross section. The remaining 9% are shared by the CH^+, C^+ and H^+ ionization channels. We have assumed that these ion fractions share the remaining 9% of the total cross section in the same proportion as they do that in the case of C_2H_2 at $E = 80$ eV. (In the C_2H_2 case, the contribution of CH^+, C^+ and H^+ fractions to the total cross section at $E = 80$ eV is 18.5% [16].) Assuming that the energy variation of this contribution is small (see Section 2.3), this procedure gives

$$\sigma(CH^+) \simeq 0.035\sigma_{tot}(C_2H), \quad (10a)$$

$$\sigma(C^+) \simeq 0.019\sigma_{tot}(C_2H), \quad (10b)$$

$$\sigma(H^+) \simeq 0.036\sigma_{tot}(C_2H). \quad (10c)$$

The values for the CH^+ and C^+ fractions are consistent with those obtained by extrapolating (linearly) the values of these fractions at $E = 75$ eV of Ref.[26] for the e + C_2H_2 and e + C_2H_4 collision systems. The cross sections for CH^+, C^+ and H^+ ion-production channels are shown in Fig. 52. In the region below ~ 40 eV, the cross sections (10) have been adjusted to account for the vicinity of the threshold.

5 Cross Sections for e + C_3H_y collision systems

5.1 Total and Partial Cross Sections for C_3H_8

5.1.1 Total Cross Section

There exist three sets of direct total ionization cross section measurements for the e + C_3H_8 collision system [18-20] which jointly cover the energy range from threshold to 12 keV. The cross sections of Refs.[18] (energy range 0.6-12 keV) and [19] (from threshold to 240 eV) are believed to be accurate to within 10%, while those of Ref.[20] (from threshold to 3000 eV) have larger uncertainties. Very extensive partial cross section measurements for this collision system were performed in Ref.[31] (including 23 ion-production channels) in the energy range up to 950 eV. The sum of these cross sections (normalized to the data of Ref.[19]

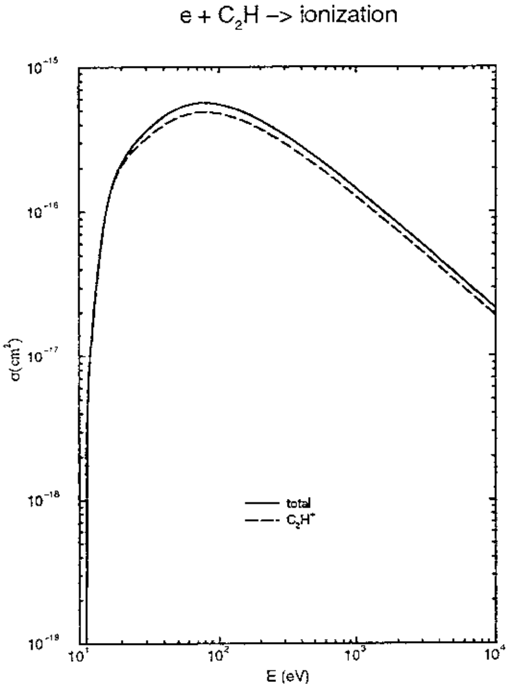

Figure 50: Total and parent ionization cross sections for C_2H (see text).

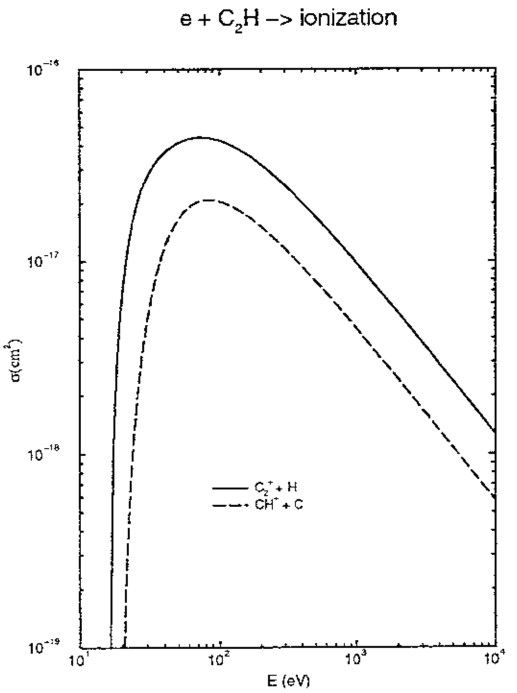

Figure 51: Partial cross sections for the C_2^+ + H and CH^+ + C dissociative channels of C_2H (see text).

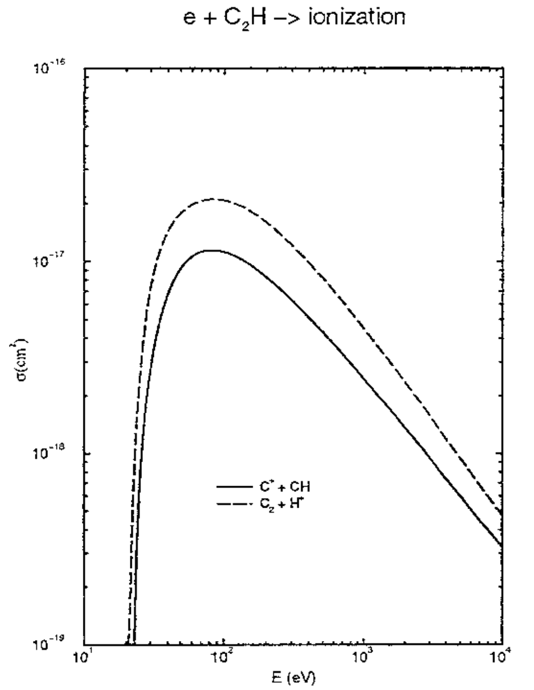

Figure 52: Partial cross sections for the C^+ + CH and H^+ + C_2 dissociative channels of C_2H (see text).

at $E = 100$ eV) should also give an accurate (to within 10%) total ionization cross section. The data from Refs.[18], [19], and [31] are shown in Fig. 53. The solid line in this figure represents a least-square fit of the data.

5.1.2 Partial Cross Sections

The number of observed ion-production channels in the e + C_3H_8 system is 23 [31], the most important of which are given in Table 4. In Table 17 we give also the dominant neutral fragmentations associated with these channels, as well as their appearance potentials [44, 45]. The ionization channels listed in Table 17 account for 95% of the total ionization cross section at 100 eV (see Table 4). As can be seen from Table 4, the dominant ion-production channels are $C_2H_5^+$, $C_2H_4^+$ and $C_2H_3^+$, which apart from the neutral fragmentations shown in Table 17 may have also other fragmentation channels. For instance, apart from the CH_3 neutral fragment, the $C_2H_5^+$ ion-production channel may contain contributions also from the CH_2 + H and CH + H_2 neutral fragmentations. The thermochemical appearance potentials for these two neutral fragmentation channels are 16.88 eV and 16.74 eV, respectively, much higher than the thermochemical appearance potential of 11.99 eV for the CH_3 neutral fragmentation channel. Their contribution to the total $C_2H_5^+$ ion-production cross section may be of the order of 10-15%. However, the amount of this contribution to $\sigma(C_2H_5^+)$

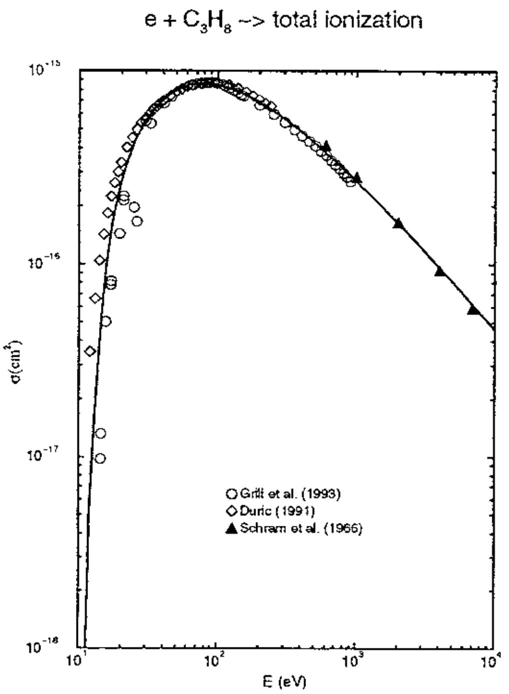

Figure 53: Total cross section for electron-impact ionization of C_3H_8. Symbols: experimental data. Solid curve: least-square fit of the data.

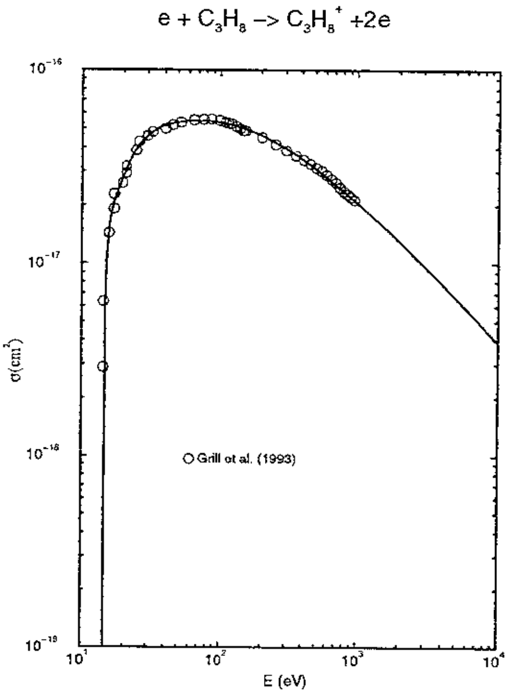

Figure 54: Partial cross section for parent (non-dissociative) ionization of C_3H_8. Symbols: experimental data, [31]. Solid curve: least-square-fit of the data, extended to higher energies by using scaling relationships (see text).

may still be, in its absolute value, comparable to the cross sections of minor ion-production channels which have similarly large appearance potentials (such as the $C_3H_2^+$, C_3H^+, C_2H^+ and CH^+ channels). In a more detailed analysis of the collisional kinetics, which takes also the minor channels into account, one has to make an appropriate partition of the cross sections of dominant ion-production channels among the dominant and sub-dominant neutral fragmentation channels. (This remark is, of course, also valid for the dominant ion-production cross sections of all C_xH_y molecules.)

We shall not, however, undertake to make this partition for the ion-production cross section in e + C_3H_8 system, since in absence of rigorous criteria, it will always contain certain level of arbitrariness and, consequently, produce large uncertainties in the derived neutral fragmentation cross sections. In case when there exist sufficiently clear basis for a plausible cross section partition among the possible neutral fragmentation channels we shall provide the corresponding suggestions (as we have been doing that in the previous sections). Such is the case, for example, with the C_2H^+ ion production cross section, which should be shared approximately equally by the $CH_3 + 2H_2$ and $CH_4 + H_2 + H$ neutral fragmentation channels because they both have almost equal appearance potentials (see Table 17).

The partial cross sections for the strongest ionization channels for the e+ C_3H_8 system are shown in Figs. 54-58 [31]. The solid lines in these figures are least-square fits of the data, continued at energies above 950 eV by maintaining the contribution of the corresponding partial cross section to the total ionization cross section of C_3H_8 at 900 eV constant.

5.2 Total Cross Sections for $C_3H_7 - C_3H$

The only total ionization cross section measurements for e + C_3H_y systems with $y \leq 7$ were performed for C_3H_6 in Refs.[18] (energy range: 0.6-12 keV) and [20] (from threshold to 3000 eV). The measurements were done both for the propene and cyclopropane isomers of C_3H_6. Total cross section calculations were performed within the Deutsch-Märk classical model for C_3H_6 and C_3H_8 [32] and C_3H_4 [33]. The measured total cross sections for C_3H_6 (propene) are shown in Fig. 59. In view of the relatively large uncertainties in the total cross sections measurements of Ref.[20], observed in the cases of CH_4, C_2H_6 and C_3H_8, we have constructed the cross section for C_3H_6 (propene) on the basis of scaling relationships discussed in Section 2.2. Figs. 3-5 immediately give the values for $E = 50$, 80, and 200 eV, and using similar diagrams one can determine the values for $\sigma_{tot}(C_3H_8)$ for other energies. For determining $\sigma_{tot}(C_3H_6)$ at a given arbitrary collision energy independently of the data from Ref.[20],

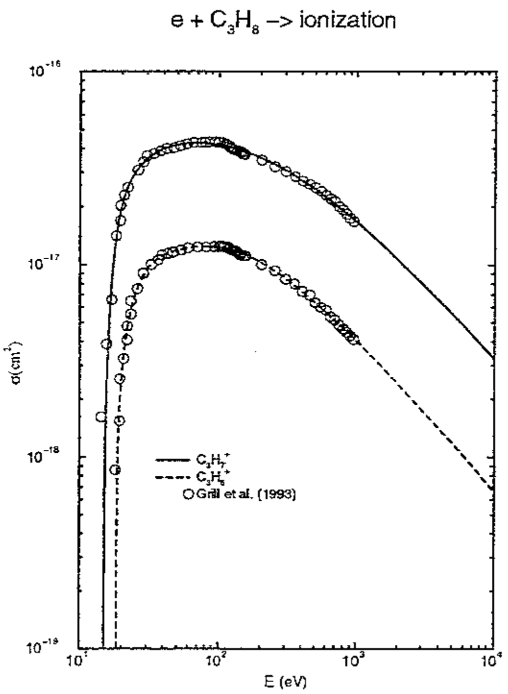

Figure 55: Same as in Fig.54, but for the $C_3H_7^+ + H$ and $C_3H_6^+ + H_2$ dissociative channels.

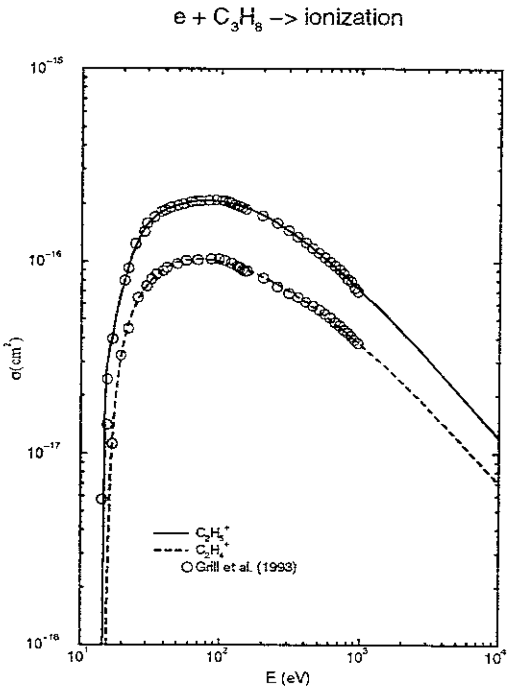

Figure 57: Same as in Fig.54, but for the $C_2H_5^+ + CH_3$ and $C_2H_4^+ + CH_4$ dissociative channels.

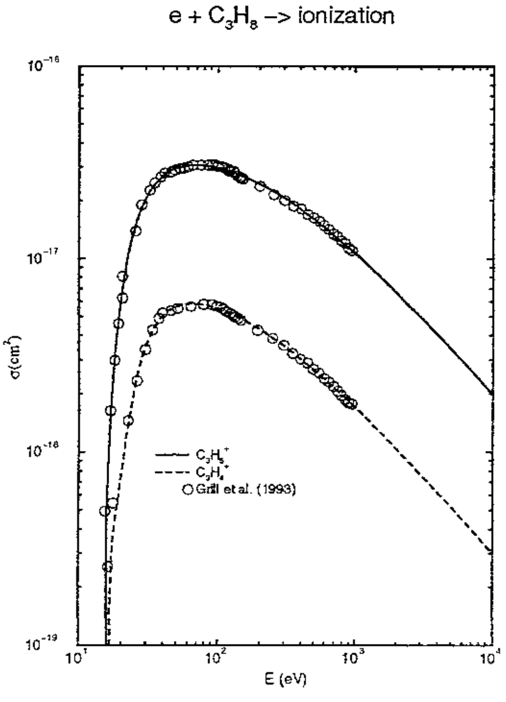

Figure 56: Same as in Fig.54, but for the $C_3H_5^+ + H_2 + H$ and $C_3H_4^+ + 2H_2$ dissociative channels.

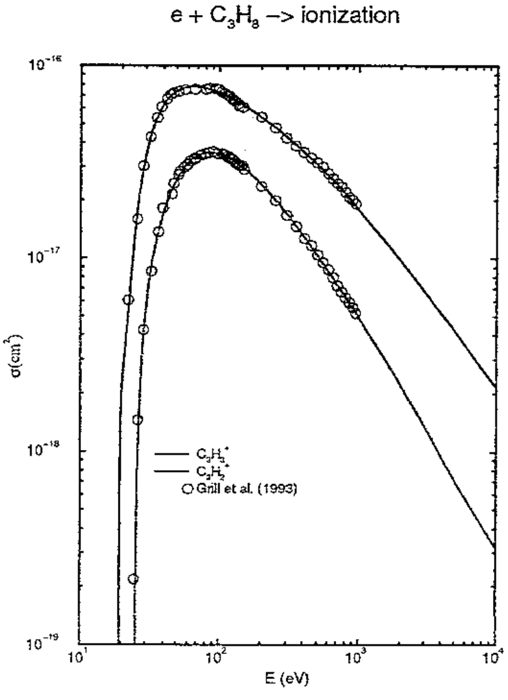

Figure 58: Same as in Fig.54, but for the $C_2H_3^+ + CH_3 + H_2$ and $C_2H_2^+ + CH_4 + H_2$ dissociative channels.

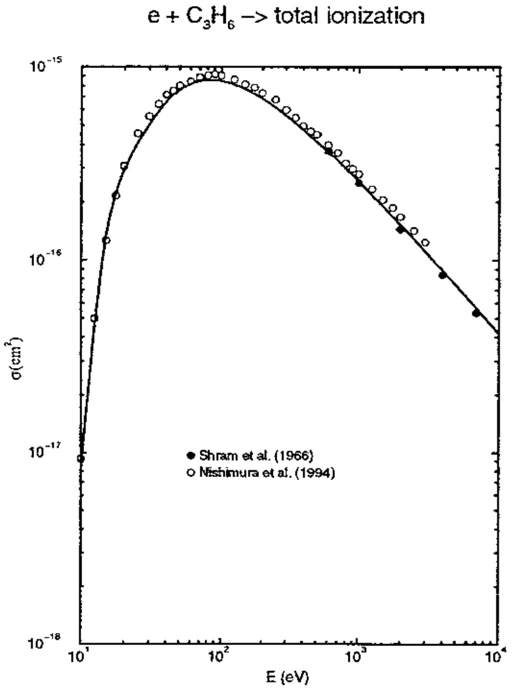

Figure 59: Total cross section for electron-impact ionization of C_3H_6. Symbols: experimental data. Solid curve: least-square fit of the data. (The data of Nishimura (1994) (Ref.[20]) were reduced by a correction factor of 0.935 before fitting; see text).

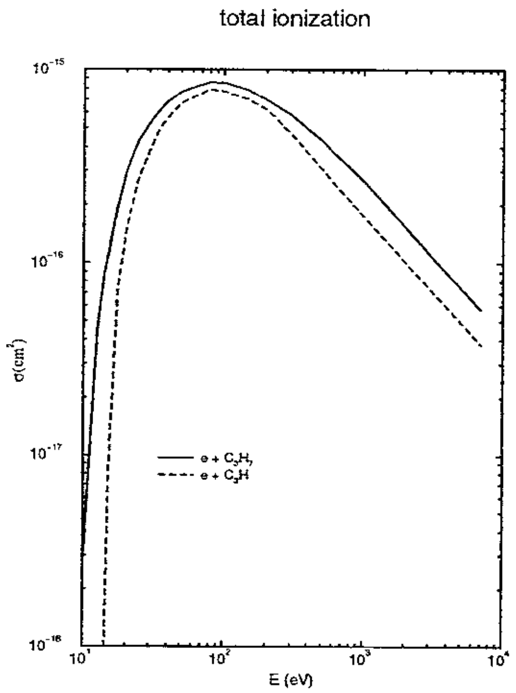

Figure 60: Total cross sections for electron-impact ionization of C_3H_7 and C_3H, based on the data of Table 18.

one needs only the values of $\sigma_{tot}(CH)$ and $\sigma_{tot}(C_2H_4)$ at that energy. Then, like in Figs. 3-5, the intersection of the line connecting $\sigma_{tot}(CH)$ and $\sigma_{tot}(C_2H_4)$ in the $\sigma_{tot}(C_xH_y) - C_xH_y$ plane with the vertical line erected at the position of C_3H_6 gives the value of $\sigma_{tot}(C_3H_6)$ at that energy. The cross section $\sigma_{tot}(C_3H_6)$ obtained by this procedure (from the known cross sections for CH and C_2H_4, see Figs. 27 and 40) is shown by the solid line in Fig. 59. This cross section goes through the data of Ref.[18] for energies above 600 eV (taken as a basis for its construction in this energy region) and by a factor 0.935 (6.5%) below the data of Ref.[20] in the energy region below 600 eV (with exception of the data points in the interval 300-500 eV which lie close to the solid line).

The total ionization cross sections for the systems e+ C_3H_7 and $e + C_3H_y$, $1 \leq y \leq 5$ have been determined by a similar procedure to the one described above. For C_3H_7, C_3H_5, C_3H_4, and C_3H_3 one can use both the linearity of total cross sections for a given energy along the C_3H_y series (with the $\sigma_{tot}(C_3H_6)$ and $\sigma_{tot}(C_3H_8)$ determining the slope of the proportionality line) and the linearity of $\sigma_{tot}(C_2H_y) - \sigma_{tot}(C_2H_{y+2})$ series (which define mutually parallel lines in the $\sigma_{tot}(C_xH_y) - C_xH_y$ plane) and their intersection with the vertical lines erected at the position of C_3H_{y+2} on the abscissa. For determining $\sigma_{tot}(C_3H_2)$ and $\sigma_{tot}(C_3H)$, only the first of these two procedures can be applied. For energies below $\sim$ 30-40 eV, particularly for processes with large energy threshold, the above described procedures had to be applied with due consideration of the rapid decrease of the cross section when the energy approaches the threshold. Since the ionization potentials of C_3H_y molecules do not show a clear regularity (with increasing y), the linearity properties of $\sigma(C_3H_y)$ for $E \lesssim 20 - 30$ eV are not any more present.

We would like to note that the C_3H_4 molecule also has two isomers, propyne and allene, with different appearance potentials (10.36 eV and 9.69 eV, respectively [44]). In deriving the total cross section for C_3H_4 we have used the appearance potential for allene.

The values of the total ionization cross section for C_3H_7 and $C_3H_5 - C_3H_1$ molecules, calculated by using the above described procedures, in the interval from an energy close to the threshold up to 7 keV, are given in Table 18. The ionization potentials of these molecules (single, non-dissociative ionization) are also given in this table. As illustration, the cross sections for C_3H_7 and C_3H are shown in Fig. 60, while in Fig. 61 is shown the cross section for C_3H_4, together with the results of calculations performed within the Deutsch-Märk (D-M) model [33]. Figure 61 shows that the two cross sections agree well in the energy region below $\sim$ 60 eV, but disagree at higher energies. The D-M model predicts the cross section maximum at $E \simeq 70$ eV,

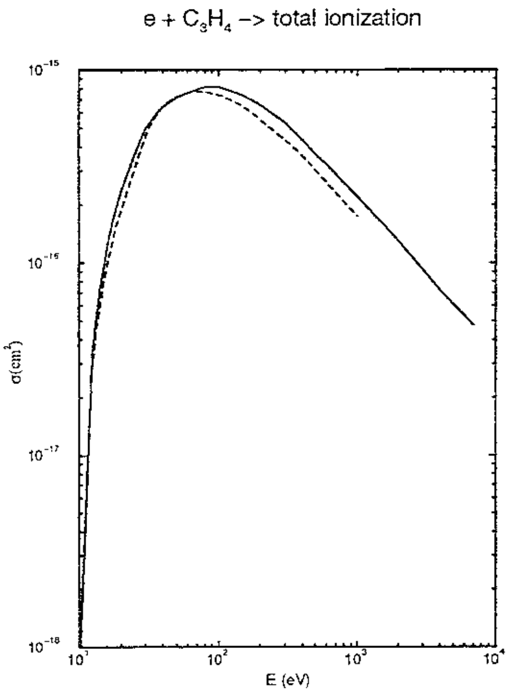

Figure 61: Total cross section for electron-impact ionization of C_3H_4. Solid curve: based on the data in Table 18. Dashed curve: results of calculations using the Deutsch-Märk model (Ref.[33]).

while the cross section obtained by the scaling procedure exhibits its maximum at around $\sim$ 80-90 eV, in accordance with experimental findings for all C_2H_y and C_3H_y hydrocarbon molecules for which total cross sections have been measured. A similar shift of the maximum of calculated D-M cross section with respect to the experimental cross section peak is observed also for C_3H_6 and C_3H_8 molecules [32]. Being based on a pure classical picture for the collision dynamics, the D-M model does not incorporate the logarithmic energy dependent factor in the cross section, typical for high-energy inelastic processes (see Eq.(2)) and, therefore, the D-M cross section decreases more rapidly at high energies than do the experimental cross sections. For the C_3H_4 molecule, the Bethe-Born formula, Eq.(2), with $M_i^2 = 9.3$ (from Table 2) and $C_i = 0.089$, gives values for $\sigma_{tot}(C_3H_4)$ which for $\gtrsim$300 eV differ from those given in Table 18 by less than 15%. In Table 19 we give the Bethe-Born total ionization cross sections for the considered molecules for a number of energies above 300 eV. From this table we see that the Bethe-Born formula, with the M_i^2 factors determined from the empirical additivity rules of Ref.[18], gives results for the C_3H_7 and C_3H_5 ionization cross sections which in the energy region above 300 eV agree with the cross sections from Table 18 to within 3.5% and 8%, respectively. With decreasing the number of H atoms in the C_3H_y molecule, the agreement becomes worse, but for C_3H_4 and C_3H_3 it is still within 15-16 %, if we exclude the E = 300 eV point for $\sigma_{tot}(C_3H_3)$. For C_3H_2 and C_3H, Bethe-Born results deviate from those given in Table 18 by about 20% and 30%, respectively, for energies above 600 eV. This analysis indicates that the empirical additivity rules for M_i^2 might be less reliable for C_xH_y molecules with small number of H atoms.

The accuracy of the total cross sections in Table 18 is not very high. The linear interpolation for $\sigma_{tot}(C_3H_7)$ from the values of $\sigma_{tot}(C_3H_6)$ and $\sigma_{tot}(C_3H_8)$ in the energy range above $\sim$ 30 eV provides cross section data perhaps with same accuracy as that of $\sigma_{tot}(C_3H_6)$ and $\sigma_{tot}(C_3H_8)$ data themselves (10-15%). The linear extrapolation to C_3H_5 should also not increase the cross section uncertainty very much. However, for the last two members of C_3H_y family, C_3H_2 and C_3H, the cross sections of which are obtained by linear extrapolation of C_3H_6 and C_3H_8 data only, the uncertainty may increase up to 4-5 times more than is the uncertainty of C_3H_6 and C_3H_8 data. In the threshold region (up to 20-30 eV), where the scaling relations for the total cross section are not anymore strictly valid, the uncertainties of derived cross sections may also be large.

5.3 Partial Cross Sections for C_3H_7 – C_3H

As we have mentioned before (see also Table 1), there is not presently any information, experimental or theoretical, regarding the partial ionization cross sections for the e + (C_3H_7 – C_3H) collision systems. On the basis of known total ionization cross section for these systems, such information is possible to derive, at least for the dominant ionization channels. This can be done by assuming that the linear behaviour of the fractional contributions of different channels to the total cross section with varying the number of H atoms in the C_xH_y hydrocarbon family, as observed for CH_y and C_2H_y (see Figs. 6 and 7) holds also for the C_3H_y family of molecules. The weak variation of these fractional contributions with the energy, at least for the dominant ionization channels and sufficiently far from the threshold region ($\sim$ 40-50 eV), has already been observed in the case of C_3H_8 molecules (see Table 7). Based on the hypothesis that all observed linearities in the total ionization cross sections with the number of C atoms in C_xH_y (Figs. 1, 3-5), or in the fractional contributions of different channels to the total cross section with the number of H atoms in C_xH_y (Figs. 6, 7), are reflection of the same additivity rules embedded in the mechanism of the ionization process, we make the additional assumption that the fractional contributions of the dominant ionization channels for the C_xH_y molecules depend linearly not only on y (is in Figs. 6 and 7), but also on x, the number of C atoms in C_xH_y. This assumption reduces to the extrapolation of exist-

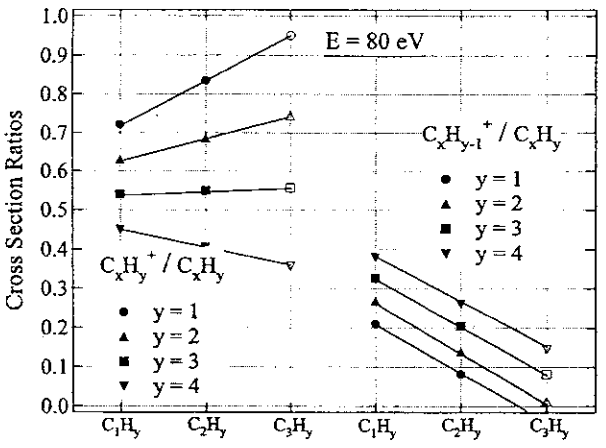

Figure 62: Cross section ratios of parent ($C_xH_y^+$) and dissociative ($C_xH_{y-1}^+$) ionization channels relative to the total ionization for C_xH_y molecules at $E = 80$ eV (see text).

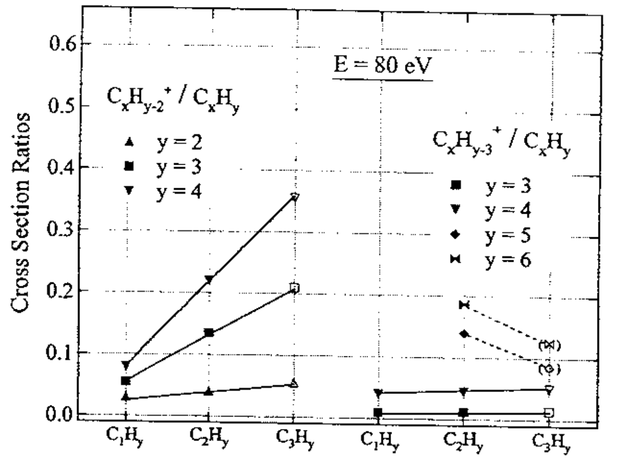

Figure 63: Cross section ratios of the dissociative $C_xH_{y-2}^+$ and $C_xH_{y-3}^+$ channels relative to the total ionization for C_xH_y molecules at $E = 80$ eV (see text).

ing (or derived) ratios of partial to total cross section of a specific ionization channel in CH_y and C_2H_y systems to the same channel in the C_3H_y system. The correctness of this assumption can be subjected to a consistency check: the derived partial cross sections should not exceed the known total cross section for any value of the collision energy (or, the fractional contributions should not exceed one).

In Fig. 62 we have plotted the ratios $\sigma(C_xH_y^+)/\sigma_{tot}(C_xH_y)$ and $\sigma(C_xH_{y-1}^+)/\sigma_{tot}(C_xH_y)$ for $x = 1$ and 2, and $y = 1 - 4$, for the energy $E = 80$ eV taken from Figs. 6 and 7, and have linearly extrapolated the values for a given number of H atoms in CH_y and C_2H_y to C_3H_y with the same number of H atoms. In Fig. 63, similar extrapolation is done for the cross section ratios $\sigma(C_xH_{y-2}^+)/\sigma_{tot}(C_xH_y)$ and $\sigma(C_xH_{y-3}^+)/\sigma_{tot}(C_xH_y)$ for $E = 80$ eV. Obviously, extrapolation of the ratios $\sigma(C_xH_{y-k}^+)/\sigma_{tot}(C_xH_y)$ to C_3H_y along the y =const series can be done only up to $y = 4$ (or $k = 4$). (The points for $C_3H_{5-3}^+$ and $C_3H_{6-3}^+$ in Fig. 63 are determined from other considerations; see later.) The determination of $\sigma(C_3H_{y-k}^+)/\sigma_{tot}(C_3H_y)$, $k = 0 - 3$, by the above extrapolation procedure can be, of course, performed for other energies (higher than $\sim 40 - 50$ eV) as well. For C_3H_y molecules with small number of H atoms, the above ionization channels are the dominant ones, as can be seen from Figs. 62 and 63. Thus, the parent ionization of C_3H accounts for 95% of the total ionization cross section, while $C_3H_{4-k}^+$ channels, $k = 0 - 3$, account for 89% of the total ionization of C_3H_4. Only in $C_3H_6 - C_3H_8$ molecules, the ionization channels associated with breakup of a C-C bond become important, or dominant (as in C_3H_8 and C_3H_7).

The extrapolated values for the ratios $\sigma(C_3H_{y-k}^+)/\sigma_{tot}(C_3H_y)$, $k = 0 - 3$, from Figs. 62 and 63 are reploted in Fig. 64 (an analogon of Fig. 7 for C_2H_y) and shown with solid symbols. In this representation they also exhibit a linear behaviour (as the corresponding ratios in Figs. 6 and 7), which may be considered as an indication of the validity of extrapolation procedure in Figs. 62 and 63. The slope of the lines for the ratios $\sigma(C_3H_y^+)/\sigma_{tot}(C_3H_y)$ and $\sigma(C_3H_{y-2}^+)/\sigma_{tot}(C_3H_y)$ is changed at C_3H_4 to account for the experimental values of these ratios for C_3H_8 [31], and to avoid unphysical consequences if they are continued with the same slope (zero-value for the $\sigma(C_3H_y^+)$ cross section for $y > 5$, in contradiction with the observation of this channel in C_3H_8, and non-conservation of unitarity of the sum of all fractional contribution in the case of $\sigma(C_3H_{y-2}^+)/\sigma_{tot}(C_3H_y)$, as well as the possible contradiction with the experimental value of this ratio for C_3H_8). Certain arguments related to the molecular structure of C_3H_4 and the possible break-up mechanisms for these reactions can also be invoked. Similar reasons have lead us to continue the lines of the ratios $\sigma(C_3H_{y-1}^+)/\sigma_{tot}(C_3H_y)$ and $\sigma(C_3H_{y-3}^+)/\sigma_{tot}(C_3H_y)$ up to C_3H_5 and C_3H_6, respectively.

In Fig. 64 we have plotted also the cross section ratios for the $C_3H_{y-5}^+$, $C_2H_3^+$, $C_2H_4^+$ and $C_3H_5^+$ ionization channels, the last three of which are dominant in the C_3H_8 electron-impact ionization (see Table 7). Since the appearance of a $C_2H_k^+$ ion from C_3H_y requires that $y \geq k$, and since the break-up of a C-C bond when $y = k$ is associated with a significant

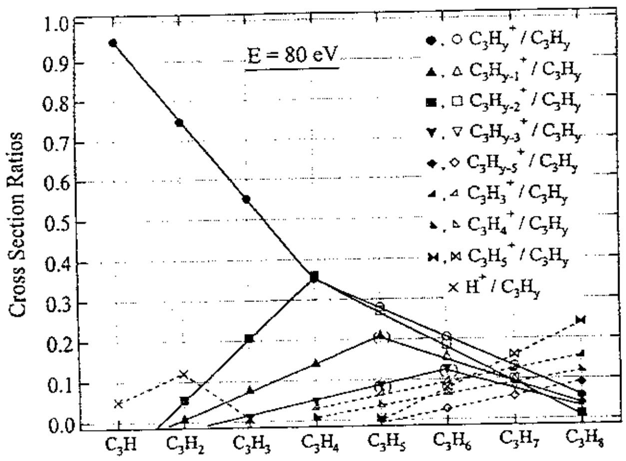

Figure 64: Relative contributions of different ion-production channels in the total electron-impact ionization cross sections of C_3H_y molecules at $E = 80$ eV.

loss of incident electron energy (high energy threshold), one can linearly extrapolate the known values of fractional contributions of $C_2H_k^+$ channels for $e + C_3H_8$ system to the systems with $k \leq y < 8$. For the C_3H_k molecule, the fractional contribution of $C_2H_k^+$ channel can be taken either zero or be assigned a very small value (which does not change the overall distribution of fractional contributions). Using these arguments, the fractional contributions for $C_2H_5^+$, $C_2H_4^+, C_2H_3^+$ and C_3H_{y-5} for C_3H_8 from Ref.[31] were extrapolated linearly to the C_3H_y molecules with smaller number of H atoms. These extrapolations are shown in Fig. 64 by dashed lines.

For the C_3H_y systems with a few H atoms, the H^+ ion-production channel is expected to have a relatively significant contribution to the total cross section, as observed in the CH_y and C_2H_y families of hydrocarbons with small value of y. Using the values of $\sigma(H^+)/\sigma_{tot}(C_xH_y)$ from the C_1H_y and C_2H_y systems, we have determined by extrapolation these ratios for the C_3H_y molecules, $y = 1 - 3$. The values of these fractional contributions are also shown in Fig. 64.

The values of the fractional contributions to the total cross section of the ion-production channels represented in Fig. 64 are given in Table 20. In this table also shown is the sum of these contributions to the total cross section of a particular C_3H_y molecule. We see from the table that the considered channels account for about 90% (or more) of the total cross section in all cases, except for the C_3H_7 molecule where this percentage is about 80%. (We note that the considered eight channels in the $e + C_3H_8$ system give a contribution of 76% to the total cross section; see Table 7.)

In Table 20 we have not included the channel $C_3H_{y-4}^+$ since in the case of C_3H_8 if its contribution to the total cross section is very small [31], and our extrapolation procedure predicts that for the other C_3H_y molecules, $4 \leq y \leq 7$, its contribution to the corresponding $\sigma_{tot}(C_3H_y)$ cross sections would be even smaller. Among the neglected channels in Table 20, which in the case of C_3H_8 gives the next in importance contribution with respect to those shown in Table 20, is the CH_3^+ ion production channel. As seen from Table 7, its contribution to $\sigma_{tot}(C_3H_8)$ is about twice smaller than that of the $C_3H_3^+$ ion-production channel for collision energies above 30 eV. Other channels with minor contributions to $\sigma_{tot}(C_3H_y)$ are the $C_2H_2^+$ and CH_2^+ ion-production channels.

In view of the uncertainties associated with the determination of fractional contributions of ion-production channels to the total cross section $\sigma_{tot}(C_3H_y)$, it would be perhaps an overestimation of the accuracy of our extrapolation procedures if we try to determine these contributions for a sufficient number of collision energies above $\sim$ 40-50 eV to determine the partial cross sections for the ion-production channels given in Table 20. Based on already established fact that fractional contributions of individual ion-production channels do not change appreciably their values in the energy region above $\sim$ 40-50 eV, we can take that the values given in Table 20 can be used for all energies above 40 eV. For the reaction channels with an energy threshold not much different (larger) than the threshold for parent ionization, their values of fractional contributions can be extended in the energy region below 40 eV without introducing a significant error in the derived partial cross section. On the other hand, the reaction channels with a threshold much higher than that for parent ionization (which is at the same time the threshold for the total cross section), the corresponding partial cross sections are already very small at $E \sim 40$ eV, i.e. their fractional contribution to the total cross section is already very small, and their improvements with respect to their values at $E = 80$ eV is immaterial. Therefore, within the accuracy of adopted procedures for determining the fractional contribution of individual reaction channels, and the accuracy of the procedures for determining the total $\sigma_{tot}(C_3H_y)$ cross sections (the combined uncertainty might be up to 30-50%, or even more), the partial cross section for an ion-production channel C_jH_k ($j = 2, 3$) given in Table 20 can be written as

$$\sigma(C_jH_k^+) = F(C_jH_k^+)\sigma_{tot}(C_3H_y), \quad j = 2, 3 \quad (11)$$

where $F(C_jH_k^+)$ is the fractional contribution of the $C_jH_k^+$ ion-production channel in $\sigma_{tot}(C_3H_y)$ for the $e + C_3H_y$ collision system given in Table 20. (Still, an adjustment of $\sigma(C_jH_k^+)$ in the threshold region is recommendable, if E_{th} is large.)

It remains now to identify the neutral fragments (or neutral fragmentation channels) associated with the ion-production channels given in Table 20. The adopted guiding principle, as before, is that the dominant neutral fragmentation channel is the one with smallest appearance potential. The application of this principle gives the following dissociation channels associated with the ions listed in Table 20:

$$e + C_3H_y \to C_3H^+_{y-k} + H, \quad k = 1 \qquad (12a)$$

$$\to C_3H^+_{y-k} + H_2, \quad k = 2 \qquad (12b)$$

$$\to C_3H^+_{y-k} + H_2 + H, \quad k = 3 \qquad (12c)$$

$$\to C_3H^+_{y-k} + 2H_2 + H, \quad k = 5 \qquad (12d)$$

$$e + C_3H_y \to C_2H^+_k + CH_{y-k}, \quad k = 3,4,5; y \geq k; \qquad (13)$$

$$e + C_3H_y \to H^+ + C_3H_{y-1} \quad y = 1,2,3 \qquad (14)$$

The appearance potentials for the dissociative channel (12), taken (or calculated) from Ref.[44], are given in Table 21, while those for the channels (13) and (14) are given in Table 22. (The appearance potentials for $C_3H_y^+$ ions coincide with the ionization potentials of C_3H_y and are given in Table 18.)

We note that the values of appearance potentials in Tables 21 and 22 are consistent with the trends of the fractional contributions of ion-production channels in the total cross section for a given C_3H_y molecule.

6 Analytic Fits of Recommended Cross Sections

All the ionization cross sections discussed in the previous three sections, for which a set of data has been selected either on the basis of critical assessment of available experimental data or derived by using the observed empirical scaling relationships, can be represented in the entire energy region by the following analytic function

$$\sigma = \frac{10^{-13}}{EI_p}\left[B_1 \ln\left(\frac{E}{I_p}\right) + \sum_{i=1}^{N-1} B_{1+i}\left(1 - \frac{I_p}{E}\right)^i\right] (\mathrm{cm}^2) \qquad (15)$$

where I_p is a parameter close (but not always equal) to the ionization or appearance potential for a given ionization channel (expressed in units of eV), E is the collision energy (expressed in units of eV) and B_i ($i = 1 - N$) are fitting coefficients. These coefficients have been determined by fitting the expression (15) to the selected set of cross section data, and their number N determined from the condition to achieve an r.m.s. deviation of the fit from the data below 3-5 %.

An expression of the form of Eq.(15) was also used in Ref.[50] for fitting the ionization cross sections of electron-atom collision systems. An attractive feature of the analytic fit function (15) is that at asymptotically large collision energies it reduces to the Bethe-Born form for the ionization cross section (see, Eq.(2))

$$\sigma_{B-B} = \frac{10^{-13}}{EI_p}\left[B_1 \ln\left(\frac{E}{I_p}\right) + B_0\right] (\mathrm{cm}^2). \qquad (16)$$

In the threshold region, the expression (15) gives a power-law increase of the cross section with the increase of energy.

For the total and partial ionization cross sections for which there were experimental data available, the selected set of data fitted by the analytic function (15) was the one obtained by critical assessment of the available data. In the figures with cross sections shown in the previous three sections, this set of data was represented by a solid line. In cases when only one set of experimental data was available, the fitting was performed on the original set of data, extended in the high energy region (when it was found necessary) by using scaling arguments. For the cases when no experimental cross section information was available, we have fitted the cross sections obtained by using the scaling procedures, as discussed in the previous three sections. However, in the energy region below ~40-50 eV, where these procedures cease to be quite reliable, especially for the reactions with large energy threshold (~ 15-20 eV), a plausible direct extrapolation of the cross section towards the threshold was used.

The neutral fragmentation channels associated with a given ion-production channel were identified (and the corresponding ion-production cross section partitioned) only in the cases when there was a sufficiently clear physical basis for that identification and partitioning. Despite of the significant effort in that direction, the uncertainties of the derived cross sections for neutral fragmentation channels within a single ion-production channel remain quite large. Such cross sections should be used with considerable caution in kinetics modeling (or other) applications.

The parameter I_p and the fitting coefficients B_i entering Eq.(15) for each of the considered reactions (for both the total and partial cross sections) are given in Appendix 1. The graphs of all cross sections represented by the analytic fit function (15), together with the corresponding reaction rate coefficients, are given in Appendix 2.

7 Reaction Rate Coefficients

With the analytic form (15) for the total and partial ionization cross sections, one can easily calculate the corresponding reaction rate coefficient $\langle\sigma v\rangle$ at a given temperature T assuming a Maxwellian velocity distribution of the particles

$$\langle \sigma v \rangle = \frac{4}{\pi^{1/2} u^3} \int_{v_{th}}^{\infty} v^3 dv \sigma(E) \exp(-v^2/u^2) \quad (17)$$

where $u = (2T/m)^{1/2}$, where $E = mv^2/2$ is the (relative) collision velocity, and v_{th} is the velocity corresponding the the threshold energy E_{th} (the ionization or appearance potential) for the ionization reaction. The rate coefficients were calculated for all the considered reactions in the temperature range from 1 eV to 1 keV. They are shown in the graphs of Appendix 2 (solid lines) together with the cross sections represented by the fit function (15) (dashed lines).

We note that with the analytic expression for $\sigma(E)$, Eq.(15), the integration in Eq.(17) can be carried out analytically, but the result is expressed in terms of integral representations of certain special functions which does not bring much practical advantages.

8 Concluding Remarks

In the present report we have critically assessed the available experimental and theoretical cross section data for the electron-impact ionization of hydrocarbon molecules C_xH_y with $x = 1, 2, 3$ and $1 \leq y \leq 2x + 2$. The analysis included both the total and partial cross sections and the energy range covered was from the reaction threshold ($\sim$ 10 eV) up to $\sim$10 keV. We have established that both the total and partial cross section obey certain empirical scaling relationships at energies above $\sim$ 40-50 eV, having their origin most probably in the additivity rules for the collision strengths for transitions of molecular electrons directly to the continuum or to dissociative states lying in the ionization continuum. On the basis of available experimental data and the empirical cross section scaling relationships, we have derived a consistent set of recommended cross sections, both for the total ionization and for the individual (direct and dissociative) ionization channels. The accuracy of the recommended cross sections is of the order of 10-15 %, when they are derived from the most accurate experimental data presently available, and about 15-30% for the cross sections derived by using the scaling relationships. In this latter case, the uncertainty may be even higher ($\sim$ 40-50%) in the threshold region, where the scalings are less reliable, particularly for the weak channels of the systems C_xH_y, $x \simeq y = 1, 2$.

The data analysis performed in the present report clearly indicates that the overall experimental information on the total and partial cross sections for electron-impact ionization of C_xH_y molecules is rather sparse and that further work in this direction would be very desirable.

When using the present database in kinetics modeling applications, one has to keep in mind that large difference in the cross section values for various ionization channels. For the molecules with small number of H atoms only a few channels (the parent ionization and dissociation with one H-atom or H_2 molecule released) give the predominant contribution (over 90%) to the total cross section. For the more complex hydrocarbons the number of dominant ionization channels increases, but is always limited to a small fraction of the total number of ionization channels. In a kinetics modeling scheme it is advisable to include only those channels for each C_xH_y molecule which in their sum contributes to the total cross section up to a certain percentage (e.g. 90%). The number of selected ionization channels which for a given C_xH_y molecule have to be included in the kinetics scheme can further be correlated with the initial concentration of C_xH_y molecules in the gas (plasma). The distinction between dominant and non-dominant ionization channels in the context of collisional kinetics is important also from the point of view of the accuracy of results of kinetics modeling: the cross sections presented in this report are, generally speaking, more accurate for the dominant channels than for the weak channels.

Acknowledgements

The authors would like to express their gratitude to Prof. Y.-K. Kim and Dr. K. K. Irikura for providing the BEB cross section for C_2H_3, and to Prof. T. Märk and Dr. H. Deutsch for providing the D-M cross section for C_3H_4. Many discussions with Prof. Y.-K. Kim and Prof. T. Märk on the physics of ionization processes of hydrocarbon molecules are also greatfully acknowledged.

References

[1] *Technical Basis for the ITER Final Design Report; ITER EDA Documentation Series No.16* (IAEA, Vienna, 1998).

[2] E. Vietzke and A.A. Haasz, in *"Physical Processes of Interaction of Fusion Plasmas with Solids"*, Eds. W.O. Hofer and J. Roth (Academic Press, San Diego, 1996), p.135.

[3] A.A. Haasz, J.A. Stephens, E. Vietzke, W. Eckstein, J.W. Davis and Y. Hirooka, Atom. Plasma-Mater. Interact. Data Fusion, vol.7 (part A) (1998), p.5.

[4] R.K. Janev, M.F.A. Harrison and H.W. Dravin, Nucl. Fusion **29**, 109 (1989).

[5] A.B. Ehrhardt and W.D. Langer, *Collisional Processes of Hydrocarbons in Hydrogen Plasmas,* Report PPPL-2477 (1987) (Princeton Plasma Physics Laboratory, Princeton, USA).

[6] H. Tawara, Y. Itikawa, H. Nishimura, H. Tanaka and Y. Nakamura, *Collision Data Involving Hydro-Carbon Molecules,* Report NIFS-DATA-6

(1990) (National Institute for Fusion Science, Toki, Japan).

[7] H. Tawara, in *"Atomic and Molecular Processes in Fusion Edge Plasmas"*, Ed. R.K. Janev (Plenum Press, New York, 1995).

[8] T. Shirai, T. Tabata, H. Tawara, and Y. Itikawa, to be published in Atomic Data and Nucl. Data Tables (2001).

[9] D.A. Alman, D.N. Ruzic, and J.N. Brooks, Phys. Plasmas **7**, 1421 (2000).

[10] R.K. Janev, J.G. Wang and T. Kato, *Cross Sections and Rate Coefficients for Charge Exchange Reactions of Protons with Hydrocarbon Molecules,* Report NIFS-DATA-64 (2001) (National Institute for Fusion Science, Toki, Japan).

[11] B. Adamczyk, A.J.H. Boerboom, B.L. Schram and J. Kistemaker, J. Chem. Phys. **44**, 4460 (1966).

[12] H. Chatham, D. Hills, R. Robertson and A. Gallagher, J. Chem. Phys. **81**, 1770 (1984).

[13] O.J. Orient and S.K. Srivastava, J. Phys. B **20**, 3923 (1987).

[14] V. Tarnovski, A. Levin, H. Deutsch and K. Becker, J. Phys. B **29**, 139 (1996).

[15] H.C. Straub, D. Lin, B.G. Lindsay, K.A. Smith and R.F. Stebbings, J. Chem. Phys. **106**, 4430 (1997).

[16] C. Tian and C.R. Vidal, J. Phys. B **31**, 895 (1998).

[17] D. Rapp and P. Englander-Golden, J. Chem. Phys. **43**, 1464 (1965).

[18] B.L. Schram, M.J. van der Wiel, F.J. de Heer and H.R. Moustafa, J. Chem. Phys. **44**, 49 (1966).

[19] N. Duric, I. Cadez and M. Kurepa, Int. J. Mass Spectrom. Ion Processes, **108**, R1 (1991).

[20] H. Nishimura and H. Tawara, J. Phys. B **27**, 2063 (1994).

[21] W. Hwang, Y.-K. Kim and M.E. Rudd, J. Chem Phys. **104**, 2956 (1996), (See also: Y.-K. Kim, W. Hwang, N.M. Weinberger, M.A. Ali and M.E. Rudd, J. Chem. Phys. **106**, 1026 (1997) for CH_4 only).

[22] F.A. Baiocchi, R.C. Wetzel and R.S. Freund, Phys. Rev. Lett. **53**, 771 (1984).

[23] D.P. Wang, L.C. Lee and S.K. Srivastava, Chem. Phys. Lett. **152**, 513 (1988).

[24] Y.-K. Kim, M.A. Ali and M.E. Rudd, J. Res. NIST **102**, 693 (1997).

[25] V. Grill, G. Walder, P. Scheir, M. Krudel and T.D. Märk, Int. J. Mass Spectrom. Ion Processes, **129**, 31 (1993).

[26] C.E. Melton, J. Chem. Phys. **37**, 562 (1962).

[27] K.K. Irikura and Y.-K. Kim (private communication, 2000).

[28] A. Gaudin and R. Hageman, J. Chim. Phys. **64**, 1209 (1967).

[29] S.-H. Zheng and S.K. Srivastava, J. Phys. B **29**, 3235 (1996).

[30] J.T. Tate and P.T. Smith, Phys. Rev. **39**, 270 (1932).

[31] V. Grill, G. Walder, D. Margreiter, T. Rauth, H.U. Poll, P. Scheir and T.D. Märk, Z. Phys. D **25**, 217 (1993).

[32] H. Deutsch, K. Becker, R.K. Janev, M. Probst and T.D. Märk, J. Phys. B **33**, L872 (2000).

[33] H. Deutsch and T.D. Märk (private communication, 2000).

[34] E. Brüche, Ann. Physik, Lpz. **4**, 387 (1930).

[35] B.A. Tozer, J. Electron. Control. **4**, 149 (1958).

[36] Y.-K. Kim and M.E. Rudd, Phys. Rev. A **50**, 3954 (1994).

[37] D. Margreiter, H. Deutsch, M. Schmidt and T.D. Märk, Int. Mass Spectrom. Ion Processes **100**, 157 (1990).

[38] E. Vogt and G.H. Wannier, Phys. Rev. **95**, 1190 (1954).

[39] Cz. Szmytkowski, Z. Phys. D **13**, 69 (1989).

[40] H. Nishimura and H. Tawara, J. Phys. B **24**, L369 (1991).

[41] J.O. Hirschfelder, C.F. Curtis and R.B. Bird, *"Molecular Theory of Gases and Liquids"*, (John Wiley, New York, 1967).

[42] P. Plessis, P. Marmet and R. Dutil, J. Phys. B **16**, 1283 (1983).

[43] R.S. Freund, S.M. Tarr and J.A.Schiavone, J. Chem. Phys. **79**, 213 (1983).

[44] H.M. Rosenstock, K. Draxl, B.M. Steiner and J.T. Herron, J. Phys. Chem. Ref. Data **6** (Suppl. 1) (1977).

[45] D.D. Wagman, W.H. Evans, V.B. Parker *et al.*, *"Selected Values of Chemical Thermodynamic Properties,"*, NBS Technical Note 270-3 (January, 1968), U.S.Gov. Printing Office, Washington D.C. (1968).

[46] P. Plessis and P.Marmet, Can. J. Chem. **65**, 1424 (1987)

[47] R.K. Janev, T. Kato, and J.G. Wang (unpublished, 2001)

[48] P. Plessis and P.Marmet, Int. J. Mass Spectrosc. Ion. Processes, **70**, 23 (1986).

[49] M. Davister and R. Locht, Chem. Phys. **189**, 805 (1994).

[50] K. L. Bell, H. B. Gilbody, J. G. Hughs, A. E. Kingston and F. J. Smith, J. Phys. Chem. Ref. Data **12**, 891 (1983).

Table 1. Cross Section Data Sources for Electron-Impact Ionization of C_xH_y(T:Theory; others:experiment)

Molecule	First Author(year)	Ref.	Cross Section Partial (No.Channels)	Cross Section Total	Remark
CH_4	Adamczyk(1966)	11	Yes(7)	Yes	(a)
	Chatham(1984)	12	Yes(7)	Yes	(a)
	Orient(1987)	13	Yes(5)	Yes	(a)
	Tarnovsky(1996)	14	Yes(4)	Yes	(a)(CD_4)
	Straub(1997)	15	Yes(7)	Yes	(a)
	Tian(1998)	16	Yes(7)	Yes	(a)
	Rapp(1965)	17	—	Yes	(b)
	Schram(1966)	18	—	Yes	(b)
	Djuric(1991)	19	—	Yes	(b)
	Nishimura(1994)	20	—	Yes	(b)
	Hwang(1996)	21	—	Yes	T(BEB)
CH_3	Baiocchi(1984)	22	Yes(2)	—	(CD_3)
	Wang(1988)	23	Yes(1)	—	
	Tarnovsky(1996)	14	Yes(2)	—	(CD_3)
	Hwang(1996)	21	—	Yes	T(BEB)
CH_2	Baiocchi(1984)	22	Yes(2)	—	(CD_2)
	Tarnovsky(1996)	14	Yes(2)	—	(CD_2)
	Hwang(1996)	21	—	Yes	T(BEB)
CH	Tarnovsky(1996)	14	Yes(2)	—	(CD)
	Kim(1997)	24	—	Yes	T(BEB)

Notes: (a):σ_{tot} is sum of partial cross sections

(b):Direct measurement of σ_{tot}

BEB:Binary-Encounter-Bethe approximation

Table 1. (Cont'd)

Molecule	First Author(year)	Ref.No	Cross Section Partial (No.Channels)	Cross Section Total	Remark
C_2H_6	Chatham(1984)	12	Yes(11)	Yes	(a)
	Grill(1993a)	25	Yes(13)	Yes	(a)
	Melton(1962)	26	Yes(13)	—	(c)
	Schram(1966)	18	—	Yes	(b)
	Duric(1991)	19	—	Yes	(b)
	Nishimura(1994)	20	—	Yes	(b)
	Hwang(1996)	21	—	Yes	T(BEB)
C_2H_5	—		—	—	
C_2H_4	Melton(1962)	26	Yes(10)	—	(c)
	Rapp(1965)	17	—	Yes	(b)
	Schram(1966)	18	—	Yes	(b)
	Nishimura(1994)	20	—	Yes	(b)
	Hwang(1996)	21	—	Yes	T(BEB)
C_2H_3	Irikura(2000)	27	—	Yes	T(BEB)
C_2H_2	Gaudin(1967)	28	Yes(7)	Yes	(a)
	Zheng(1996)	29	Yes(6)	Yes	(a)
	Tian(1998)	16	Yes(6)	Yes	(a)
	Melton(1962)	26	Yes(7)	—	(c)
	Tate(1932)	30	—	Yes	(b)
	Kim(1997)	24	—	Yes	T(BEB)
C_2H	—		—	—	

Remark: (c):Relative cross sections for E=75eV and 3.5MeV only.

Table 1. (Cont'd)

Molecule	First Author(year)	Ref.No	Cross Section Partial (No.Channels)	Cross Section Total	Remark
C_3H_8	Grill(1993b)	31	Yes(23)	Yes	(a)
	Schram(1966)	18	—	Yes	(b)
	Djuric(1991)	19	—	Yes	(b)
	Nishimura(1994)	20	—	Yes	(b)
	Hwang(1996)	21	—	Yes	T(BEB)
	Deutsch(2000)	32	—	Yes	T(DM)
C_3H_7	—		—	—	
C_3H_6	Schram(1966)	18	—	Yes	(b)
(propene and	Nishimura(1994)	20	—	Yes	(b)
cyclopropane)	Deutsch(2000)	32	—	Yes	T(DM)
C_3H_5	—		—	—	
C_3H_4	Deutsch(2000)	33	—	Yes	T(DM)
C_3H_3					
C_3H_2	—		—	—	
C_3H					

Note: DM: Deutsch-Märk model

Table 2. Values of Mi^2 for C_xH_y Calculated by the Additivity Rule. (Experimental values, when available, are also shown.)

Molecule	$Mi^2(CH_y)$ Calc.	$Mi^2(CH_y)$ Exp.	$Mi^2(C_2H_y)$ Calc.	$Mi^2(C_2H_y)$ Exp.	$Mi^2(C_3H_y)$ Calc.	$Mi^2(C_3H_y)$ Exp.
C_xH	1.07		3.6		6.11	
C_xH_2	2.14		4.64	5.33[28]	7.15	
C_xH_3	3.21		5.71		8.2	
C_xH_4	4.28	4.28[18]	6.78	7.25[17]	9.3	
C_xH_5			7.85		10.35	
C_xH_6			8.92	8.63[18]	11.4	12.0[18][(a)]
C_xH_7					12.5	
C_xH_8					13.6	13.0[31] 13.8[18]

(a) This value is for the propen isomer. For cyclopropane Mi^2=10.2[18].

Table 3. Polarizabilities α_{pol} of C_xH_y Molecules (in a_0^3 units). (From Ref. 9, and Ref. 41 for C_3H_8)

Molecule	CH_y	C_2H_y	C_3H_y
C_xH	12.03	22.49	33.10
C_xH_2	13.44	24.05	34.58
C_xH_3	14.93	25.47	36.00
C_xH_4	16.41	26.95	37.49
C_xH_5		28.37	38.98
C_xH_6		29.86	40.39
C_xH_7			(41.80)[a]
C_xH_8			42.49

a: Interpolated value

Table 4. Fractional Contributions of Partial Cross Sections of Dominant Ion-Production Channels to the Total Ionization Cross Section of C_3H_8 at E=100 eV.(From Ref.[31])

$C_3H_8^+$	0.063	$C_2H_5^+$	0.239	CH_3^+	0.051
$C_3H_7^+$	0.049	$C_2H_4^+$	0.119	CH_2^+	0.019
$C_3H_6^+$	0.015	$C_2H_3^+$	0.156	CH^+	0.006
$C_3H_5^+$	0.035	$C_2H_2^+$	0.062		
$C_3H_4^+$	0.009	C_2H^+	0.009		
$C_3H_3^+$	0.087				
$C_3H_2^+$	0.025				
C_3H^+	0.005				

Table 5. Fractions of Partial Cross Sections of Dominant Ion-Production Channels in Total Ionization Cross Section of CH_4. (From Ref.15; for last two energies, from Ref.11)

E(eV)	CH_4^+	CH_3^+	CH_2^+	CH^+	H^+
20	0.62	0.36	0.011	—	—
30	0.52	0.40	0.051	0.011	0.11
50	0.45	0.36	0.082	0.041	0.073
100	0.41	0.33	0.079	0.043	0.11
200	0.42	0.34	0.074	0.037	0.11
300	0.41	0.34	0.070	0.032	0.092
500	0.47	0.38	0.070	0.030	0.086
1000	0.46	0.37	0.062	0.025	0.066
1500	0.47	0.44	0.065	0.022	—
2000	0.47	0.43	0.066	0.021	—

Table 6. Fractions of Partial Cross Sections of Dominant Ion-Production Channels in Total Ionization Cross Section of C_2H_6. (From Ref.25; the values for E=3.5MeV are from Ref.26)

E(eV)	$C_2H_6^+$	$C_2H_5^+$	$C_2H_4^+$	$C_2H_3^+$	$C_2H_2^+$	C_2H^+
20	0.13	0.095	0.37	0.20	0.067	0.002
30	0.11	0.087	0.42	0.19	0.092	0.006
50	0.08	0.079	0.39	0.19	0.13	0.022
100	0.08	0.078	0.38	0.19	0.13	0.032
200	0.085	0.085	0.39	0.18	0.12	0.026
300	0.09	0.087	0.40	0.18	0.11	0.022
500	0.10	0.089	0.43	0.185	0.11	0.018
900	0.11	0.092	0.46	0.18	0.095	0.014
3.5×10^6	0.14	0.102	0.49	0.14	0.071	0.013

Table 7. Fractions of Partial Cross Sections of Dominant Ion-Production Channels in Total Ionization Cross Section of C_3H_8.(From Ref.[31])

E(eV)	$C_3H_8^+$	$C_3H_7^+$	$C_3H_3^+$	$C_2H_5^+$	$C_2H_4^+$	$C_2H_3^+$	CH_3^+
20	0.091	0.061	0.020	0.28	0.15	0.157	0.036
30	0.080	0.059	0.074	0.27	0.14	0.170	0.040
50	0.069	0.054	0.089	0.25	0.13	0.160	0.052
100	0.063	0.049	0.087	0.24	0.12	0.156	0.051
200	0.065	0.051	0.079	0.24	0.12	0.158	0.047
300	0.069	0.054	0.083	0.25	0.12	0.164	0.046
500	0.070	0.051	0.080	0.24	0.13	0.163	0.044
900	0.066	0.052	0.080	0.25	0.12	0.162	0.043

Table 8. Ionization Channels for CH4 and Their Threshold Energies, Eth(in eV).

Ionization Channel	E_{th} Ref.[42]	E_{th} (Ref.[12])	Thermochemical value[43]
$CH_4 \rightarrow CH_4^+$	12.63(a)	12.6	—
$\rightarrow CH_3^+ + H^{**}$	14.01	14.3	14.35
$\rightarrow CH_2^+ + H_2$	15.06	15.1	15.24
$\rightarrow CH^+ + H_2 + H^{(*)}$	19.87	22.2	19.85
$\rightarrow C^+ + 2H_2$	19.56	25±2	19.46
$\rightarrow H^+ + CH_3$	(18.11)		18.11
$\rightarrow H_2^+ + CH_2$	(20.27)		20.27

Note: (a): The most recent value for $I_p(CH_4)$ is 12.51eV.
**: H atom in a highly excited (Rydberg) state[43].

Table 9. Ionization Channels for CH_3 and Their Threshold Energies, E_{th} (From Refs.[44,45]).

Ionization Channel	E_{th} (eV)
$CH_3 \rightarrow CH_3^+$	9.84
$\rightarrow CH_2^+ + H$	15.27
$\rightarrow CH^+ + H_2$	15.88
$\rightarrow C^+ + H_2 + H$	19.54
$\rightarrow H^+ + CH_2$	18.48
$\rightarrow H_2^+ + CH$	20.18

Table10. Ionization Channels for CH_2 and CH and Their Threshold Energies, E_{th} (From Refs.[44,45]).

CH_2		CH	
Ionization Channel	E_{th}(eV)	Ionization Channel	E_{th}(eV)
$e + CH_2 \rightarrow CH_2^+$	10.40	$e + CH \rightarrow CH^+$	11.13
$\rightarrow CH^+ + H$	15.53	$\rightarrow C^+ + H$	14.80
$\rightarrow C^+ + H_2$	14.67	$\rightarrow H^+ + C$	17.14
$\rightarrow H^+ + CH$	18.01	—	—
$\rightarrow H_2^+ + C$	18.83	—	—

Table11. Ionization Channels for C2H6 and Their Threshold Energies, E_{th}.

Ionization Channel	E_{th}(eV) Ref.[46]	E_{th}(eV) Ref.[12]	Thermochemical value[43]
$e+C_2H_6 \rightarrow C_2H_6^+$	11.56(a)	11.4	—
$\rightarrow C_2H_5^+ + H^{**}$	12.45	12.1	12.61
$\rightarrow C_2H_4^+ + H_2$	11.81	12.1	11.93
$\rightarrow C_2H_3^+ + H_2 + H^{**}$	14.50	14.5	—
$\rightarrow C_2H_2^+ + 2H_2$	14.51	15.2±1	14.64
$\rightarrow C_2H^+ + 2H_2 + H^{**}$	22.4	—	—
$\rightarrow C_2^+ + 3H_2$	22.9	—	21.56
$\rightarrow CH_4^+ + CH_2$ (c)	16.63	—	16.77
$\rightarrow CH_3^+ + CH_3$	13.65	14.2±2	13.67
$\rightarrow CH_2^+ + CH_4$	14.69	17.0±2	14.57
$\rightarrow CH^+ + CH_3 + H_2$	20.10	26.7 (b)	19.17
$+CH_4 + H^{(*)}$	—	26.7 (b)	19.18
$\rightarrow C^+ + CH_4 + H_2$	20.3	—	18.18
$\rightarrow H^+ + C_2H_5$ (c)	—	23.5 (b)	17.85
$\rightarrow H_2^+ + C_2H_4$ (c)	—	35 (b)	16.85
$\rightarrow C_2H_5^{2+} + H$	32.3		—
$\rightarrow C_2H_3^{2+} + H_2 + H$	35.5		—

Notes: (a)The most recent value for $I_p(C_2H_6)$ is 11.52eV.
(b)Appearance potentials from Ref.[43].
(c)This ion-production channel was not observed in experiments.
**: H atom in a highly excited state(n~20-30)[43].

Table12. Ionization Channels for C_2H_5 and Their Threshold Energies, E_{th}.

Ionization Channel	E_{th}(eV)
$e+C_2H_5 \rightarrow C_2H_5^+$	8.25
$\rightarrow C_2H_4^+ + H$	12.14
$\rightarrow C_2H_3^+ + H_2$	10.59
$\rightarrow C_2H_2^+ + H_2 + H$	14.93
$\rightarrow C_2H^+ + 2H_2$	16.23
$\rightarrow C_2^+ + 2H_2 + H$	21.79
$\rightarrow CH_3^+ + CH_2$	14.22
$\rightarrow CH_2^+ + CH_3$	14.78
$\rightarrow CH^+ + CH_4$	15.42
$\rightarrow C^+ + CH_4 + H$	19.10
$\rightarrow$ $+CH_3 + H_2$	18.06

Table13. Ionization Channels for C_2H_4 and Their Threshold Energies, E_{th}.

Ionization Channel	E_{th}(eV)
$e+C_2H_4 \rightarrow C_2H_4^+$	10.45
$\rightarrow C_2H_3^+ + H$	13.42
$\rightarrow C_2H_2^+ + H_2$	13.25 (a)
$\rightarrow C_2H^+ + H_2 + H$	19.01
$\rightarrow C_2^+ + 2H_2$	20.11
$\rightarrow CH_3^+ + CH$	16.94
$\rightarrow CH_2^+ + CH_2$	17.96
$\rightarrow CH^+ + CH_3$	18.22
$\rightarrow C^+ + CH_3 + H$	21.89
$\rightarrow$ $+CH_2 + H_2$	22.24

Note: (a) The appearance potential for $C_2H_2^+ + 2H$ channel is 17.77eV.

Table14. Ionization Channels for C_2H_3 and Their Threshold Energies, E_{th}.

Ionization Channel	E_{th}(eV)	
$e+C_2H_3 \rightarrow C_2H_3^+$	9.45	
$\rightarrow C_2H_2^+ + H$	12.80	
$\rightarrow C_2H^+ + H_2$	15.11	(a)
$\rightarrow C_2^+ + H_2 + H$	20.66	
$\rightarrow CH_2^+ + CH$	18.40	
$\rightarrow CH^+ + CH_2$	19.52	
$\rightarrow C^+ + CH_3$	17.92	
$\rightarrow H^+ + C_2H_2$	16.01	

Note: The appearance potential for C_2H^++2H channel is 19.63eV.

Table15. Ionization Channels for C_2H_2 and Their Threshold Energies, E_{th} (in eV).

Ionization Channel	E_{th}(eV) Ref.[48]	E_{th}(eV) Ref.[29]	Thermochem. value.[44,45]
$e+C_2H_2 \rightarrow C_2H_2^+$	11.40	11.4±0.2	—
$\rightarrow C_2H^+ + H$	16.70	17.2±0.2	17.22
$\rightarrow C_2^+ + H_2$	22.60	22.9±0.3	18.28 (b)
$\rightarrow CH^+ + CH$	23.9	23.6±0.5	21.12 (c)
$\rightarrow C^+ + CH_2$	—	24.9±0.5	20.39 (d)
$\rightarrow H^+ + C_2H$	18.93 (a)	19.2±0.5	18.43

Notes: (a) Value from Ref.[49].
(b) The appearance potential for C_2^++2H channel is 22.79 eV.
(c) The appearance potential for CH^++C+H channel is 24.65 eV.
(d) The appearance potential for C^++CH+H channel is 24.79 eV.

Table16. Ionization Channels for C_2H and Their Threshold Energies, E_{th}.

Ionization Channel	E_{th}(eV)
$e+C_2H \rightarrow C_2H^+$	12.41
$\rightarrow C_2^+ + H$	17.97
$\rightarrow CH^+ + C$	19.83
$\rightarrow C^+ + CH$	19.87
$\rightarrow H^+ + C_2$	19.58

Table17. Ionization Channels for C_3H_8 and Associated Threshold Energies.

Ionization Channel	I_p/A_p(eV) [44]	Thermochemical value[44,45]
$e+C_3H_8 \rightarrow C_3H_8^+$	11.08	—
$\rightarrow C_3H_7^+ + H$	11.53	12.39
$\rightarrow C_3H_6^+ + H_2$	12.2	11.00
$\rightarrow C_3H_5^+ + H_2 + H$	14.76	12.71
$\rightarrow C_3H_4^+ + 2H_2$	—	13.23
$\rightarrow C_3H_3^+ + 2H_2 + H$	—	14.41
$\rightarrow C_3H_2^+ + 3H_2$	—	16.93
$\rightarrow C_3H^+ + 3H_2 + H$	—	18.47
$\rightarrow C_2H_5^+ + CH_3$	12.15	11.99
$\rightarrow C_2H_4^+ + CH_4$	11.35	11.26
$\rightarrow C_2H_3^+ + CH_3 + H_2$	14.5	14.18
$\rightarrow C_2H_2^+ + CH_4 + H_2$	14.1	15.60
$\rightarrow C_2H^+ + CH_3 + 2H_2$	—	19.61
$\rightarrow$ $+CH_4 + H_2 + H$	—	19.65
$\rightarrow CH_3^+ + C_2H_5$	14.0	13.43
$\rightarrow CH_2^+ + C_2H_6$	—	13.92
$\rightarrow CH^+ + C_2H_4 + H_2$	—	17.84

Table 18. Total Ionization Cross Sections for C_3H_y Molecules (y=7,5-1) in units of 10^{-16} cm^2
The Ionization Potentials are also given (in eV) [44].

I_p(eV) / E(eV)	C_3H_7	C_3H_5	C_3H_4	C_3H_3	C_3H_2	C_3H
	9.10	9.90	9.69	8.34	12.50	13.40
12	0.25	0.10	0.15	0.37	—	—
13	0.50	0.25	0.35	0.57	—	—
14	0.75	0.46	0.66	0.85	0.08	0.01
15	1.10	0.83	0.90	1.15	0.30	0.03
16	1.50	1.17	1.20	1.50	0.60	0.15
18	2.15	1.90	1.80	2.10	1.30	0.70
20	2.92	2.71	2.34	2.70	2.01	1.46
22	3.50	3.30	2.95	3.30	2.70	2.10
25	4.31	4.02	3.62	3.93	3.45	2.77
28	5.00	4.70	4.35	4.51	4.10	3.50
30	5.27	5.01	4.95	4.88	4.48	4.00
35	6.11	5.86	5.70	5.64	5.36	4.90
40	6.84	6.56	6.43	6.28	6.03	5.65
45	7.20	6.90	6.85	6.68	6.50	6.20
50	7.65	7.31	7.18	7.00	6.85	6.70
55	7.80	7.60	7.40	7.20	7.15	6.95
60	8.02	7.76	7.60	7.45	7.45	7.15
70	8.30	8.10	7.95	7.85	7.80	7.55
80	8.60	8.35	8.18	8.07	7.97	7.87
90	8.54	8.34	8.25	8.10	7.92	7.80
100	8.47	8.33	8.17	8.01	7.85	7.70
120	8.25	8.10	8.00	7.75	7.60	7.40
130	8.15	8.00	7.80	7.60	7.45	7.30
150	7.81	7.54	7.50	7.28	7.13	6.99
170	7.50	7.20	7.20	7.00	6.85	6.80
200	7.02	6.82	6.73	6.63	6.42	6.35
250	6.20	6.20	6.00	5.90	5.70	5.65
300	5.58	5.44	5.32	5.20	5.09	4.98
400	4.60	4.60	4.50	4.18	4.00	3.90
500	4.00	3.90	3.80	3.53	3.30	3.30
600	3.60	3.48	3.25	3.03	2.82	2.80
800	2.95	2.80	2.62	2.35	2.30	2.20
1000	2.50	2.37	2.20	2.00	1.93	1.85
1500	1.90	1.67	1.60	1.42	1.37	1.30
2000	1.50	1.34	1.24	1.14	1.10	1.05
3000	1.10	1.00	0.93	0.84	0.78	0.75
4000	0.88	0.80	0.75	0.68	0.62	0.60
5000	0.73	0.66	0.63	0.56	0.52	0.50
7000	0.57	0.50	0.48	0.43	0.40	0.38

Table19. Bethe-Born Ionization Cross Sections for C_3H_7 and C_3H_5-C_3H for E≧300eV (in units of 10^{-16}cm^2). (From Eq.(2) and Table 2.)

E(eV)	C_3H_7	C_3H_5	C_3H_4	C_3H_3	C_3H_2	C_3H
300	6.56	5.45	4.89	4.31	3.77	3.22
600	3.98	3.29	2.96	2.61	2.27	1.95
1000	2.69	2.23	2.00	1.77	1.54	1.32
2000	1.55	1.29	1.16	1.02	0.887	0.758
4000	0.879	0.729	0.655	0.577	0.503	0.430
7000	0.551	0.456	0.410	0.361	0.315	0.269

Table 20. Fractional Contributions of Dominant Ion-Production Channels to Total Ionization Cross Section in $e+C_3H_y$ (y=1-7) Collisions at E=80eV.

Ion-Channel	C_3H	C_3H_2	C_3H_3	C_3H_4	C_3H_5	C_3H_6	C_3H_7
$C_3H_y^+$	0.95	0.745	0.552	0.355	0.282	0.206	0.184
$C_3H_{y-1}^+$	—	0.010	0.077	0.145	0.213	0.156	0.102
$C_3H_{y-2}^+$	—	0.055	0.206	0.310	0.272	0.137	0.100
$C_3H_{y-3}^+$	—	—	0.010	0.047	0.083	0.125	0.077
$C_3H_{y-5}^+$	—	—	—	—	0.005	0.030	0.057
$C_2H_5^+$	—	—	—	—	0.006	0.082	0.160
$C_2H_4^+$	—	—	—	0.008	0.035	0.065	0.094
$C_2H_3^+$	—	—	0.006	0.034	0.064	0.093	0.122
H^+	0.05	0.120	0.010	—	—	—	—
Total	1.00	0.930	0.861	0.899	0.960	0.894	0.796

Table 21. Appearance Potential A_p(in eV) for $C_3H_{y-k}^+$(k=1-3,5) Dissociation of C_3H_y Molecules. (From Ref.[44,45])

C_3H_y	$C_3H_{y-1}^+$	$C_3H_{y-2}^+$	$C_3H_{y-3}^+$	$C_3H_{y-5}^+$
C_3H	14.67	—	—	—
C_3H_2	13.0	16.4	—	—
C_3H_3	15.38	12.40	20.39	—
C_3H_4	12.34	13.86	15.40	—
C_3H_5	13.10	9.76	16.80	21.90
C_3H_6	11.44	11.96	13.15	17.20
C_3H_7	11.23	8.42	13.47	17.14

Table 22. Appearance Potentials A_p(in eV) for $C_2H_k^+$(k=3,4,5) and H^+ Ion-Production Channels in e+C3Hy (y=1-7) Dissociative Ionization. (From[44,45])

C_3H_y	$C_2H_3^+$	$C_2H_4^+$	$C_2H_5^+$	H^+
C_3H	—	—	—	21.40 (a)
C_3H_2	—	—	—	14.15
C_3H_3	16.38	—	—	17.59
C_3H_4	15.86	16.41	—	—
C_3H_5	14.40	15.83	15.61	—
C_3H_6	13.31	14.73	15.48	—
C_3H_7	9.92	11.44	12.59	—

Note: (a)The C^+ and C_2^+ ion-produciton channels from C_3H dissociative ionization fave A_p's 25.3eV and 24.1eV, respectively.

Appendix 1. Values of fitting coefficients in Eq.(15) for total and partial ionization cross sections in $e + C_xH_y$ collisions

For each process, I_p, N and B_i (i runs from 1 to N) are listed. 5.1090E+02 means 5.1090×10^2.

A-1.1 $e + CH_y$ systems

A-1.1.1 e + CH

(a) Total cross section

process	I_p	N	B_i					
$e + CH \rightarrow$ total ionization	1.1200E+01	8	1.2258E+00	-3.0764E+00	2.6182E+01	-1.4891E+02	4.3224E+02	-6.6387E+02
			5.1090E+02	-1.5314E+02				

(b) Partial cross sections

process	I_p	N	B_i					
$e + CH \rightarrow CH^+ + 2e$	1.1300E+01	6	1.4439E+00	-1.2724E+00	-2.2221E+00	9.2822E+00	-1.5506E+01	8.2778E+00
$e + CH \rightarrow C^+H + 2e$	1.4800E+01	6	4.3045E-01	-4.1305E-01	-5.6881E-01	3.2957E+00	-5.6549E+00	3.4295E+00
$e + CH \rightarrow C + H^+ + 2e$	1.7140E+01	6	4.4144E-02	-1.8579E-02	-4.1046E-01	2.3115E+00	-4.1040E+00	2.7436E+00

A-1.1.2 $e + CH_2$

(a) Total cross section

process	I_p	N	B_i					
$e + CH_2 \rightarrow$ total ionization	1.0910E+01	6	2.9597E+00	-2.6451E+00	-3.7136E+00	8.9168E+00	-1.2872E+01	5.8594E+00

(b) Partial cross sections

process	I_p	N	B_i					
$e + CH_2 \rightarrow CH_2^+ + 2e$	1.0400E+01	6	1.7159E+00	-1.7164E+00	-6.5529E-01	2.1724E+00	-5.4186E+00	3.1616E+00
$e + CH_2 \rightarrow CH^+ + H + 2e$	1.5530E+01	6	8.1919E-01	-7.5016E-01	-3.8063E-03	1.4065E+00	-3.6447E+00	2.6220E+00
$e + CH_2 \rightarrow C^+ + H_2 + 2e$	1.7100E+01	6	3.8400E-02	-2.91786E-02	-0.98490E-01	0.73008E+00	-1.2111E+00	0.85722E+00
$e + CH_2 \rightarrow CH + H^+ + 2e$	2.2300E+01	6	-5.8168E-02	8.2064E-02	5.2048E-02	3.1915E-01	-1.3363E-01	2.3477E-01
$e + CH_2 \rightarrow C + H_2^+ + 2e$	2.4800E+01	6	2.7682E-02	5.0215E-02	3.7494E-04	5.1300E-01	-6.1525E-01	6.2835E-01

A-1.1.3 $e + CH_3$

(a) Total cross section

process	I_p	N	B_i					
$e + CH_3 \rightarrow$ total ionization	9.8400E+00	6	2.4221E+00	-2.4368E+00	-7.4454E-01	4.6634E-01	-4.1606E+00	4.5799E+00

(b) Partial cross sections

process	I_p	N	B_i					
$e + CH_3 \rightarrow CH_3^+ + 2e$	9.8000E+00	6	1.9725E+00	-2.1011E+00	1.0593E+00	-6.3438E+00	8.0140E+00	-4.2440E+00
$e + CH_3 \rightarrow CH_2^+ + H + 2e$	1.4000E+01	6	1.2824E+00	-1.3906E+00	6.2993E-01	9.4521E-01	-5.3629E+00	4.3087E+00
$e + CH_3 \rightarrow CH^+ + H_2 + 2e$	1.6000E+01	6	1.1666E-01	-1.1254E-01	1.5594E-01	-7.3177E-02	-2.1307E-01	5.5290E-01
$e + CH_3 \rightarrow CH_2 + H^+ + 2e$	1.8480E+01	6	-2.1667E-02	3.2699E-02	-1.3308E-01	1.1473E+00	-1.9437E+00	1.5827E+00
$e + CH_3 \rightarrow CH + H_2^+ + 2e$	2.0180E+01	6	-4.4067E-03	8.6072E-03	-2.0148E-02	1.6728E-01	-2.6542E-01	2.1110E-01
$e + CH_3 \rightarrow C^+ + H_2 + H + 2e$	1.9540E+01	6	-9.5279E-03	1.7251E-02	-5.1275E-02	4.0755E-01	-6.5843E-01	5.1835E-01

A-1.1.4 $e + CH_4$

(a) Total cross section

process	I_p	N	B_i					
$e + CH_4 \rightarrow$ total ionization	1.2630E+01	6	2.3449E+00	-2.6163E+00	2.1843E-01	1.0890E+01	-2.9718E+01	2.4582E+01

(b) Partial cross sections

process	I_p	N	B_i					
$e + CH_4 \rightarrow CH_4^+ + 2e$	1.2630E+01	6	1.3541E+00	-1.4665E+00	1.6787E-01	6.1801E+00	-1.5638E+01	1.0767E+01
$e + CH_4 \rightarrow CH_3^+ + H + 2e$	1.4010E+01	6	1.6074E+00	-1.4713E+00	-2.7386E-01	1.9556E-01	1.1343E-01	9.0166E-03
$e + CH_4 \rightarrow CH_2^+ + H_2 + 2e$	1.6200E+01	6	1.6252E-01	-1.0708E-01	-3.2252E-01	8.7125E-01	-1.8747E-02	1.3071E-01
$e + CH_4 \rightarrow CH^+ + H_2 + H + 2e$	2.2200E+01	6	-1.2458E-01	1.6287E-01	-3.3395E-01	3.5738E+00	-5.0472E+00	2.8240E+00
$e + CH_4 \rightarrow C^+ + 2H_2 + 2e$	2.2000E+01	6	-6.2138E-02	4.4747E-02	1.7054E-01	-2.2989E-01	7.7426E-01	-2.9020E-01
$e + CH_4 \rightarrow CH_2 + H_2^+ + 2e$	2.2300E+01	6	-1.7615E-02	1.8347E-02	-5.0664E-02	2.6118E-01	1.5316E-01	-1.7314E-01
$e + CH_4 \rightarrow CH_3 + H^+ + 2e$	2.1100E+01	6	-3.4698E-01	-1.6026E-02	4.3296E+00	-1.5155E+01	2.4766E+01	-1.0873E+01

A-1.2 $e + C_2H_y$ systems

A-1.2.1 $e + C_2H$

(a) **Total cross section**

process	I_p	N	B_i					
$e + C_2H \rightarrow$ total ionization	1.1220E+01	6	3.2202E+00	-2.8152E+00	-5.8088E+00	2.9504E+01	-5.8412E+01	3.9669E+01

(b) **Partial cross sections**

process	I_p	N	B_i					
$e + C_2H \rightarrow C_2H^+ + 2e$	1.1000E+01	6	2.8838E+00	-2.5628E+00	-5.4320E+00	2.8889E+01	-5.7295E+01	3.7708E+01
$e + C_2H \rightarrow C_2^+ + H + 2e$	1.6600E+01	6	1.8190E-01	-1.3742E-01	1.9606E-01	1.5691E+00	-3.4910E+00	2.8130E+00
$e + C_2H \rightarrow CH^+ + C + 2e$	2.0000E+01	6	1.0185E-01	-9.2971E-02	2.0310E-02	1.8823E-01	9.2660E-01	-5.2016E-01
$e + C_2H \rightarrow C^+ + CH + 2e$	2.1500E+01	6	6.8836E-02	-7.7999E-02	2.6112E-01	-4.3316E-01	1.0820E+00	-5.5750E-01
$e + C_2H \rightarrow C_2 + H^+ + 2e$	1.8100E+01	6	-5.1850E-03	4.5961E-02	-7.0162E-01	3.8420E+00	-5.5680E+00	3.2844E+00

A-1.2.2 $e + C_2H_2$

(a) **Total cross section**

process	I_p	N	B_i					
$e + C_2H_2 \rightarrow$ total ionization	1.5500E+01	6	4.4672E+00	-1.3171E+00	-1.9831E+01	8.1048E+01	-1.3186E+02	7.8763E+01

(b) **Partial cross sections**

process	I_p	N	B_i					
$e + C_2H_2 \rightarrow C_2H_2^+ + 2e$	1.5400E+01	6	4.2151E+00	-1.4139E+00	-1.5703E+01	6.1345E+01	-1.0070E+02	5.6335E+01
$e + C_2H_2 \rightarrow C_2H^+ + H + 2e$	1.7700E+01	6	6.1452E-01	-3.4326E-01	-1.9464E+00	1.3746E+01	-2.4790E+01	1.4872E+01
$e + C_2H_2 \rightarrow C_2^+ + H_2 + 2e$	2.2600E+01	6	-1.2316E-01	1.7484E-01	7.3057E-01	8.9691E-01	-2.7137E+00	2.4490E+00
$e + C_2H_2 \rightarrow CH^+ + CH + 2e$	2.3900E+01	6	-9.6563E-02	1.7049E-01	1.6868E+00	-4.9120E+00	1.0656E+01	-5.5749E+00
$e + C_2H_2 \rightarrow C^+ + CH_2 + 2e$	2.8500E+01	6	2.9296E-02	1.0247E-01	1.5647E+00	-6.8246E+00	1.4659E+01	-8.3645E+00
$e + C_2H_2 \rightarrow H^+ + C_2H + 2e$	2.4000E+01	6	2.6407E-03	2.0240E-01	7.3429E-03	-9.3824E-01	7.7448E+00	-5.1682E+00
$e + C_2H_2 \rightarrow C_2H_2^{2+} + 3e$	5.0000E+01	6	5.8712E-02	-9.1017E+00	5.5948E+01	-1.2562E+02	1.2516E+02	-4.6304E+01
$e + C_2H_2 \rightarrow C_2H^{2+} + H + 3e$	7.0000E+01	6	1.4407E-04	-6.8112E-04	5.1788E-02	-1.2682E-01	1.2149E-01	-4.3423E-02

A-1.2.3 $e + C_2H_3$

(a) **Total cross section**

process	I_p	N	B_i					
$e + C_2H_3 \rightarrow$ total ionization	1.0230E+01	6	3.7814E+00	-3.1886E+00	-8.8629E+00	3.6097E+01	-6.6447E+01	4.1577E+01

(b) Partial cross sections

process	I_p	N	B_i					
$e + C_2H_3 \rightarrow C_2H_3^+ + 2e$	1.0000E+01	6	2.1638E+00	-1.8885E+00	-3.9536E+00	1.6627E+01	-3.1823E+01	1.9787E+01
$e + C_2H_3 \rightarrow C_2H_2^+ + H + 2e$	1.2300E+01	6	9.1180E-01	-8.4482E-01	-8.3155E-01	4.7606E+00	-1.0715E+01	7.7800E+00
$e + C_2H_3 \rightarrow C_2H^+ + H_2/2H + 2e$	1.3100E+01	6	3.6351E-01	-3.1960E-01	-6.6137E-01	4.2235E+00	-8.4395E+00	6.1642E+00
$e + C_2H_3 \rightarrow C_2H^+ + H_2 + 2e$	1.3100E+01	6	3.3047E-01	-2.9055E-01	-6.0125E-01	3.8396E+00	-7.6723E+00	5.6039E+00
$e + C_2H_3 \rightarrow C_2H^+ + 2H + 2e$	1.3100E+01	6	3.3047E-02	-2.9055E-02	-6.0125E-02	3.8396E-01	-7.6723E-01	5.6039E-01
$e + C_2H_3 \rightarrow C_2^+ + H_2 + H + 2e$	2.3400E+01	6	5.1232E-02	-3.4944E-02	3.3463E-01	-7.4796E-01	1.3188E+00	-5.9278E-01
$e + C_2H_3 \rightarrow CH_2^+ + CH + 2e$	2.0000E+01	6	2.6169E-02	-1.8406E-02	3.0591E-02	7.0391E-02	-1.3010E-01	1.6045E-01
$e + C_2H_3 \rightarrow CH^+ + CH_2 + 2e$	2.5000E+01	6	3.6483E-02	-6.5833E-02	1.6869E+00	-4.2141E+00	6.0795E+00	-2.6635E+00
$e + C_2H_3 \rightarrow C^+ + CH_3 + 2e$	2.1100E+01	6	1.0349E-01	-1.1251E-01	5.2156E-01	-1.6825E+00	2.8676E+00	-1.3848E+00
$e + C_2H_3 \rightarrow H^+ + C_2H_2 + 2e$	2.1100E+01	6	1.1828E-01	-1.2858E-01	5.9606E-01	-1.9229E+00	3.2773E+00	-1.5826E+00

A-1.2.4 $e + C_2H_4$

(a) Total cross section

process	I_p	N	B_i					
$e + C_2H_4 \rightarrow$ total ionization	1.0450E+01	6	4.3521E+00	-4.0953E+00	-5.4465E+00	1.9260E+01	-3.9235E+01	2.7143E+01

(b) Partial cross sections

process	I_p	N	B_i					
$e + C_2H_4 \rightarrow C_2H_4^+ + 2e$	1.1000E+01	6	2.1339E+00	-2.1027E+00	-1.4991E+00	7.6831E+00	-1.8586E+01	1.3248E+01
$e + C_2H_4 \rightarrow C_2H_3^+ + H + 2e$	1.2600E+01	6	1.0771E+00	-1.1006E+00	-7.1624E-01	5.6861E+00	-1.3597E+01	1.0568E+01
$e + C_2H_4 \rightarrow C_2H_2^+ + H_2 + 2e$	1.4300E+01	6	6.3131E-01	-5.7812E-01	-6.2781E-01	5.3546E+00	-1.1487E+01	9.5818E+00
$e + C_2H_4 \rightarrow C_2H^+ + H_2 + H + 2e$	2.3500E+01	6	3.0122E-01	-2.8740E-01	-1.9558E-01	1.8746E+00	-1.8614E+00	7.4894E-01
$e + C_2H_4 \rightarrow C_2^+ + 2H_2 + 2e$	2.5600E+01	6	1.4016E-02	-3.3329E-02	4.8119E-01	-1.2222E+00	2.0053E+00	-9.5120E-01
$e + C_2H_4 \rightarrow CH_3^+ + CH + 2e$	2.1500E+01	6	6.7093E-02	-3.2712E-02	-2.5428E-01	1.5686E+00	-2.2885E+00	1.3626E+00
$e + C_2H_4 \rightarrow CH_2^+ + CH_2 + 2e$	2.1500E+01	6	6.1553E-02	-3.0011E-02	-2.3328E-01	1.4391E+00	-2.0995E+00	1.2501E+00
$e + C_2H_4 \rightarrow CH^+ + CH_3 + 2e$	2.7400E+01	6	4.7646E-02	-3.0637E-02	2.2730E-01	-4.6992E-01	7.4920E-01	-3.5489E-01
$e + C_2H_4 \rightarrow C^+ + (CH_2 + H_2)/(CH_3 + H) + 2e$	2.8800E+01	6	2.0449E-02	-7.1556E-03	2.1225E-01	-6.3042E-01	9.6428E-01	-4.3114E-01

A-1.2.5 $e + C_2H_5$

(a) **Total cross section**

process	I_p	N	B_i					
$e + C_2H_5 \rightarrow$ total ionization	1.0720E+01	6	3.2266E+00	-2.9214E+00	-4.6995E+00	2.0847E+01	-4.3907E+01	3.2627E+01

(b) **Partial cross sections**

process	I_p	N	B_i					
$e + C_2H_5 \rightarrow C_2H_5^+ + 2e$	9.2900E+00	6	1.0396E+00	-1.0585E+00	-7.8373E-01	4.4709E+00	-1.0590E+01	7.2951E+00
$e + C_2H_5 \rightarrow C_2H_4^+ + H + 2e$	1.1500E+01	6	7.3095E-01	-7.1416E-01	-5.0556E-01	4.1229E+00	-9.9820E+00	7.4219E+00
$e + C_2H_5 \rightarrow C_2H_3^+ + H_2 + 2e$	1.2100E+01	6	8.1673E-01	-7.8552E-01	-1.1560E+00	9.7883E+00	-2.1341E+01	1.5713E+01
$e + C_2H_5 \rightarrow C_2H_2^+ + H_2 + H + 2e$	1.6300E+01	6	3.8144E-01	-3.7062E-01	-1.8209E-01	2.1859E+00	-2.5851E+00	2.3403E+00
$e + C_2H_5 \rightarrow C_2H^+ + 2H_2 + 2e$	1.8100E+01	6	2.6686E-01	-3.2896E-01	8.6054E-01	-2.9524E+00	5.1638E+00	-2.4925E+00
$e + C_2H_5 \rightarrow CH_3^+ + CH_2 + 2e$	1.8100E+01	6	2.1412E-01	-2.8591E-01	1.0153E+00	-3.9444E+00	6.5300E+00	-3.4506E+00
$e + C_2H_5 \rightarrow CH_2^+ + CH_3 + 2e$	1.8700E+01	6	8.0482E-02	-1.3470E-01	8.2172E-01	-3.0297E+00	4.7510E+00	-2.1714E+00
$e + C_2H_5 \rightarrow CH^+ + CH_4 + 2e$	2.0000E+01	6	3.5922E-02	-7.9976E-02	5.6120E-01	-1.6337E+00	2.1472E+00	-7.6633E-01
$e + C_2H_5 \rightarrow C^+ + (CH_4 + H)/(CH_3 + H_2) + 2e$	2.4600E+01	6	-3.4867E-03	1.6590E-02	9.1837E-02	-3.1695E-02	6.7634E-03	1.7756E-01

A-1.2.6 $e + C_2H_6$

(a) **Total cross section**

process	I_p	N	B_i					
$e + C_2H_6 \rightarrow$ total ionization	1.1520E+01	6	5.2541E+00	-5.4485E+00	4.0002E-01	-1.4406E+00	-8.0654E+00	1.1302E+01

(b) **Partial cross sections**

process	I_p	N	B_i					
$e + C_2H_6 \rightarrow C_2H_6^+ + 2e$	1.1600E+01	6	8.2615E-01	-8.2021E-01	-5.6633E-02	-2.1538E-01	-3.3404E-01	-2.2170E-01
$e + C_2H_6 \rightarrow C_2H_5^+ + H + 2e$	1.2650E+01	6	5.5541E-01	-5.4868E-01	-6.5438E-01	4.1294E+00	-8.2258E+00	4.8497E+00
$e + C_2H_6 \rightarrow C_2H_4^+ + H_2 + 2e$	1.1810E+01	5	3.2570E+00	-3.2295E+00	-2.3531E+00	4.2286E+00	-4.0175E+00	
$e + C_2H_6 \rightarrow C_2H_3^+ + H_2 + H + 2e$	1.5000E+01	5	1.2029E+00	-1.0931E+00	-9.2486E-01	2.5826E+00	-1.0069E+00	
$e + C_2H_6 \rightarrow C_2H_2^+ + 2H_2 + 2e$	1.6000E+01	6	2.2917E-01	-7.6755E-02	-5.1260E-01	4.2754E-01	3.4436E+00	-1.5903E+00
$e + C_2H_6 \rightarrow C_2H^+ + 2H_2 + H + 2e$	2.7500E+01	6	-1.0284E-01	1.0591E-01	2.4415E+00	-7.2489E+00	1.2360E+01	-6.6793E+00
$e + C_2H_6 \rightarrow CH_3^+ + CH_3 + 2e$	1.5500E+01	6	2.9446E-01	-3.4463E-01	4.1525E-01	-7.9157E-01	7.6763E-01	-1.7526E-01
$e + C_2H_6 \rightarrow CH_2^+ + CH_4 + 2e$	2.6000E+01	6	-1.5131E-01	8.9757E-02	9.5436E-01	4.9445E-01	-9.6513E-01	6.8539E-01
$e + C_2H_6 \rightarrow CH^+ + (CH_3 + H_2)/(CH_4 + H) + 2e$	2.4200E+01	6	-9.2310E-02	-1.2519E-02	1.1308E+00	-2.9895E+00	5.0173E+00	-2.4317E+00
$e + C_2H_6 \rightarrow C_2^+ + 3H_2 + 2e$	3.0200E+01	6	-2.4726E-02	-1.2327E-01	1.6520E+00	-5.5917E+00	8.8261E+00	-4.4963E+00
$e + C_2H_6 \rightarrow C^+ + CH_4 + H_2 + 2e$	3.0500E+01	6	-3.3797E-02	-2.7912E-02	7.5677E-01	-2.3435E+00	4.1065E+00	-2.2066E+00
$e + C_2H_6 \rightarrow C_2H_5^{2+} + H + 3e$	3.5500E+01	6	-3.8235E-03	4.7880E-03	1.0142E-01	-1.0201E-01	4.6253E-02	-2.4543E-03

A-1.3 $e + C_3H_y$ systems

A-1.3.1 $e + C_3H$

process	I_p	N	B_i					
$e + C_3H \rightarrow$ total ionization	1.3400E+01	6	2.9764E+00	-2.3477E+00	-1.3216E+01	7.3427E+01	-1.3479E+02	9.1416E+01

A-1.3.2 $e + C_3H_2$

process	I_p	N	B_i					
$e + C_3H_2 \rightarrow$ total ionization	1.2500E+01	6	3.4541E+00	-2.5401E+00	-1.5431E+01	7.8784E+01	-1.4284E+02	9.3027E+01

A-1.3.3 $e + C_3H_3$

process	I_p	N	B_i					
$e + C_3H_3 \rightarrow$ total ionization	8.3400E+00	6	3.9516E+00	6.1981E+00	-8.5488E+01	2.4758E+02	-3.1654E+02	1.4805E+02

A-1.3.4 $e + C_3H_4$

process	I_p	N	B_i					
$e + C_3H_4 \rightarrow$ total ionization	9.6900E+00	6	5.6635E+00	-3.4929E+00	-2.5611E+01	8.4138E+01	-1.2944E+02	7.1372E+01

A-1.3.5 $e + C_3H_5$

process	I_p	N	B_i					
$e + C_3H_5 \rightarrow$ total ionization	9.9000E+00	6	6.1485E+00	-3.4551E+00	-3.2501E+01	1.0869E+02	-1.6248E+02	8.5999E+01

A-1.3.6 $e + C_3H_6$

process	I_p	N	B_i					
$e + C_3H_6 \rightarrow$ total ionization	9.9000E+00	6	6.8619E+00	-5.7820E+00	-1.5514E+01	5.3625E+01	-9.3645E+01	5.5264E+01

A-1.3.7 $e + C_3H_7$

process	I_p	N	B_i					
$e + C_3H_7 \rightarrow$ total ionization	9.1000E+00	6	6.3672E+00	-2.3655E+00	-4.0355E+01	1.2121E+02	-1.6787E+02	8.3031E+01

A-1.3.8 $e + C_3H_8$

(a) Total cross section

process	I_p	N	B_i					
$e + C_3H_8 \rightarrow$ total ionization	1.1080E+01	6	9.2375E+00	-8.9512E+00	-8.1610E+00	2.0096E+01	-3.5203E+01	2.0414E+01

(b) Partial cross sections

process	I_p	N	B_i					
$e + C_3H_8 \rightarrow C_3H_8^+ + 2e$	1.4300E+01	6	1.1449E+00	-6.1376E-01	-2.7962E+00	6.2843E+00	-7.7244E+00	2.8788E+00
$e + C_3H_8 \rightarrow C_3H_7^+ + H + 2e$	1.4320E+01	6	1.0161E+00	-1.0639E+00	1.1574E+00	-4.4077E+00	5.0090E+00	-2.6962E+00
$e + C_3H_8 \rightarrow C_3H_6^+ + H_2 + 2e$	1.8110E+01	6	2.0241E-01	-1.0303E-01	-1.5354E-01	6.5766E-01	-1.5173E+00	1.0456E+00
$e + C_3H_8 \rightarrow C_3H_5^+ + H_2 + H + 2e$	1.5400E+01	6	6.2959E-01	-5.7820E-01	-4.2275E-01	1.0438E+00	-1.2310E+00	1.5894E-01
$e + C_3H_8 \rightarrow C_3H_4^+ + 2H_2 + 2e$	1.6250E+01	6	9.2480E-02	-7.0635E-02	-1.9218E-01	6.0213E-01	-6.7201E-01	2.2408E-01
$e + C_3H_8 \rightarrow C_3H_3^+ + 2H_2 + H + 2e$	1.9000E+01	6	8.5033E-01	-5.9487E-01	-2.9271E+00	1.4455E+01	-1.9396E+01	8.6935E+00
$e + C_3H_8 \rightarrow C_3H_2^+ + 3H_2 + 2e$	2.5030E+01	6	-2.6317E-01	3.3089E-01	1.6290E+00	-3.4753E+00	7.9786E+00	-4.1578E+00
$e + C_3H_8 \rightarrow C_3H^+ + 3H_2 + H + 2e$	2.6000E+01	6	-1.8486E-01	1.9884E-01	1.0565E+00	-3.8196E+00	9.3217E+00	-5.2271E+00
$e + C_3H_8 \rightarrow C_3^+ + 4H_2 + 2e$	3.7000E+01	6	-1.8126E-02	-1.2458E-02	7.8290E-01	-2.2762E+00	4.4177E+00	-2.6932E+00
$e + C_3H_8 \rightarrow C_2H_5^+$ (total)	1.5500E+01	6	3.3493E+00	-1.4701E+00	-1.1776E+01	3.7323E+01	-5.4124E+01	2.7061E+01
$e + C_3H_8 \rightarrow C_2H_5^+ + CH_3 + 2e$	1.3920E+01	6	1.8084E+00	-1.4952E+00	-2.6108E+00	9.2923E+00	-1.5153E+01	7.6576E+00
$e + C_3H_8 \rightarrow C_2H_5^+ + CH_2 + H + 2e$	1.3520E+01	6	9.6666E-01	-8.2170E-01	-1.4347E+00	5.0765E+00	-8.1327E+00	4.0249E+00
$e + C_3H_8 \rightarrow C_2H_5^+ + CH + H_2 + 2e$	1.5440E+01	6	4.9612E-01	-2.0251E-01	-1.9007E+00	6.0396E+00	-8.6886E+00	4.3218E+00
$e + C_3H_8 \rightarrow C_2H_4^+$ (total)	1.4190E+01	6	2.0981E+00	-2.3192E+00	2.6151E+00	-9.6433E+00	1.1904E+01	-6.4075E+00
$e + C_3H_8 \rightarrow C_2H_4^+ + CH_4 + 2e$	1.4190E+01	6	9.4413E-01	-1.0436E+00	1.1768E+00	-4.3395E+00	5.3567E+00	-2.8834E+00
$e + C_3H_8 \rightarrow C_2H_4^+ + CH_3 + H + 2e$	1.4190E+01	6	7.3433E-01	-8.1173E-01	9.1530E-01	-3.3752E+00	4.1664E+00	-2.2426E+00
$e + C_3H_8 \rightarrow C_2H_4^+ + CH_2 + H_2 + 2e$	1.4190E+01	6	3.1471E-01	-3.4788E-01	3.9227E-01	-1.4465E+00	1.7856E+00	-9.6113E-01
$e + C_3H_8 \rightarrow C_2H_4^+ + CH + H_2 + H + 2e$	1.4190E+01	6	1.0490E-01	-1.1596E-01	1.3076E-01	-4.8217E-01	5.9519E-01	-3.2038E-01
$e + C_3H_8 \rightarrow C_2H_3^+$ (total)	2.4600E+01	6	3.1460E+00	-2.2731E+00	1.6790E+01	-5.9326E+01	7.6575E+01	-3.3943E+01
$e + C_3H_8 \rightarrow C_2H_3^+ + CH_4 + H + 2e$	1.7500E+01	6	4.8967E-01	-1.6033E-01	-2.3282E-01	-8.4995E-01	2.3019E+00	-1.1694E+00
$e + C_3H_8 \rightarrow C_2H_3^+ + CH_3 + H_2 + 2e$	2.4600E+01	6	1.5074E+00	-1.6355E-01	-1.1436E+00	3.4966E-01	1.9949E+00	-9.9793E-01
$e + C_3H_8 \rightarrow C_2H_3^+ + CH_2 + H_2 + H + 2e$	3.3000E+01	6	1.0379E-01	4.1519E-01	-2.7020E+00	7.2257E+00	-8.2132E+00	3.4544E+00
$e + C_3H_8 \rightarrow C_2H_3^+ + CH + 2H_2 + 2e$	2.8700E+01	6	1.9840E-01	1.2298E-01	-9.1546E-01	2.2331E+00	-2.4088E+00	9.6347E-01
$e + C_3H_8 \rightarrow C_2H_2^+$ (total)	2.1380E+01	6	4.0247E-01	-2.9371E-01	-1.4692E-01	1.0883E+00	2.9111E+00	-2.7502E+00
$e + C_3H_8 \rightarrow C_2H_2^+ + CH_4 + H_2 + 2e$	2.1380E+01	6	2.4148E-01	-1.7622E-01	-8.8151E-02	6.5296E-01	1.7467E+00	-1.6501E+00
$e + C_3H_8 \rightarrow C_2H_2^+ + CH_3 + H_2 + H + 2e$	2.1380E+01	6	1.0062E-01	-7.3427E-02	-3.6730E-02	2.7207E-01	7.2778E-01	-6.8754E-01
$e + C_3H_8 \rightarrow C_2H_2^+ + CH_2 + 2H_2 + 2e$	2.1380E+01	6	6.0371E-02	-4.4056E-02	-2.2038E-02	1.6324E-01	4.3667E-01	-4.1252E-01

process	I_p	N	B_i					
$e + C_3H_8 \rightarrow C_2H^+$ (total)	2.3060E+01	6	2.0075E-01	-2.4075E-01	4.4626E-01	-2.0128E+00	3.2211E+00	-1.6941E+00
$e + C_3H_8 \rightarrow C_2H^+ + CH_4 + H_2 + H + 2e$	2.3060E+01	6	1.0037E-01	-1.2037E-01	2.2313E-01	-1.0064E+00	1.6105E+00	-8.4706E-01
$e + C_3H_8 \rightarrow C_2H^+ + CH_3 + 2H_2 + 2e$	2.3060E+01	6	6.0225E-02	-7.2224E-02	1.3388E-01	-6.0384E-01	9.6632E-01	-5.0824E-01
$e + C_3H_8 \rightarrow C_2H^+ + CH_2 + 2H_2 + H + 2e$	2.3060E+01	6	4.0150E-02	-4.8150E-02	8.9252E-02	-4.0256E-01	6.4421E-01	-3.3882E-01
$e + C_3H_8 \rightarrow C_2^+$ (total)	3.9000E+01	6	-6.7956E-02	4.9925E-02	4.8662E-01	-2.0569E+00	4.0249E+00	-2.2366E+00
$e + C_3H_8 \rightarrow C_2^+ + CH_2 + 3H_2 + 2e$	3.9000E+01	6	-3.0580E-02	2.2466E-02	2.1898E-01	-9.2560E-01	1.8112E+00	-1.0065E+00
$e + C_3H_8 \rightarrow C_2^+ + CH_4 + 2H_2 + 2e$	3.9000E+01	6	-3.7376E-02	2.7459E-02	2.6764E-01	-1.1313E+00	2.2137E+00	-1.2301E+00
$e + C_3H_8 \rightarrow CH_3^+$ (total)	2.4200E+01	6	-2.9172E-02	3.9988E-01	-2.2765E+00	9.4140E+00	-7.6602E+00	2.2697E+00
$e + C_3H_8 \rightarrow CH_3^+ + C_2H_5 + 2e$	2.3000E+01	6	4.9544E-02	-3.9462E-01	3.5653E+00	-1.0382E+01	1.4136E+01	-6.4721E+00
$e + C_3H_8 \rightarrow CH_3^+ + C_2H_4 + H + 2e$	2.3000E+01	6	1.6084E-02	-3.1169E-01	2.8600E+00	-8.1452E+00	1.1321E+01	-5.2918E+00
$e + C_3H_8 \rightarrow CH_3^+ + C_2H_3 + H_2 + 2e$	2.0000E+01	6	-3.0758E-02	5.5540E-02	-1.1295E-01	7.2093E-01	-5.3867E-01	3.4627E-01
$e + C_3H_8 \rightarrow CH_3^+ + C_2H_2 + H_2 + H + 2e$	3.2900E+01	6	4.9495E-02	-7.9001E-02	9.3415E-01	-2.5830E+00	3.2824E+00	-1.4886E+00
$e + C_3H_8 \rightarrow CH_2^+$ (total)	2.1000E+01	6	1.2721E-02	-1.0856E-01	1.1754E+00	-4.9652E+00	9.1847E+00	-4.7603E+00
$e + C_3H_8 \rightarrow CH_2^+ + C_2H_6 + 2e$	2.1000E+01	6	5.7257E-03	-4.8853E-02	5.2894E-01	-2.2344E+00	4.1331E+00	-2.1422E+00
$e + C_3H_8 \rightarrow CH_2^+ + C_2H_5 + H + 2e$	2.1000E+01	6	2.5446E-03	-2.1712E-02	2.3508E-01	-9.9305E-01	1.8369E+00	-9.5207E-01
$e + C_3H_8 \rightarrow CH_2^+ + C_2H_4 + H_2 + 2e$	2.1000E+01	6	4.4531E-03	-3.7996E-02	4.1140E-01	-1.7378E+00	3.2147E+00	-1.6661E+00
$e + C_3H_8 \rightarrow CH^+$ (total)	3.0770E+01	6	-3.9297E-02	5.5189E-02	5.0500E-01	-2.7586E+00	6.3715E+00	-3.8831E+00
$e + C_3H_8 \rightarrow C_3H_4^{2+} + 2H_2 + 3e$	4.7550E+01	4	-7.4397E-02	2.5027E-01	-5.0397E-02	1.0253E-01		
$e + C_3H_8 \rightarrow C_3H_3^{2+} + 2H_2 + H + 3e$	4.0040E+01	6	-5.5762E-02	4.0342E-02	2.2088E-01	4.4344E-01	-1.0952E+00	6.9354E-01
$e + C_3H_8 \rightarrow C_3H_2^{2+} + 3H_2 + 3e$	4.0880E+01	6	-5.7684E-02	1.0316E-01	-3.7592E-01	2.8206E+00	-4.0827E+00	1.9574E+00
$e + C_3H_8 \rightarrow C_3H_5^{2+} + H_2 + H + 3e$	3.4390E+01	6	1.3656E-03	-4.7994E-05	-2.7414E-03	1.4041E-02	-6.6982E-03	-5.3844E-03
$e + C_3H_8 \rightarrow C^+$ (total)	3.9040E+01	6	-1.9446E-01	2.5057E-01	2.0994E-02	-9.4116E-02	1.6798E+00	-1.1035E+00
$e + C_3H_8 \rightarrow C^+ + C_2H_6 + H_2 + 2e$	3.7040E+01	6	-1.3571E-02	-9.1608E-03	4.8370E-01	-2.0265E+00	3.7257E+00	-2.1042E+00
$e + C_3H_8 \rightarrow C^+ + C_2H_4 + 2H_2 + 2e$	3.7040E+01	6	-1.4702E-02	-9.9242E-03	5.2401E-01	-2.1954E+00	4.0362E+00	-2.2795E+00

Appendix 2. Graphs of cross sections and rate coefficients for total, direct and dissociative ionization in $e + C_xH_y$ collisions

A-2.1 $e + CH_y$ systems

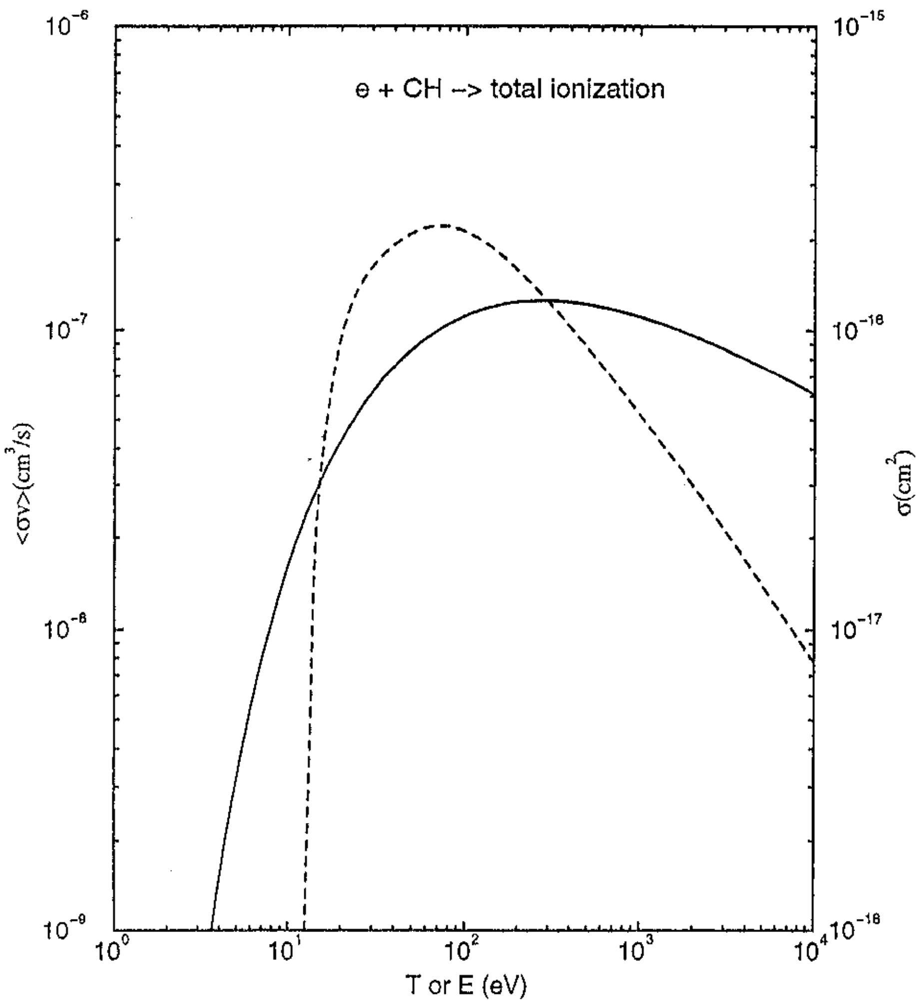

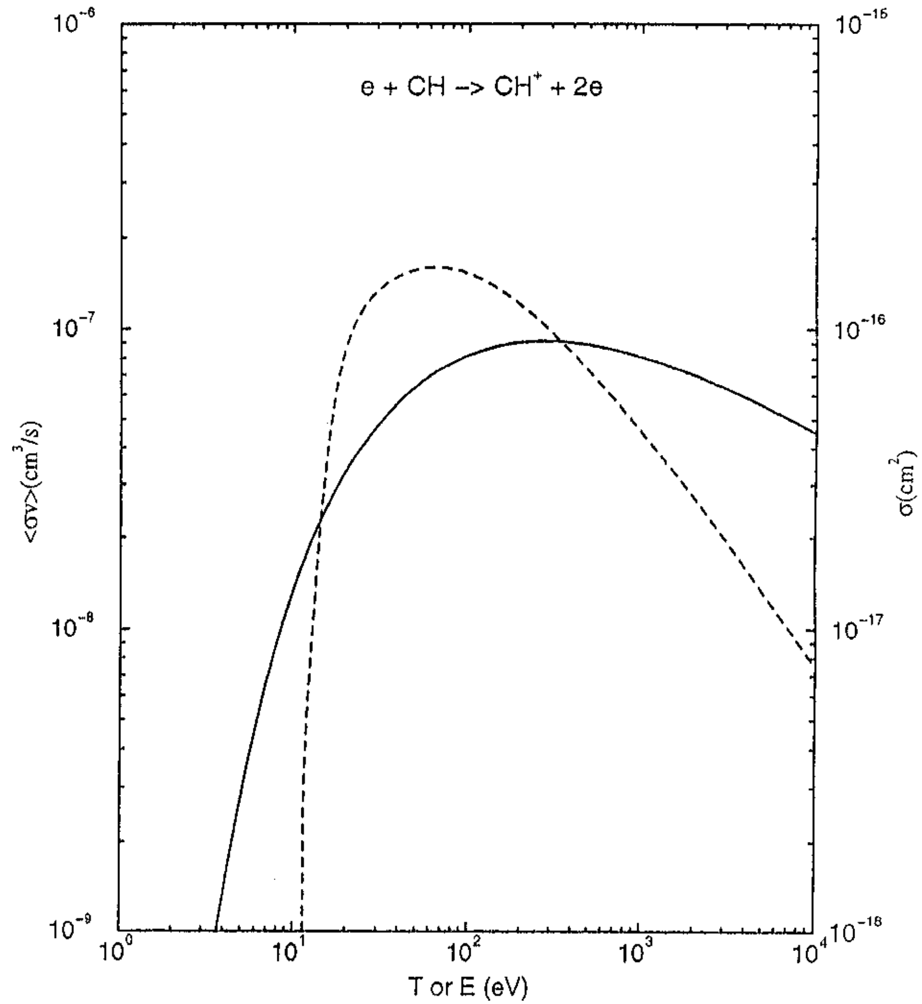

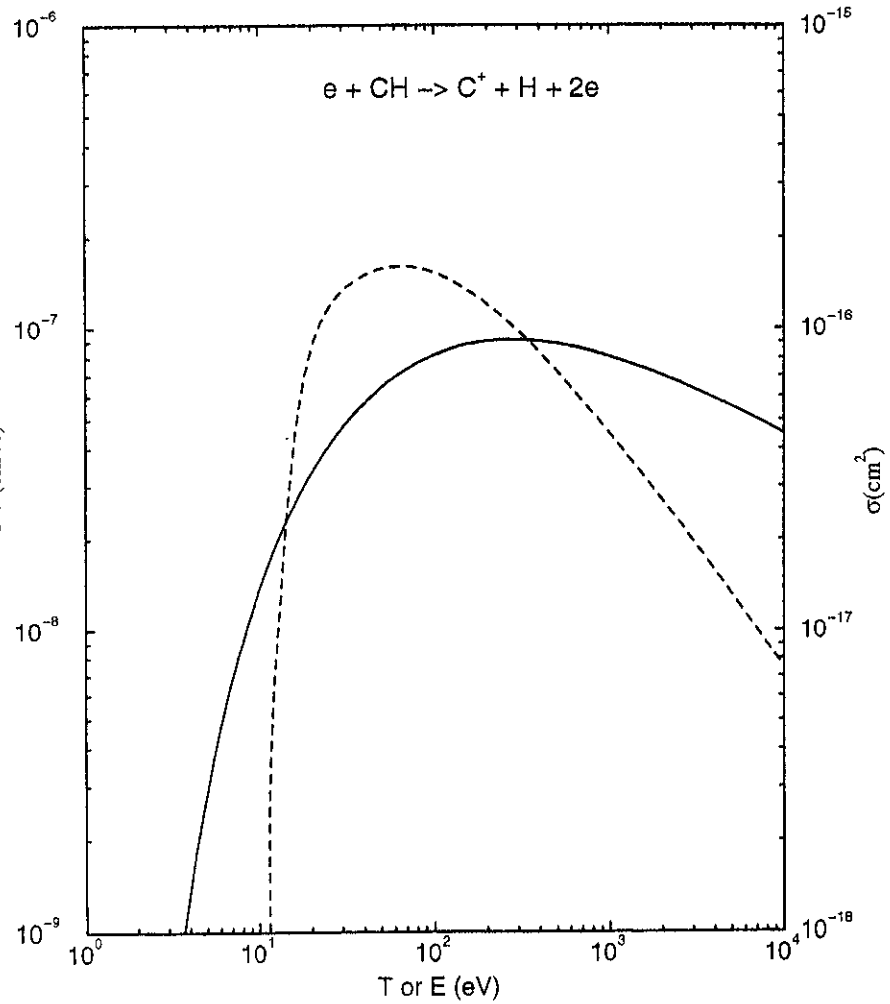
e + CH -> C+ + H + 2e
<σv>(cm3/s)
σ(cm2)
T or E (eV)
10-6
10-7
10-8
10-9
10-15
10-16
10-17
10-18
100
101
102
103
104

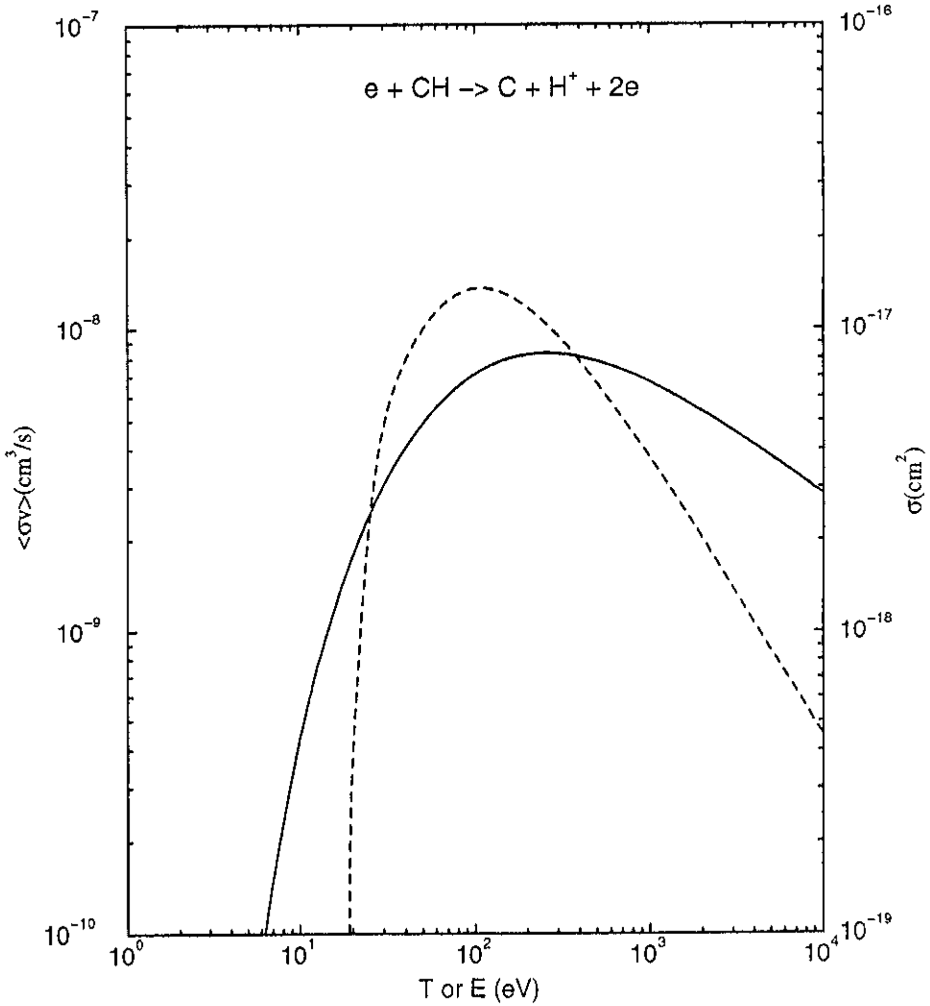
e + CH -> C + H+ + 2e
<σv>(cm3/s)
σ(cm2)
T or E (eV)
10-7
10-8
10-9
10-10
10-16
10-17
10-18
10-19
100
101
102
103
104

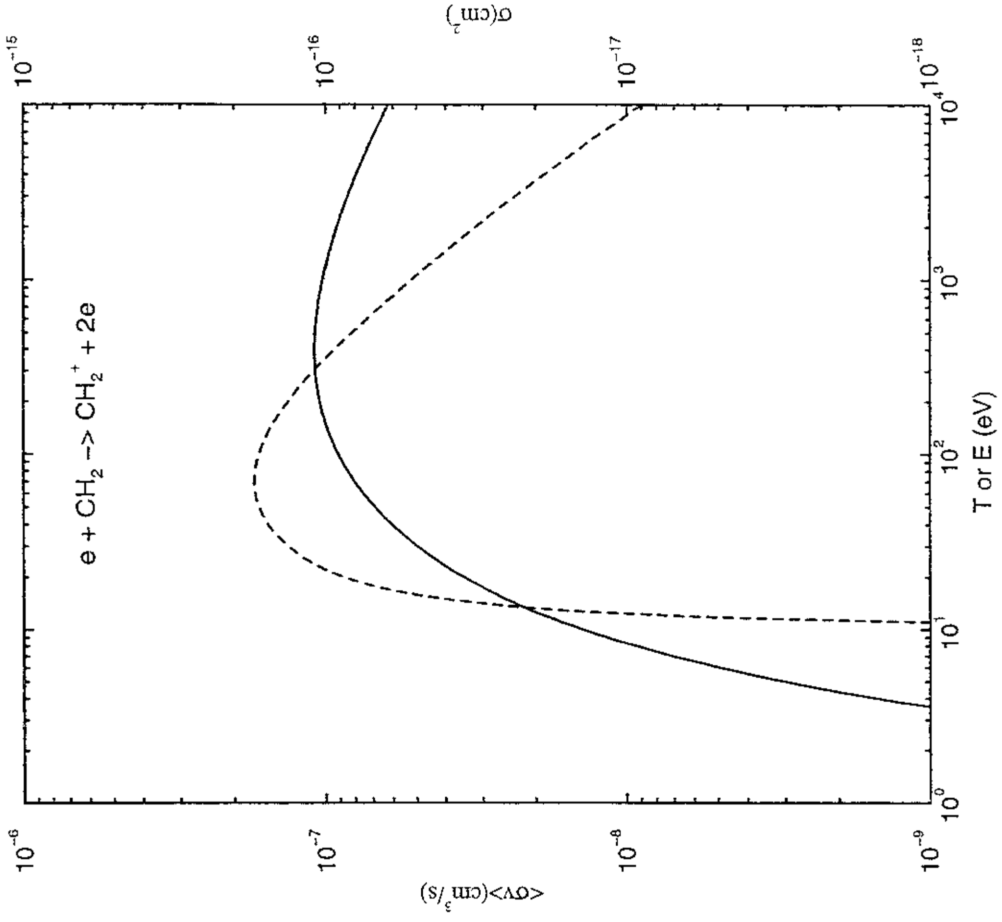
e + CH_2 –> CH_2^+ + 2e
T or E (eV)
<σv>(cm^3/s)
σ(cm^2)
10^0
10^1
10^2
10^3
10^4
10^{-6}
10^{-7}
10^{-8}
10^{-9}
10^{-15}
10^{-16}
10^{-17}
10^{-18}

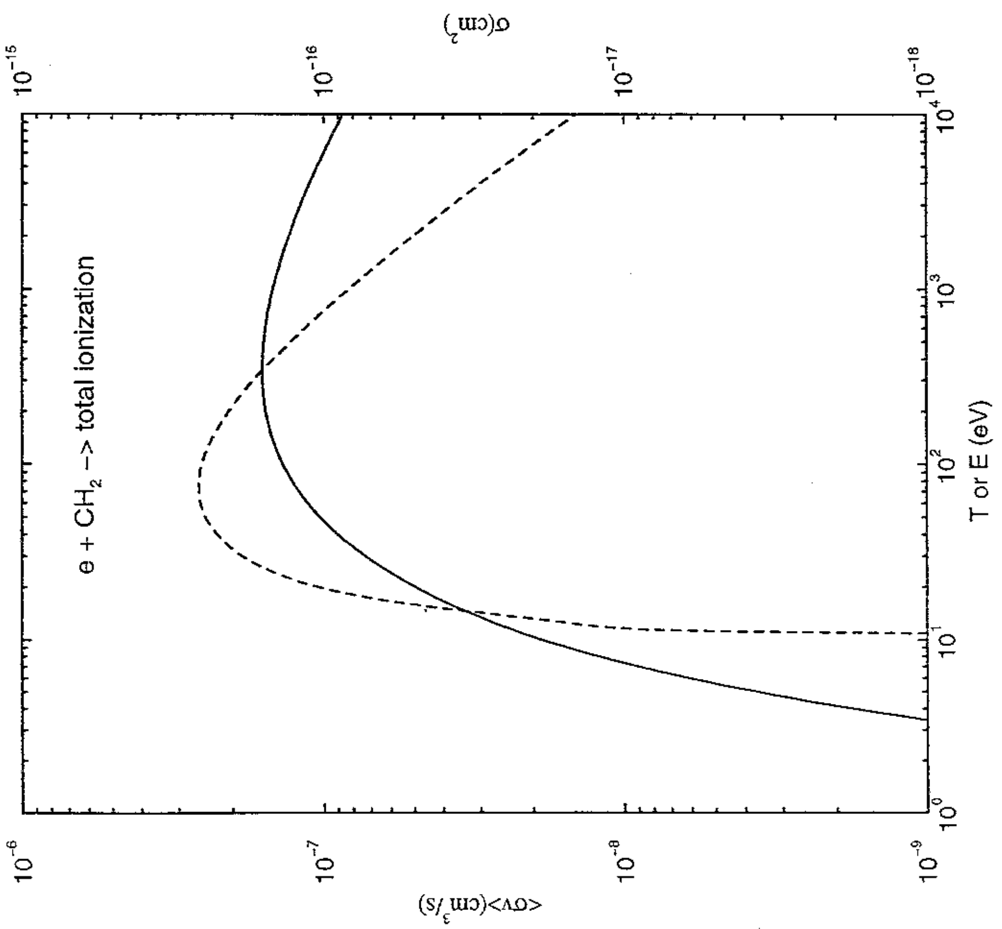
e + CH_2 –> total ionization
T or E (eV)
<σv>(cm^3/s)
σ(cm^2)
10^0
10^1
10^2
10^3
10^4
10^{-6}
10^{-7}
10^{-8}
10^{-9}
10^{-15}
10^{-16}
10^{-17}
10^{-18}

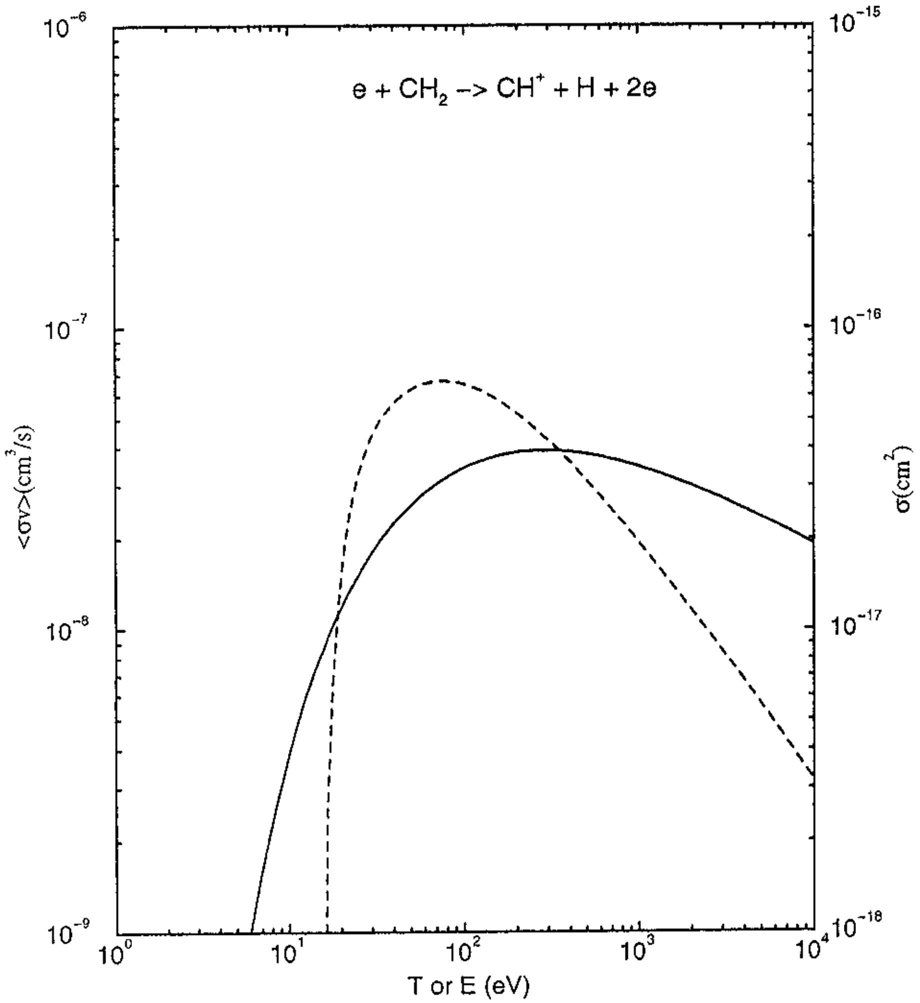
e + CH2 -> CH+ + H + 2e
<σv>(cm3/s)
σ(cm2)
T or E (eV)
10-6
10-7
10-8
10-9
10-15
10-16
10-17
10-18
100
101
102
103
104

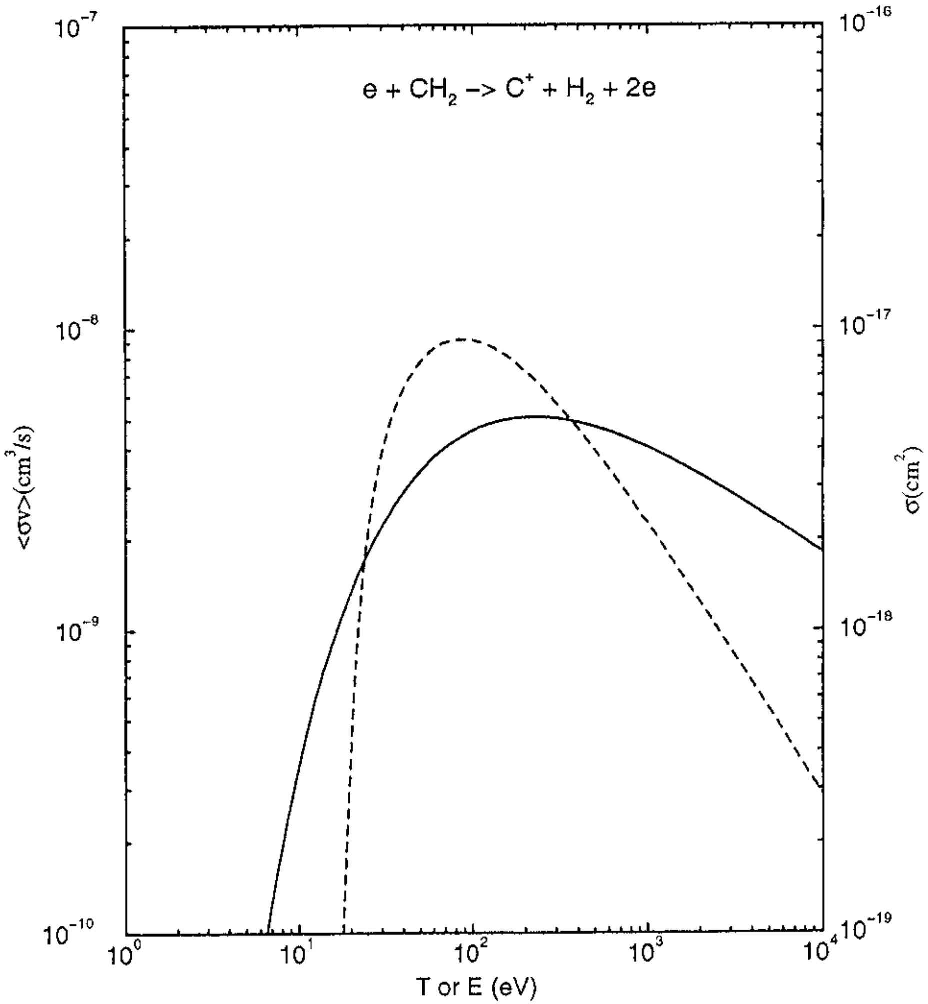
e + CH2 -> C+ + H2 + 2e
<σv>(cm3/s)
σ(cm2)
T or E (eV)
10-7
10-8
10-9
10-10
10-16
10-17
10-18
10-19
100
101
102
103
104

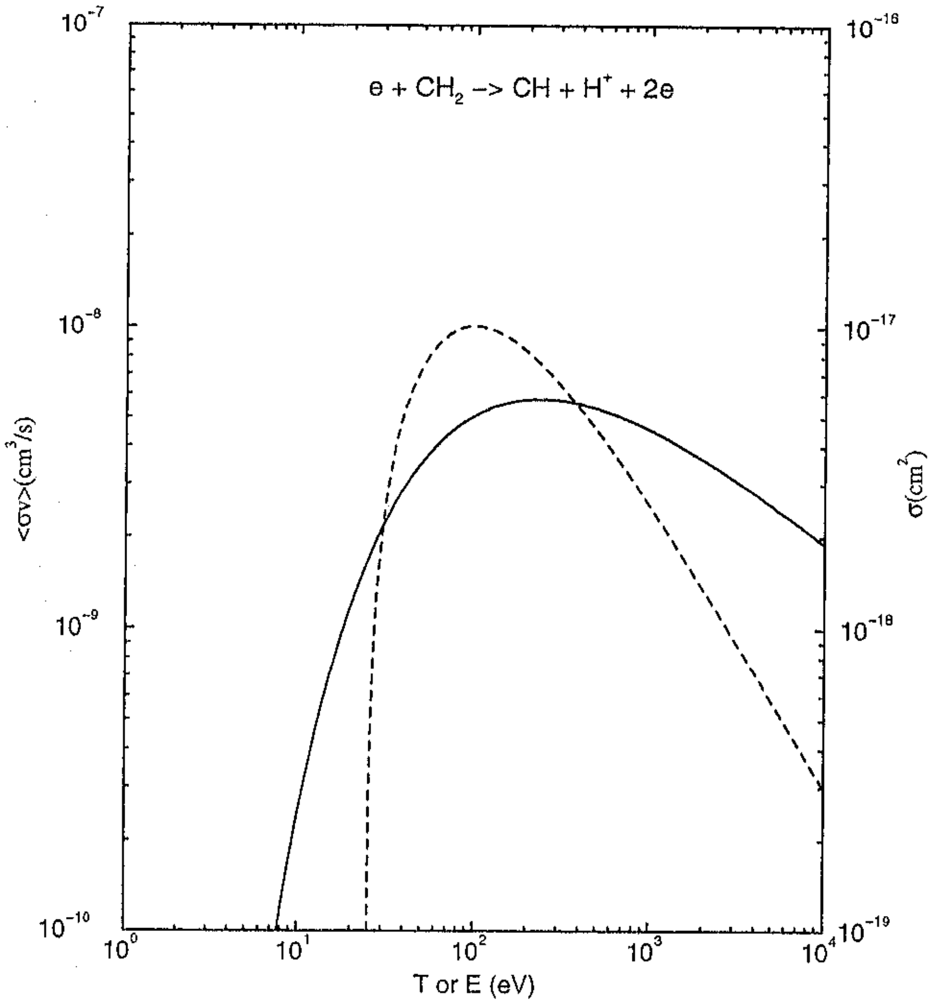

e + CH2 -> CH + H+ + 2e
<σv>(cm3/s)
σ(cm2)
T or E (eV)

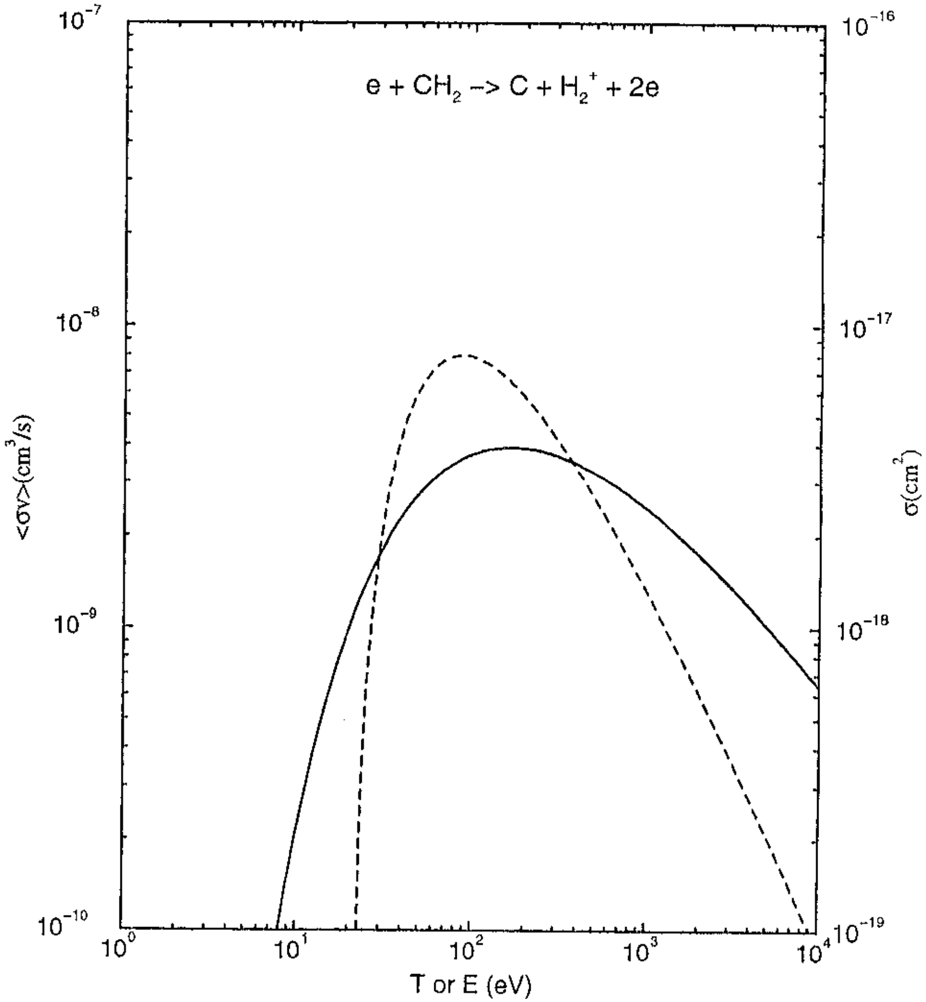

e + CH2 -> C + H2+ + 2e
<σv>(cm3/s)
σ(cm2)
T or E (eV)

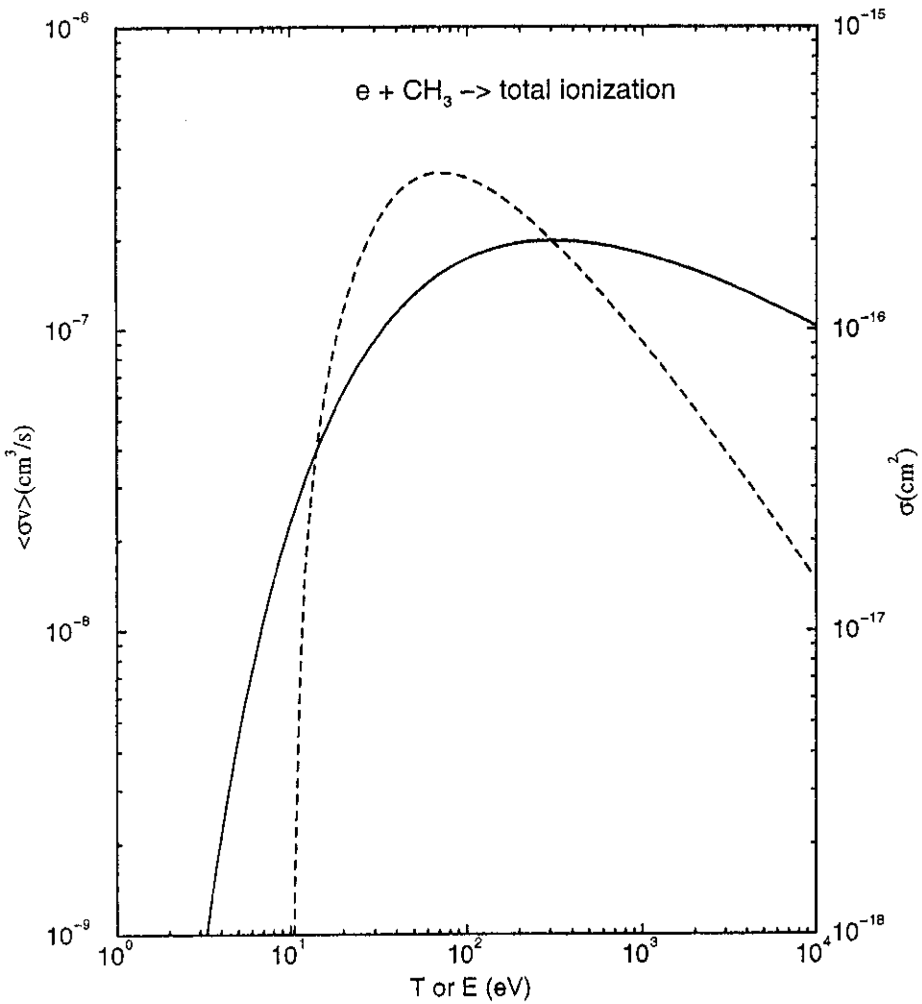
e + CH3 -> total ionization
<σv>(cm3/s)
σ(cm2)
T or E (eV)
10^-6
10^-7
10^-8
10^-9
10^-15
10^-16
10^-17
10^-18
10^0
10^1
10^2
10^3
10^4

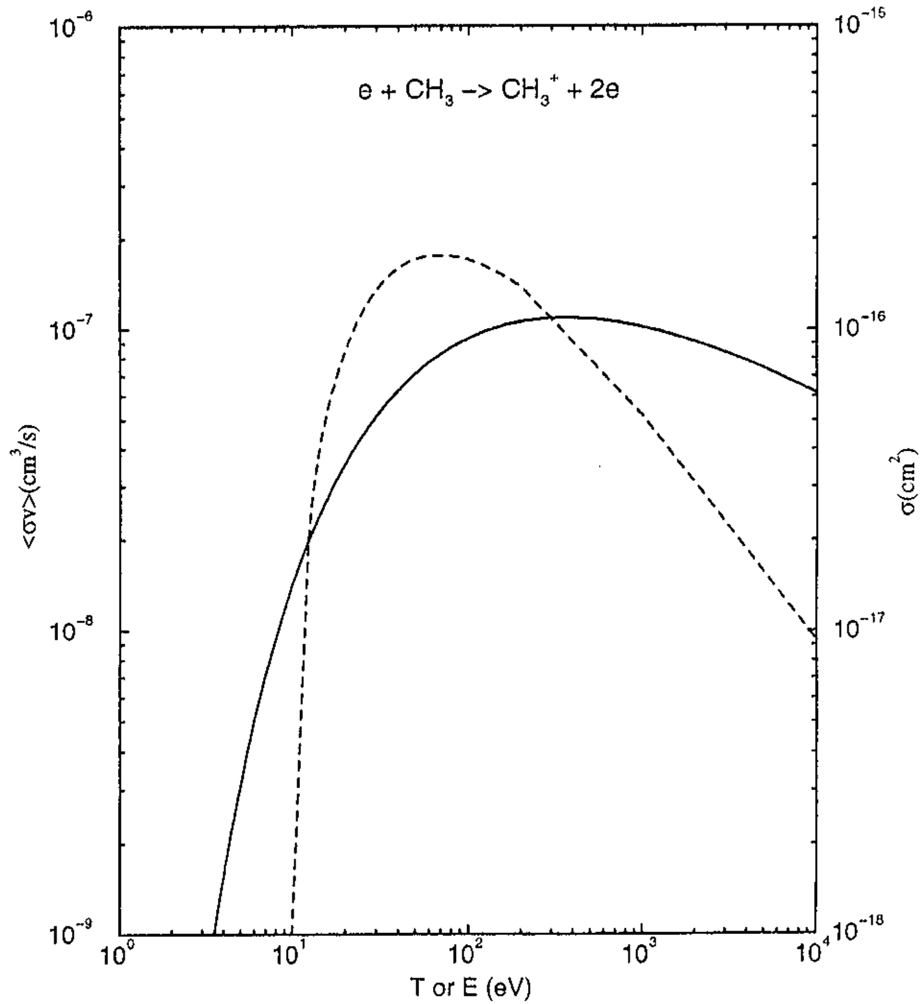
e + CH3 -> CH3+ + 2e
<σv>(cm3/s)
σ(cm2)
T or E (eV)
10^-6
10^-7
10^-8
10^-9
10^-15
10^-16
10^-17
10^-18
10^0
10^1
10^2
10^3
10^4

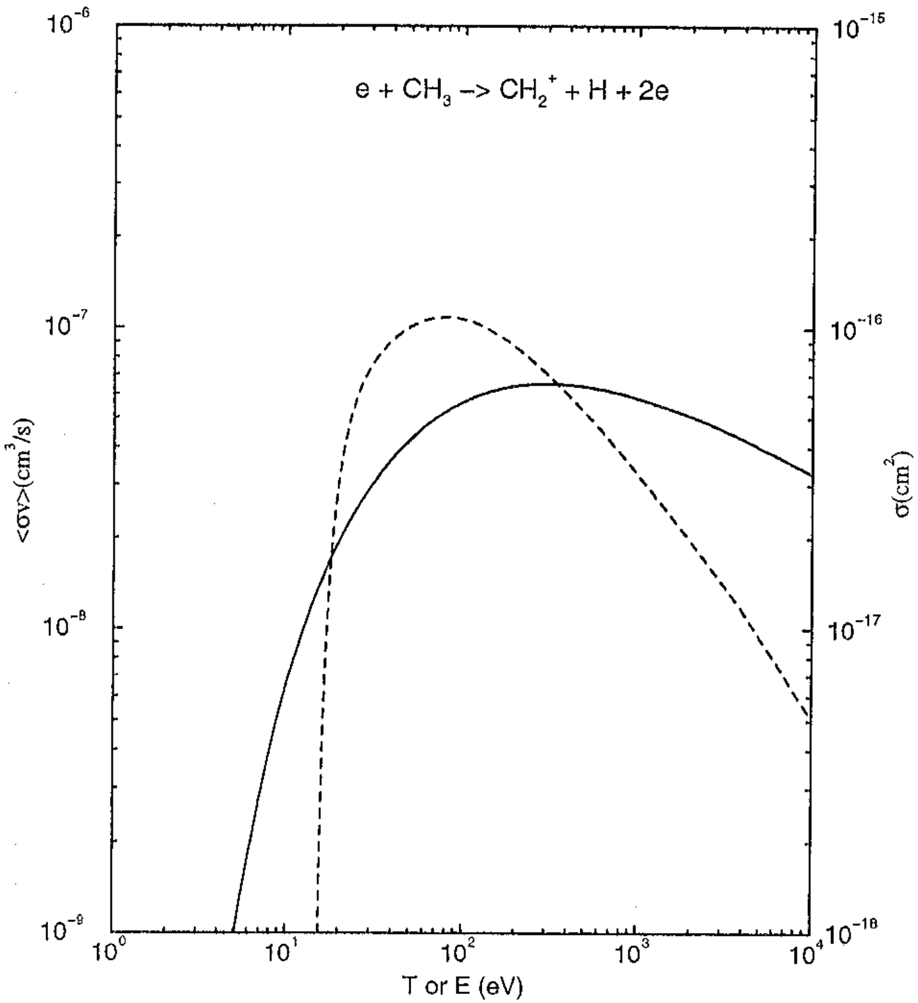
e + CH3 -> CH2+ + H + 2e
<σv>(cm3/s)
σ(cm2)
T or E (eV)
10^-6
10^-7
10^-8
10^-9
10^-15
10^-16
10^-17
10^-18
10^0
10^1
10^2
10^3
10^4

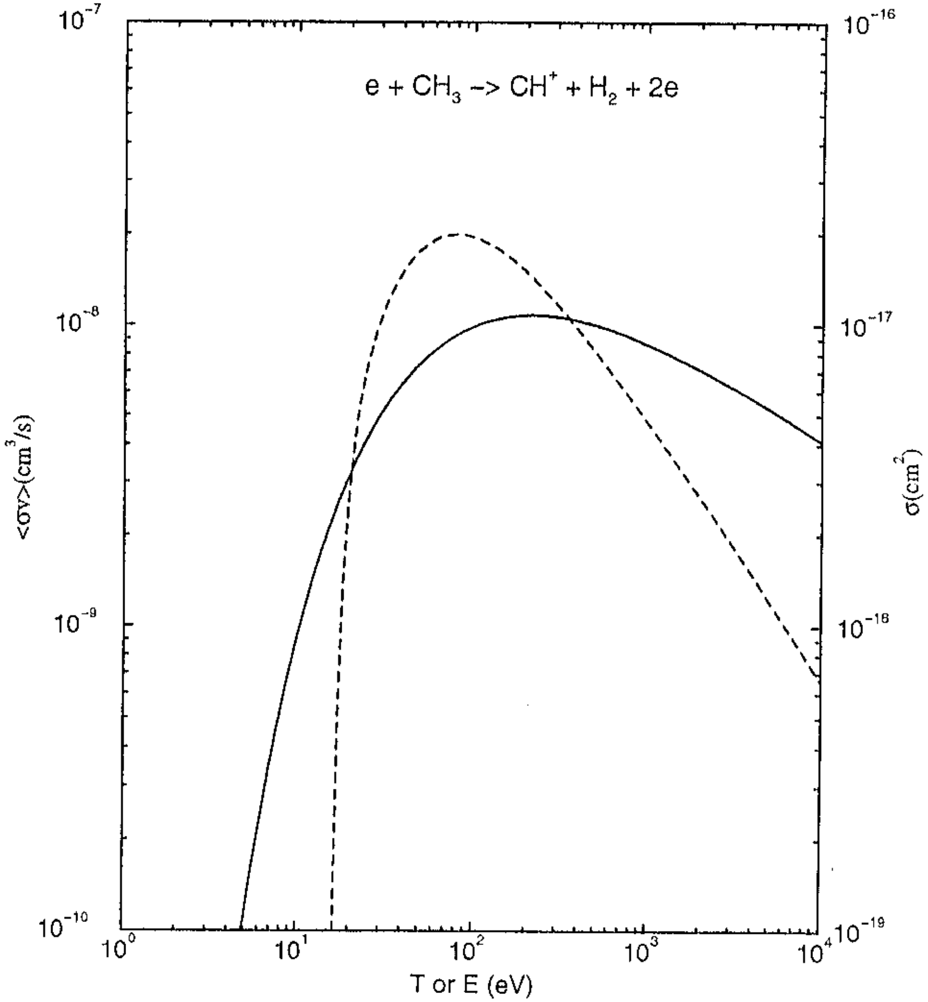
e + CH3 -> CH+ + H2 + 2e
<σv>(cm3/s)
σ(cm2)
T or E (eV)
10^-7
10^-8
10^-9
10^-10
10^-16
10^-17
10^-18
10^-19
10^0
10^1
10^2
10^3
10^4

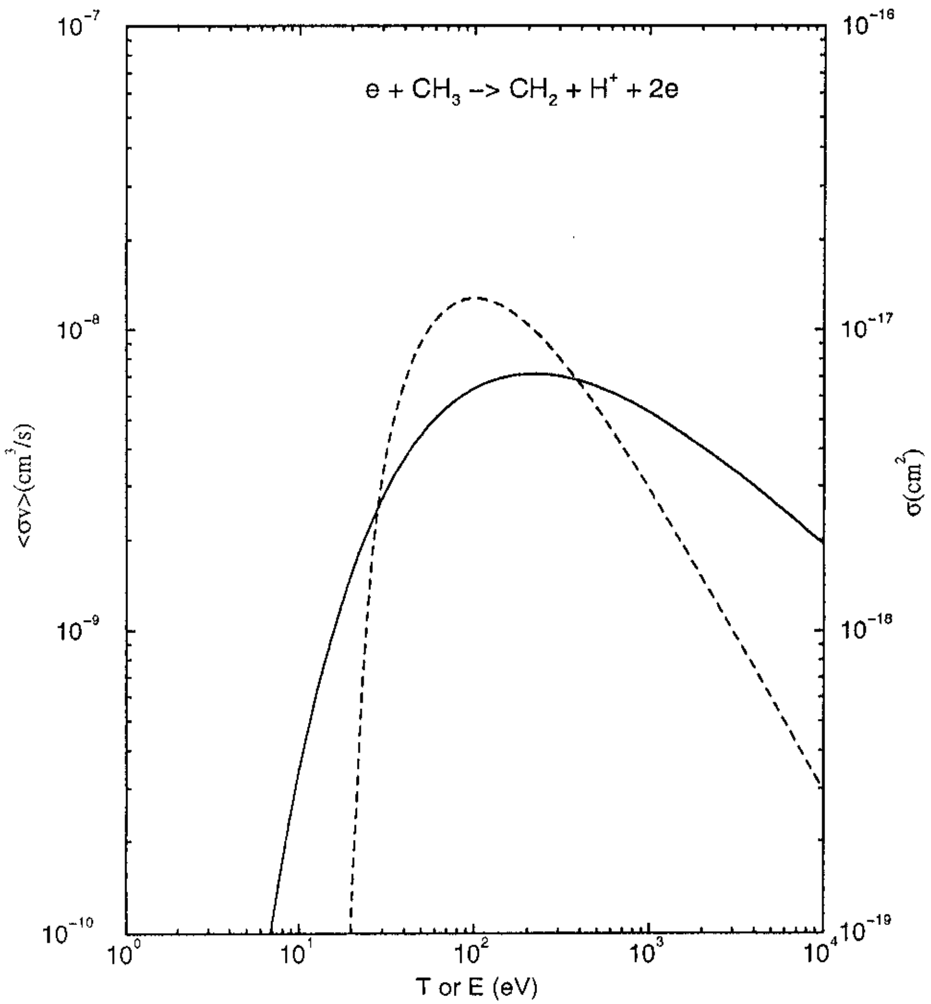
e + CH3 -> CH2 + H+ + 2e
<σv>(cm3/s)
σ(cm2)
T or E (eV)
10−7
10−8
10−9
10−10
10−16
10−17
10−18
10−19
100
101
102
103
104

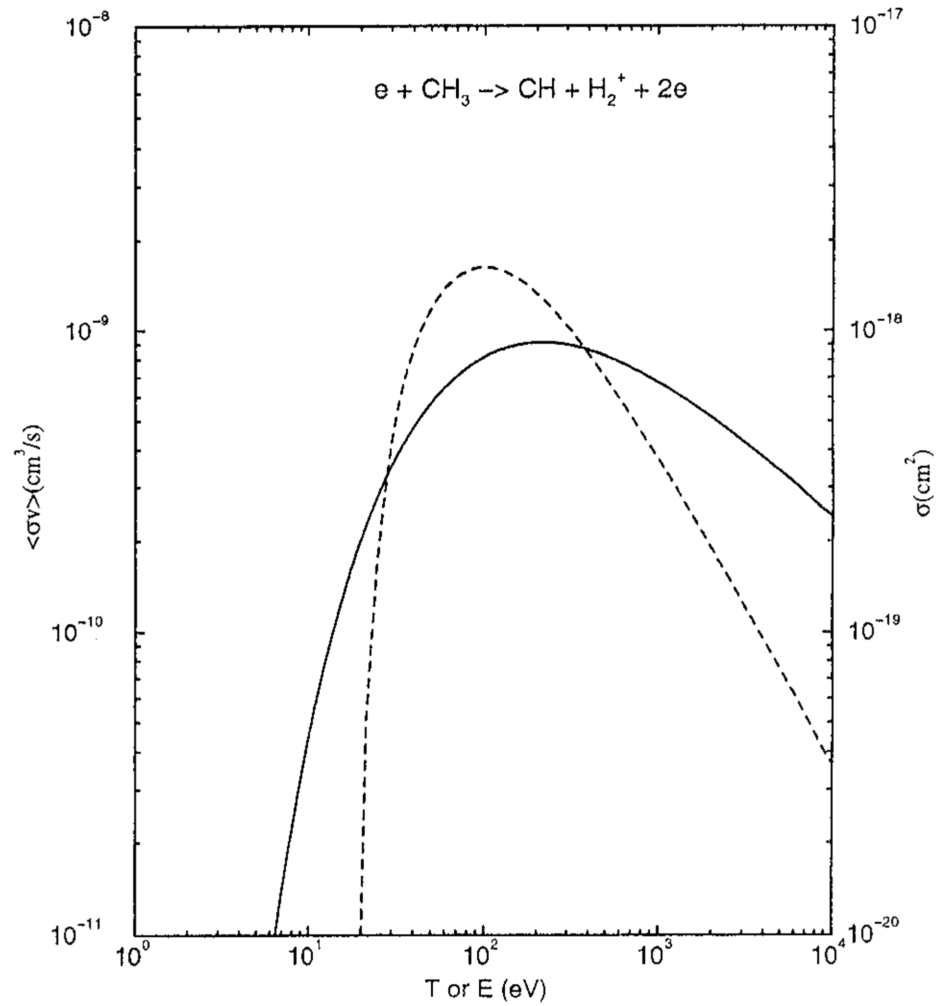
e + CH3 -> CH + H2+ + 2e
<σv>(cm3/s)
σ(cm2)
T or E (eV)
10−8
10−9
10−10
10−11
10−17
10−18
10−19
10−20
100
101
102
103
104

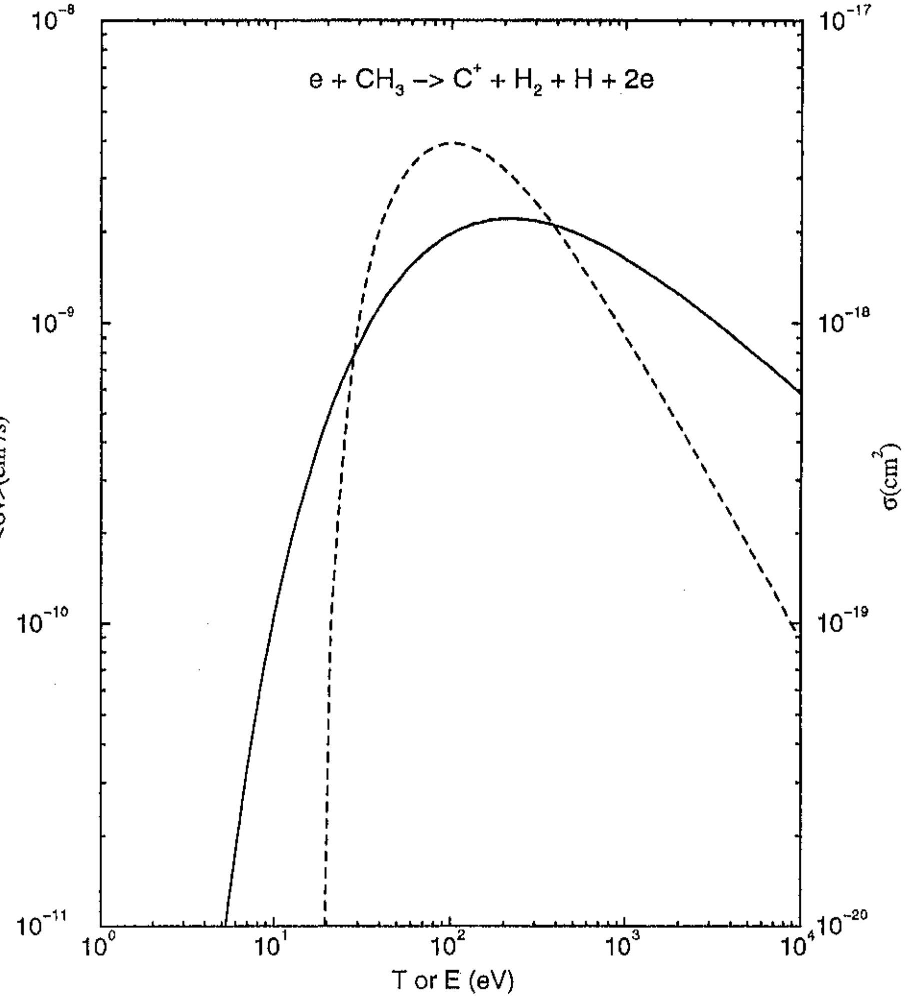
e + CH3 -> C+ + H2 + H + 2e
<σv>(cm3/s)
σ(cm2)
T or E (eV)
10−8
10−9
10−10
10−11
10−17
10−18
10−19
10−20
10^0
10^1
10^2
10^3
10^4

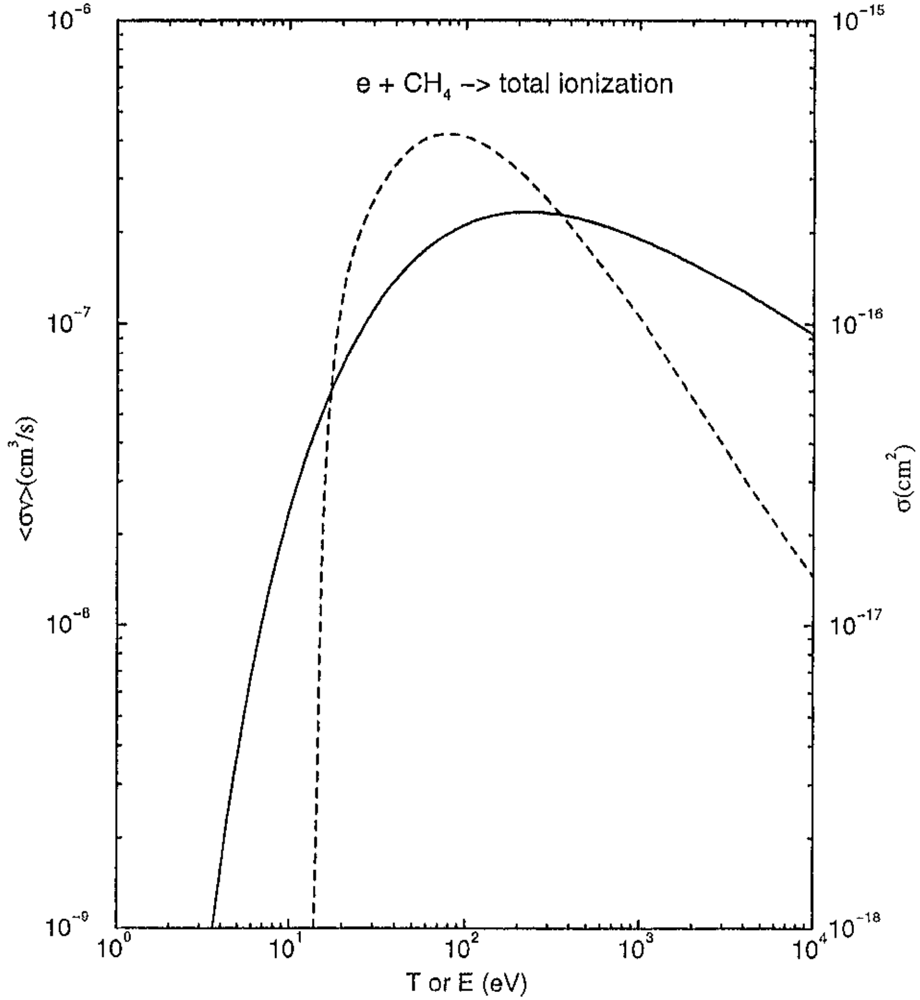
e + CH4 -> total ionization
<σv>(cm3/s)
σ(cm2)
T or E (eV)
10−6
10−7
10−8
10−9
10−15
10−16
10−17
10−18
10^0
10^1
10^2
10^3
10^4

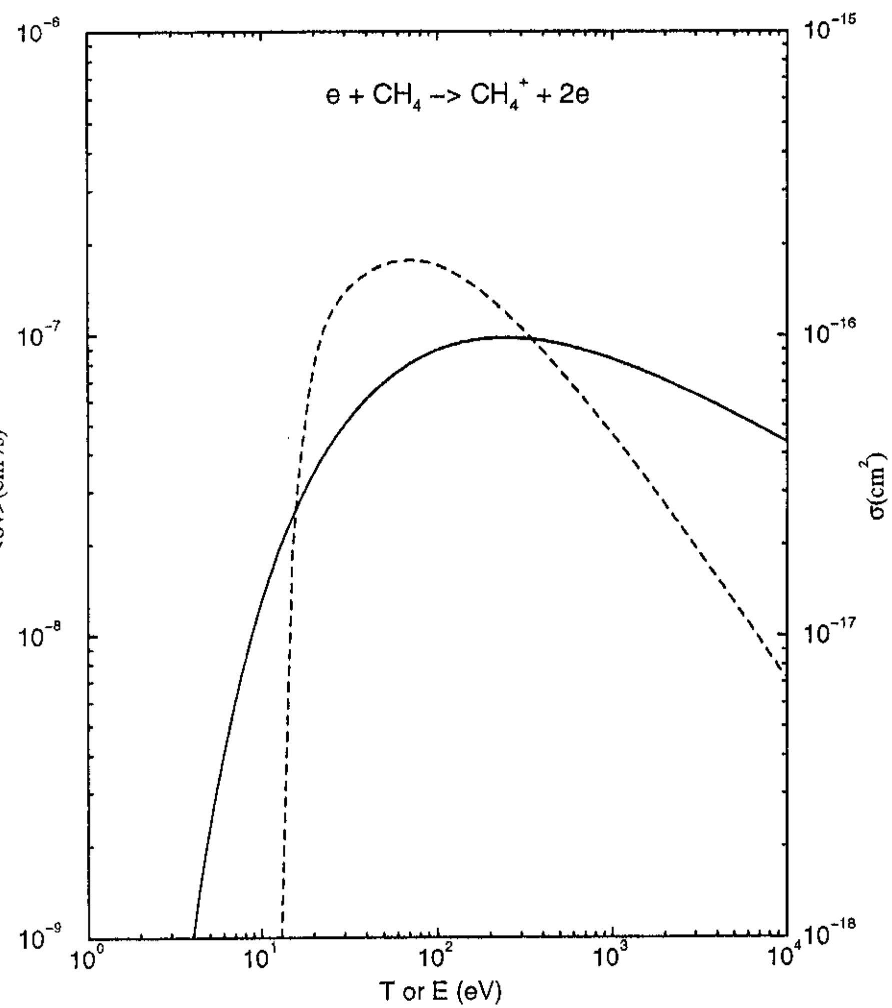
e + CH4 -> CH4+ + 2e
<σv>(cm3/s)
σ(cm2)
T or E (eV)
10-6
10-7
10-8
10-9
10-15
10-16
10-17
10-18
10^0
10^1
10^2
10^3
10^4

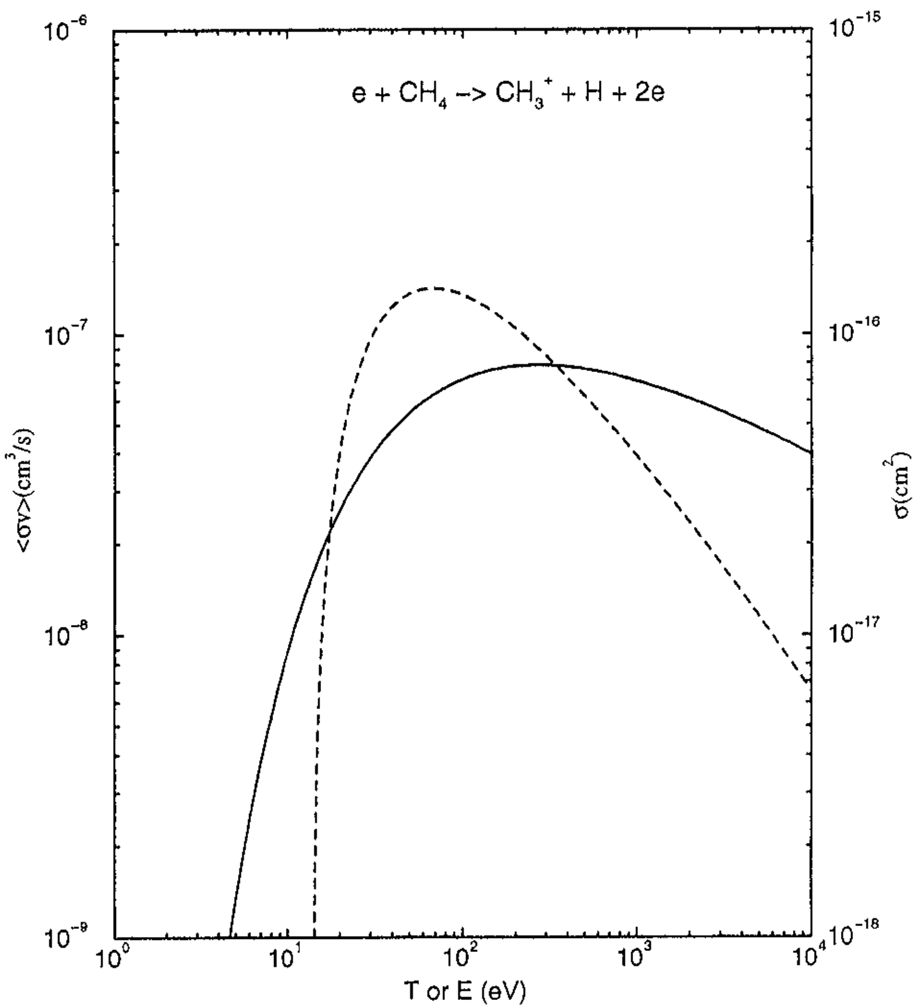
e + CH4 -> CH3+ + H + 2e
<σv>(cm3/s)
σ(cm2)
T or E (eV)
10-6
10-7
10-8
10-9
10-15
10-16
10-17
10-18
10^0
10^1
10^2
10^3
10^4

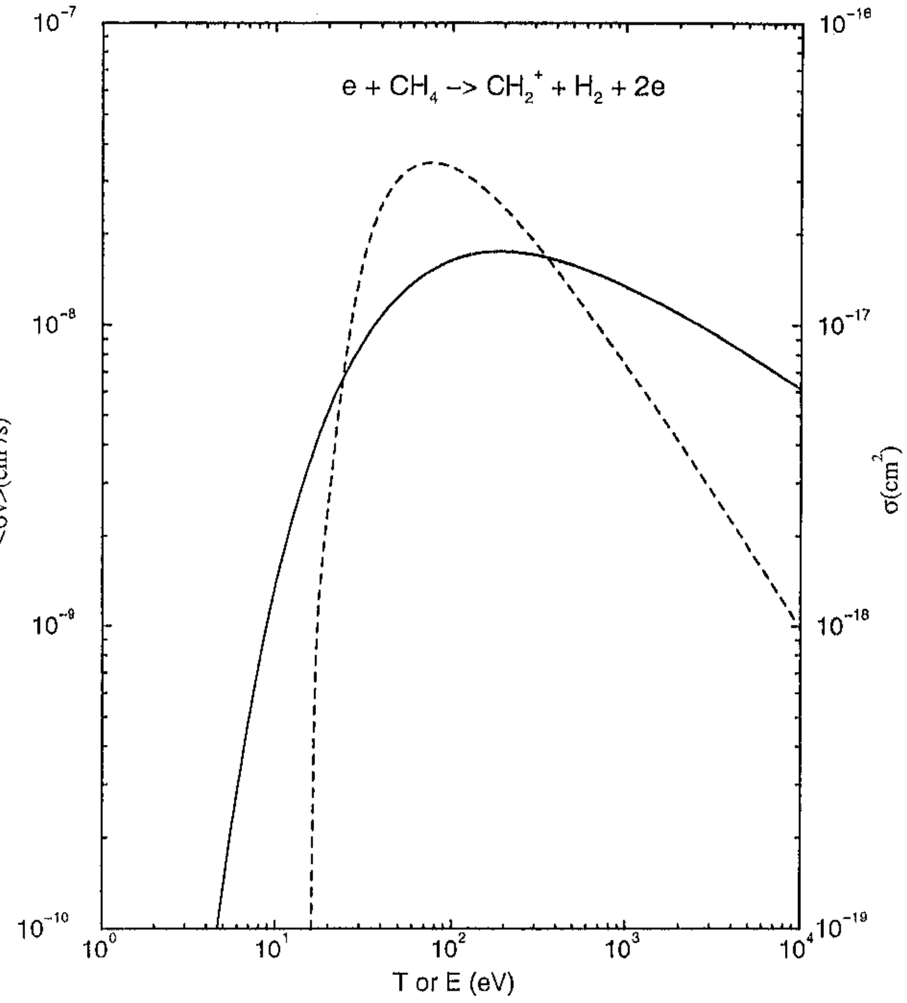

e + CH4 -> CH2+ + H2 + 2e
<σv>(cm3/s)
σ(cm2)
T or E (eV)

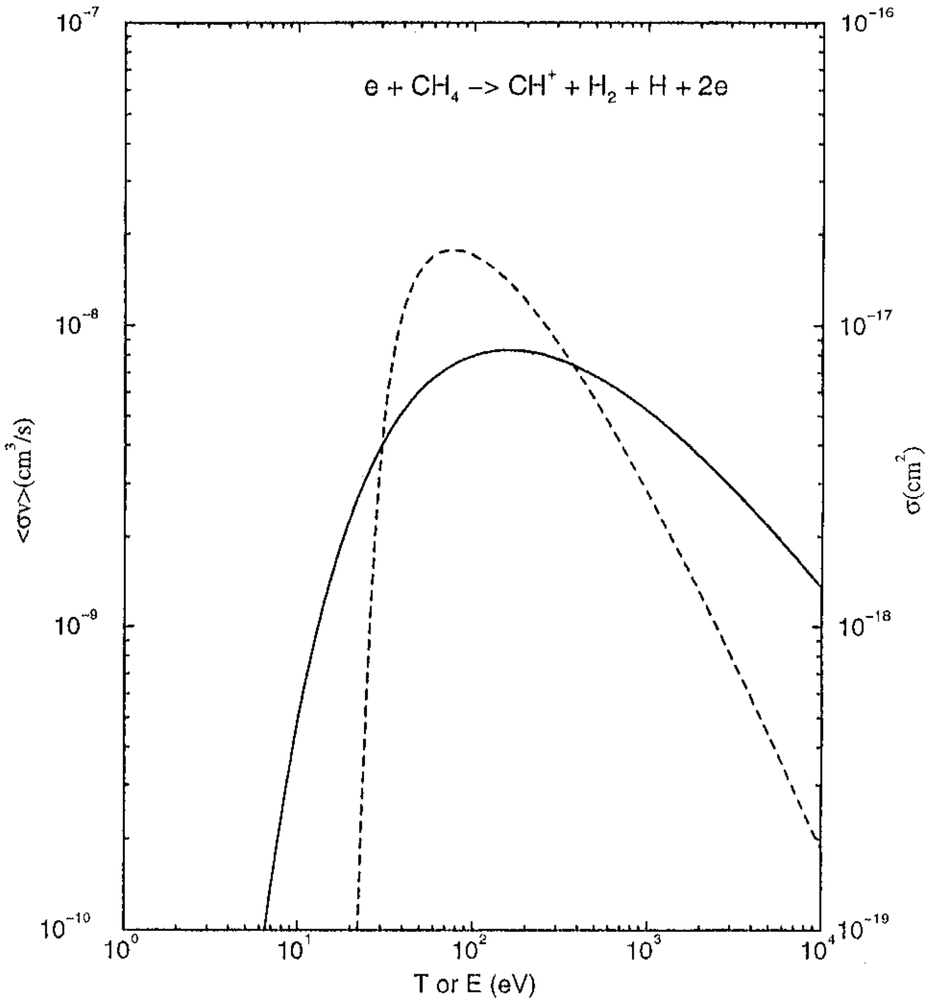

e + CH4 -> CH+ + H2 + H + 2e
<σv>(cm3/s)
σ(cm2)
T or E (eV)

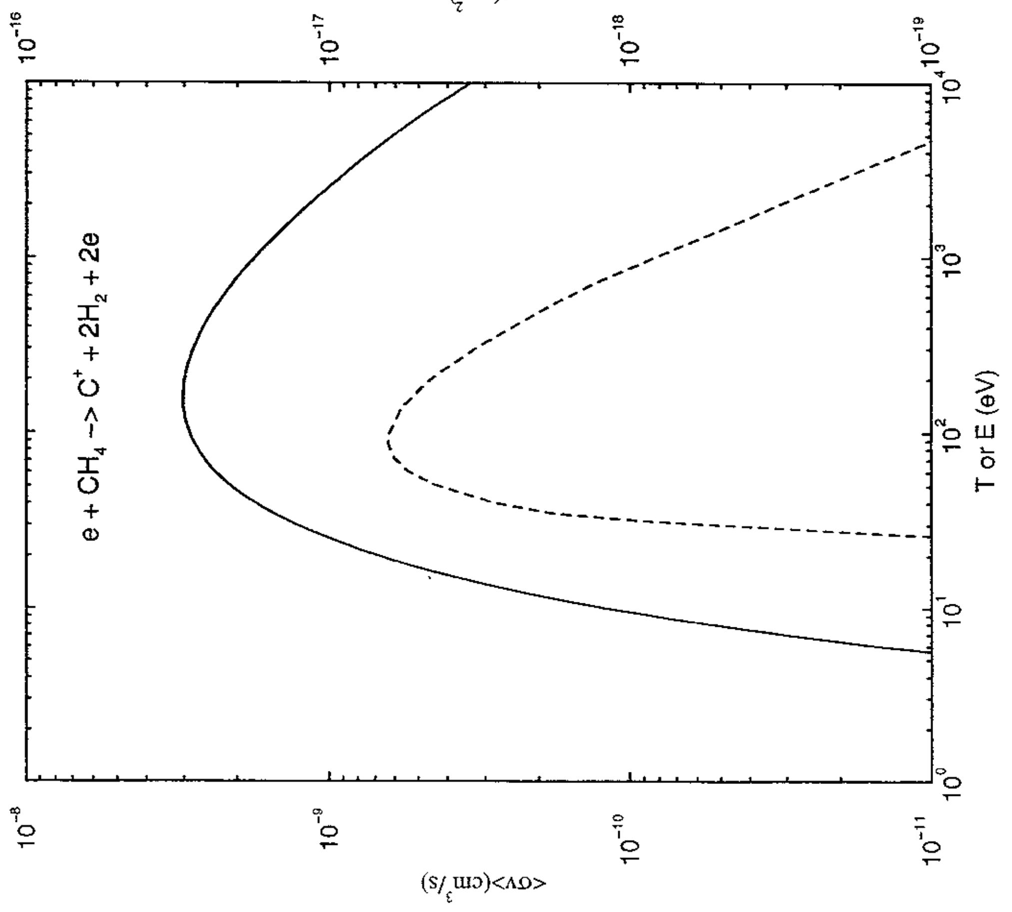
e + CH4 -> C+ + 2H2 + 2e
T or E (eV)
<σv>(cm3/s)
σ(cm2)

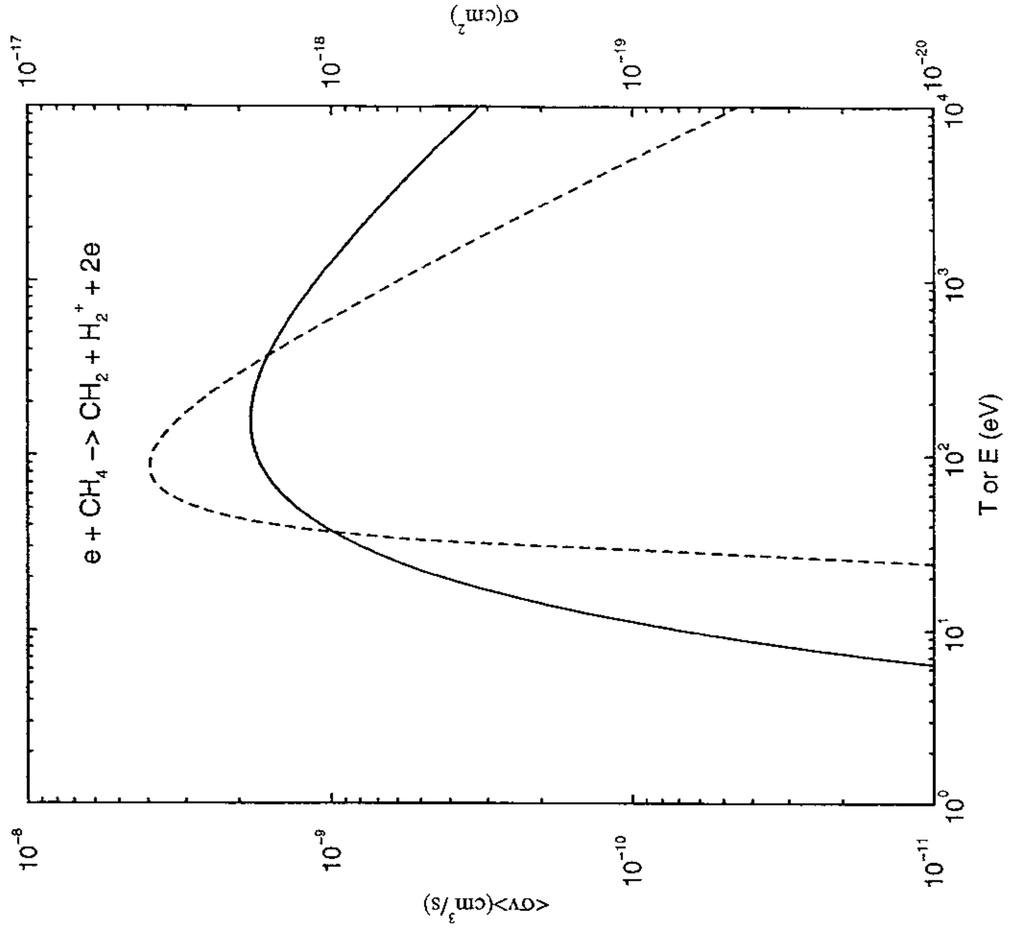
e + CH4 -> CH2 + H2+ + 2e
T or E (eV)
<σv>(cm3/s)
σ(cm2)

A-2.2 e + C_2H_y systems

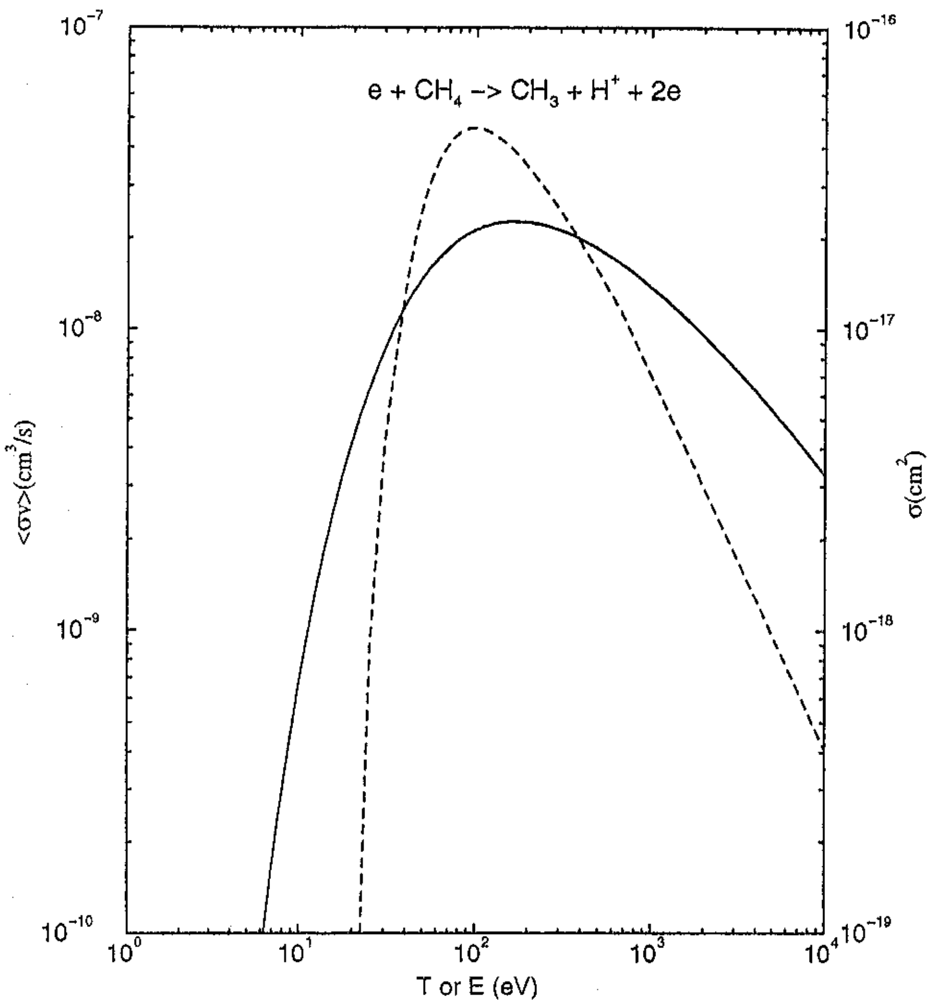

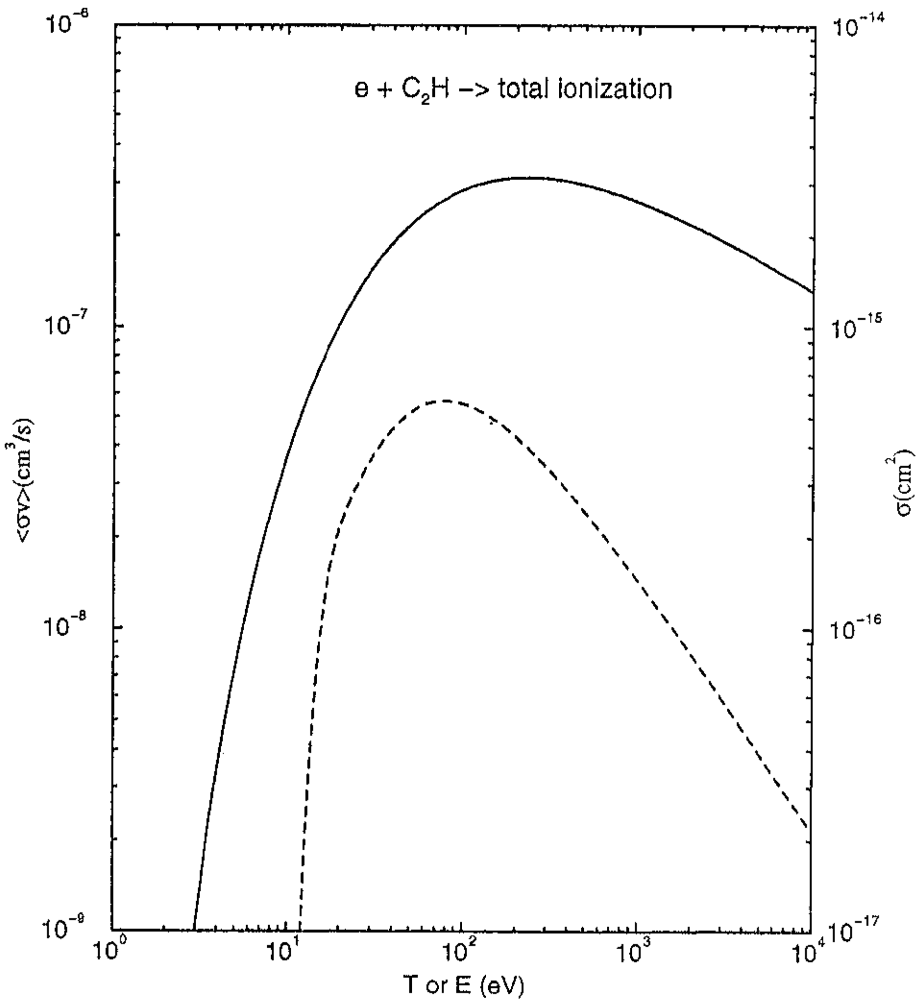

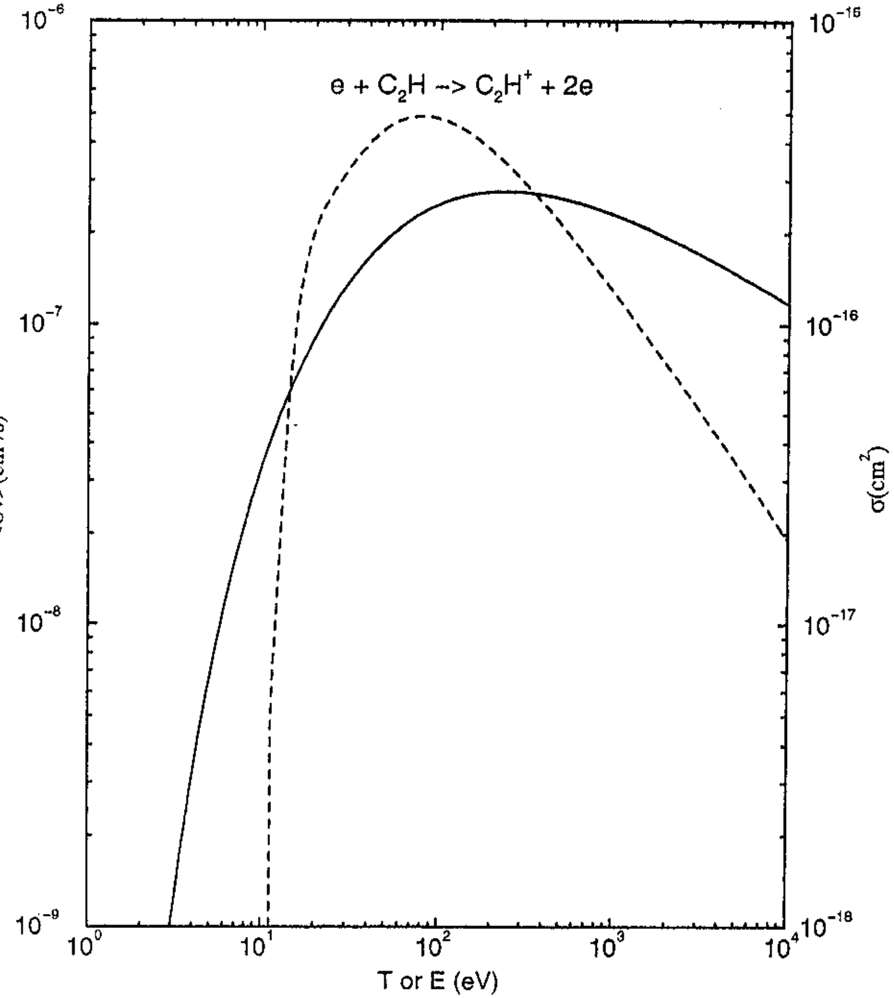
e + C2H --> C2H+ + 2e
<σv>(cm3/s)
σ(cm2)
T or E (eV)
10−6
10−7
10−8
10−9
10−15
10−16
10−17
10−18
100
101
102
103
104

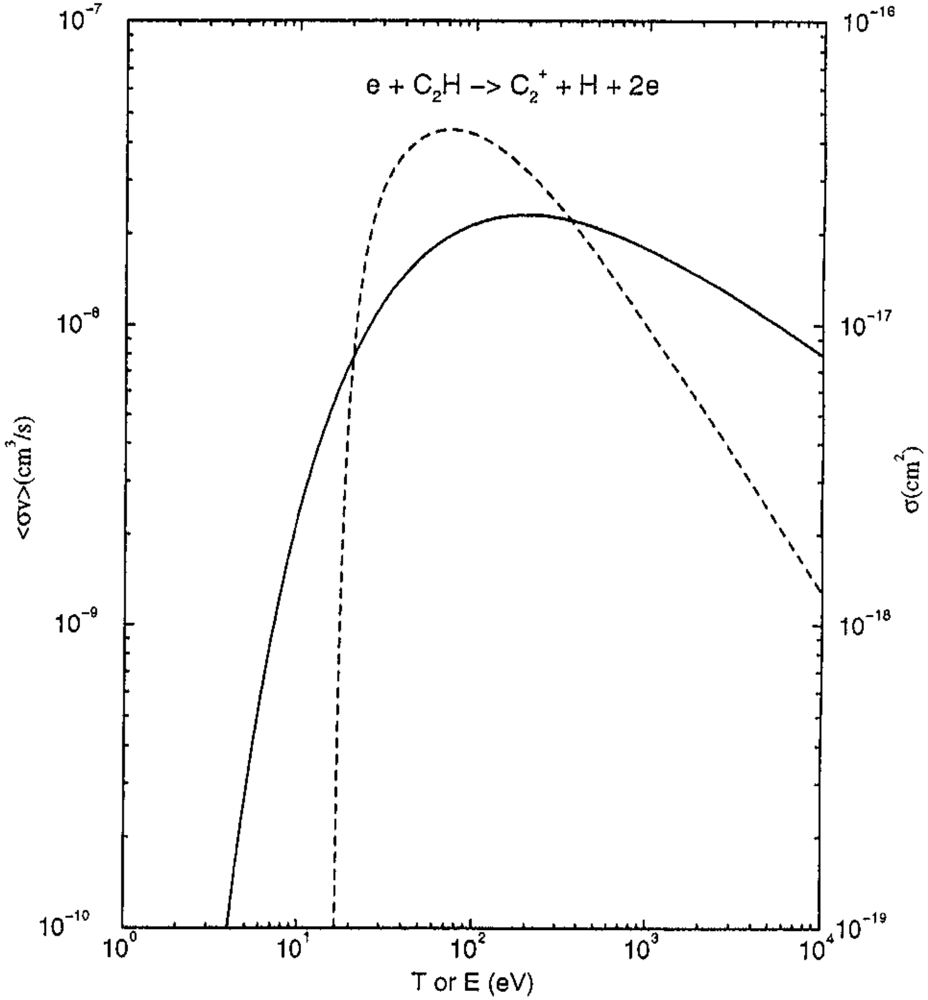
e + C2H -> C2+ + H + 2e
<σv>(cm3/s)
σ(cm2)
T or E (eV)
10−7
10−8
10−9
10−10
10−16
10−17
10−18
10−19
100
101
102
103
104

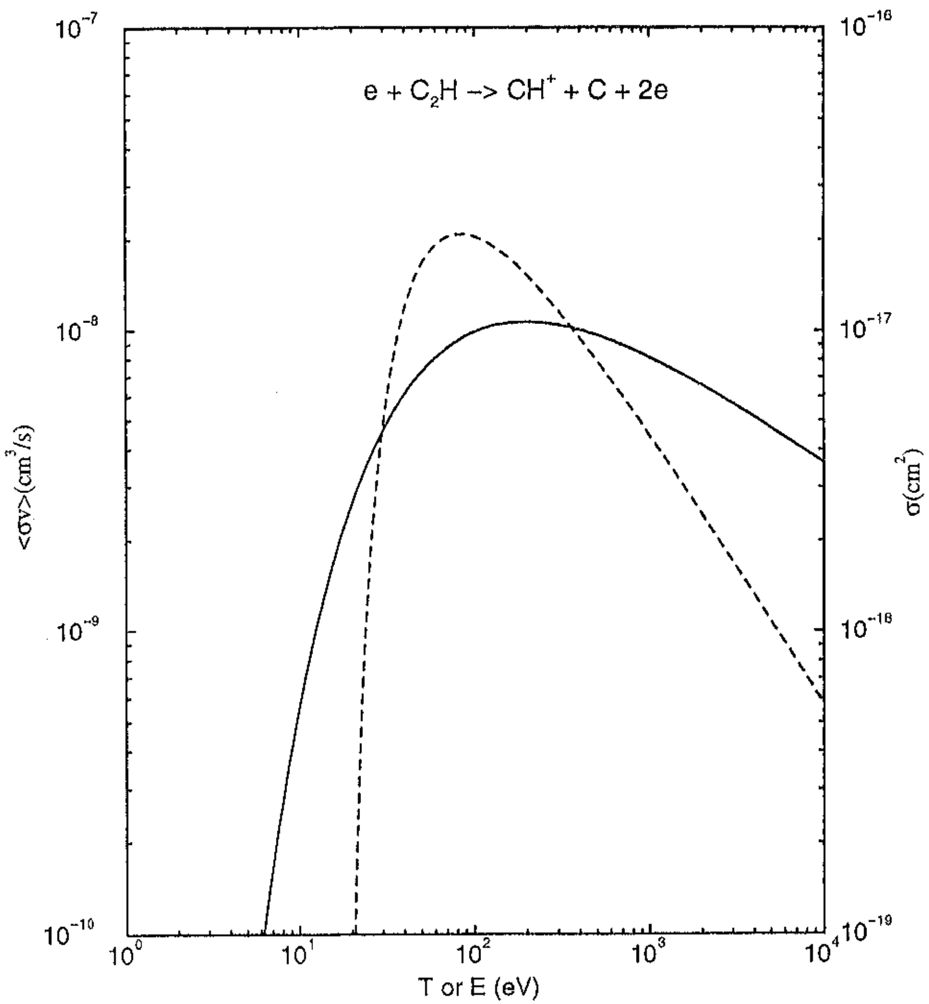
e + C2H -> CH+ + C + 2e
<σv>(cm3/s)
σ(cm2)
T or E (eV)
10−7
10−8
10−9
10−10
10−16
10−17
10−18
10−19
100
101
102
103
104

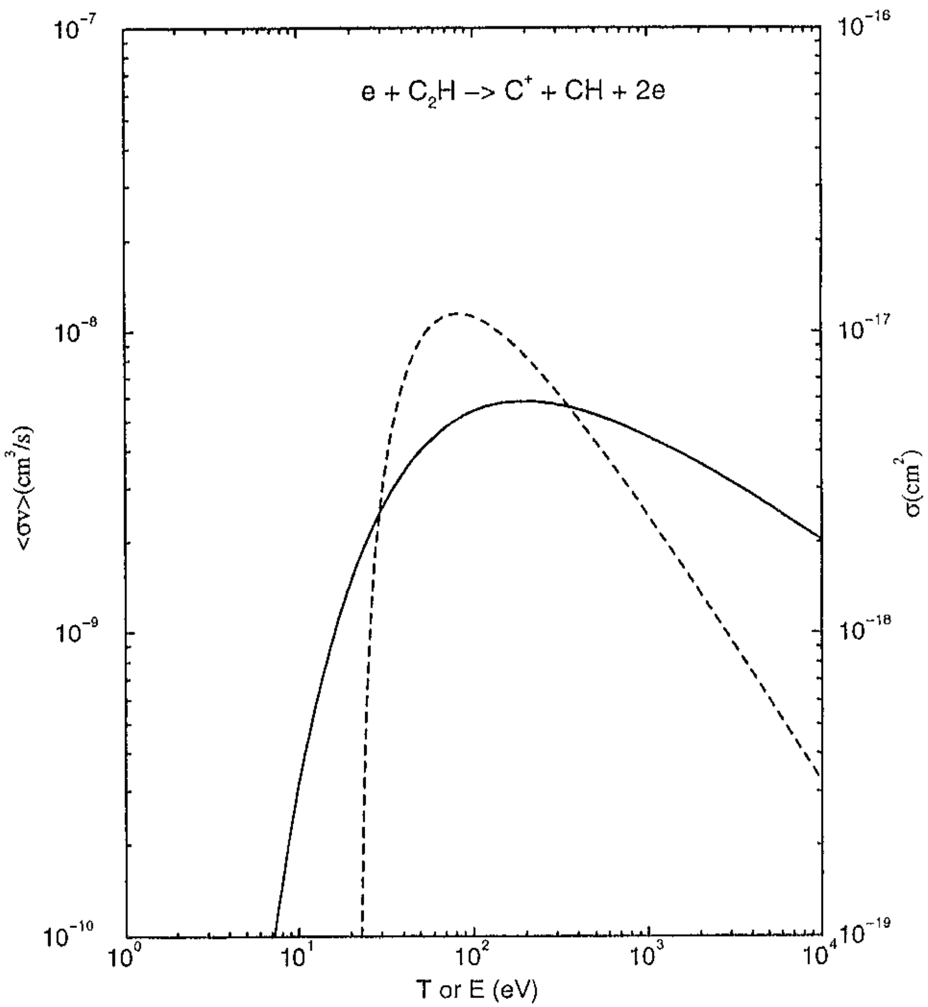
e + C2H -> C+ + CH + 2e
<σv>(cm3/s)
σ(cm2)
T or E (eV)
10−7
10−8
10−9
10−10
10−16
10−17
10−18
10−19
100
101
102
103
104

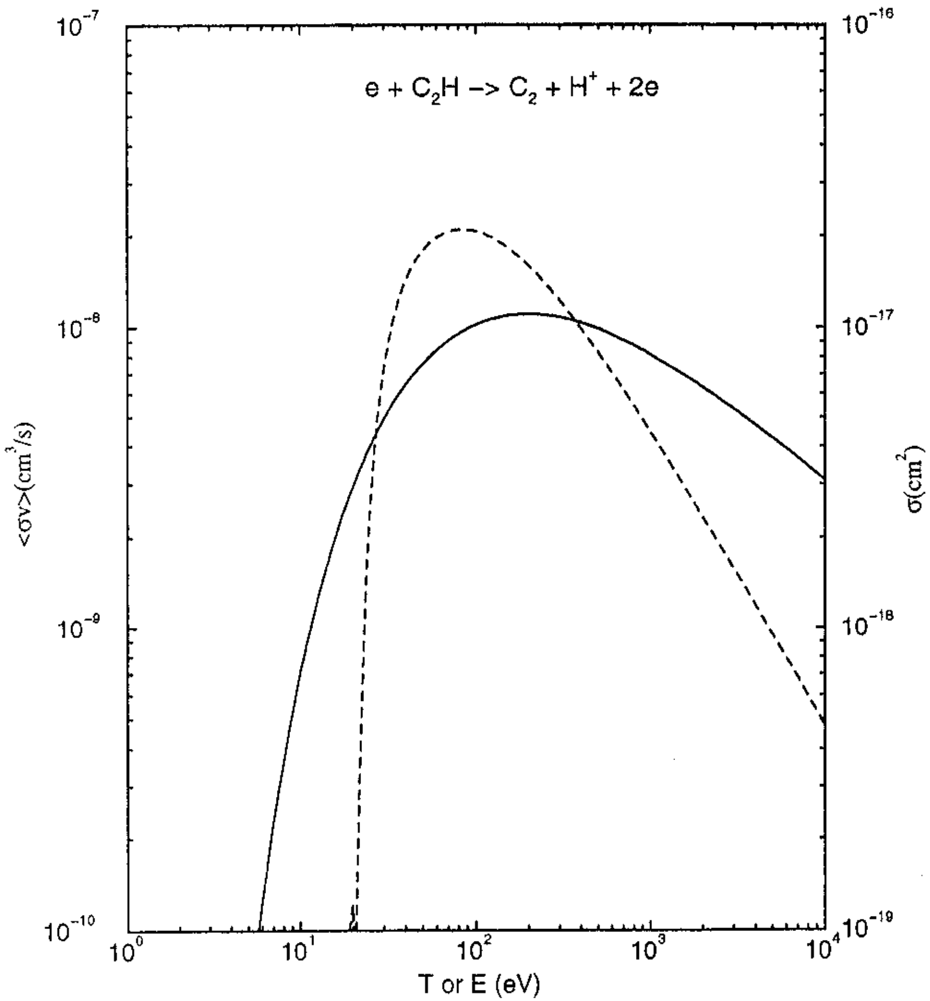
e + C_2H -> C_2 + H^+ + 2e
<σv>(cm³/s)
σ(cm²)
T or E (eV)

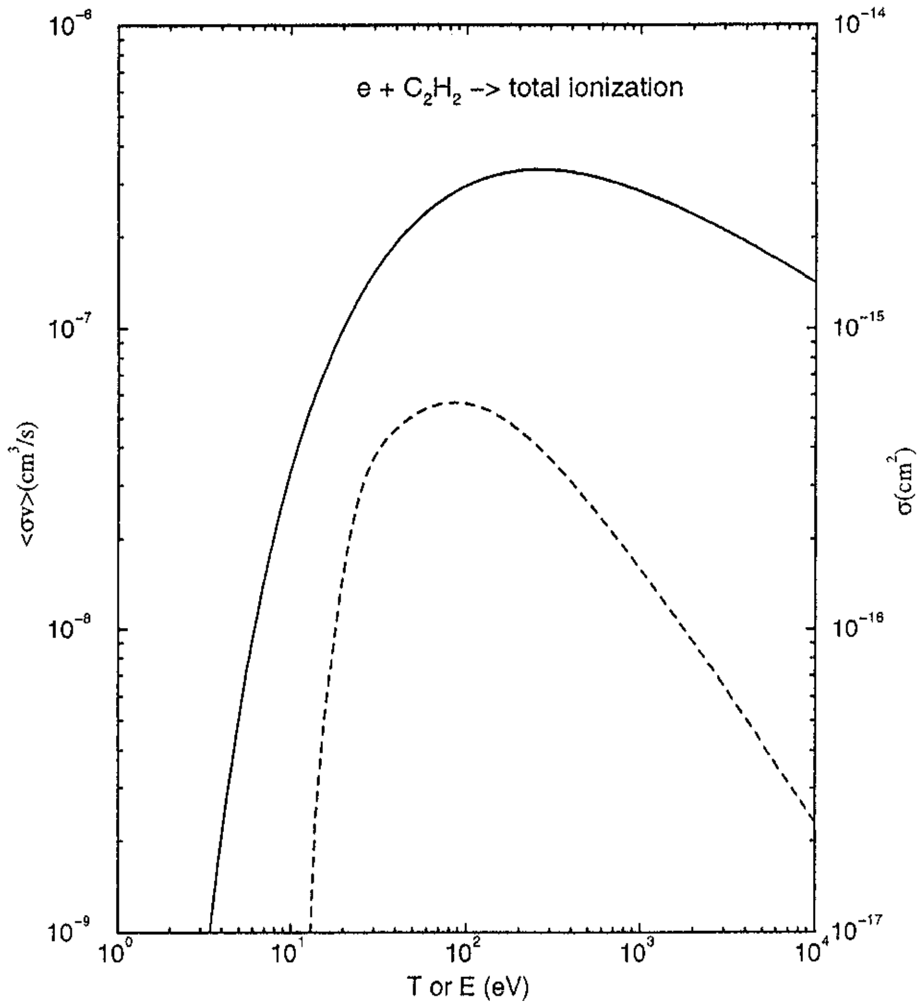
e + C_2H_2 -> total ionization
<σv>(cm³/s)
σ(cm²)
T or E (eV)

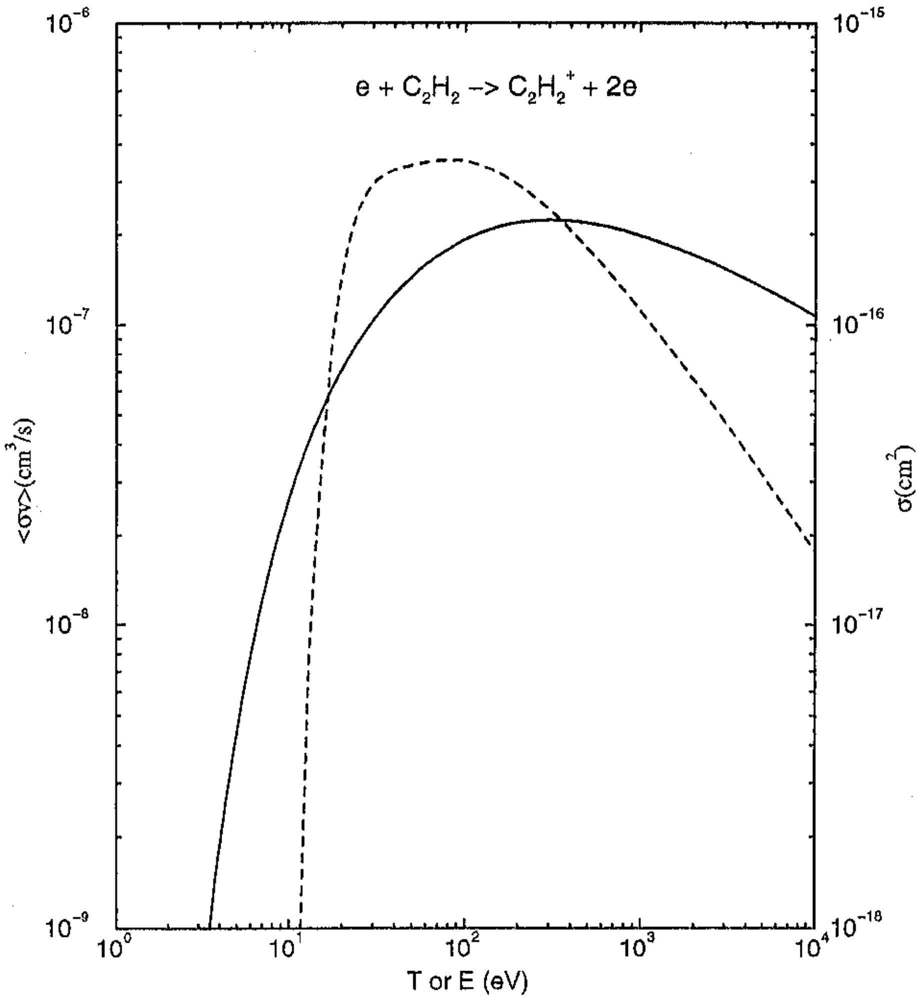
e + C_2H_2 --> $C_2H_2^+$ + 2e
<σv>(cm^3/s)
σ(cm^2)
T or E (eV)
10^{-6}
10^{-7}
10^{-8}
10^{-9}
10^{-15}
10^{-16}
10^{-17}
10^{-18}
10^0
10^1
10^2
10^3
10^4

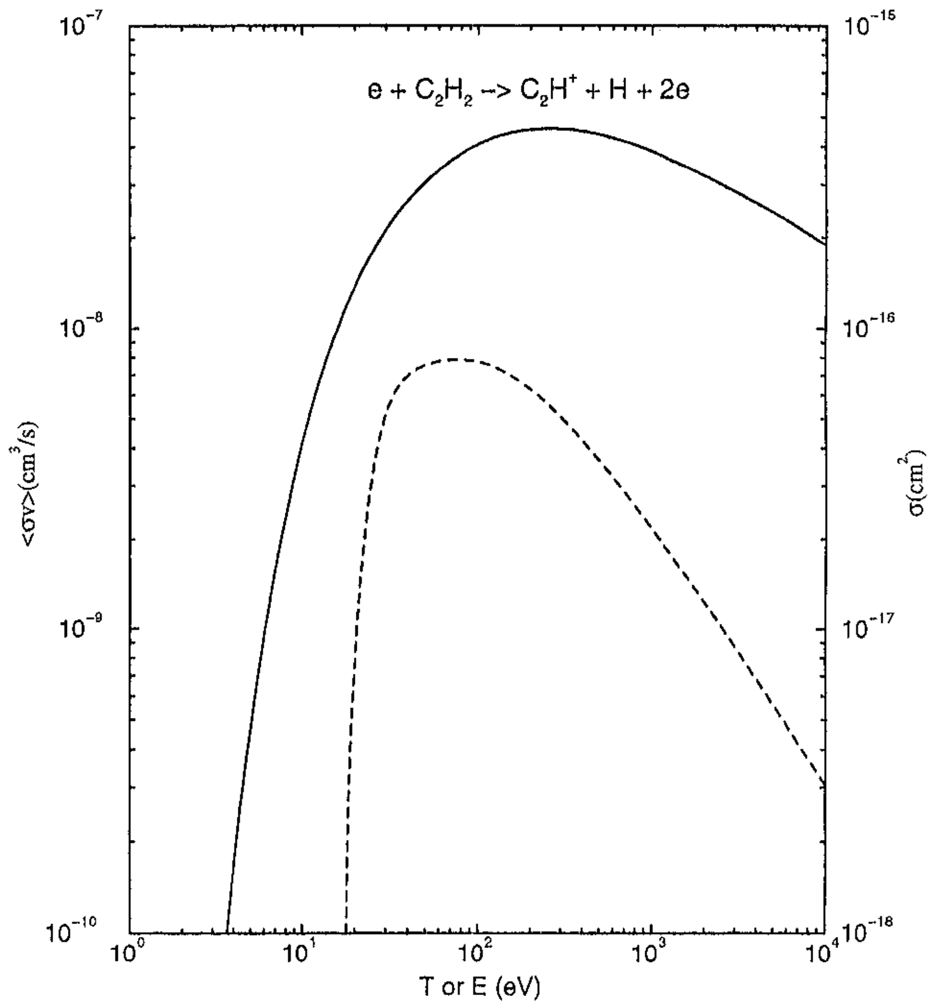
e + C_2H_2 --> C_2H^+ + H + 2e
<σv>(cm^3/s)
σ(cm^2)
T or E (eV)
10^{-7}
10^{-8}
10^{-9}
10^{-10}
10^{-15}
10^{-16}
10^{-17}
10^{-18}
10^0
10^1
10^2
10^3
10^4

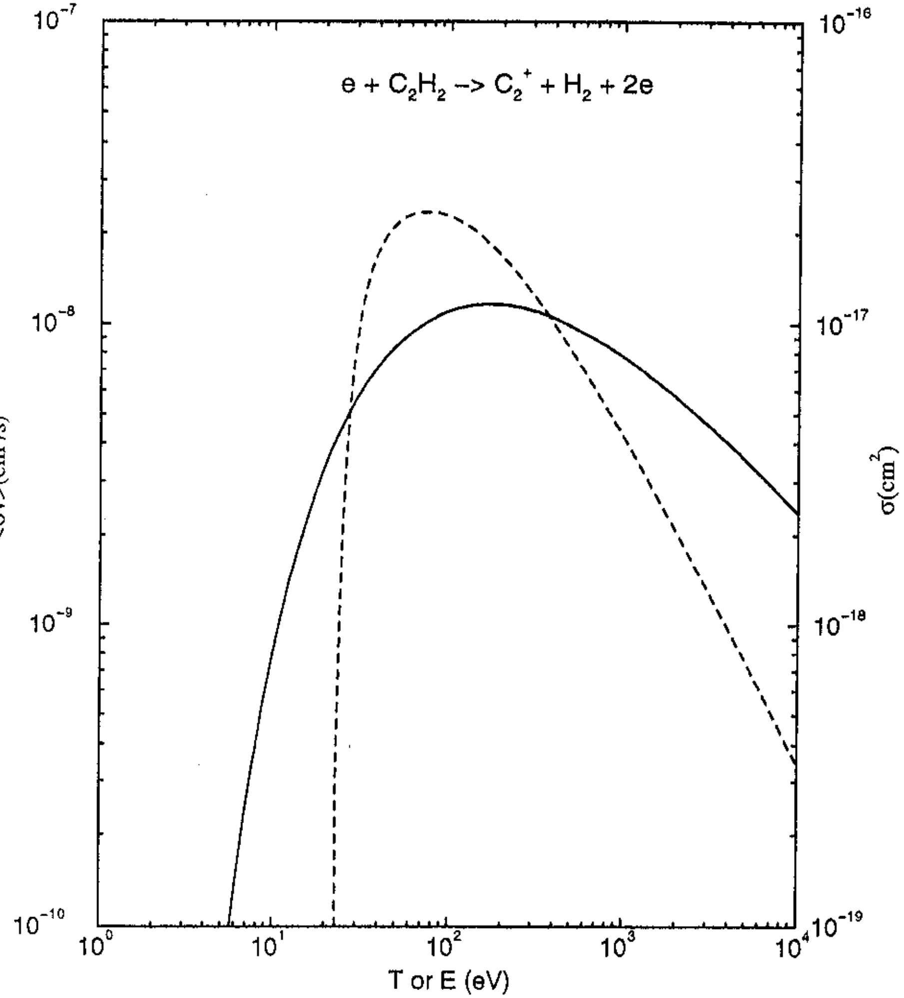

e + C2H2 -> C2+ + H2 + 2e
<σv>(cm3/s)
σ(cm2)
T or E (eV)

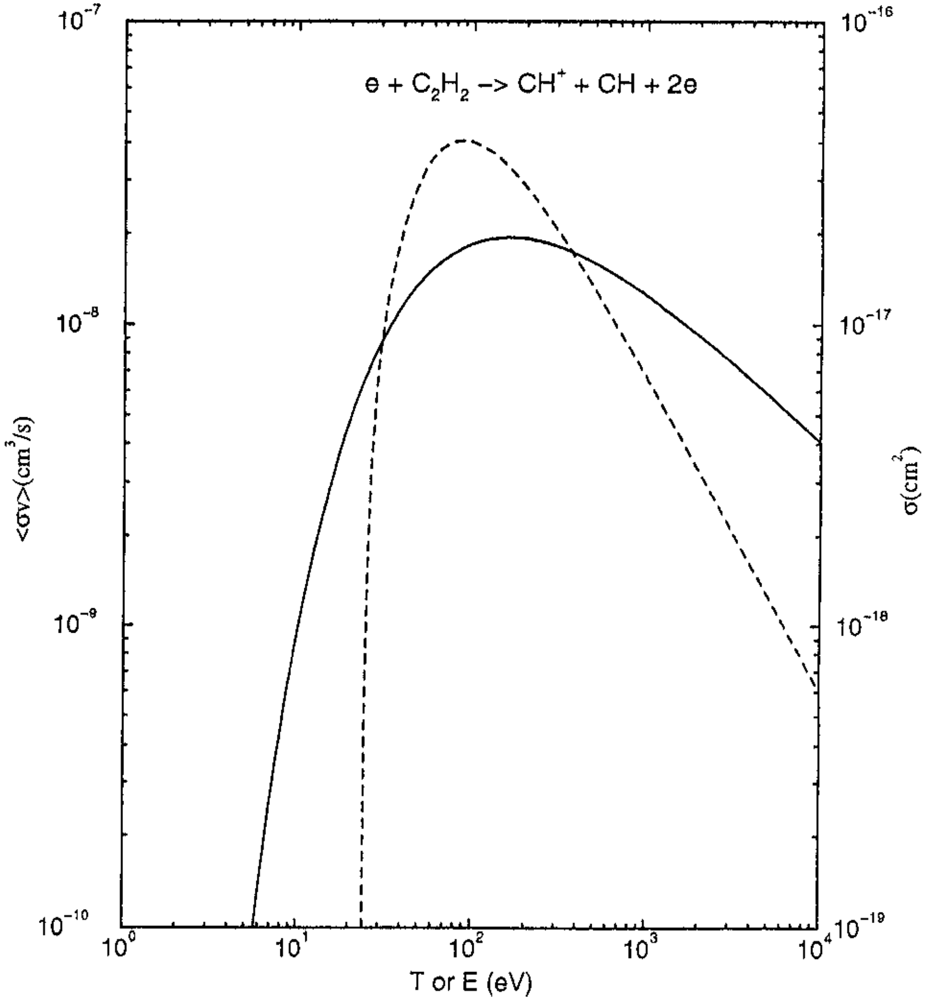

e + C2H2 -> CH+ + CH + 2e
<σv>(cm3/s)
σ(cm2)
T or E (eV)

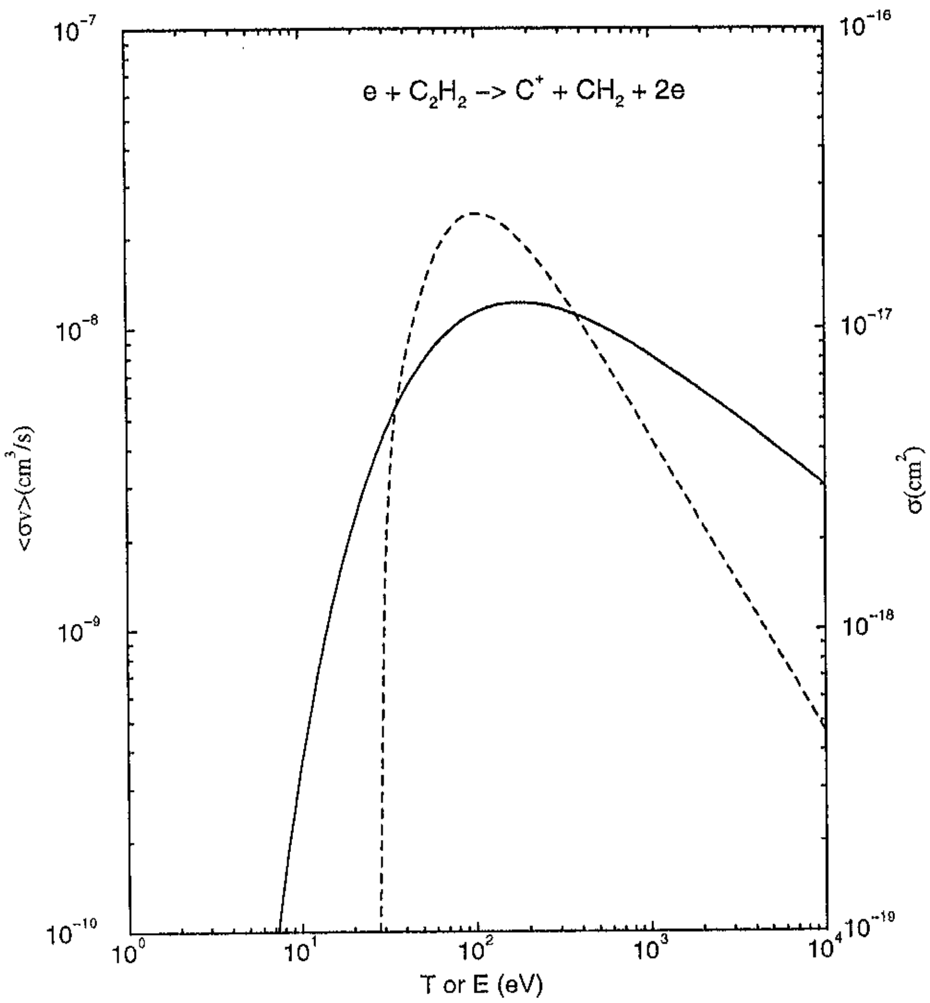
e + C2H2 -> C+ + CH2 + 2e
<σv>(cm3/s)
σ(cm2)
T or E (eV)
10−7
10−8
10−9
10−10
10−16
10−17
10−18
10−19
100
101
102
103
104

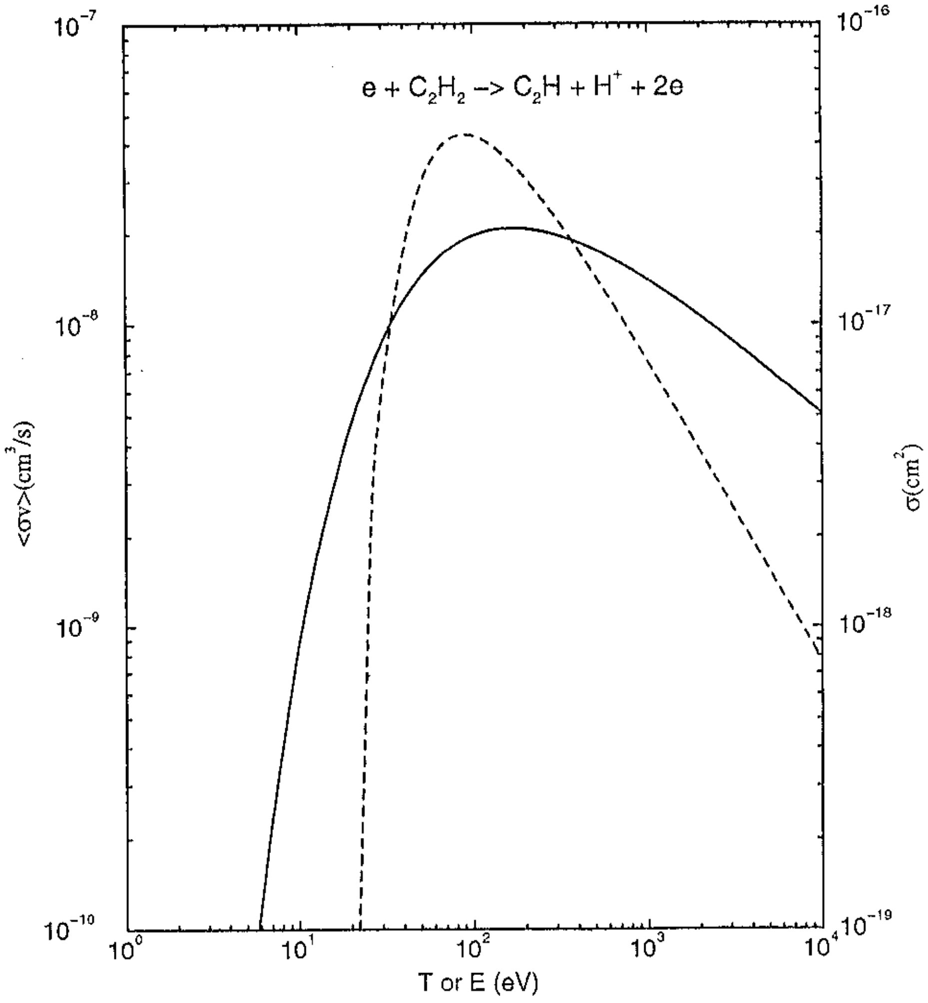
e + C2H2 -> C2H + H+ + 2e
<σv>(cm3/s)
σ(cm2)
T or E (eV)
10−7
10−8
10−9
10−10
10−16
10−17
10−18
10−19
100
101
102
103
104

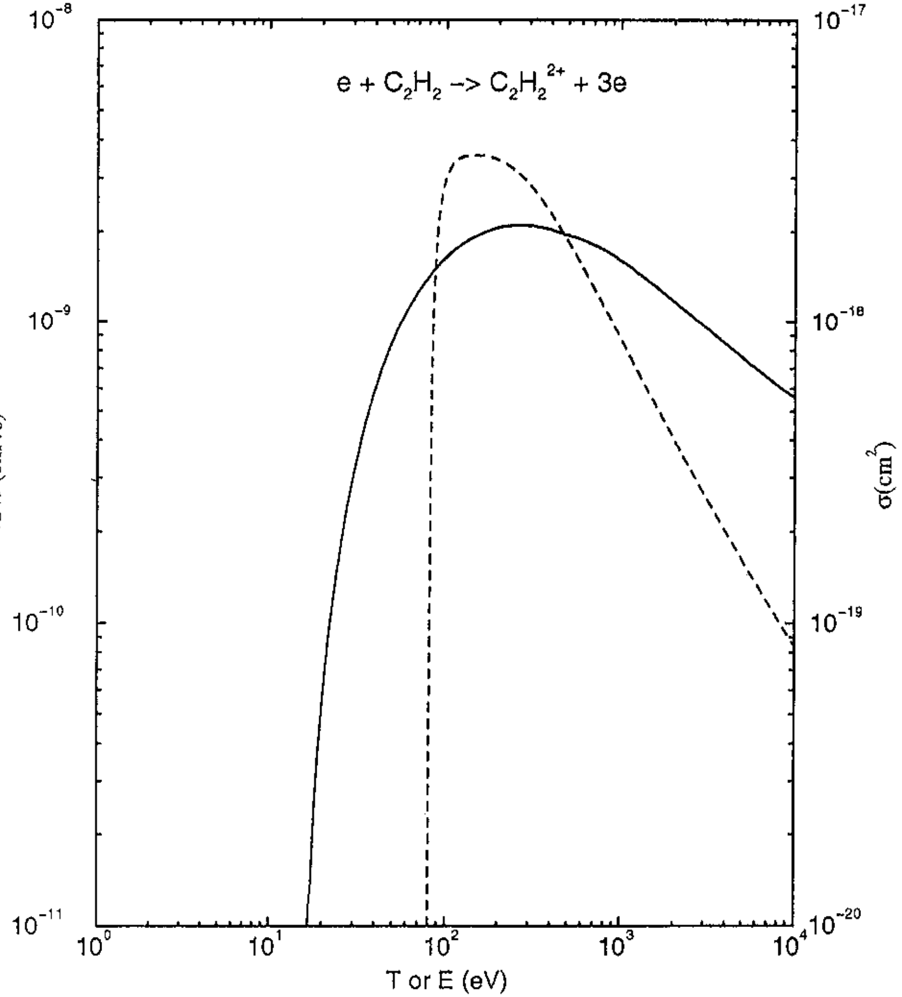
e + C2H2 -> C2H2 2+ + 3e
<σv>(cm3/s)
σ(cm2)
T or E (eV)
10−8
10−9
10−10
10−11
10−17
10−18
10−19
10−20
100
101
102
103
104

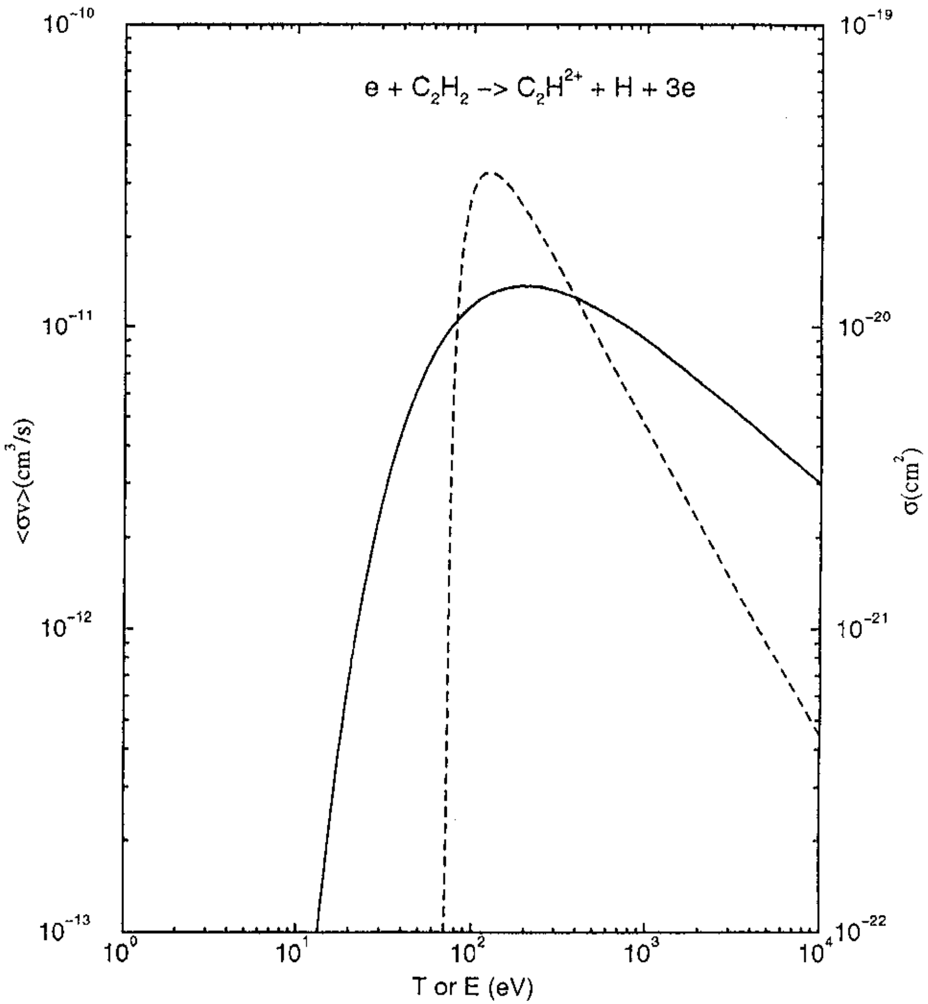
e + C2H2 -> C2H2+ + H + 3e
<σv>(cm3/s)
σ(cm2)
T or E (eV)
10−10
10−11
10−12
10−13
10−19
10−20
10−21
10−22
100
101
102
103
104

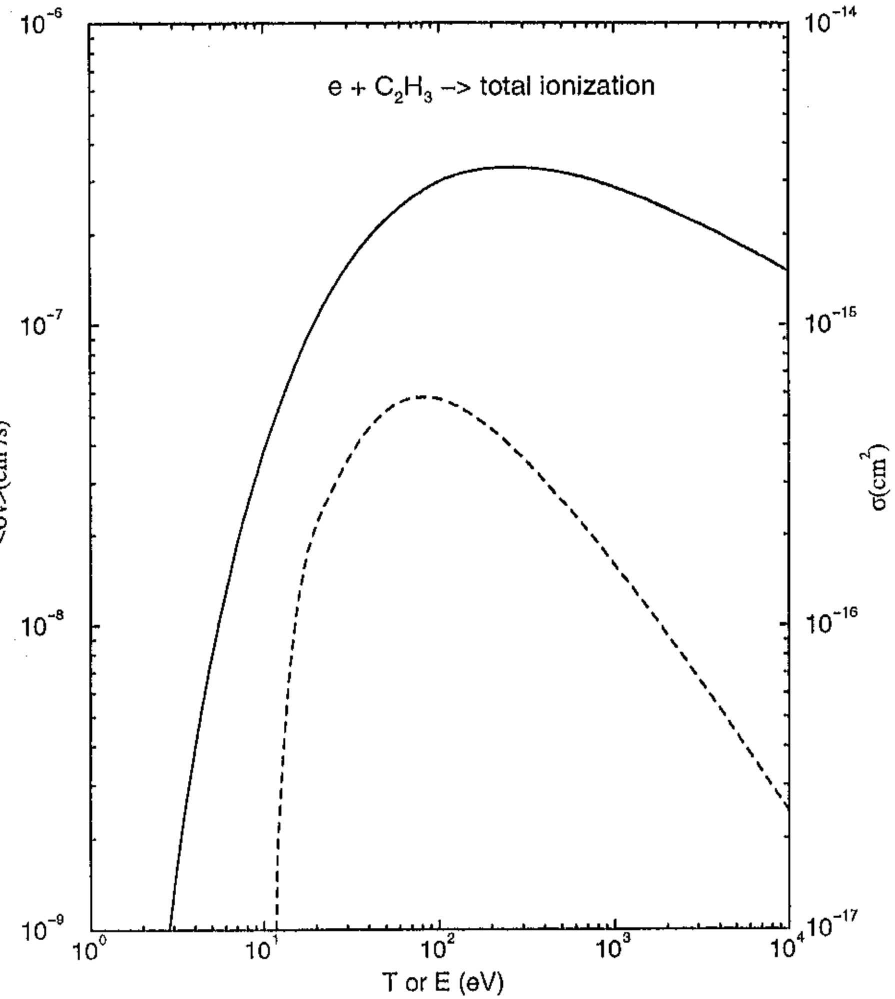
e + C_2H_3 –> total ionization
<σv>(cm^3/s)
σ(cm^2)
T or E (eV)
10^{-6}
10^{-7}
10^{-8}
10^{-9}
10^{-14}
10^{-15}
10^{-16}
10^{-17}
10^0
10^1
10^2
10^3
10^4

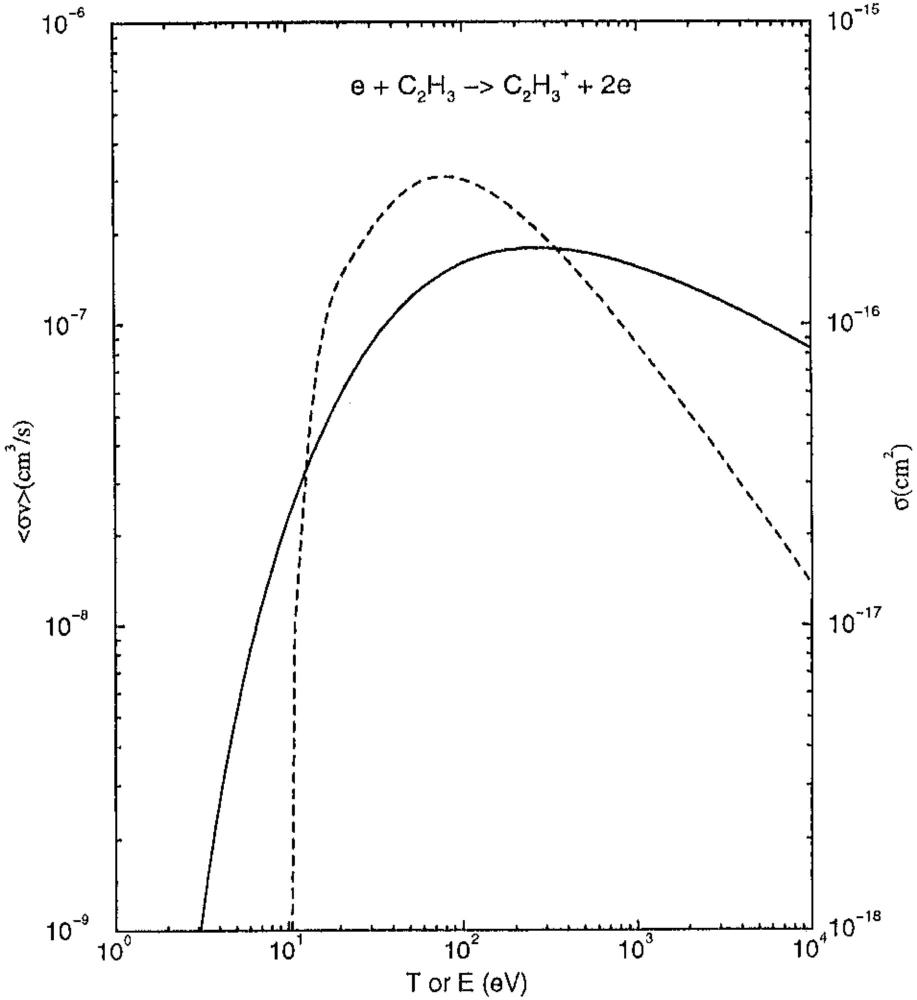
e + C_2H_3 –> $C_2H_3^+$ + 2e
<σv>(cm^3/s)
σ(cm^2)
T or E (eV)
10^{-6}
10^{-7}
10^{-8}
10^{-9}
10^{-15}
10^{-16}
10^{-17}
10^{-18}
10^0
10^1
10^2
10^3
10^4

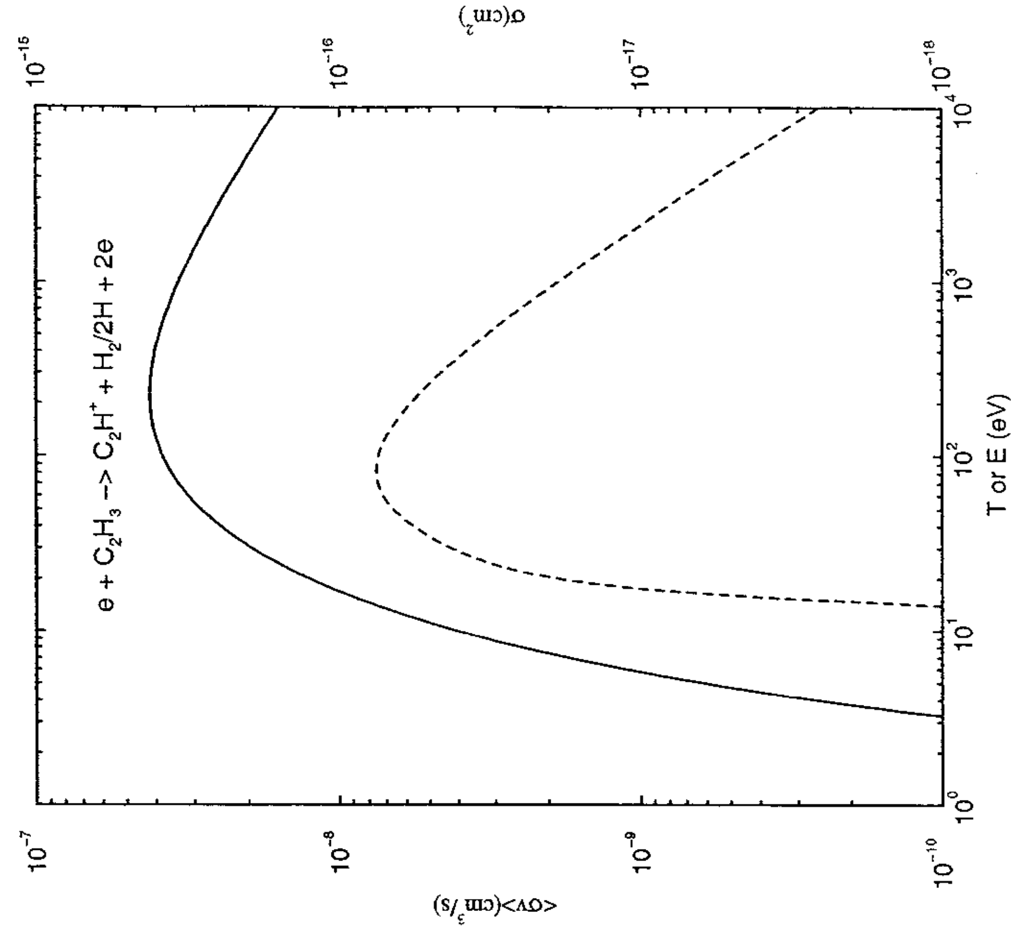

e + C2H3 -> C2H+ + H2/2H + 2e
T or E (eV)
<σv>(cm3/s)
σ(cm2)

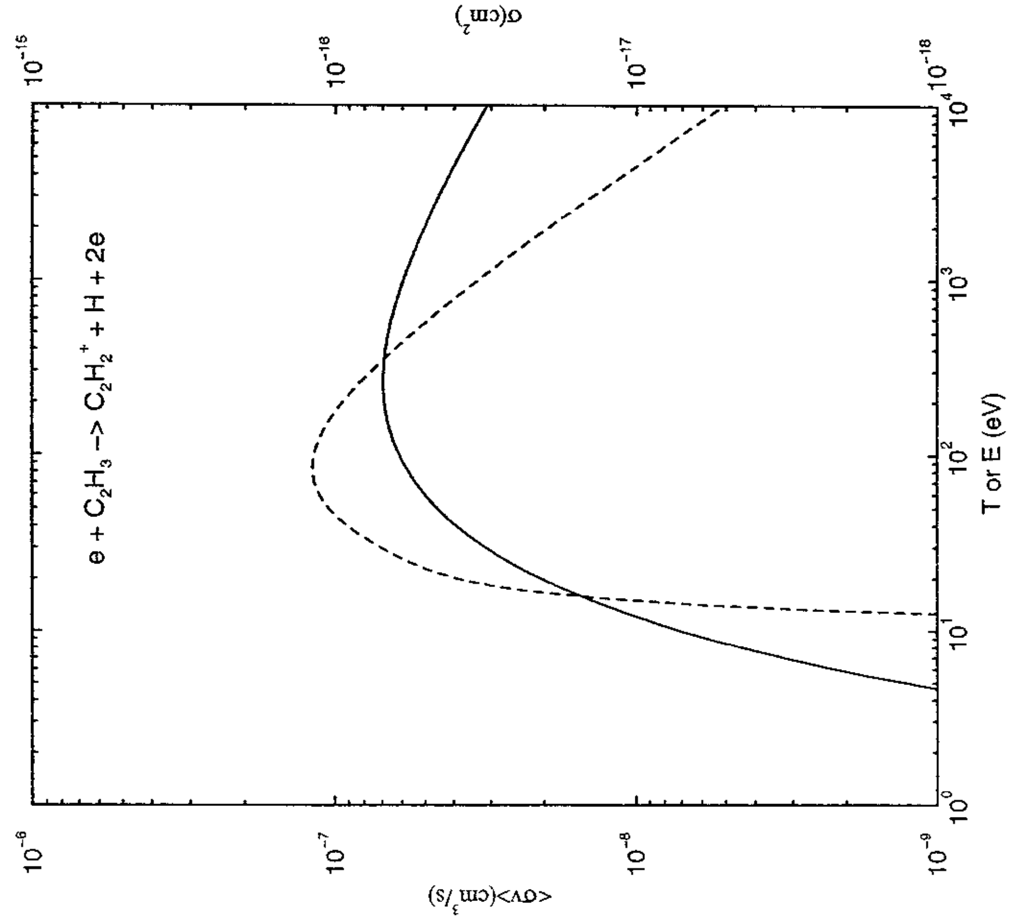

e + C2H3 -> C2H2+ + H + 2e
T or E (eV)
<σv>(cm3/s)
σ(cm2)

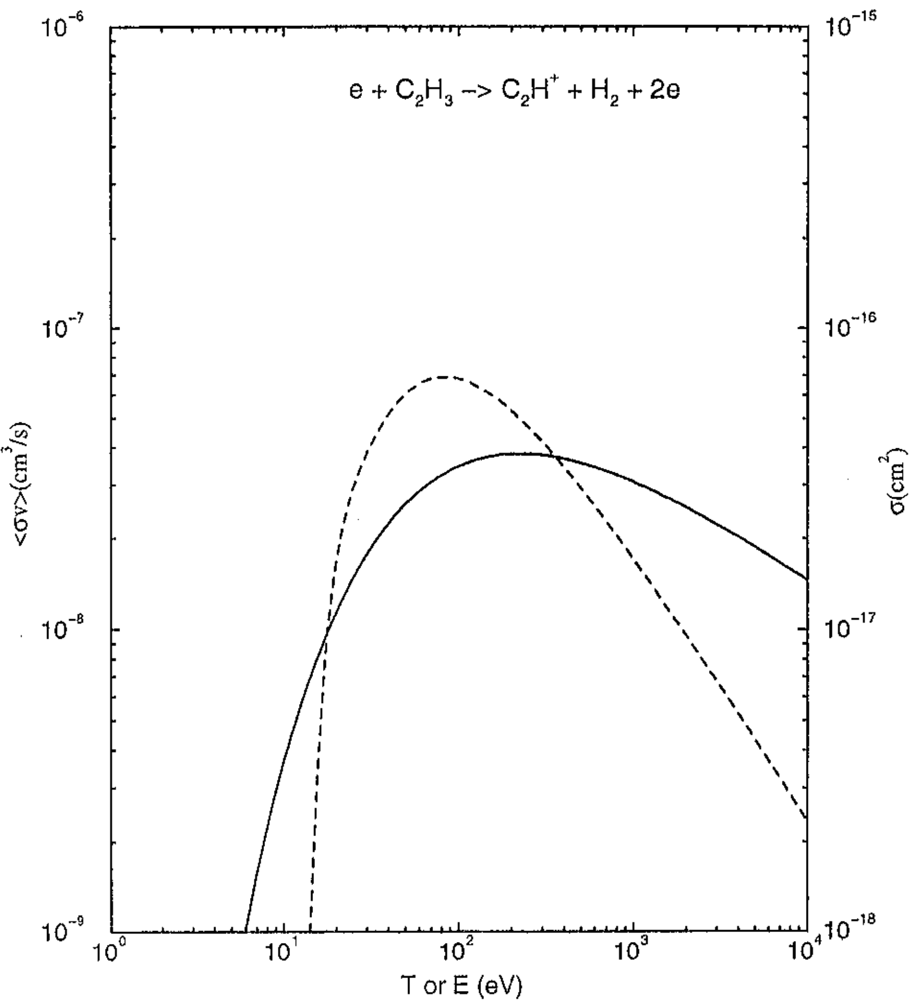

e + C2H3 -> C2H+ + H2 + 2e
<σv>(cm3/s)
σ(cm2)
T or E (eV)

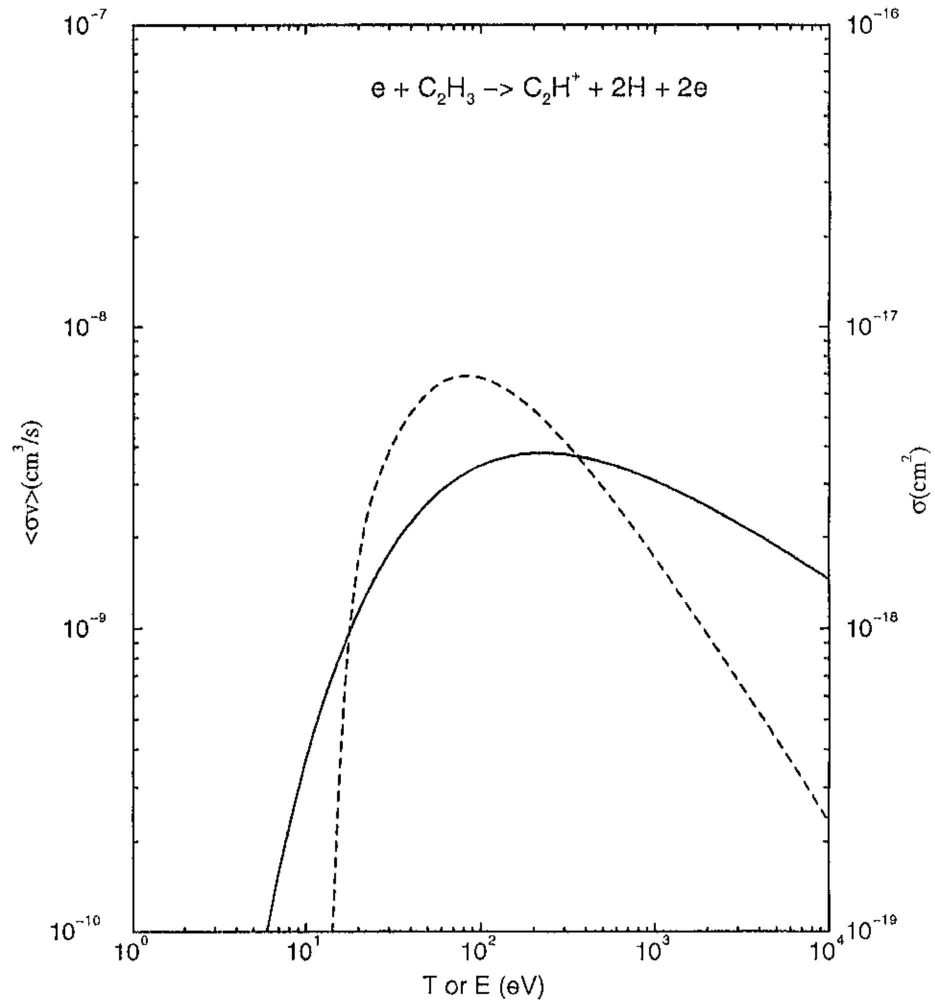

e + C2H3 -> C2H+ + 2H + 2e
<σv>(cm3/s)
σ(cm2)
T or E (eV)

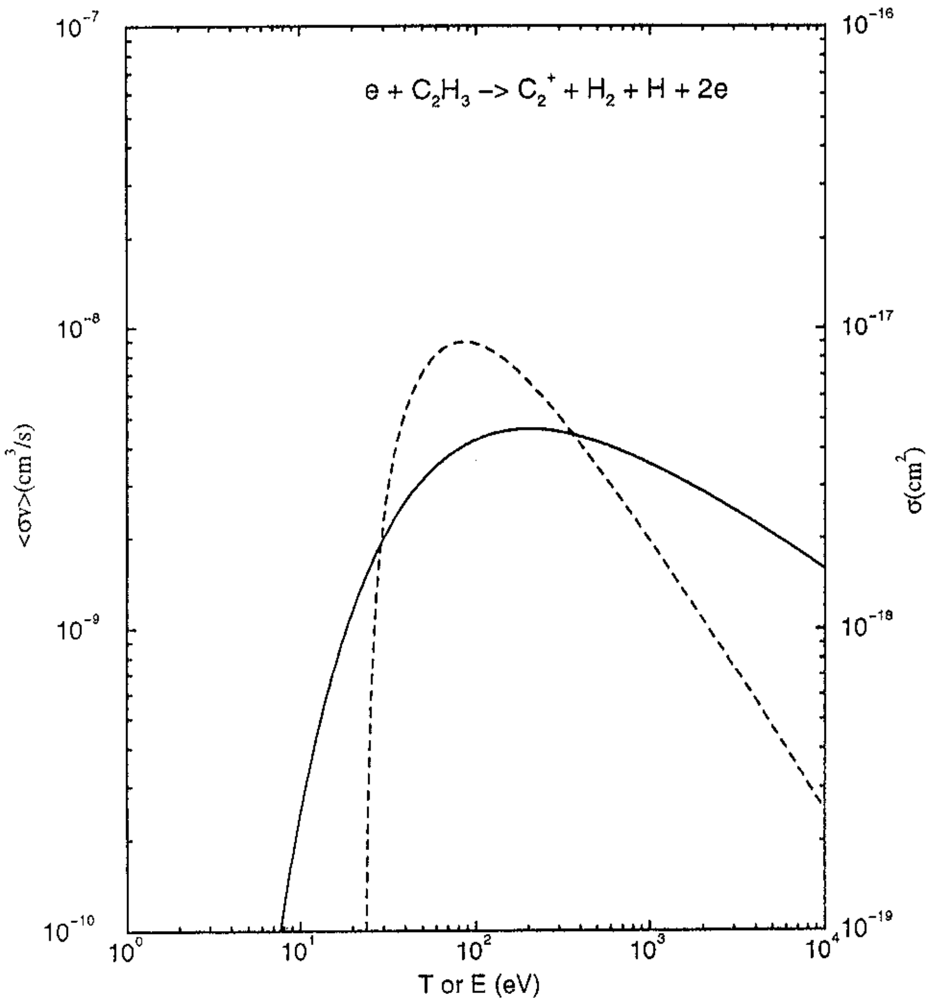
e + C_2H_3 -> C_2^+ + H_2 + H + 2e
<σv>(cm^3/s)
σ(cm^2)
T or E (eV)
10^{-7}
10^{-8}
10^{-9}
10^{-10}
10^{-16}
10^{-17}
10^{-18}
10^{-19}
10^0
10^1
10^2
10^3
10^4

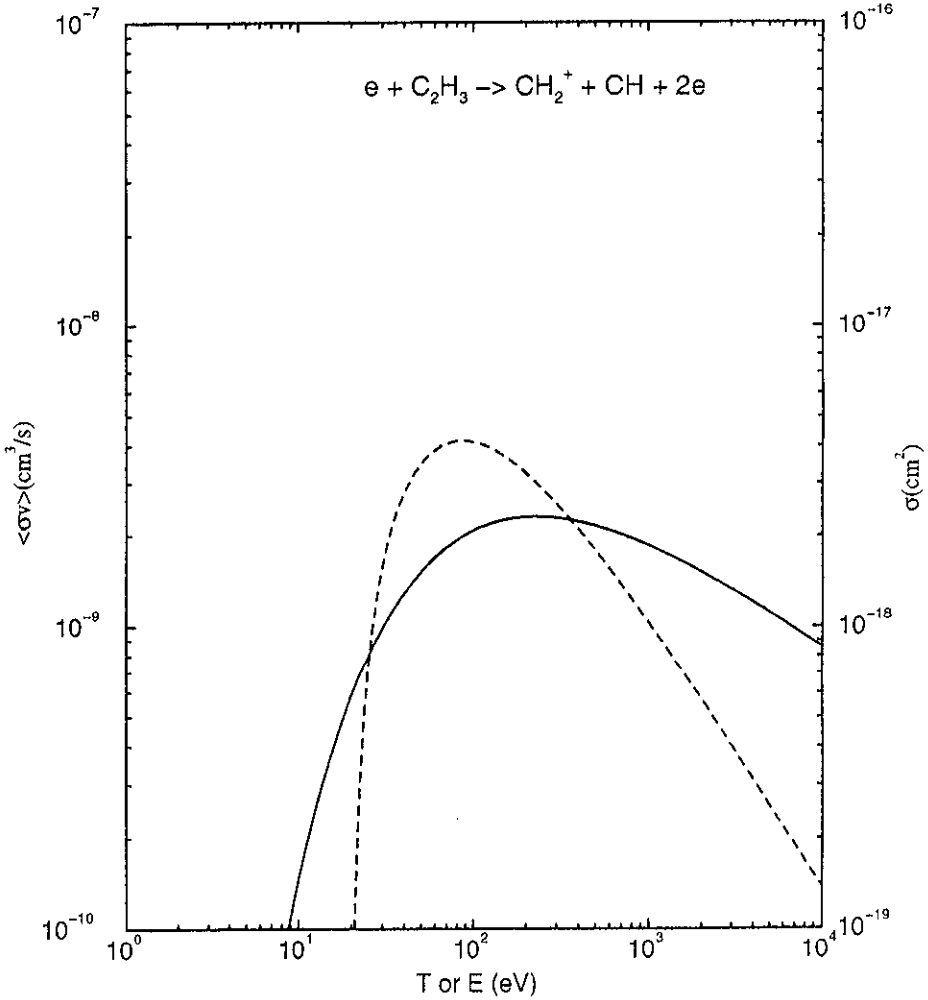
e + C_2H_3 -> CH_2^+ + CH + 2e
<σv>(cm^3/s)
σ(cm^2)
T or E (eV)
10^{-7}
10^{-8}
10^{-9}
10^{-10}
10^{-16}
10^{-17}
10^{-18}
10^{-19}
10^0
10^1
10^2
10^3
10^4

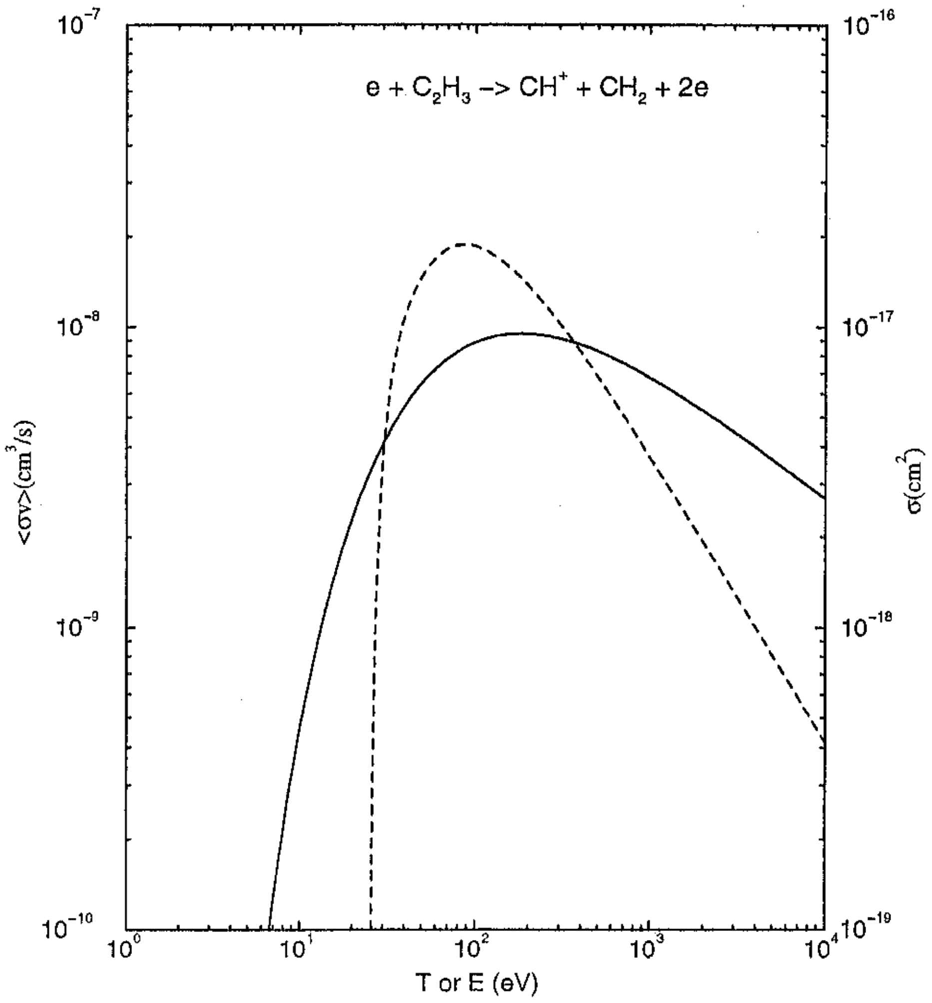
e + C_2H_3 -> CH^+ + CH_2 + 2e
<σv>(cm^3/s)
σ(cm^2)
T or E (eV)
10^{-7}
10^{-8}
10^{-9}
10^{-10}
10^{-16}
10^{-17}
10^{-18}
10^{-19}
10^0
10^1
10^2
10^3
10^4

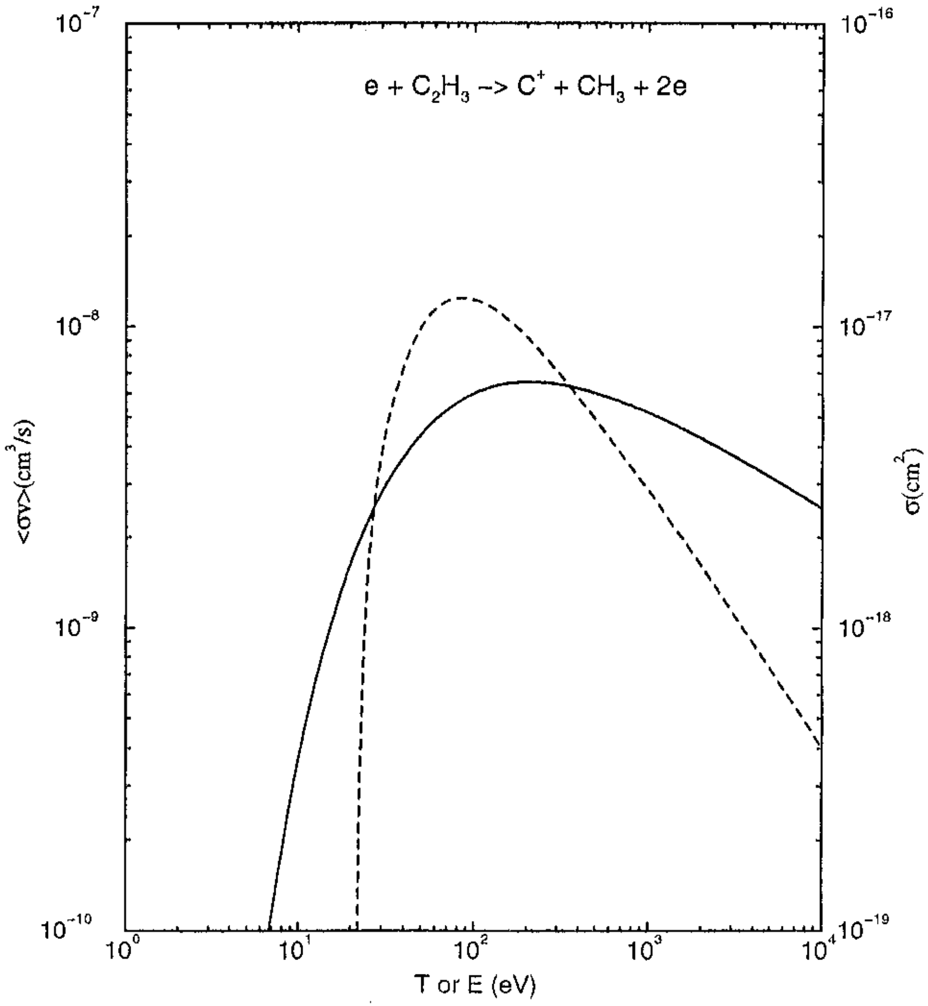
e + C_2H_3 -> C^+ + CH_3 + 2e
<σv>(cm^3/s)
σ(cm^2)
T or E (eV)
10^{-7}
10^{-8}
10^{-9}
10^{-10}
10^{-16}
10^{-17}
10^{-18}
10^{-19}
10^0
10^1
10^2
10^3
10^4

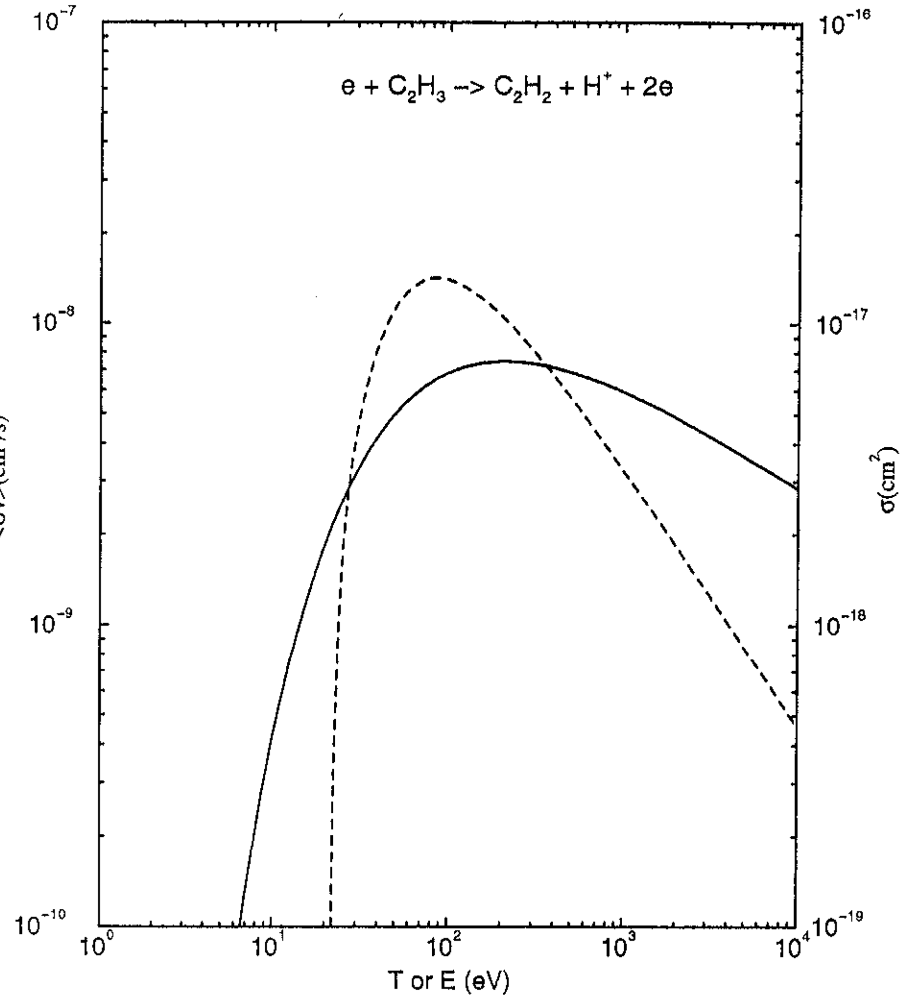

e + C_2H_3 -> C_2H_2 + H^+ + 2e
$<\sigma v>(cm^3/s)$
$\sigma(cm^2)$
T or E (eV)
10^{-7}
10^{-8}
10^{-9}
10^{-10}
10^{-16}
10^{-17}
10^{-18}
10^{-19}
10^0
10^1
10^2
10^3
10^4

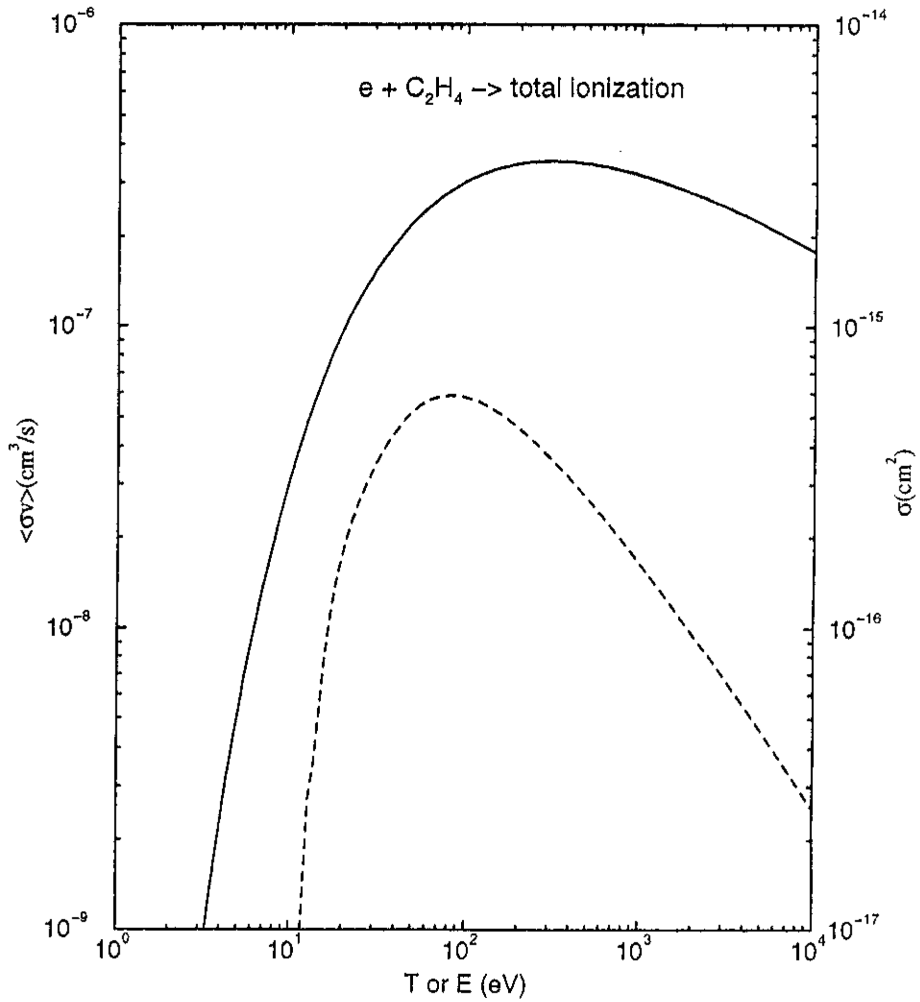

e + C_2H_4 -> total Ionization
$<\sigma v>(cm^3/s)$
$\sigma(cm^2)$
T or E (eV)
10^{-6}
10^{-7}
10^{-8}
10^{-9}
10^{-14}
10^{-15}
10^{-16}
10^{-17}
10^0
10^1
10^2
10^3
10^4

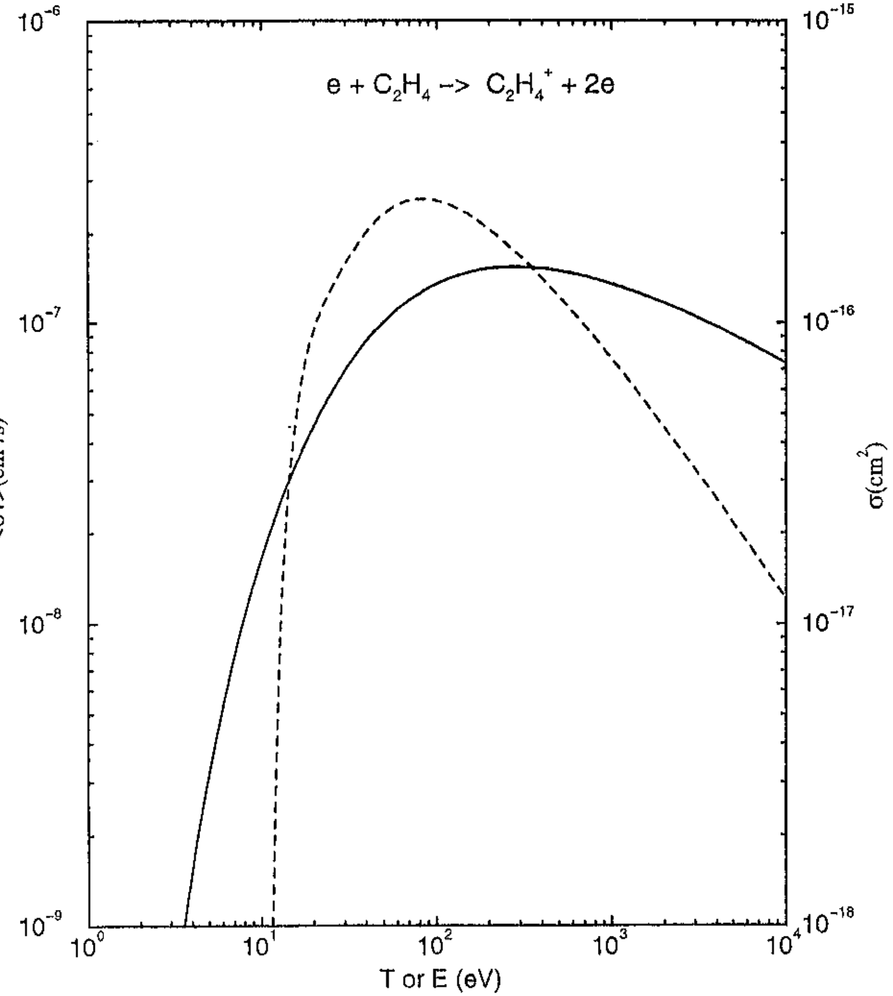
e + C_2H_4 -> $C_2H_4^+$ + 2e
<σv>(cm^3/s)
σ(cm^2)
T or E (eV)
10^{-6}
10^{-7}
10^{-8}
10^{-9}
10^{-15}
10^{-16}
10^{-17}
10^{-18}
10^0
10^1
10^2
10^3
10^4

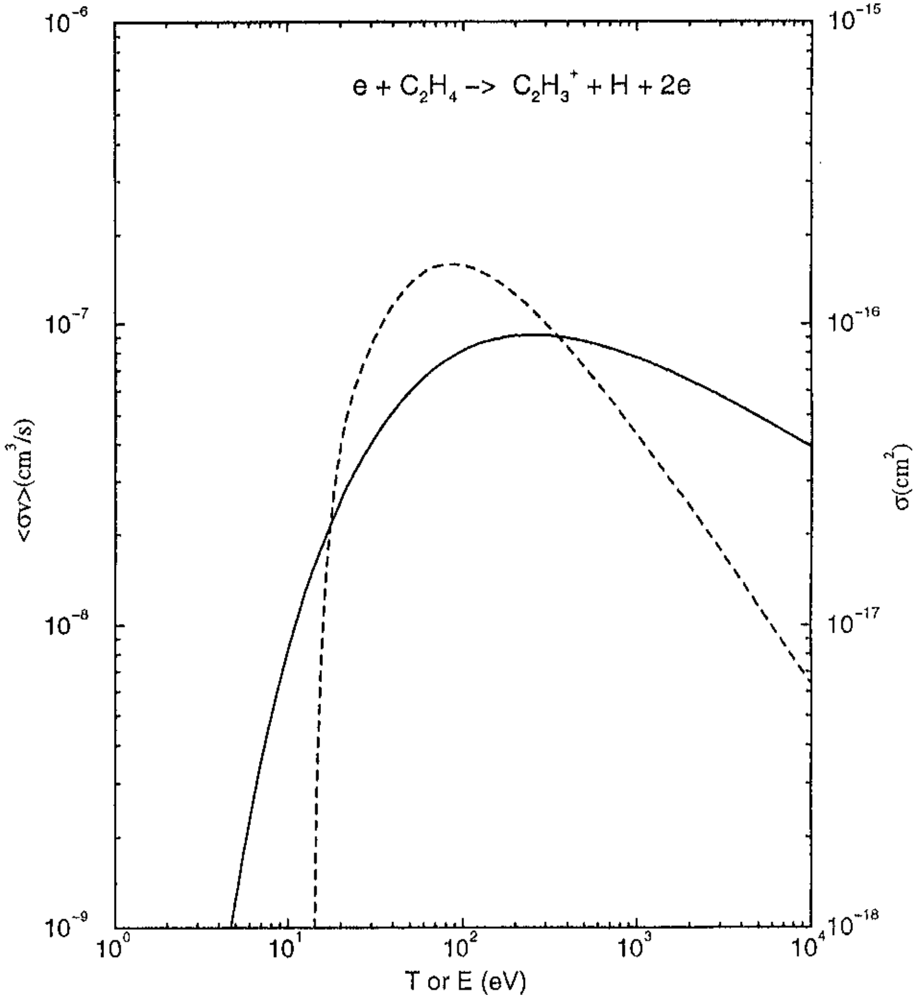
e + C_2H_4 -> $C_2H_3^+$ + H + 2e
<σv>(cm^3/s)
σ(cm^2)
T or E (eV)
10^{-6}
10^{-7}
10^{-8}
10^{-9}
10^{-15}
10^{-16}
10^{-17}
10^{-18}
10^0
10^1
10^2
10^3
10^4

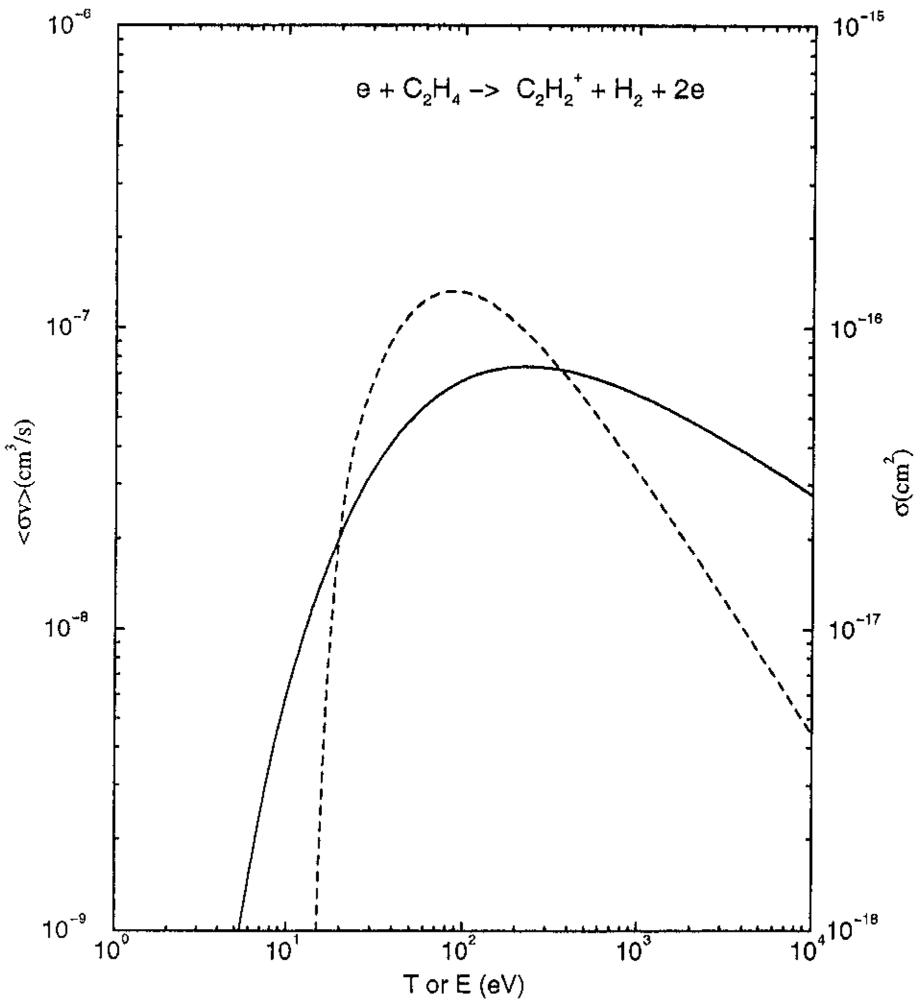

e + C_2H_4 -> $C_2H_2^+$ + H_2 + 2e
<σv>(cm³/s)
σ(cm²)
T or E (eV)

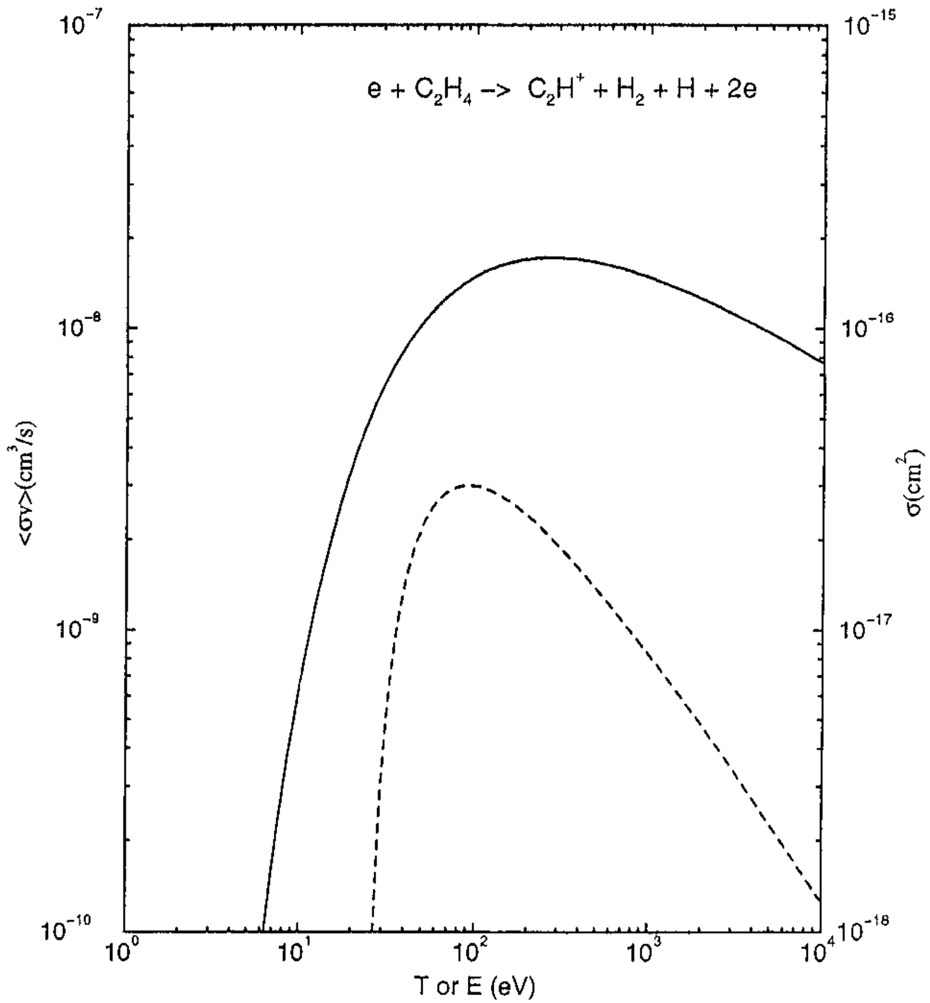

e + C_2H_4 -> C_2H^+ + H_2 + H + 2e
<σv>(cm³/s)
σ(cm²)
T or E (eV)

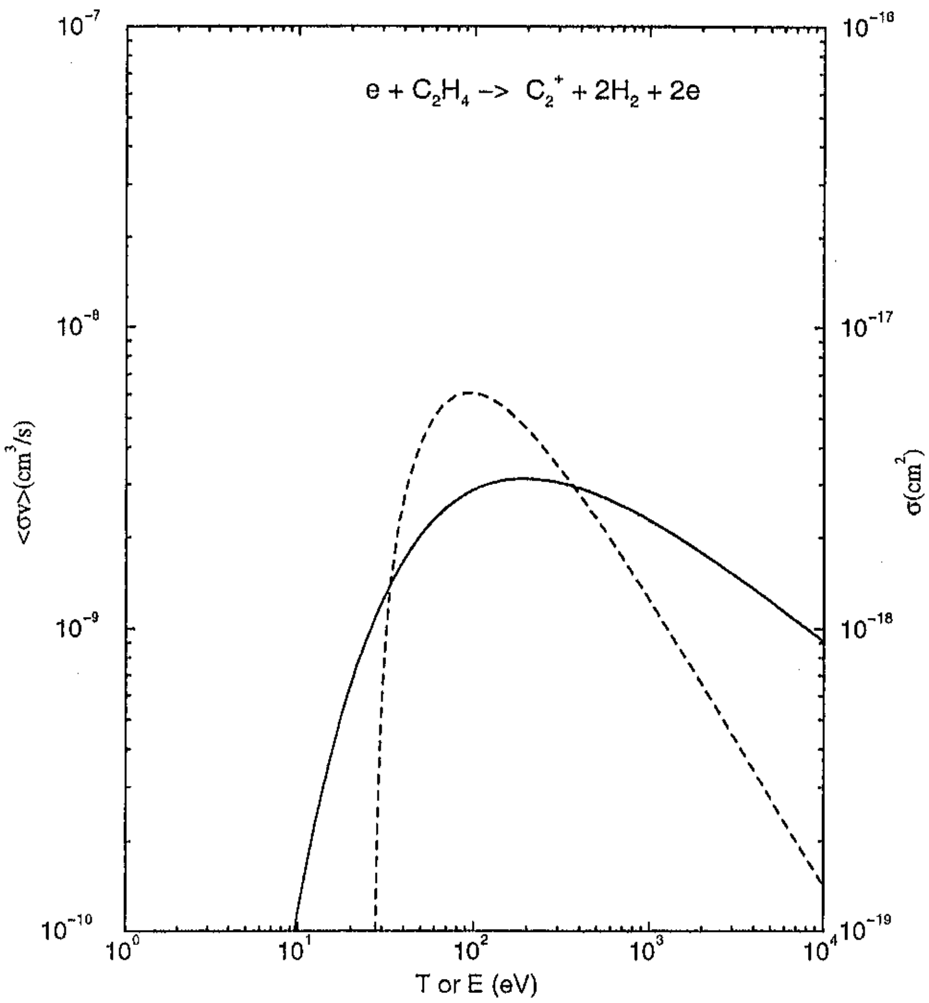
e + C_2H_4 -> C_2^+ + $2H_2$ + 2e
<σv>(cm^3/s)
σ(cm^2)
T or E (eV)
10^{-7}
10^{-8}
10^{-9}
10^{-10}
10^{-16}
10^{-17}
10^{-18}
10^{-19}
10^0
10^1
10^2
10^3
10^4

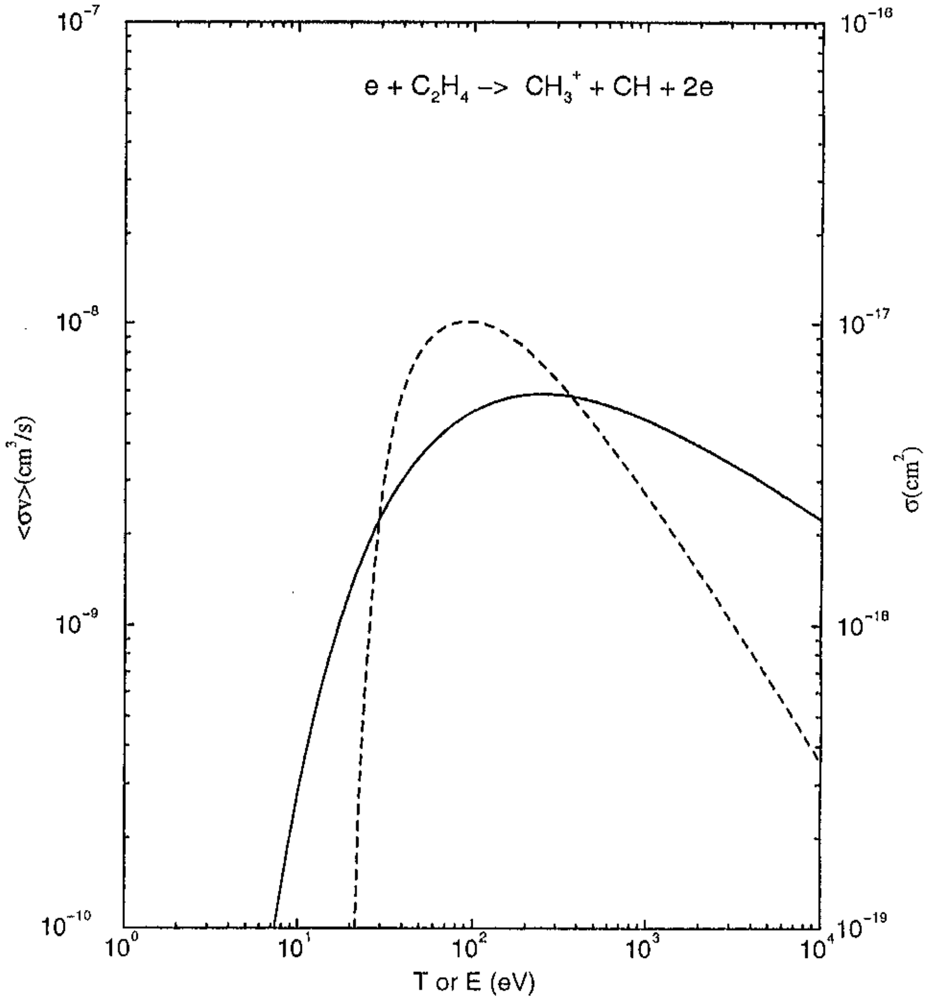
e + C_2H_4 -> CH_3^+ + CH + 2e
<σv>(cm^3/s)
σ(cm^2)
T or E (eV)
10^{-7}
10^{-8}
10^{-9}
10^{-10}
10^{-16}
10^{-17}
10^{-18}
10^{-19}
10^0
10^1
10^2
10^3
10^4

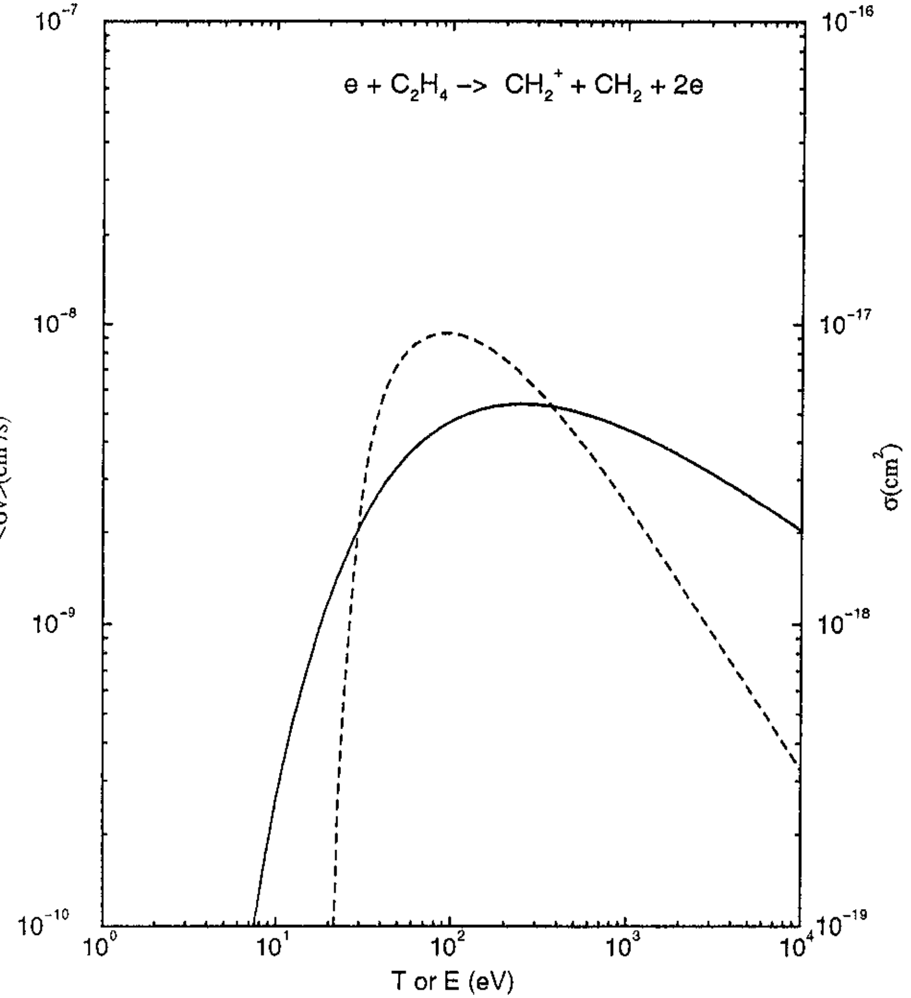
e + C2H4 -> CH2+ + CH2 + 2e
<σv>(cm3/s)
σ(cm2)
T or E (eV)
10-7
10-8
10-9
10-10
10-16
10-17
10-18
10-19
10^0
10^1
10^2
10^3
10^4

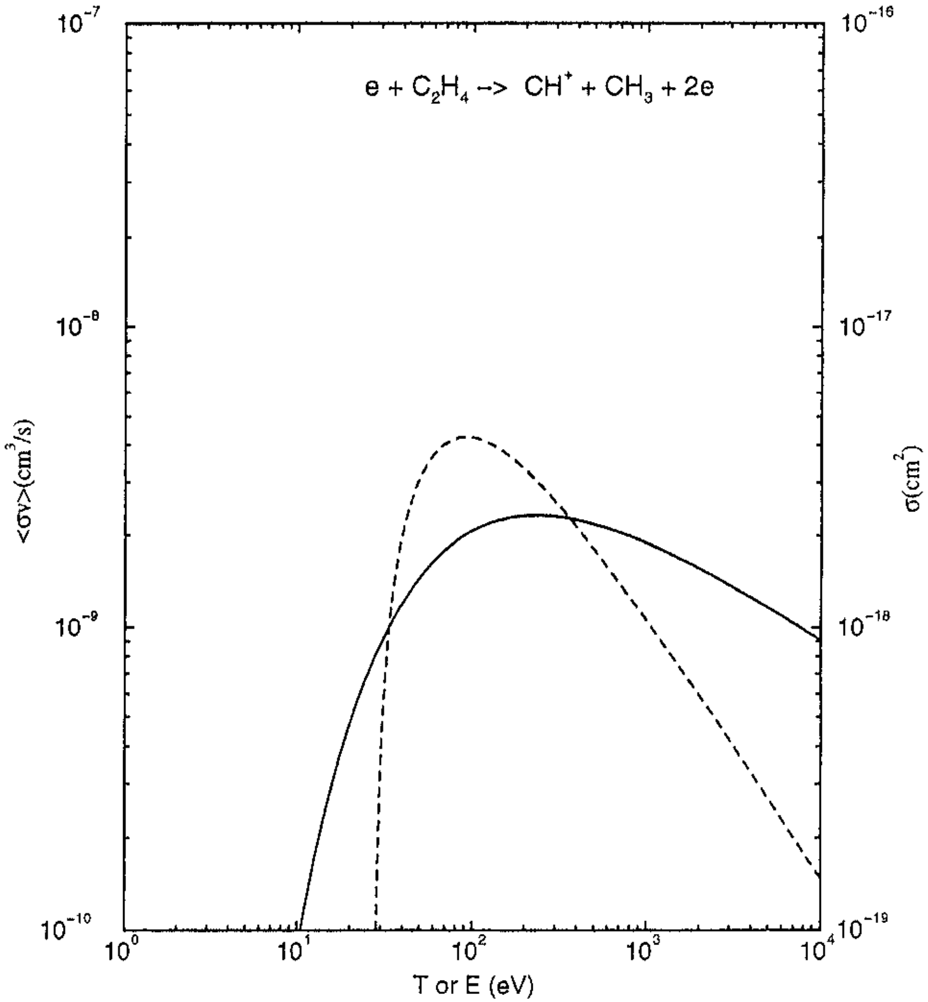
e + C2H4 -> CH+ + CH3 + 2e
<σv>(cm3/s)
σ(cm2)
T or E (eV)
10-7
10-8
10-9
10-10
10-16
10-17
10-18
10-19
10^0
10^1
10^2
10^3
10^4

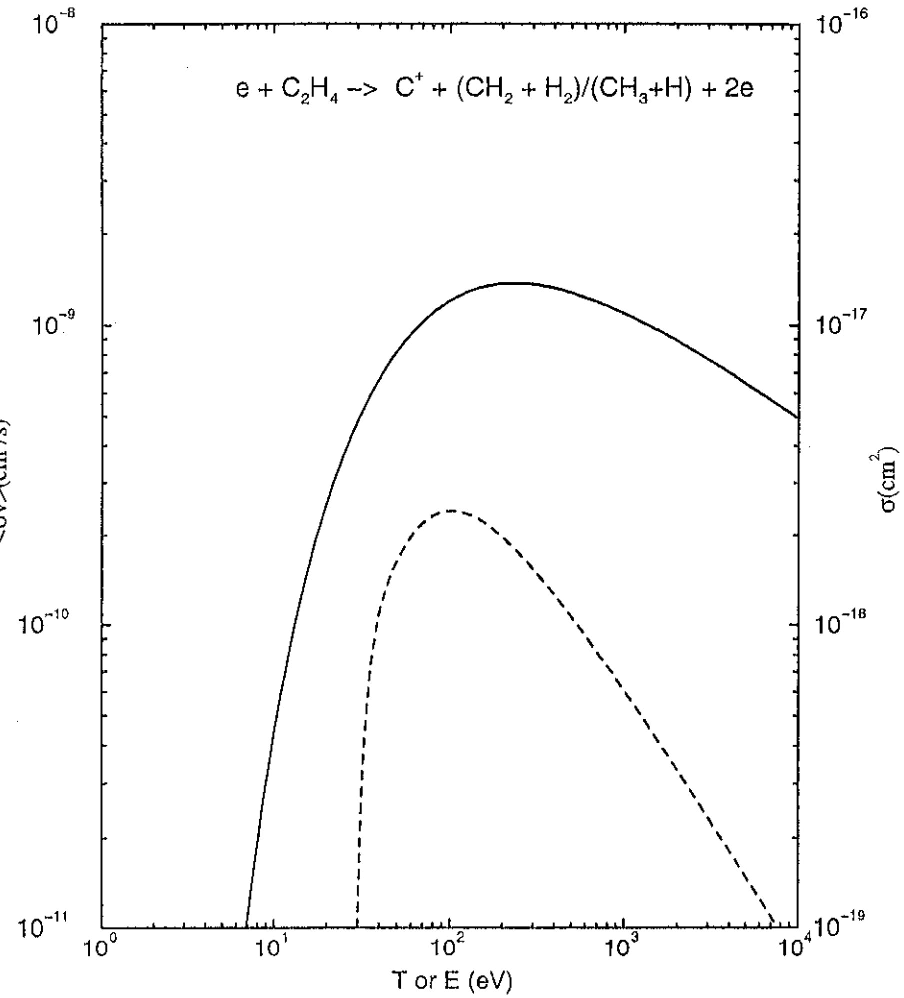

e + C2H4 --> C+ + (CH2 + H2)/(CH3+H) + 2e
<σv>(cm3/s)
σ(cm2)
T or E (eV)

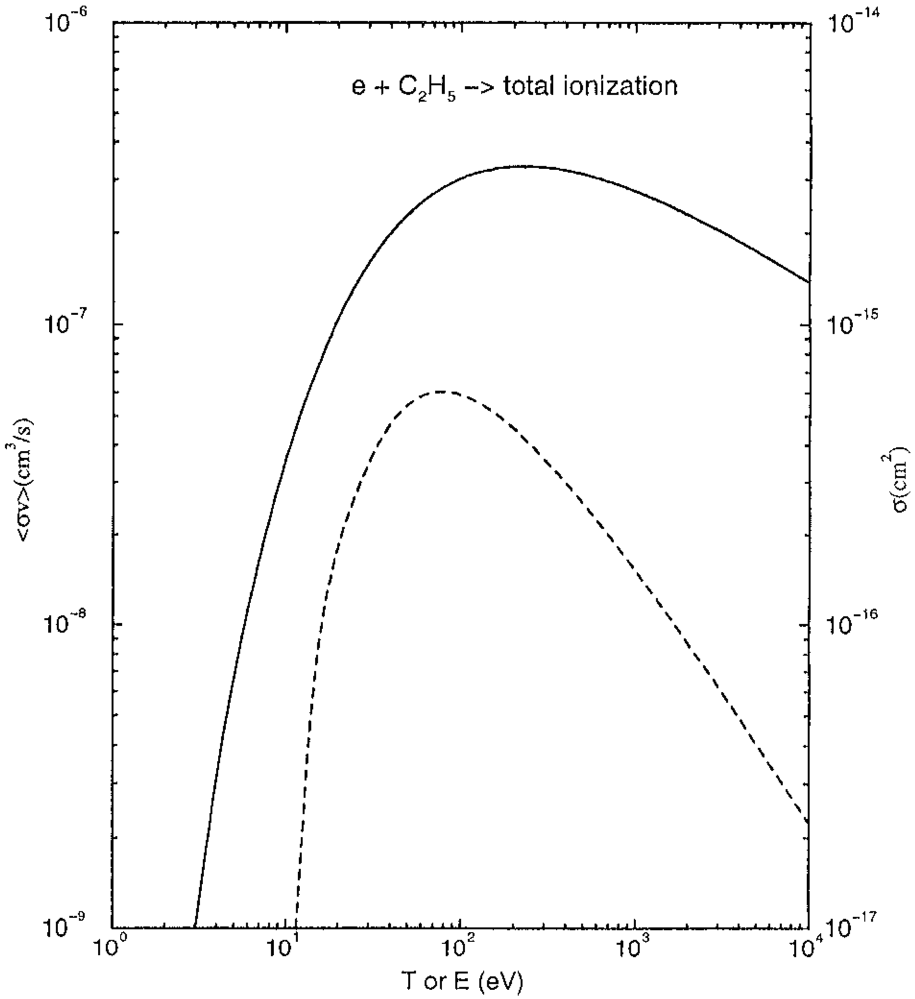

e + C2H5 --> total ionization
<σv>(cm3/s)
σ(cm2)
T or E (eV)

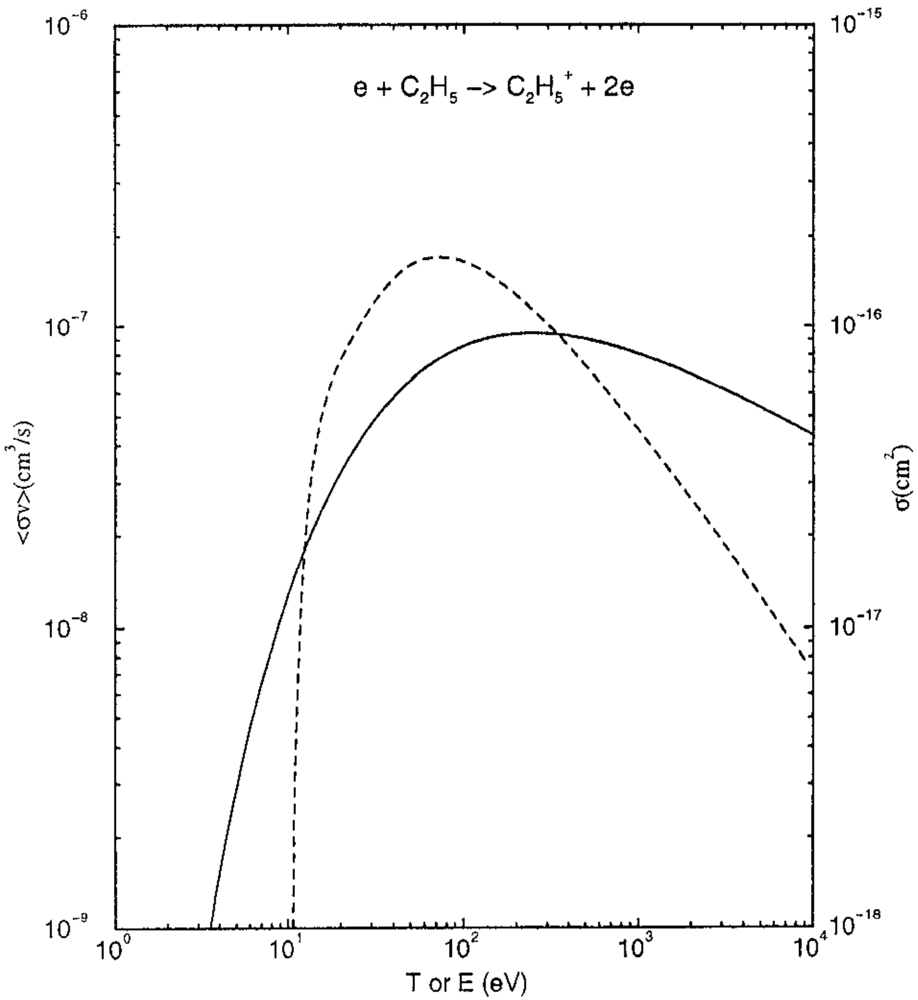
e + C_2H_5 -> $C_2H_5^+$ + 2e
<σv>(cm^3/s)
σ(cm^2)
T or E (eV)
10^{-6}
10^{-7}
10^{-8}
10^{-9}
10^{-15}
10^{-16}
10^{-17}
10^{-18}
10^0
10^1
10^2
10^3
10^4

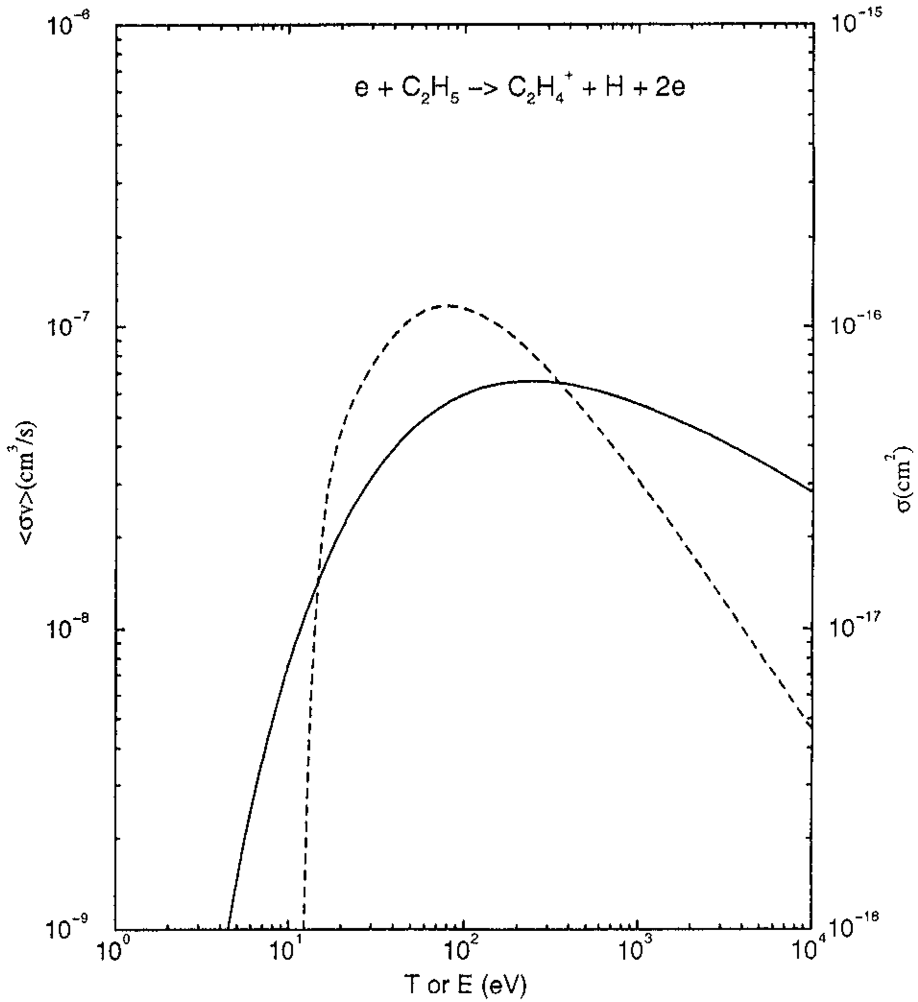
e + C_2H_5 -> $C_2H_4^+$ + H + 2e
<σv>(cm^3/s)
σ(cm^2)
T or E (eV)
10^{-6}
10^{-7}
10^{-8}
10^{-9}
10^{-15}
10^{-16}
10^{-17}
10^{-18}
10^0
10^1
10^2
10^3
10^4

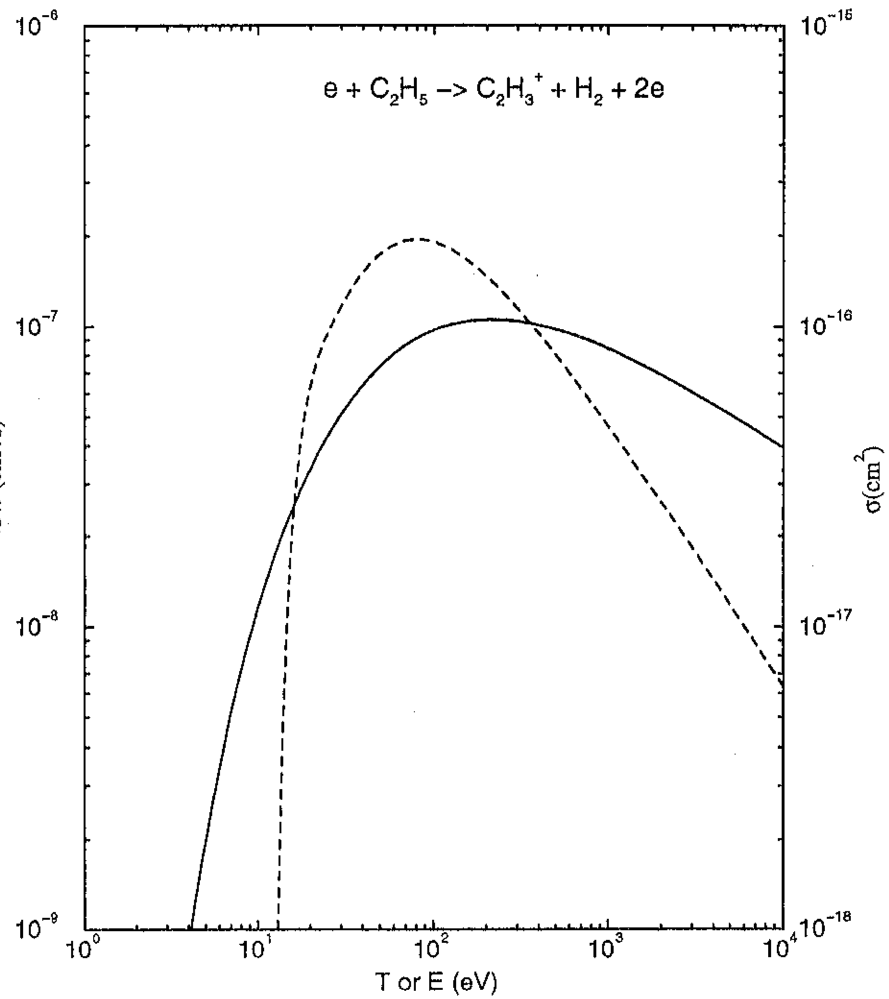

e + C2H5 -> C2H3+ + H2 + 2e
<σv>(cm3/s)
σ(cm2)
T or E (eV)

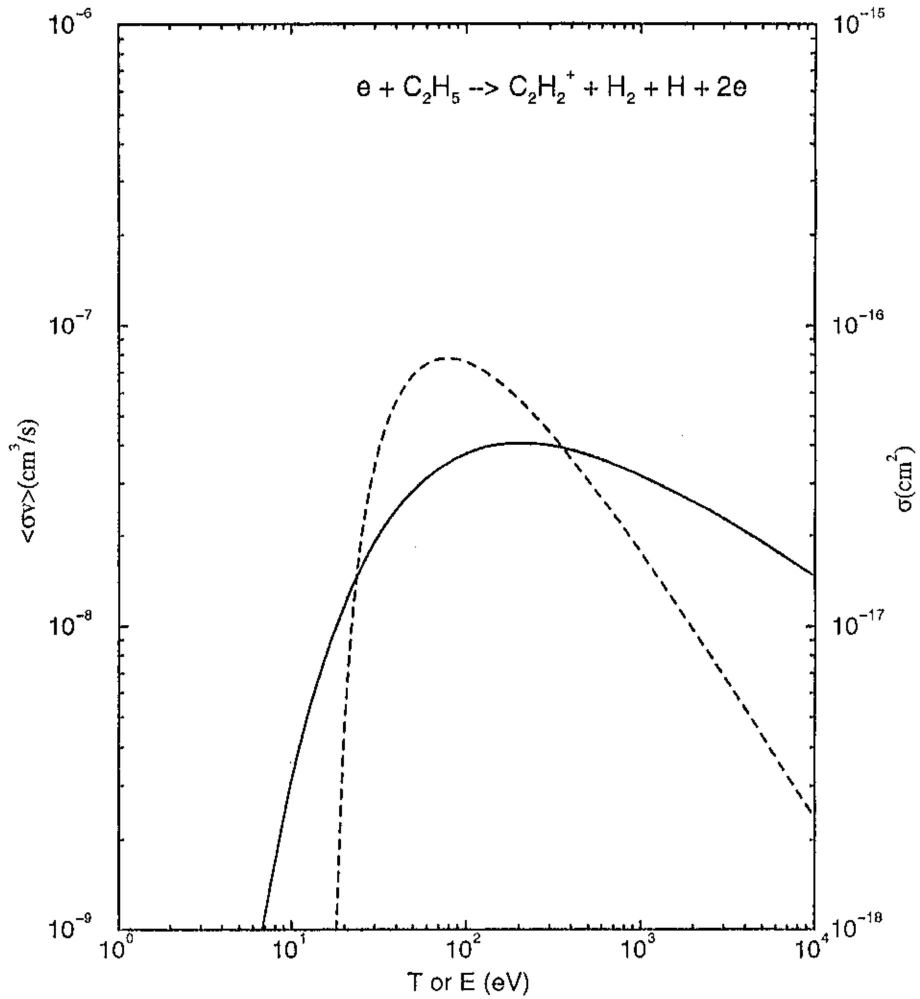

e + C2H5 --> C2H2+ + H2 + H + 2e
<σv>(cm3/s)
σ(cm2)
T or E (eV)

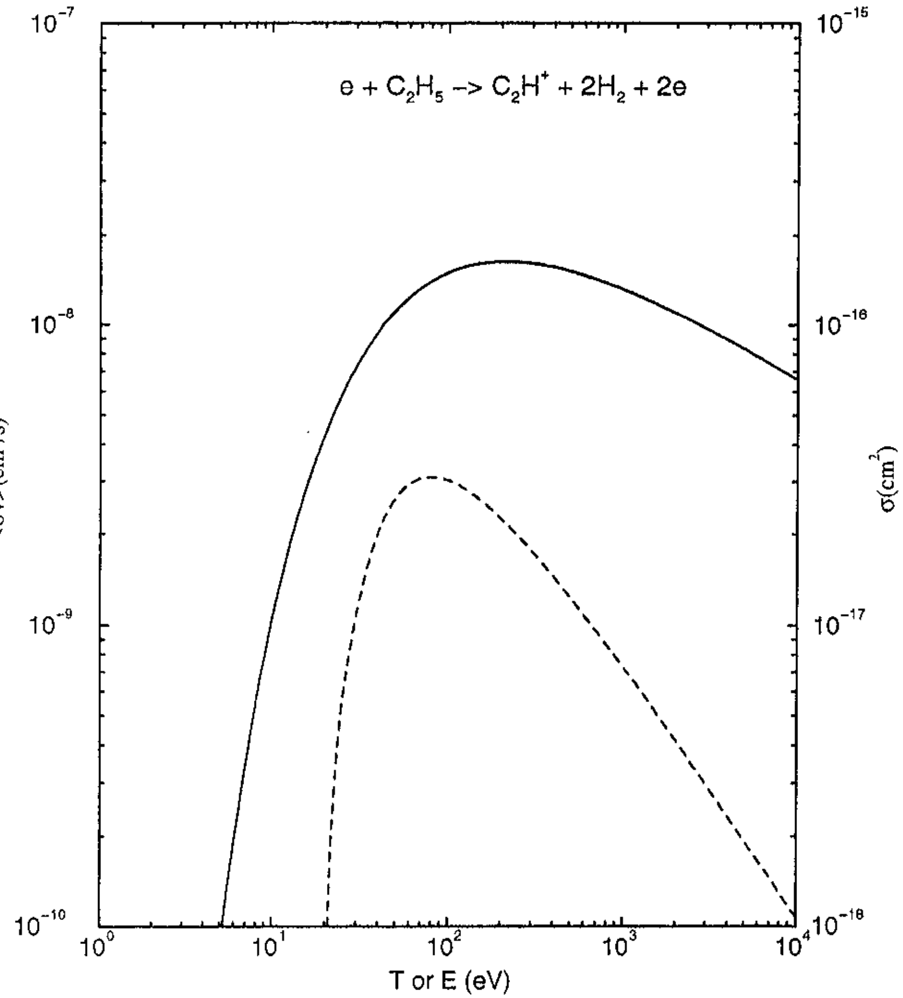

e + C2H5 -> C2H+ + 2H2 + 2e
<σv>(cm3/s)
σ(cm2)
T or E (eV)
10-7
10-8
10-9
10-10
10-15
10-16
10-17
10-18
100
101
102
103
104

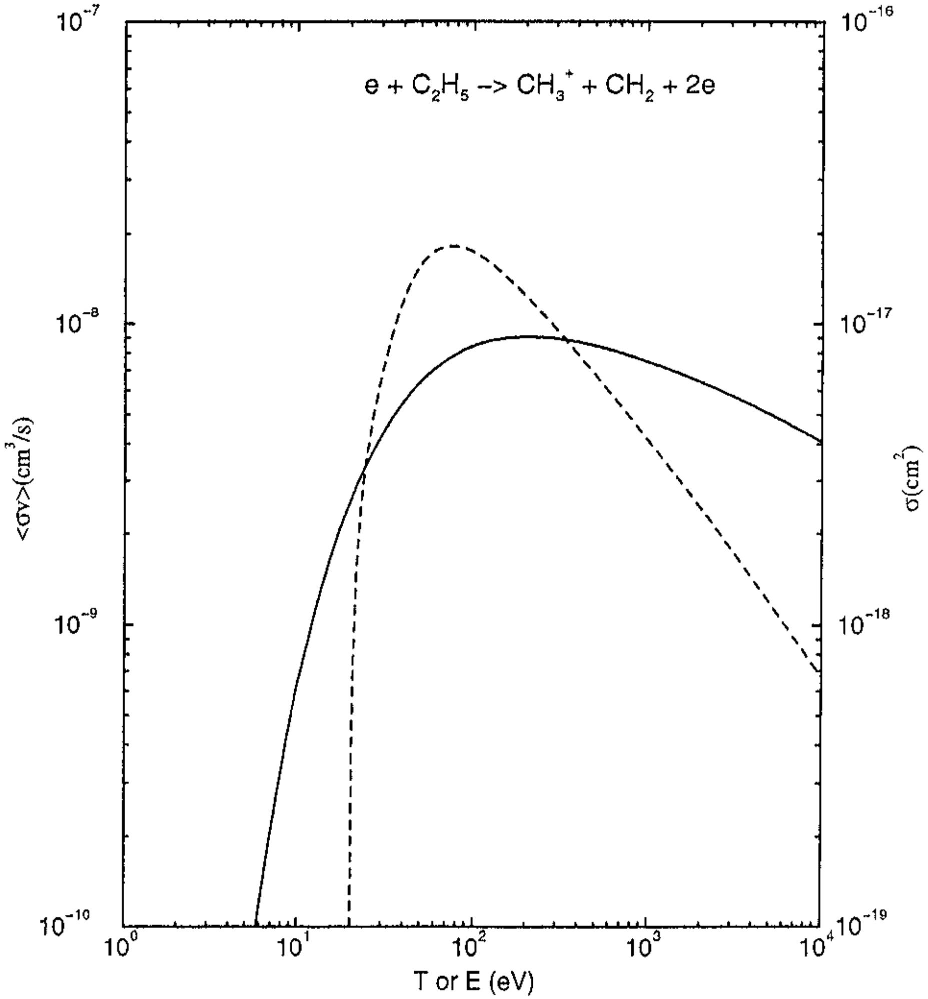

e + C2H5 -> CH3+ + CH2 + 2e
<σv>(cm3/s)
σ(cm2)
T or E (eV)
10-7
10-8
10-9
10-10
10-16
10-17
10-18
10-19
100
101
102
103
104

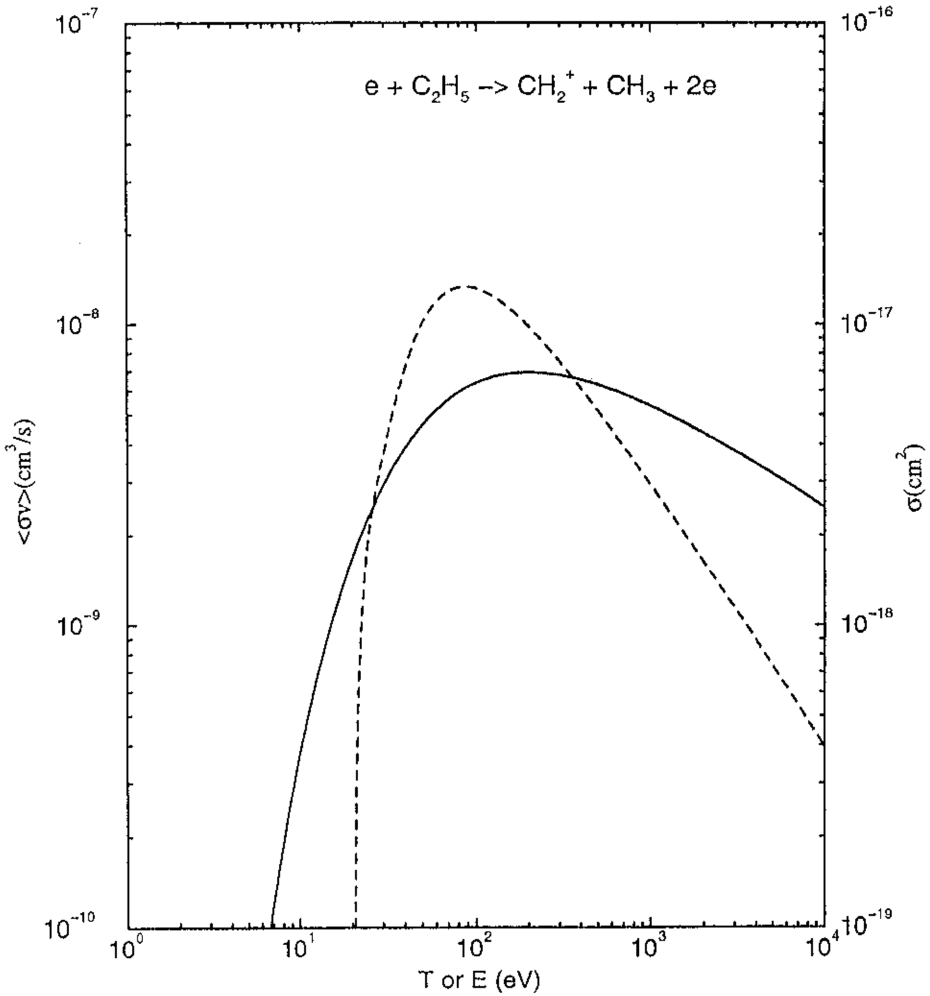
e + C2H5 -> CH2+ + CH3 + 2e
<σv>(cm3/s)
σ(cm2)
T or E (eV)
10−7
10−8
10−9
10−10
10−16
10−17
10−18
10−19
100
101
102
103
104

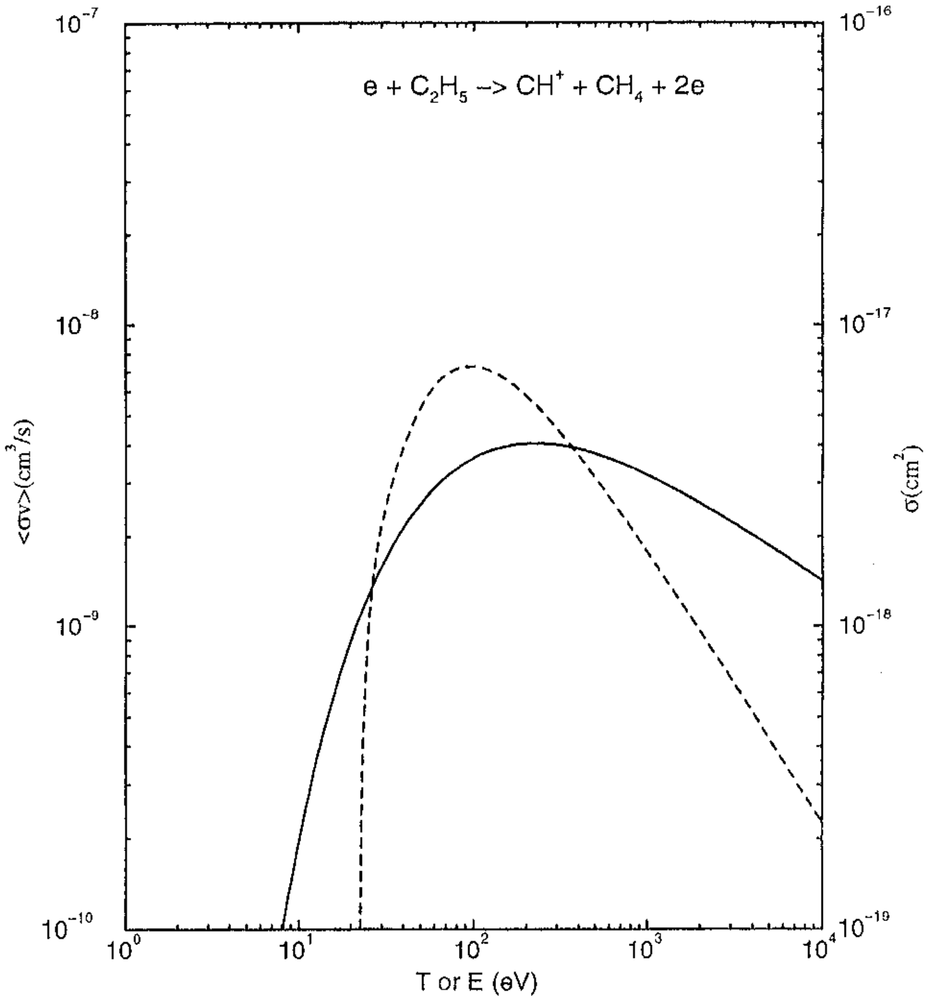
e + C2H5 -> CH+ + CH4 + 2e
<σv>(cm3/s)
σ(cm2)
T or E (eV)
10−7
10−8
10−9
10−10
10−16
10−17
10−18
10−19
100
101
102
103
104

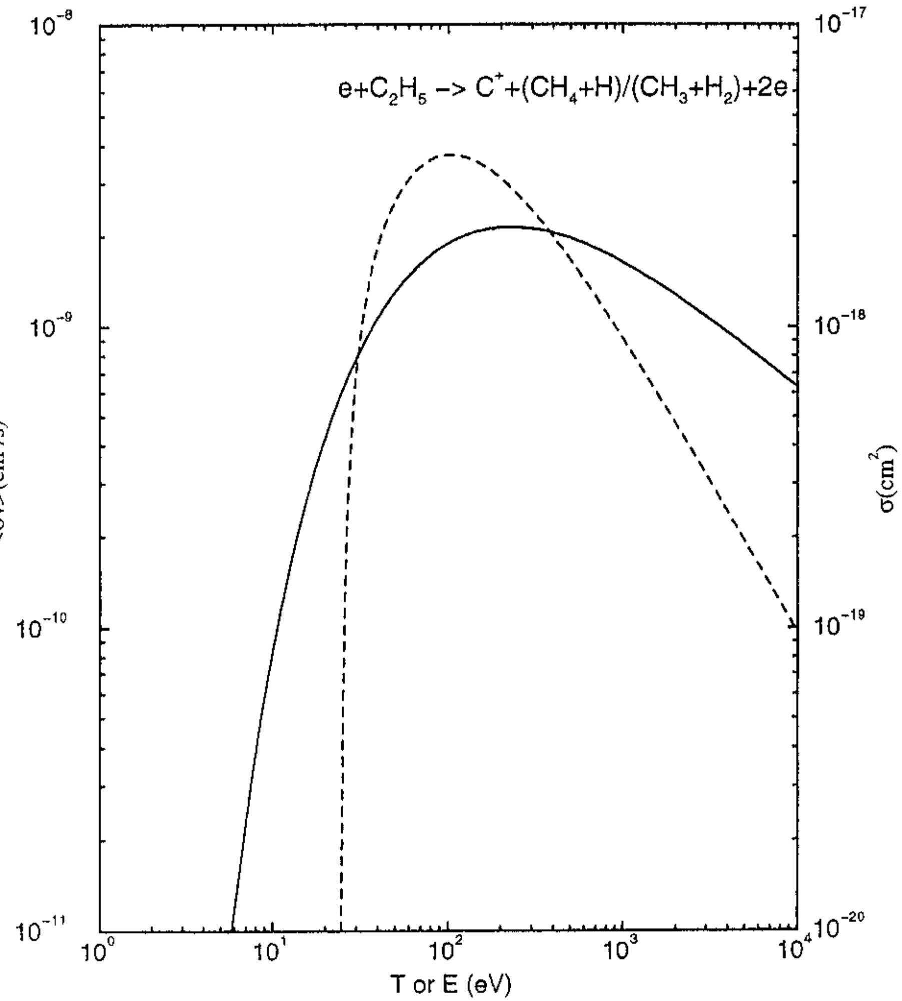
e+C2H5 -> C+ +(CH4+H)/(CH3+H2)+2e
<σv>(cm3/s)
σ(cm2)
T or E (eV)

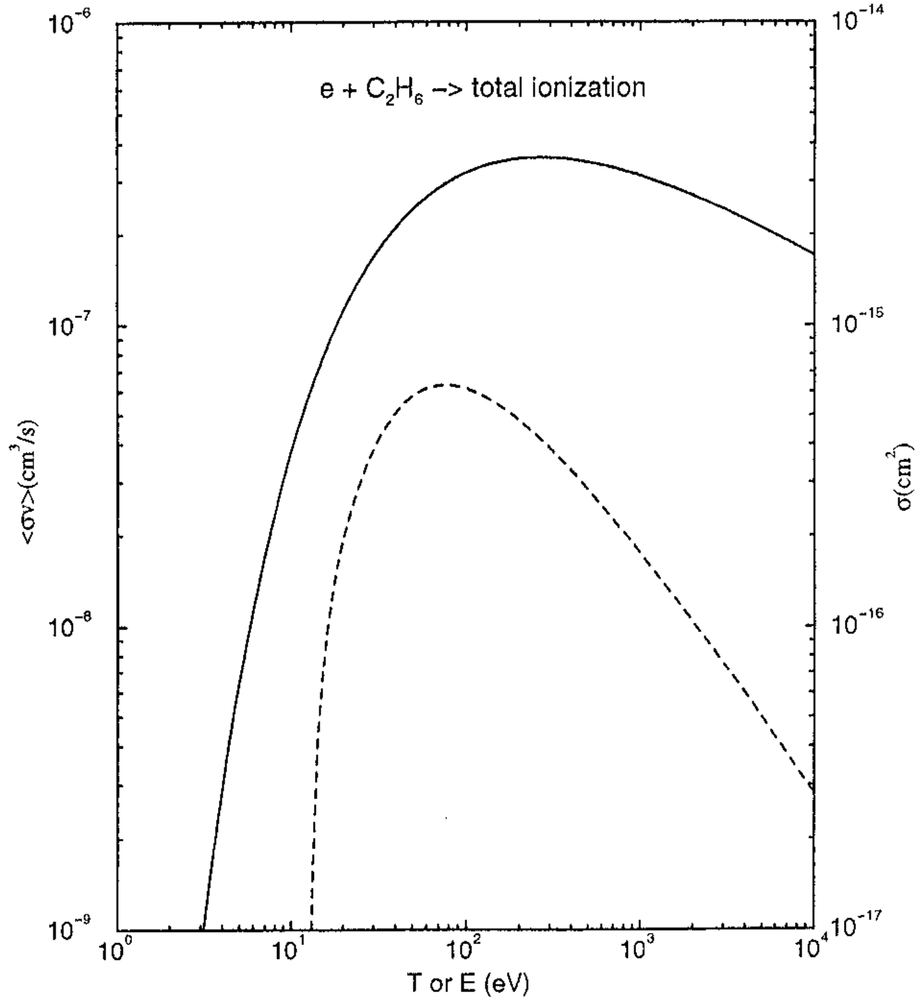
e + C2H6 -> total ionization
<σv>(cm3/s)
σ(cm2)
T or E (eV)

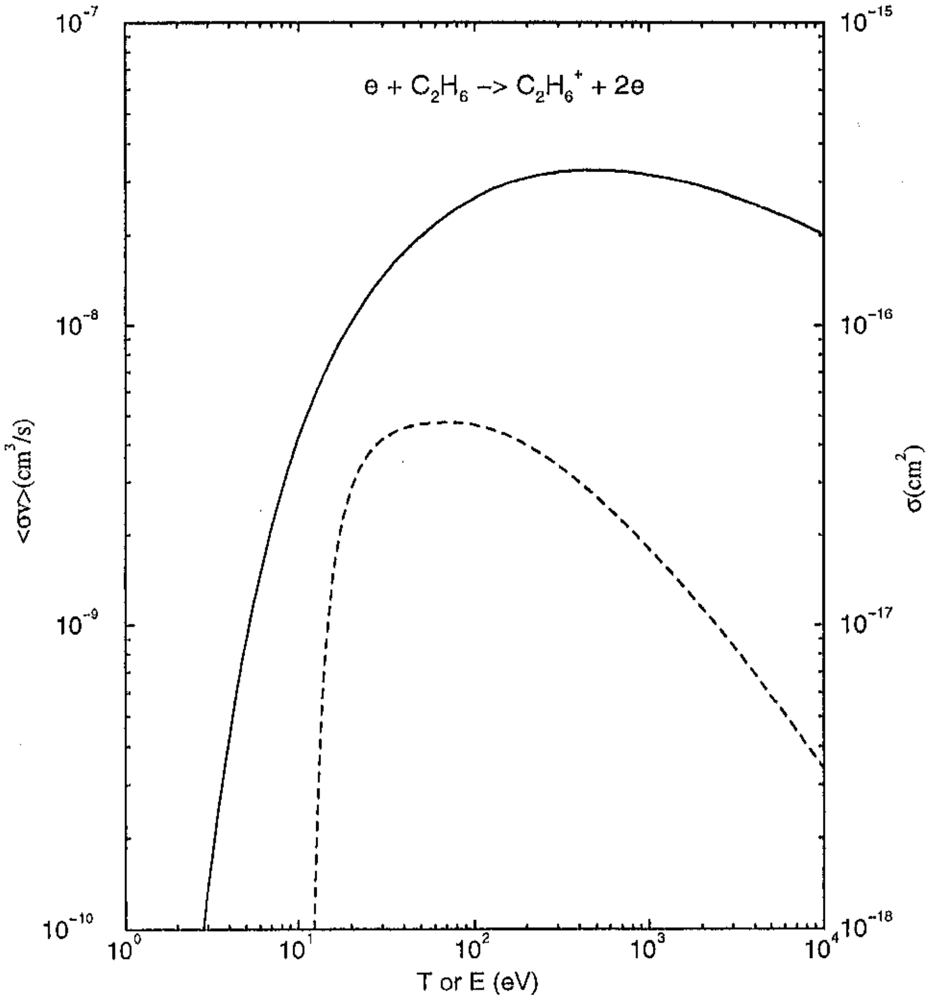
e + C2H6 -> C2H6+ + 2e
<σv>(cm3/s)
σ(cm2)
T or E (eV)
10^-7
10^-8
10^-9
10^-10
10^-15
10^-16
10^-17
10^-18
10^0
10^1
10^2
10^3
10^4

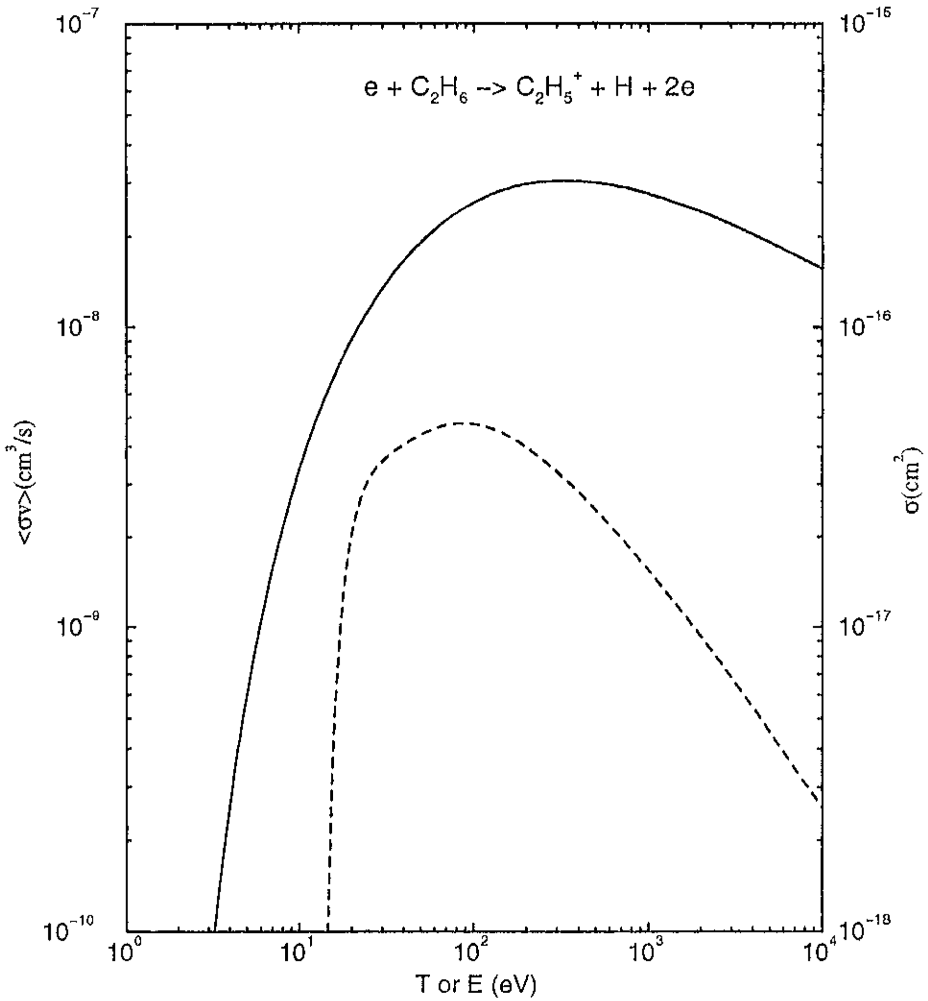
e + C2H6 -> C2H5+ + H + 2e
<σv>(cm3/s)
σ(cm2)
T or E (eV)
10^-7
10^-8
10^-9
10^-10
10^-15
10^-16
10^-17
10^-18
10^0
10^1
10^2
10^3
10^4

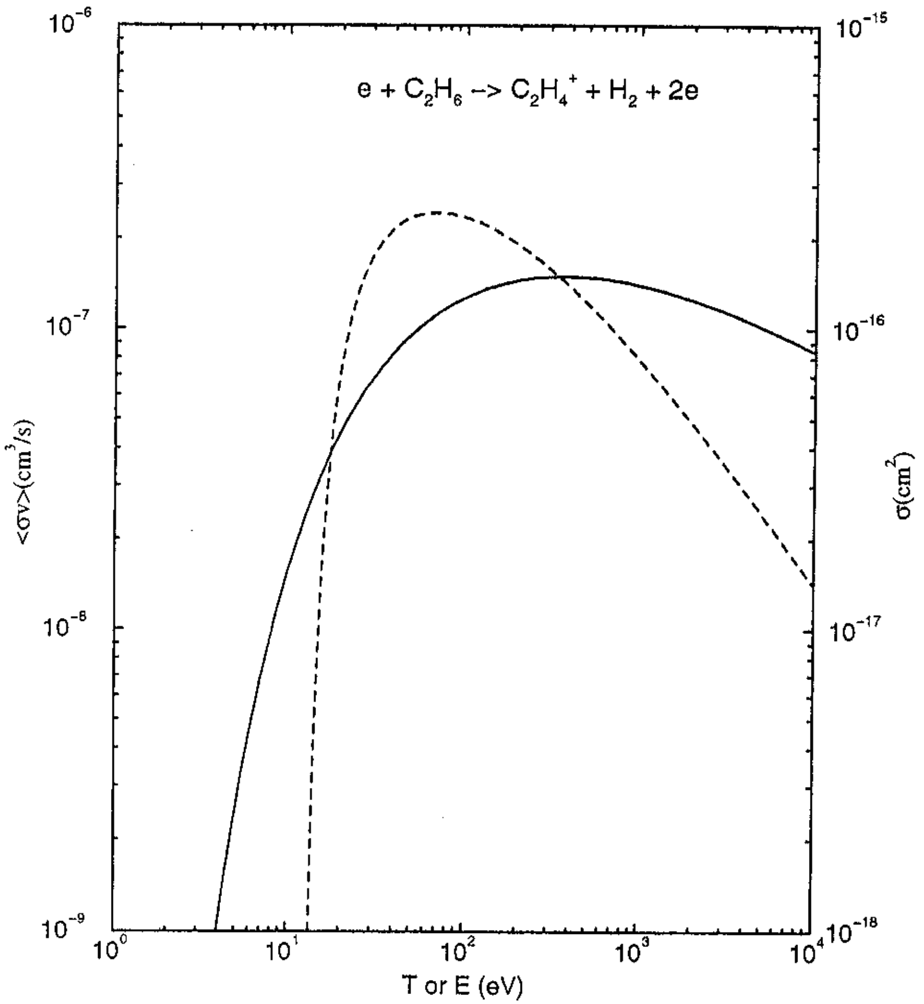
e + C2H6 -> C2H4+ + H2 + 2e
<σv>(cm3/s)
σ(cm2)
T or E (eV)

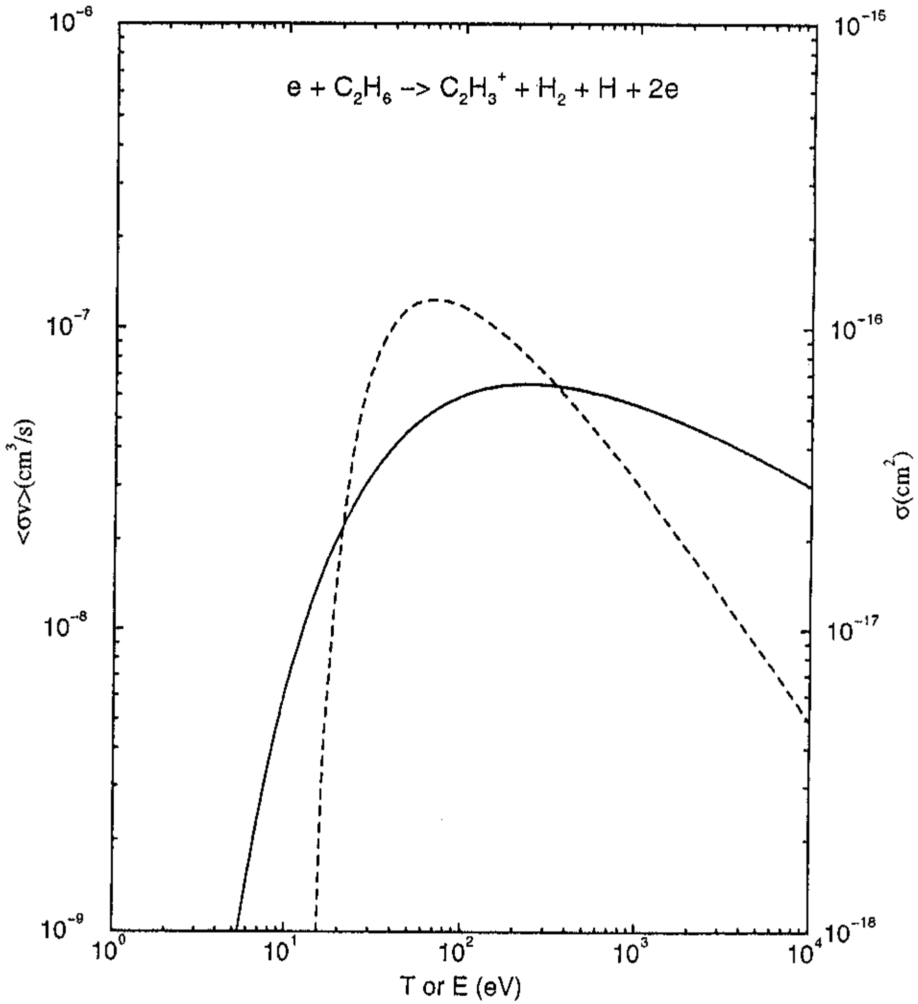
e + C2H6 -> C2H3+ + H2 + H + 2e
<σv>(cm3/s)
σ(cm2)
T or E (eV)

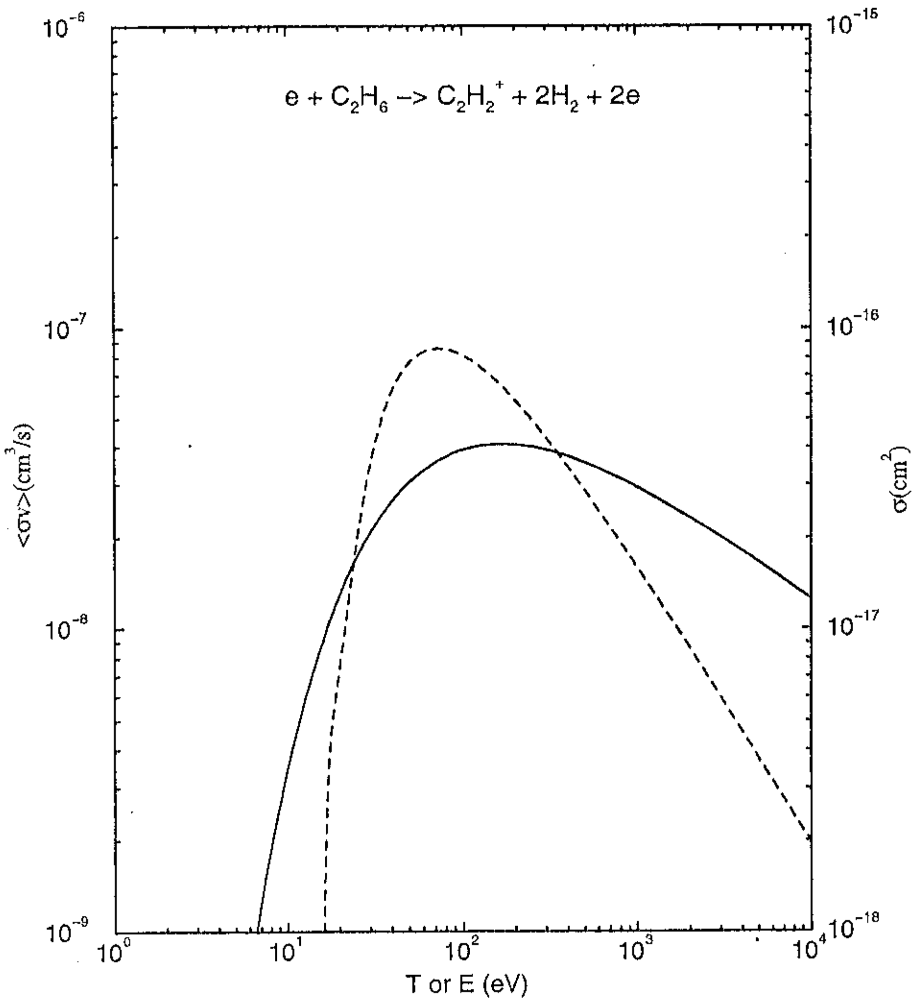
e + C2H6 -> C2H2+ + 2H2 + 2e
<σv>(cm3/s)
σ(cm2)
T or E (eV)
10-6
10-7
10-8
10-9
10-15
10-16
10-17
10-18
100
101
102
103
104

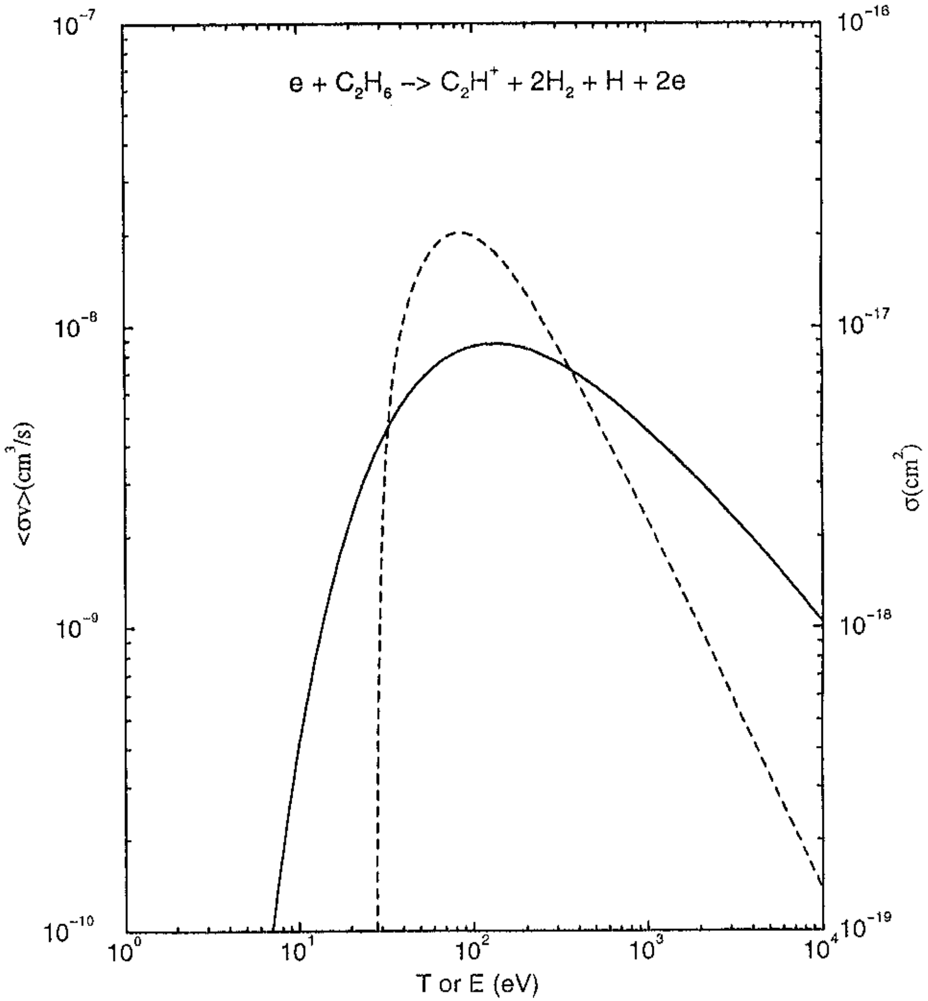
e + C2H6 -> C2H+ + 2H2 + H + 2e
<σv>(cm3/s)
σ(cm2)
T or E (eV)
10-7
10-8
10-9
10-10
10-16
10-17
10-18
10-19
100
101
102
103
104

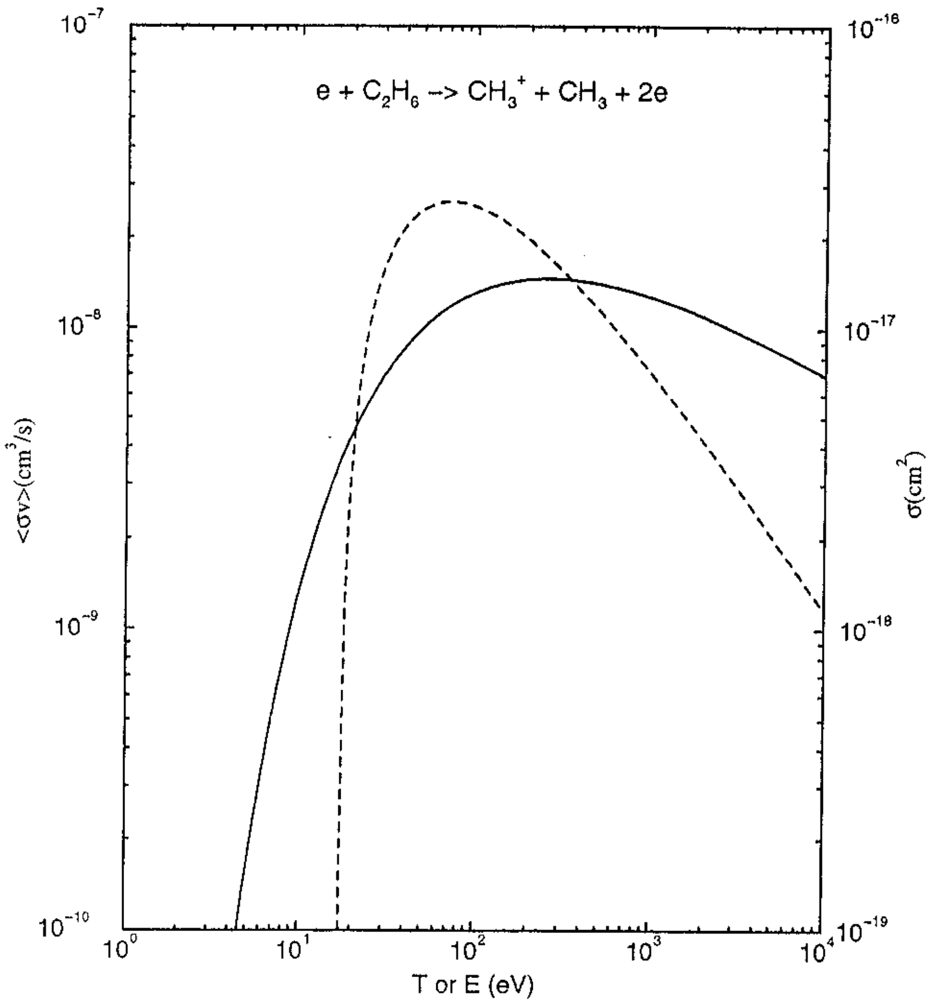
e + C2H6 -> CH3+ + CH3 + 2e
<σv>(cm3/s)
σ(cm2)
T or E (eV)
10-7
10-8
10-9
10-10
10-16
10-17
10-18
10-19
10^0
10^1
10^2
10^3
10^4

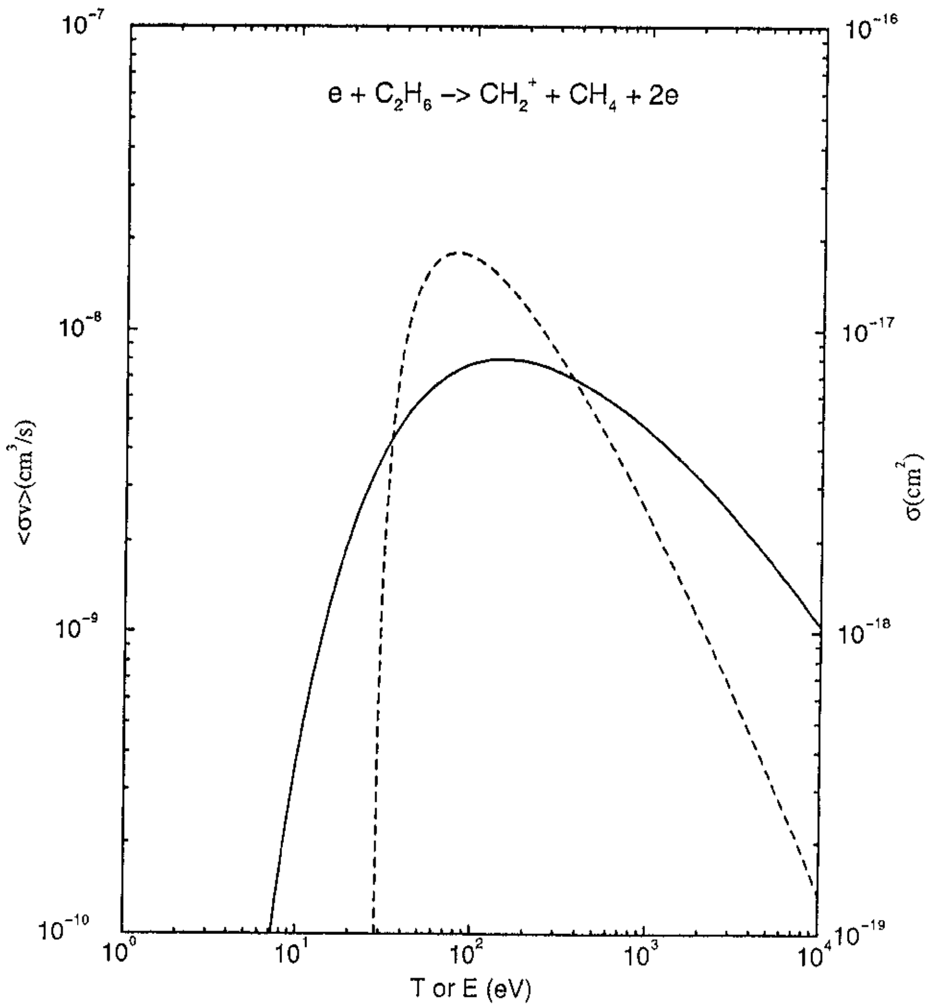
e + C2H6 -> CH2+ + CH4 + 2e
<σv>(cm3/s)
σ(cm2)
T or E (eV)
10-7
10-8
10-9
10-10
10-16
10-17
10-18
10-19
10^0
10^1
10^2
10^3
10^4

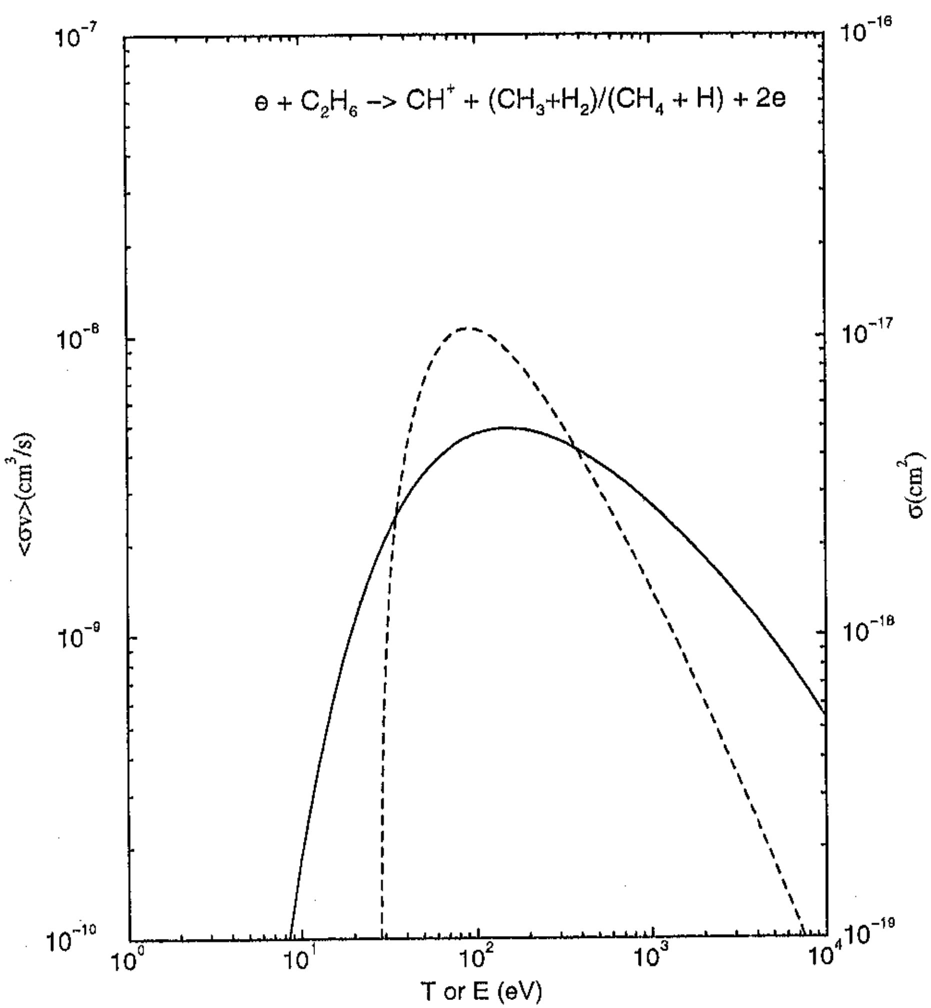

e + C2H6 -> CH+ + (CH3+H2)/(CH4 + H) + 2e
<σv>(cm3/s)
σ(cm2)
T or E (eV)

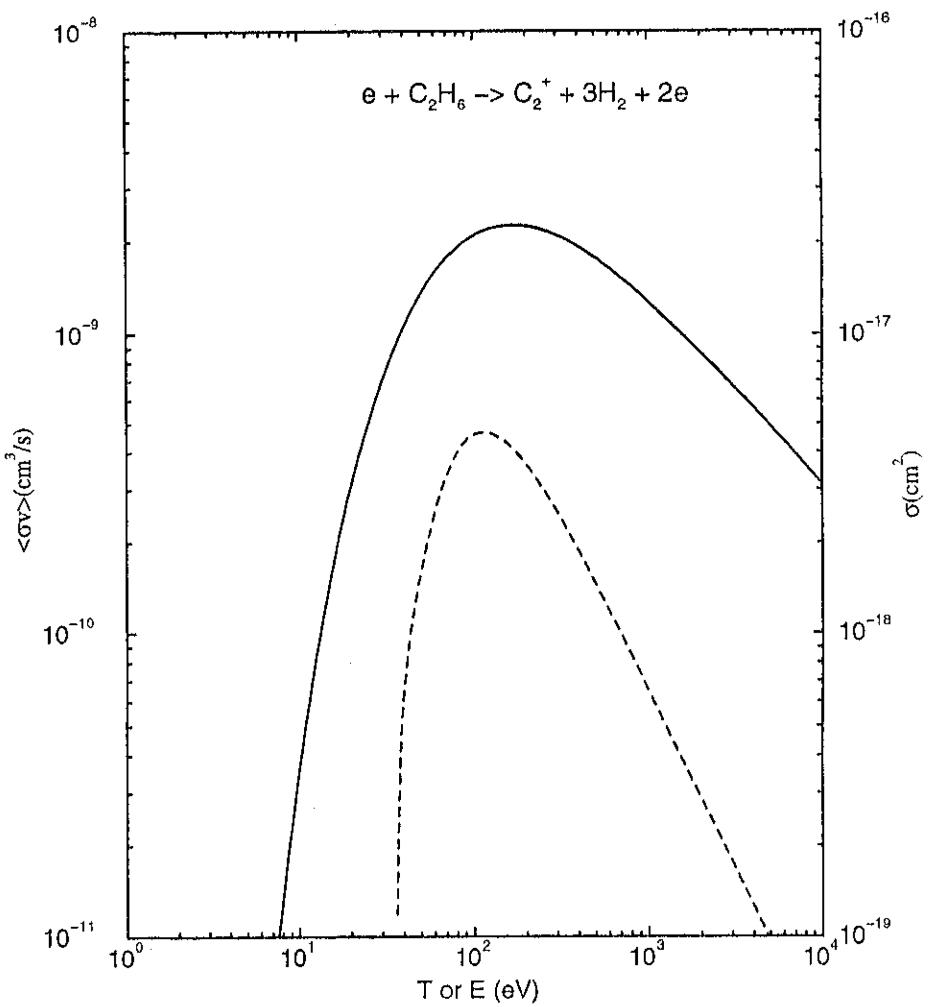

e + C2H6 -> C2+ + 3H2 + 2e
<σv>(cm3/s)
σ(cm2)
T or E (eV)

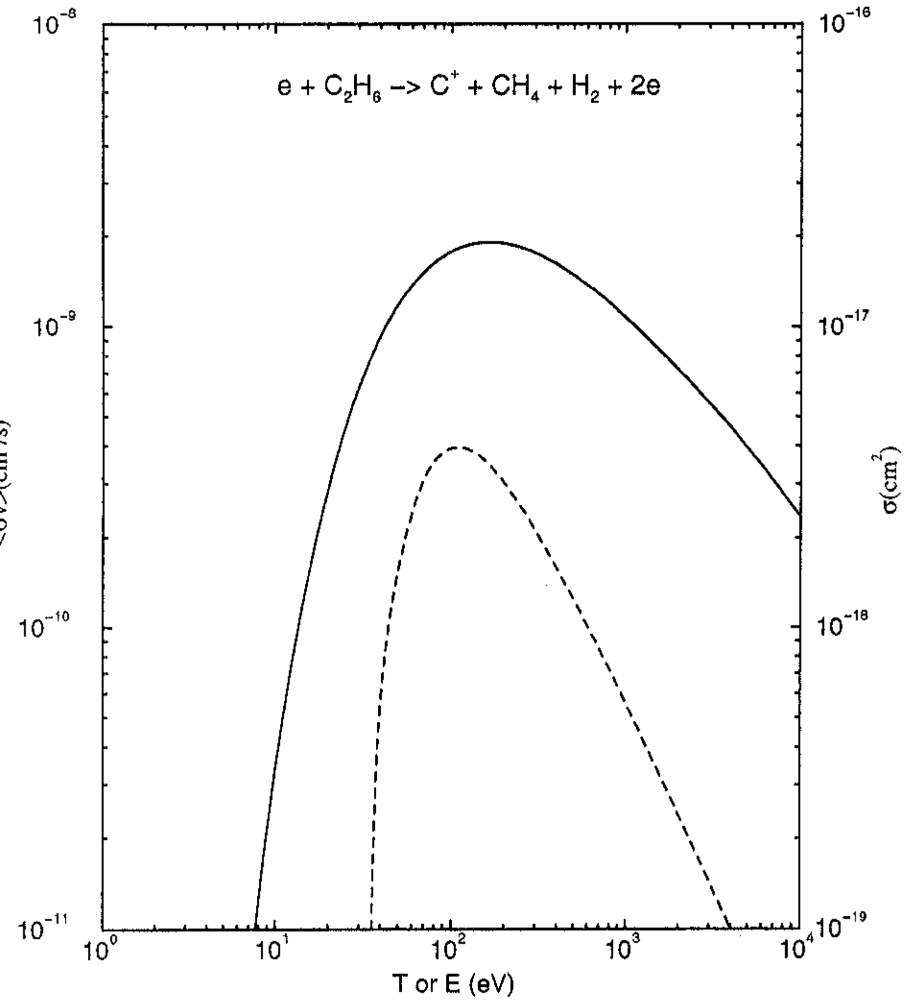
e + C2H6 -> C+ + CH4 + H2 + 2e
<σv>(cm3/s)
σ(cm2)
T or E (eV)

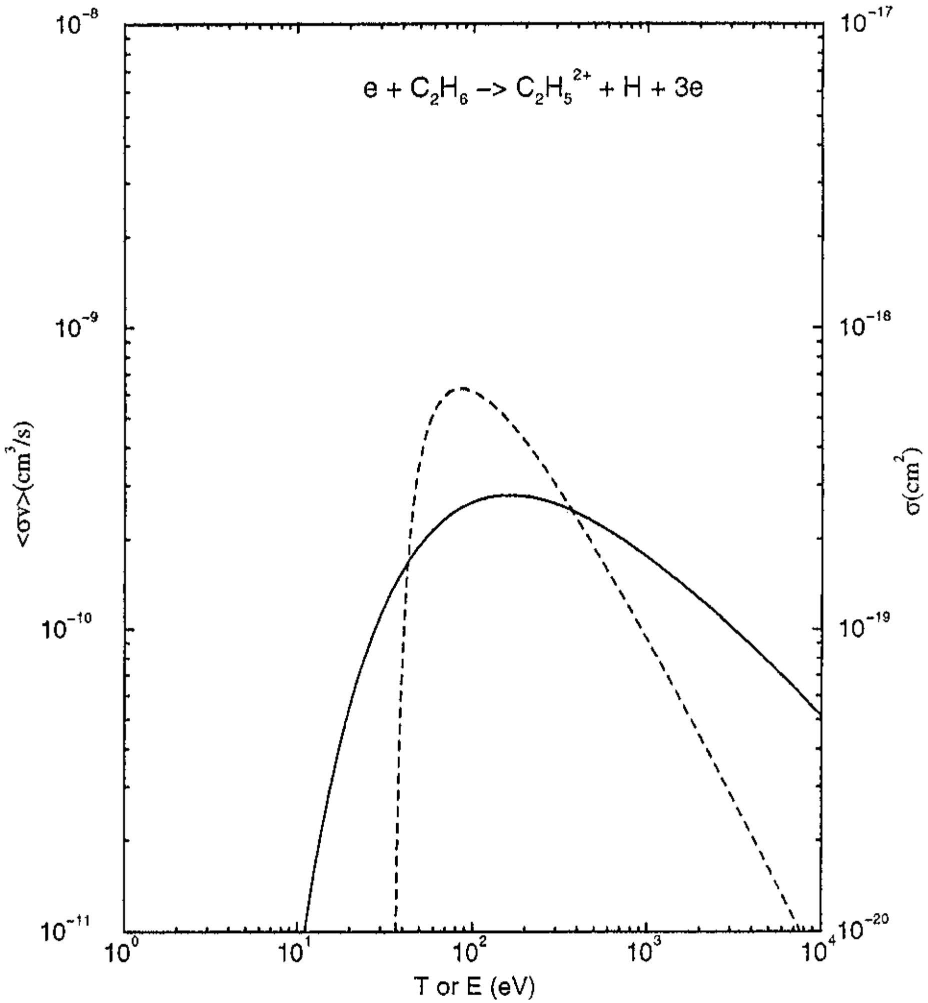
e + C2H6 -> C2H5 2+ + H + 3e
<σv>(cm3/s)
σ(cm2)
T or E (eV)

A-2.3 $e + C_3H_y$ systems

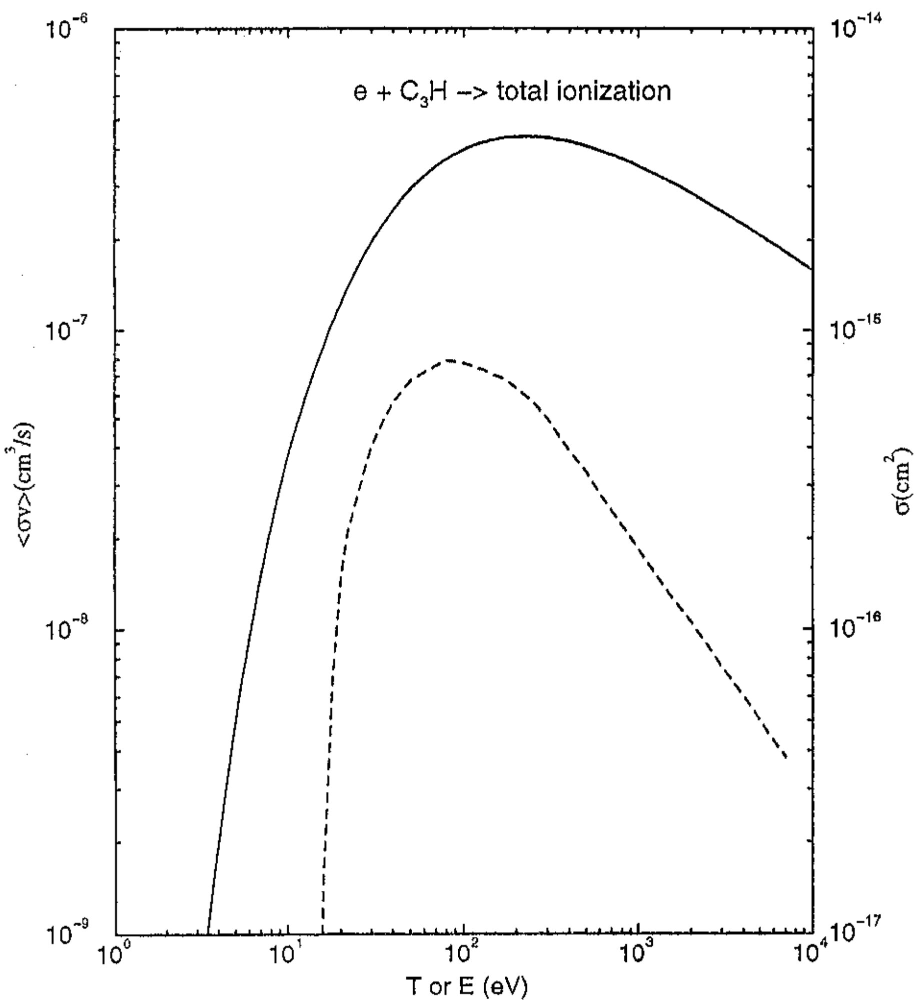

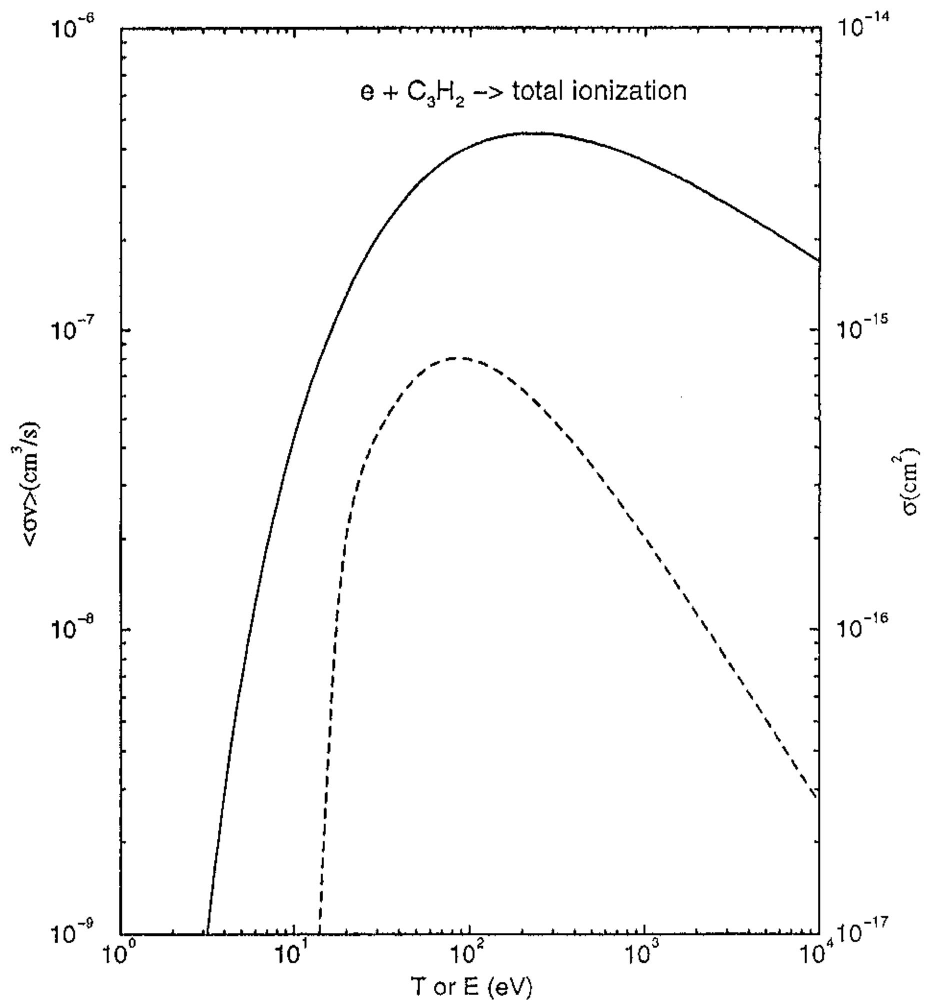

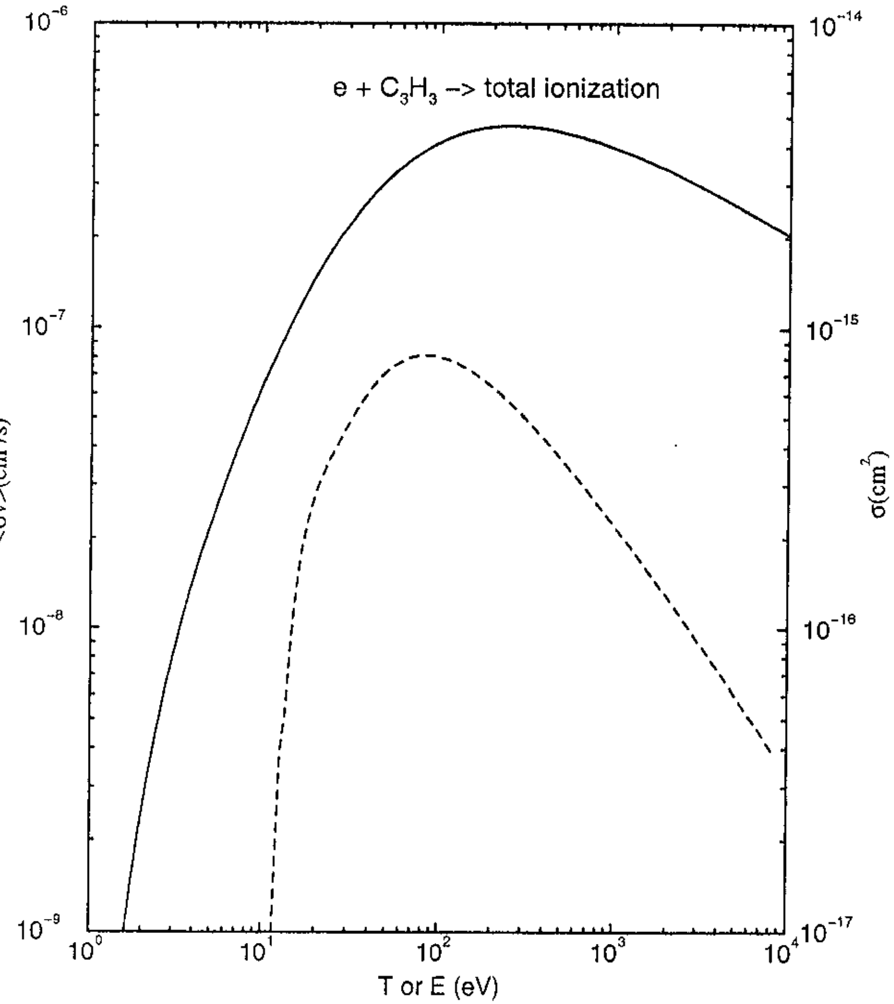
e + C3H3 -> total ionization
10^-6
10^-7
10^-8
10^-9
<σv>(cm^3/s)
10^-14
10^-15
10^-16
10^-17
σ(cm^2)
10^0
10^1
10^2
10^3
10^4
T or E (eV)

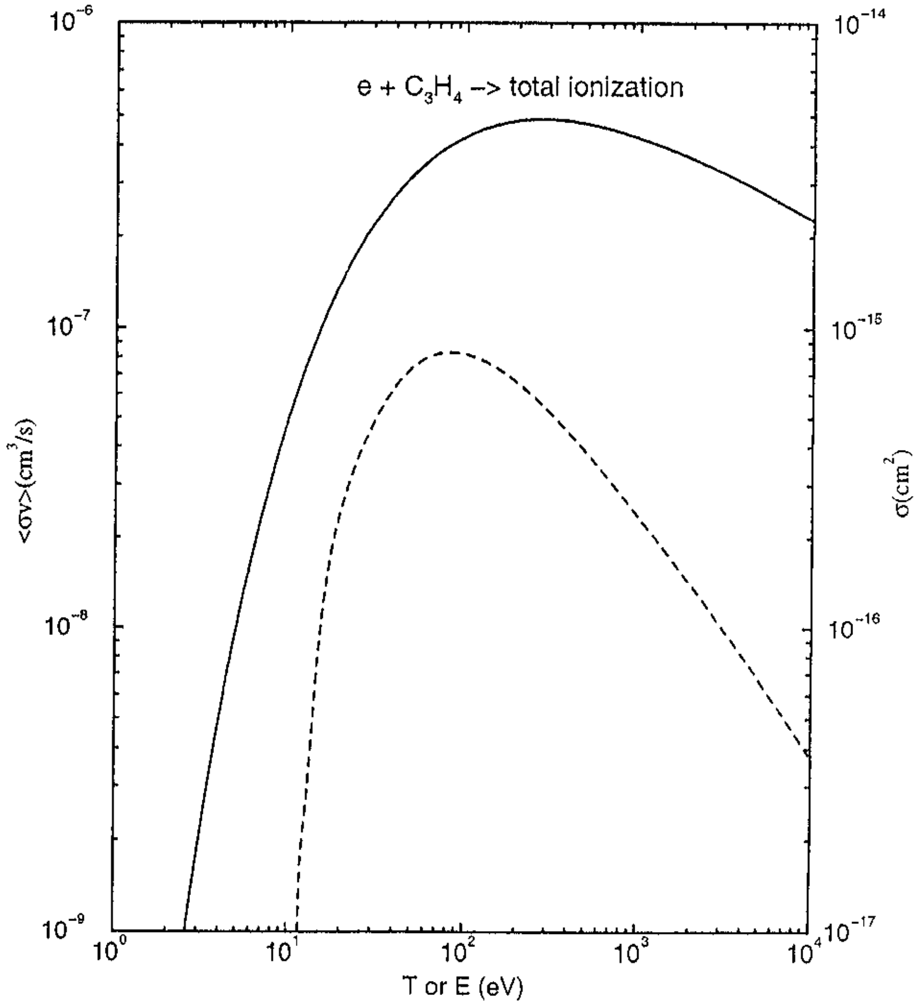
e + C3H4 -> total ionization
10^-6
10^-7
10^-8
10^-9
<σv>(cm^3/s)
10^-14
10^-15
10^-16
10^-17
σ(cm^2)
10^0
10^1
10^2
10^3
10^4
T or E (eV)

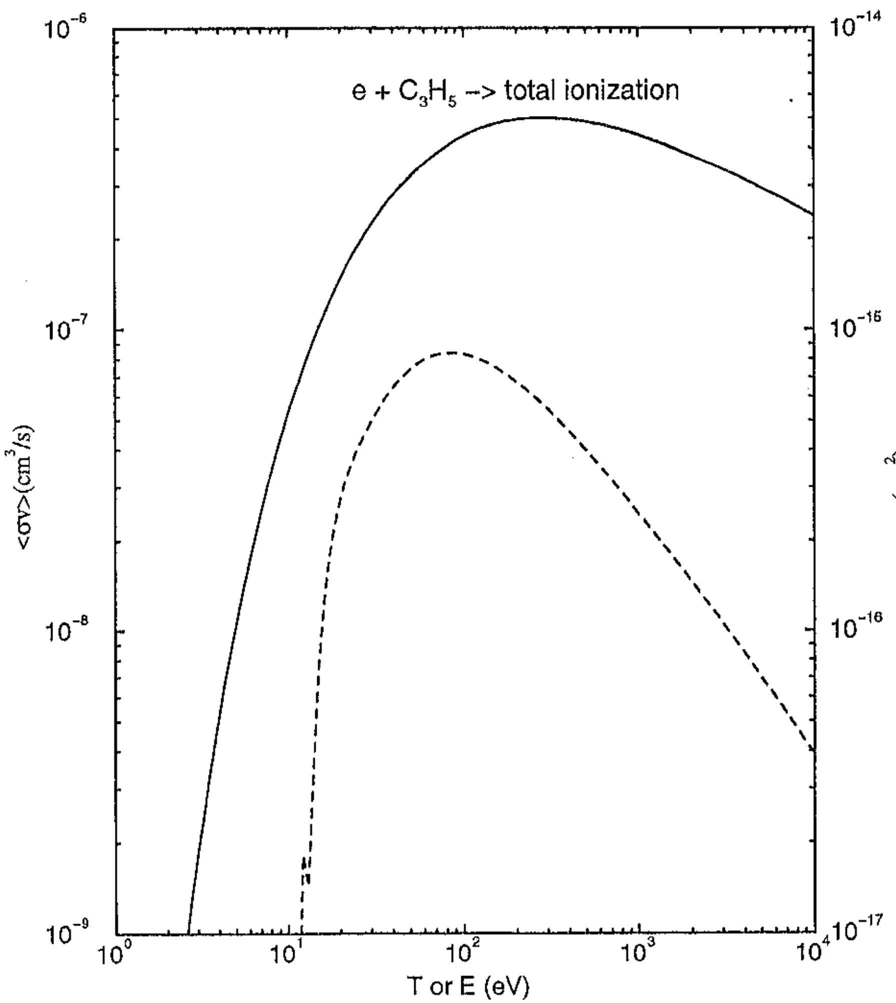
e + C3H5 -> total ionization
10^-6
10^-7
10^-8
10^-9
<σv>(cm^3/s)
10^-14
10^-15
10^-16
10^-17
σ(cm^2)
10^0
10^1
10^2
10^3
10^4
T or E (eV)

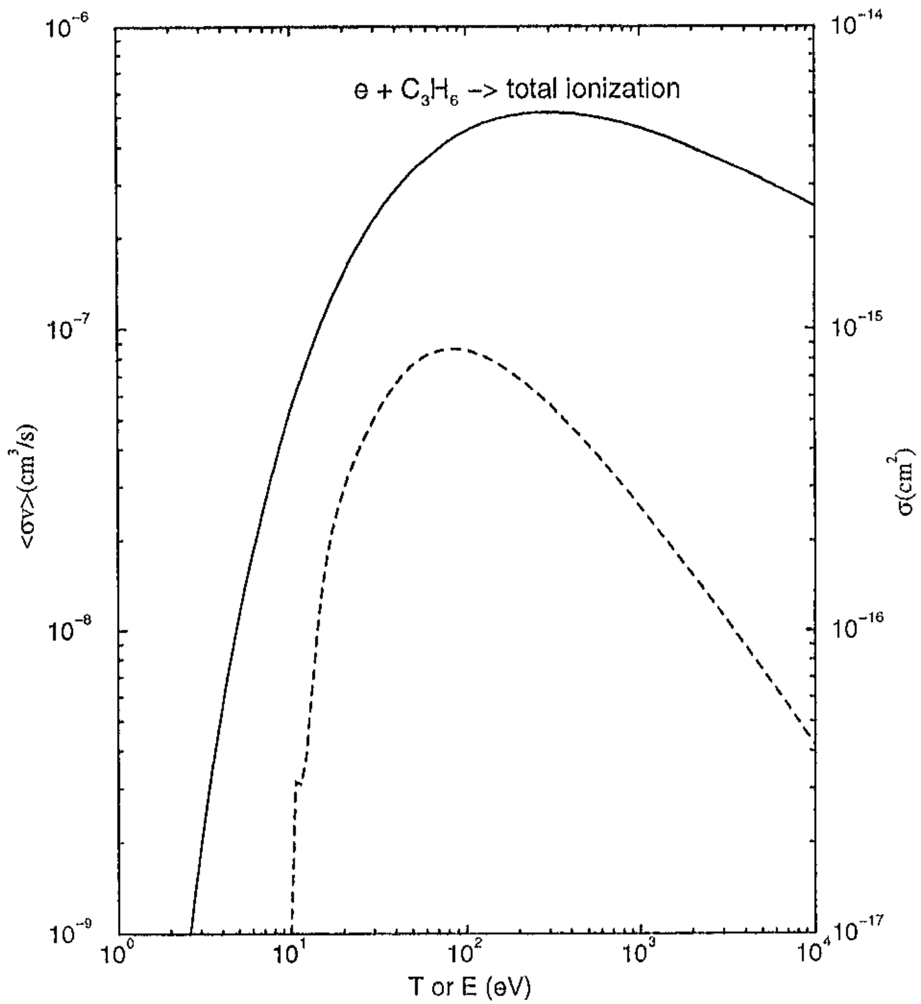
e + C3H6 -> total ionization
10^-6
10^-7
10^-8
10^-9
<σv>(cm^3/s)
10^-14
10^-15
10^-16
10^-17
σ(cm^2)
10^0
10^1
10^2
10^3
10^4
T or E (eV)

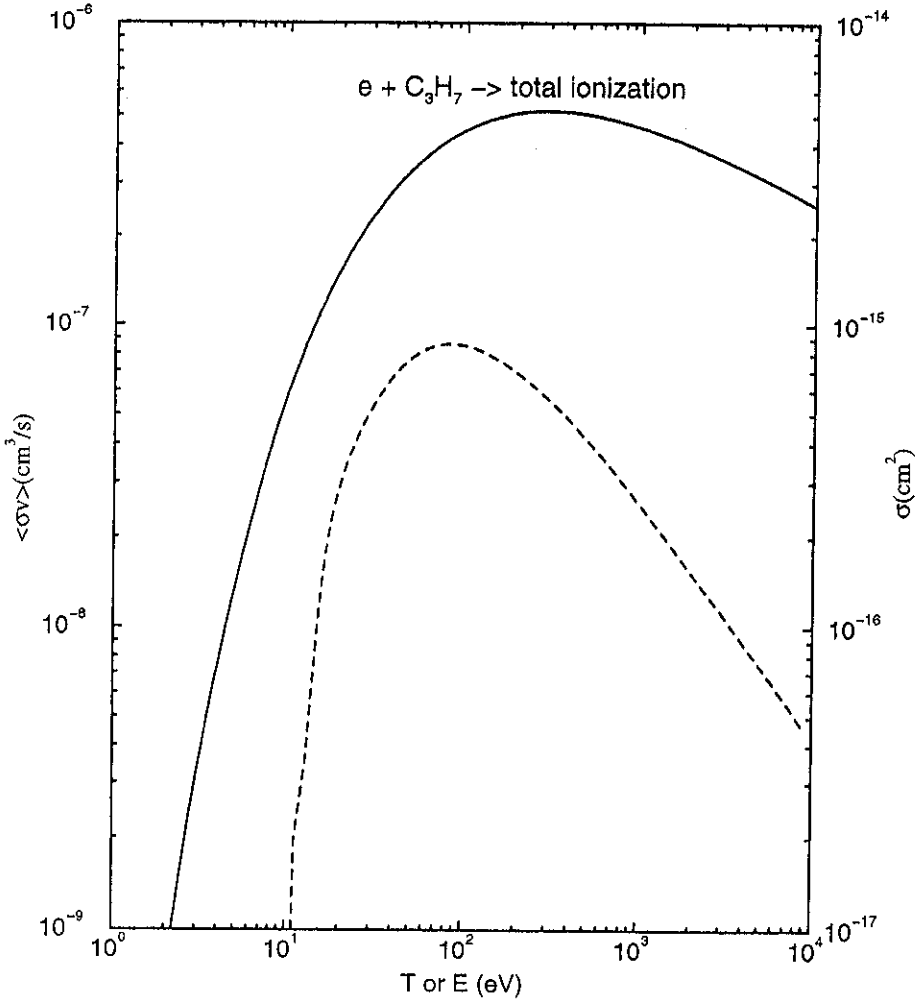

e + C_3H_7 -> total ionization
10^{-6}
10^{-7}
10^{-8}
10^{-9}
<σv>(cm^3/s)
10^{-14}
10^{-15}
10^{-16}
10^{-17}
σ(cm^2)
10^0
10^1
10^2
10^3
10^4
T or E (eV)

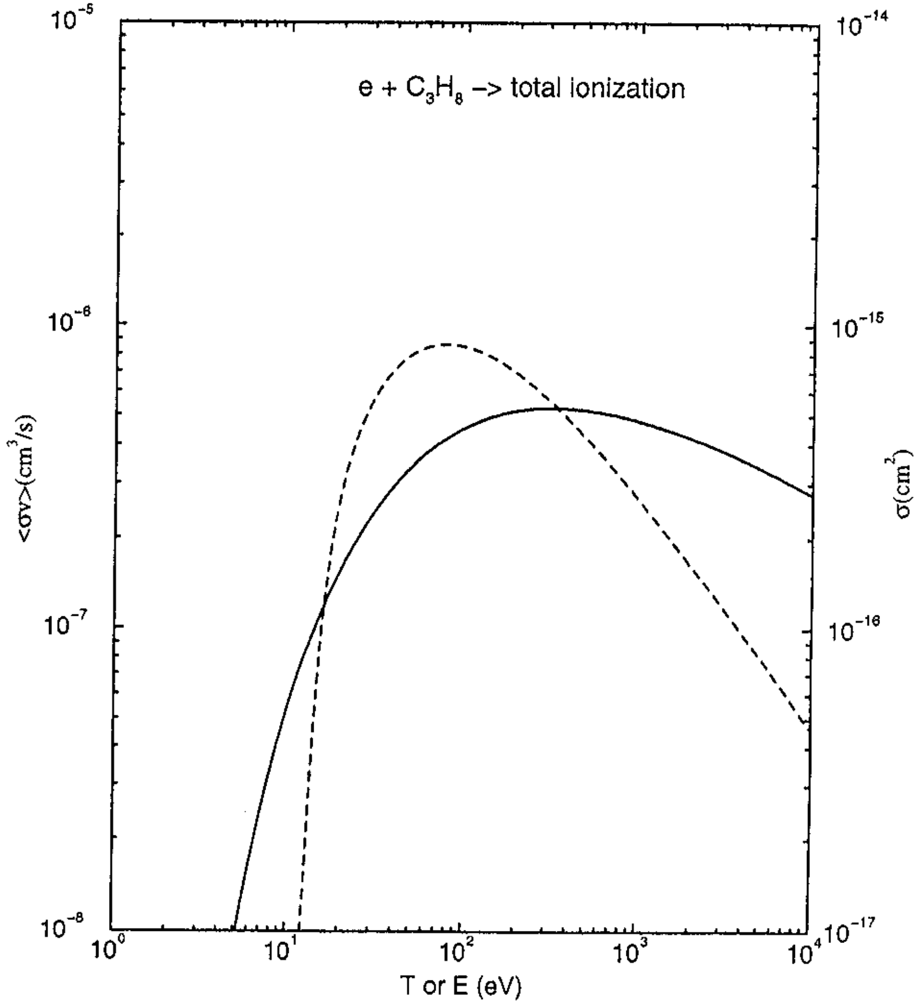

e + C_3H_8 -> total ionization
10^{-5}
10^{-6}
10^{-7}
10^{-8}
<σv>(cm^3/s)
10^{-14}
10^{-15}
10^{-16}
10^{-17}
σ(cm^2)
10^0
10^1
10^2
10^3
10^4
T or E (eV)

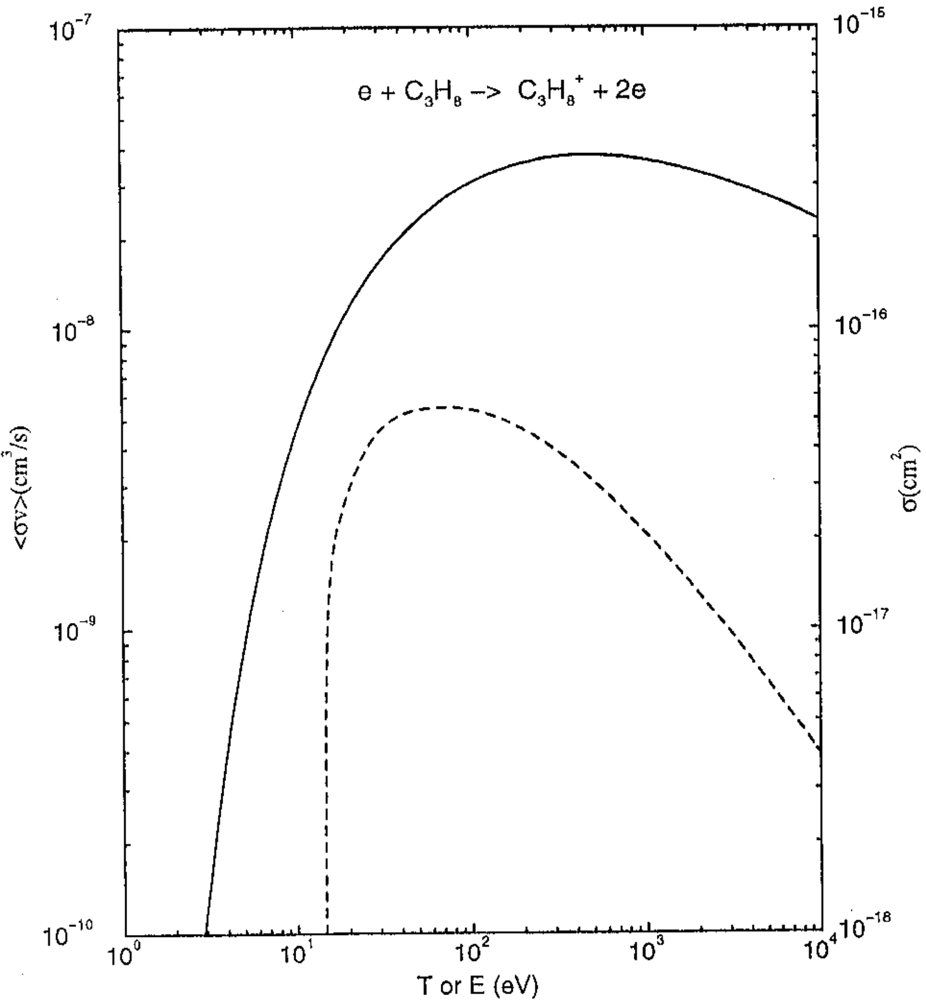
e + C3H8 -> C3H8+ + 2e
<σv>(cm3/s)
σ(cm2)
T or E (eV)
10−7
10−8
10−9
10−10
10−15
10−16
10−17
10−18
100
101
102
103
104

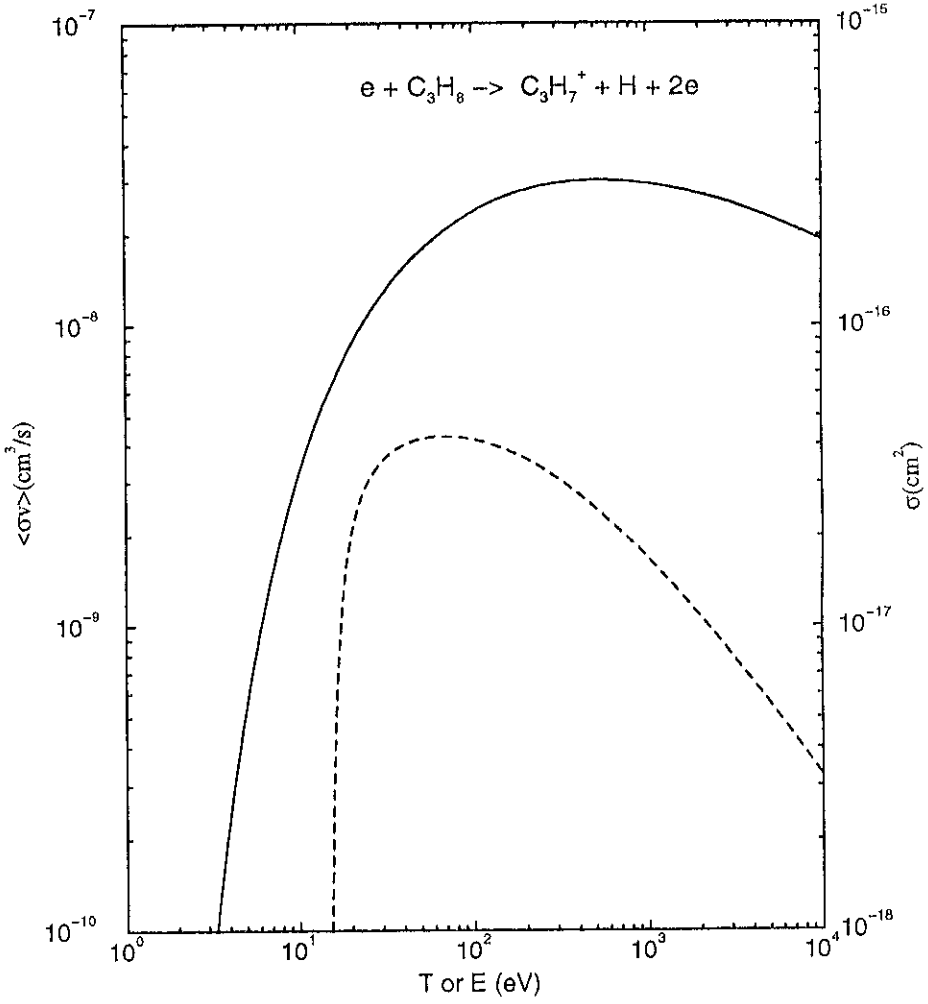
e + C3H8 -> C3H7+ + H + 2e
<σv>(cm3/s)
σ(cm2)
T or E (eV)
10−7
10−8
10−9
10−10
10−15
10−16
10−17
10−18
100
101
102
103
104

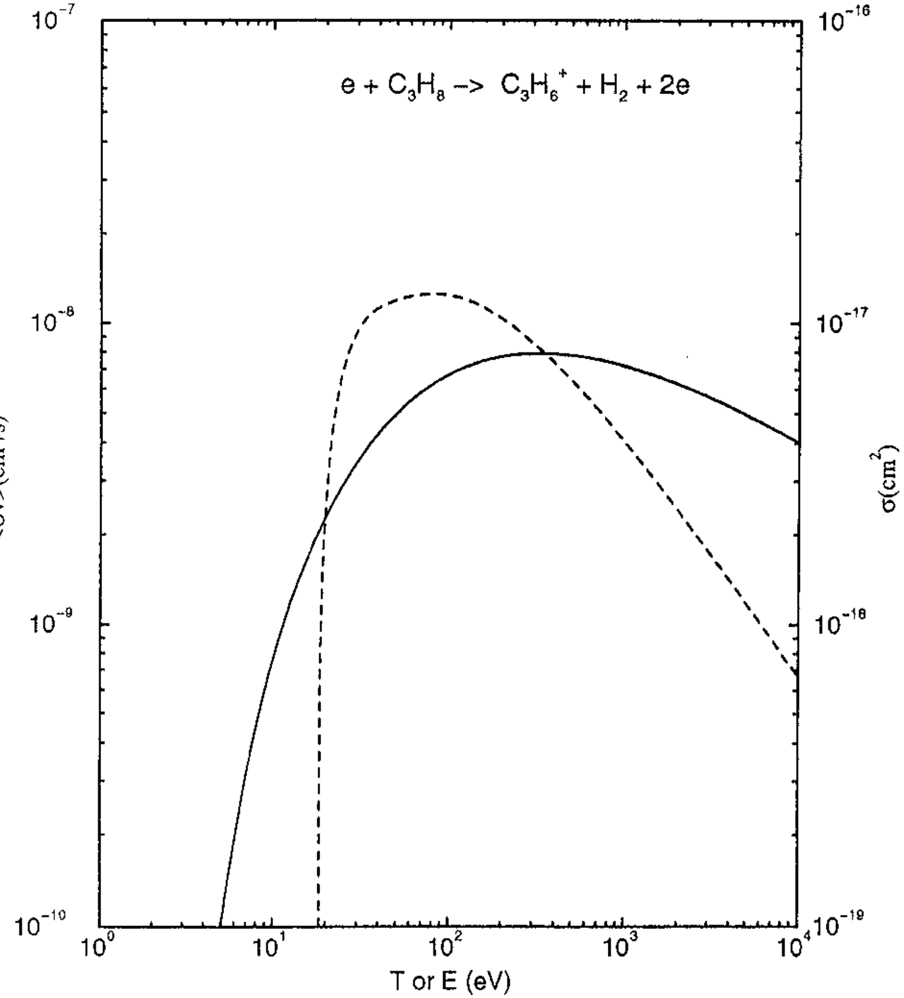
e + C3H8 -> C3H6+ + H2 + 2e
<σv>(cm3/s)
σ(cm2)
T or E (eV)
10−7
10−8
10−9
10−10
10−16
10−17
10−18
10−19
100
101
102
103
104

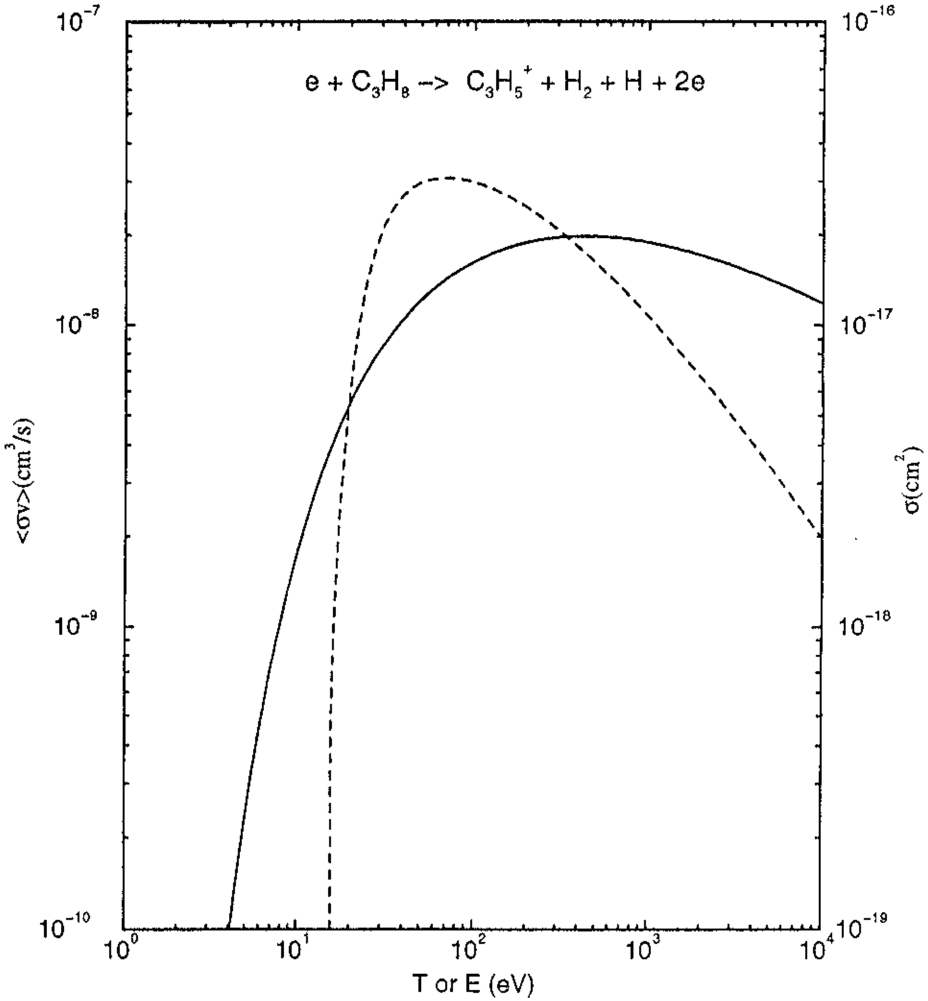
e + C3H8 -> C3H5+ + H2 + H + 2e
<σv>(cm3/s)
σ(cm2)
T or E (eV)
10−7
10−8
10−9
10−10
10−16
10−17
10−18
10−19
100
101
102
103
104

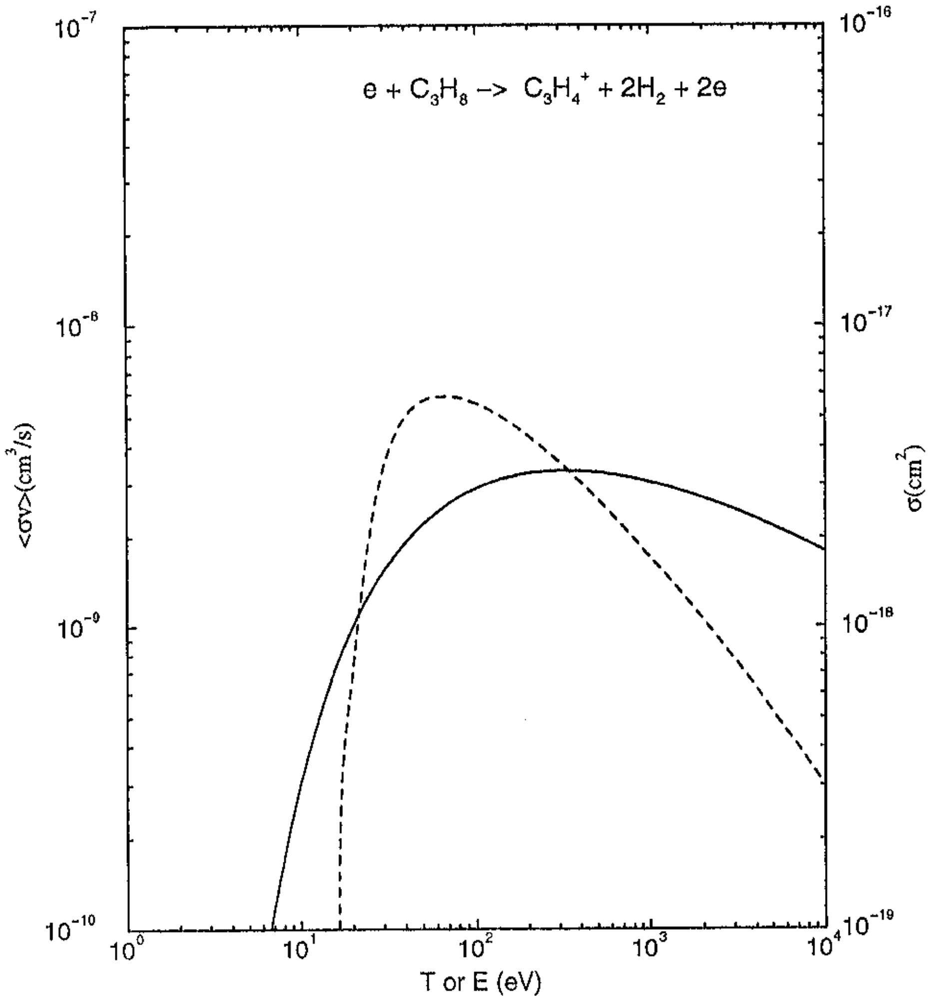
e + C3H8 -> C3H4+ + 2H2 + 2e
<σv>(cm3/s)
σ(cm2)
T or E (eV)
10−7
10−8
10−9
10−10
10−16
10−17
10−18
10−19
100
101
102
103
104

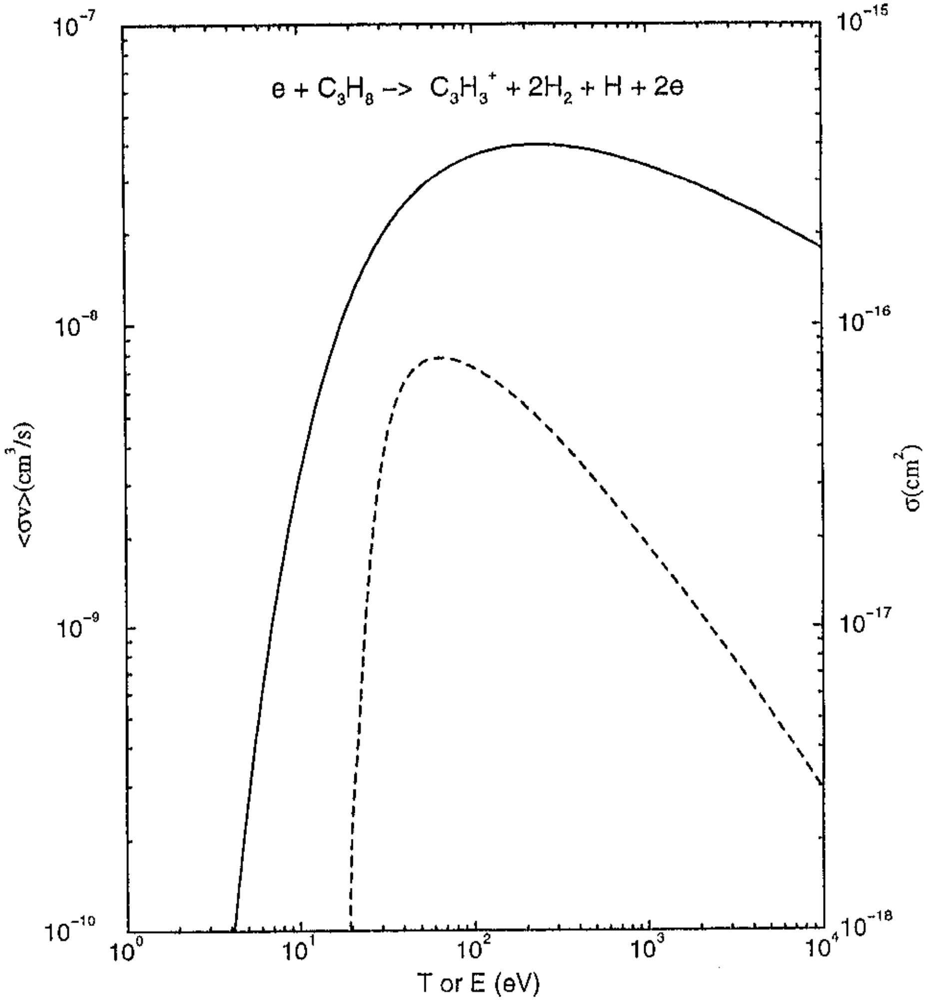
e + C3H8 -> C3H3+ + 2H2 + H + 2e
<σv>(cm3/s)
σ(cm2)
T or E (eV)
10−7
10−8
10−9
10−10
10−15
10−16
10−17
10−18
100
101
102
103
104

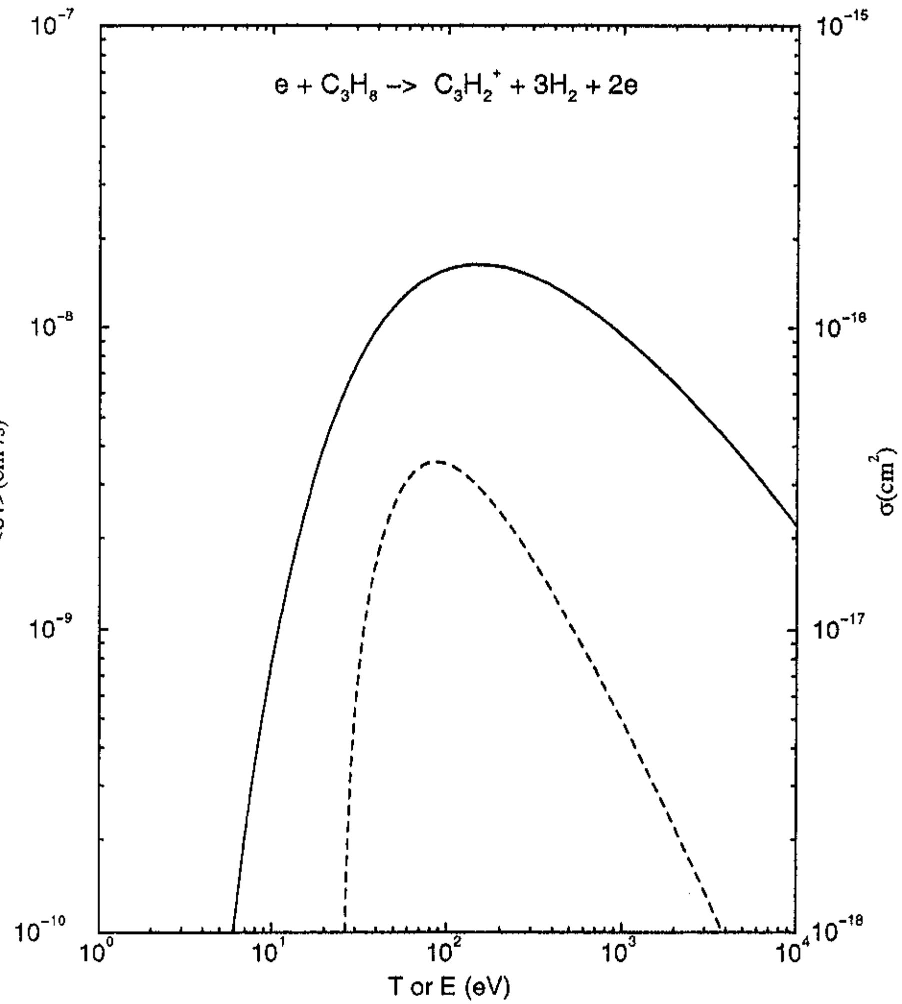
e + C3H8 -> C3H2+ + 3H2 + 2e
<σv>(cm3/s)
σ(cm2)
T or E (eV)
10−7
10−8
10−9
10−10
10−15
10−16
10−17
10−18
100
101
102
103
104

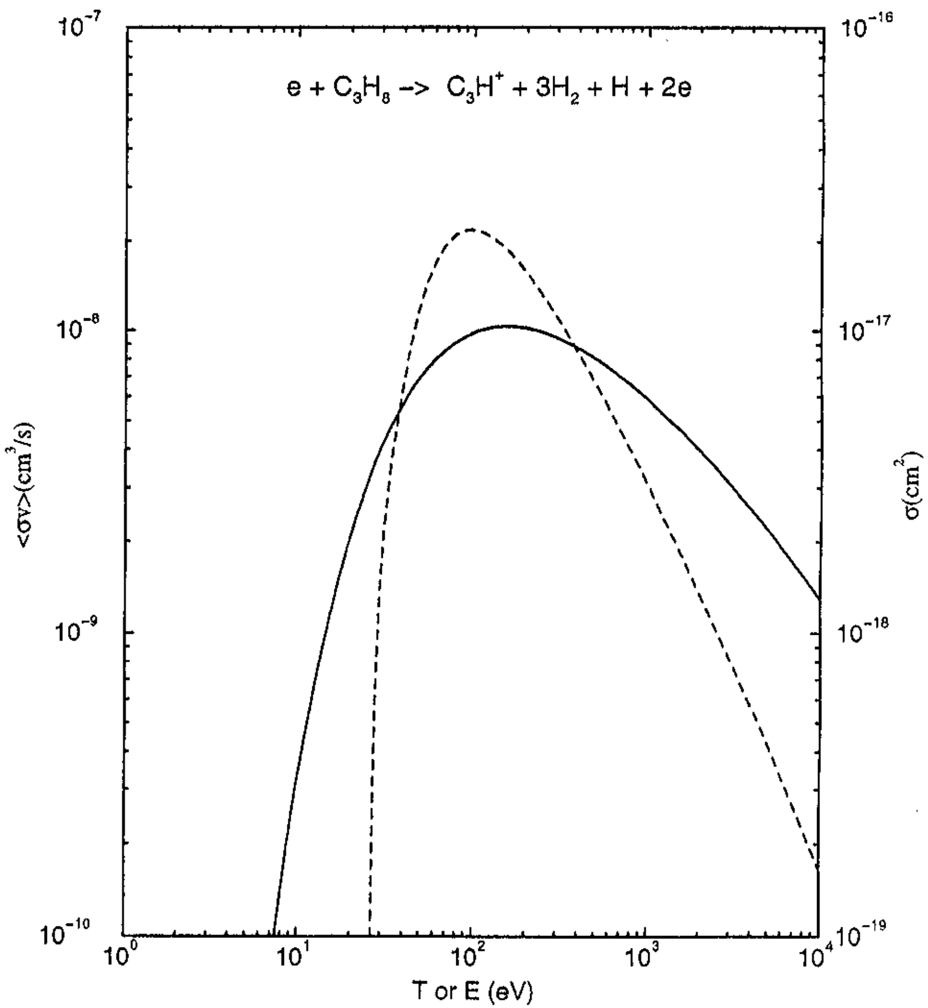
e + C3H8 -> C3H+ + 3H2 + H + 2e
<σv>(cm3/s)
σ(cm2)
T or E (eV)
10−7
10−8
10−9
10−10
10−16
10−17
10−18
10−19
100
101
102
103
104

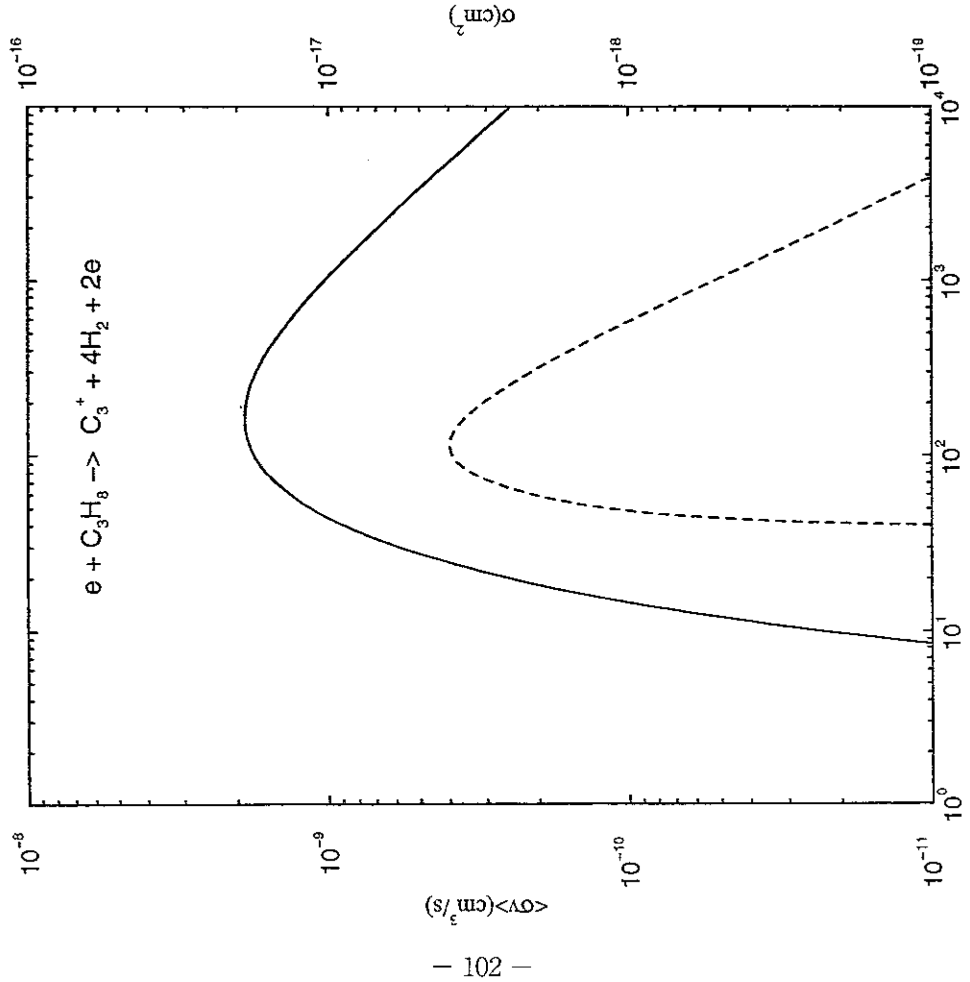
e + C3H8 -> C3+ + 4H2 + 2e
<σv>(cm3/s)
σ(cm2)
T or E (eV)
10^-8
10^-9
10^-10
10^-11
10^-16
10^-17
10^-18
10^-19
10^0
10^1
10^2
10^3
10^4

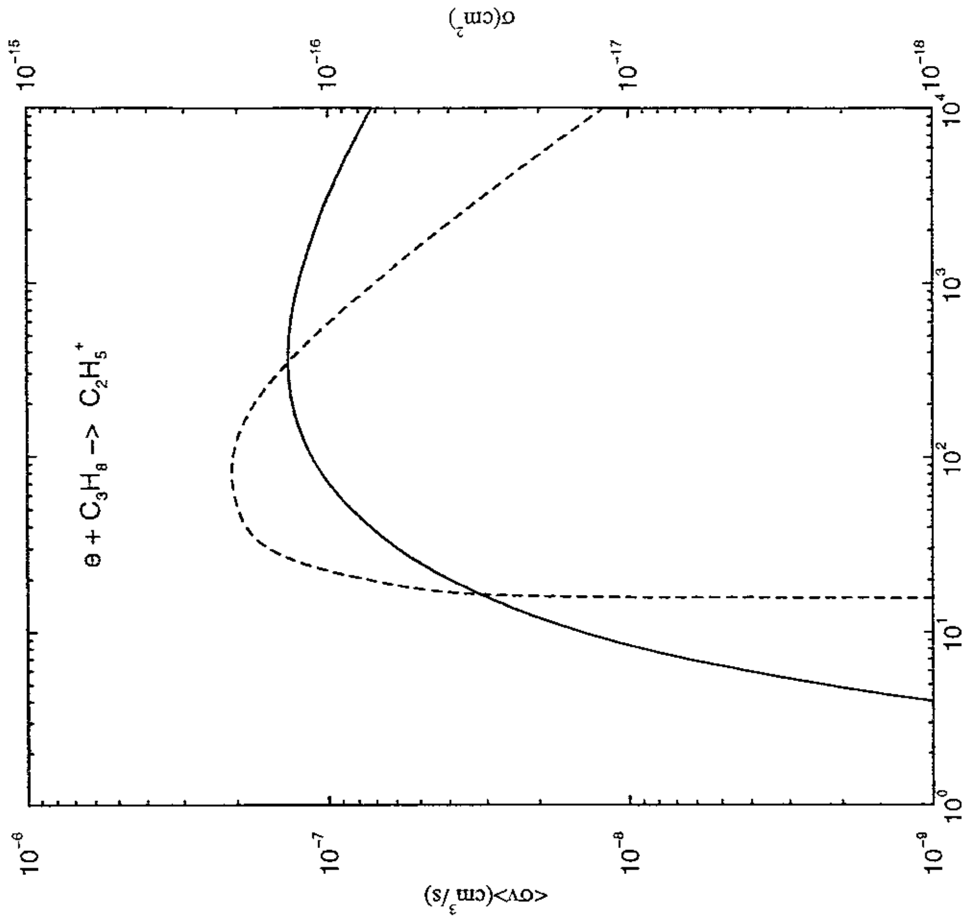
e + C3H8 -> C2H5+
<σv>(cm3/s)
σ(cm2)
T or E (eV)
10^-6
10^-7
10^-8
10^-9
10^-15
10^-16
10^-17
10^-18
10^0
10^1
10^2
10^3
10^4

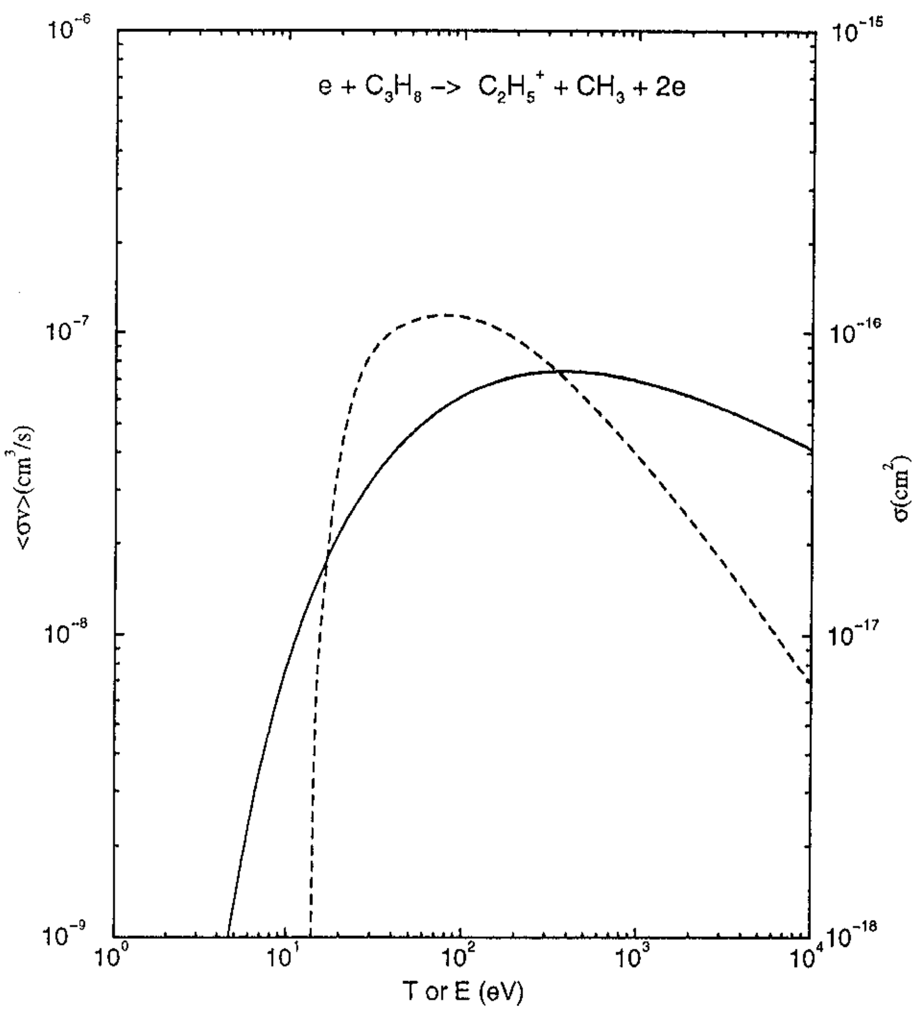
e + C3H8 -> C2H5+ + CH3 + 2e
<σv>(cm3/s)
σ(cm2)
T or E (eV)
10−6
10−7
10−8
10−9
10−15
10−16
10−17
10−18
100
101
102
103
104

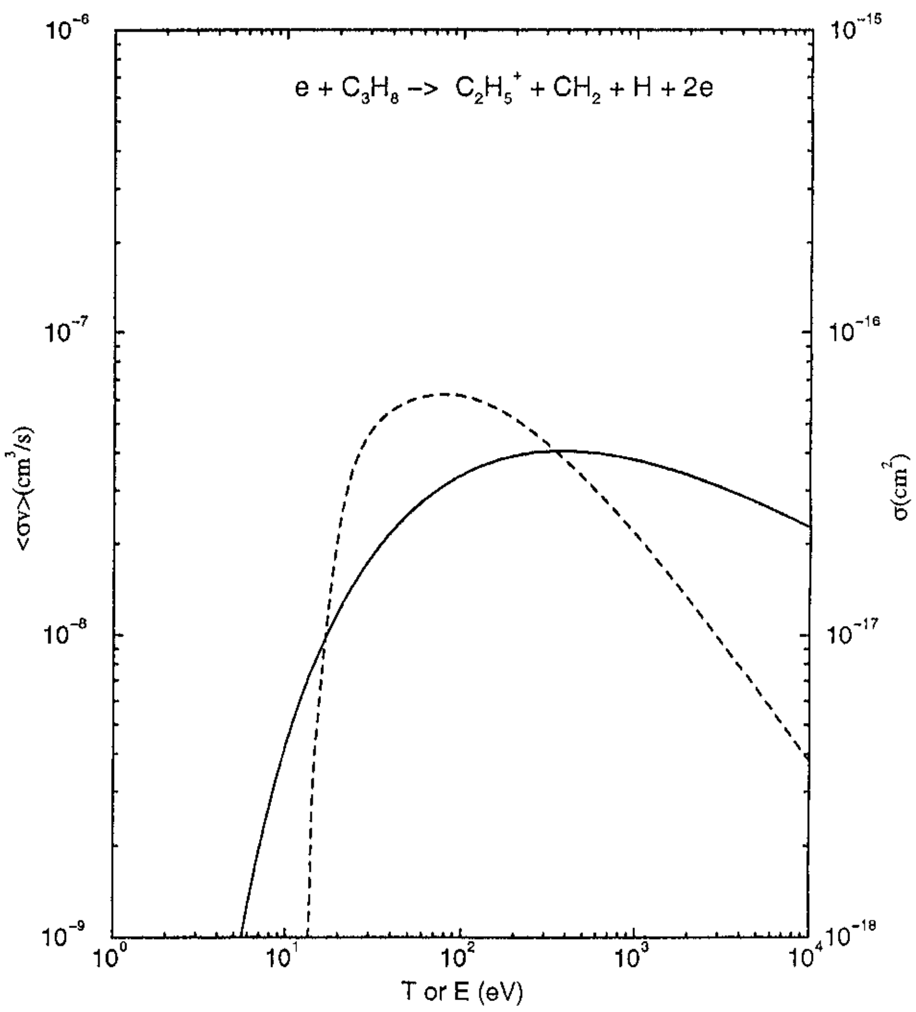
e + C3H8 -> C2H5+ + CH2 + H + 2e
<σv>(cm3/s)
σ(cm2)
T or E (eV)
10−6
10−7
10−8
10−9
10−15
10−16
10−17
10−18
100
101
102
103
104

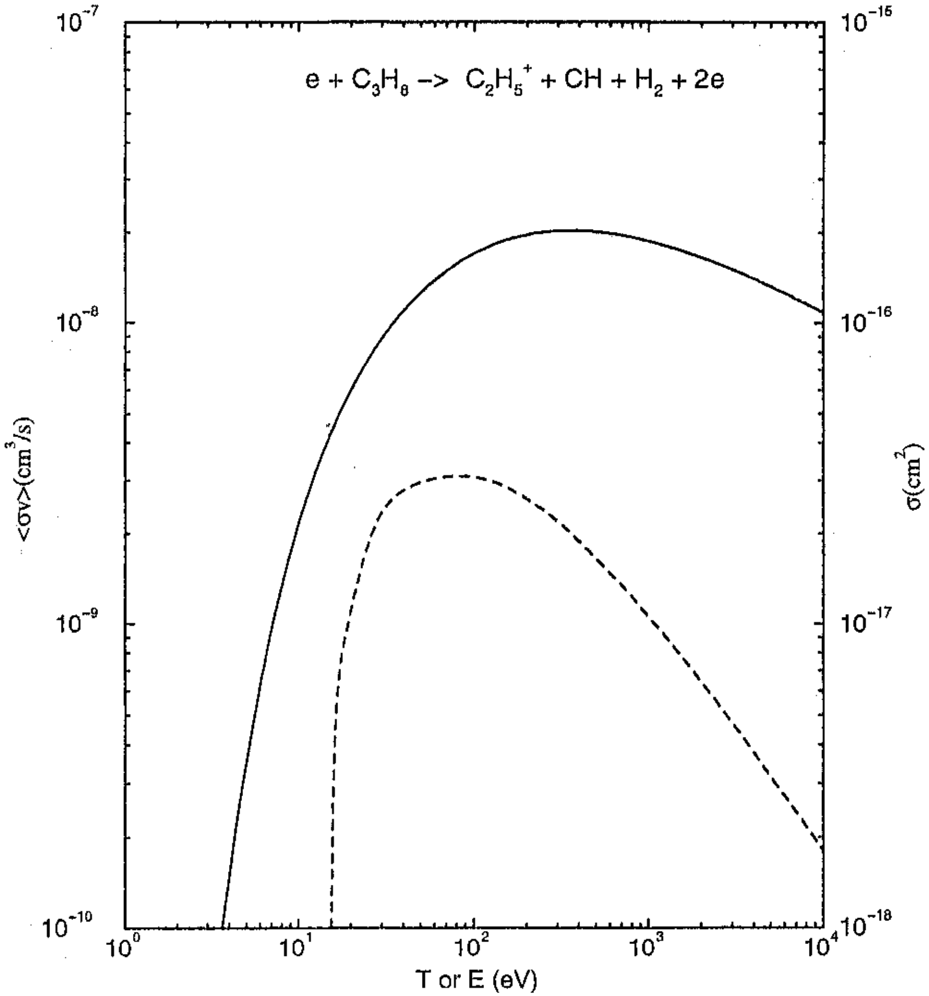

e + C3H8 -> C2H5+ + CH + H2 + 2e
<σv>(cm3/s)
σ(cm2)
T or E (eV)

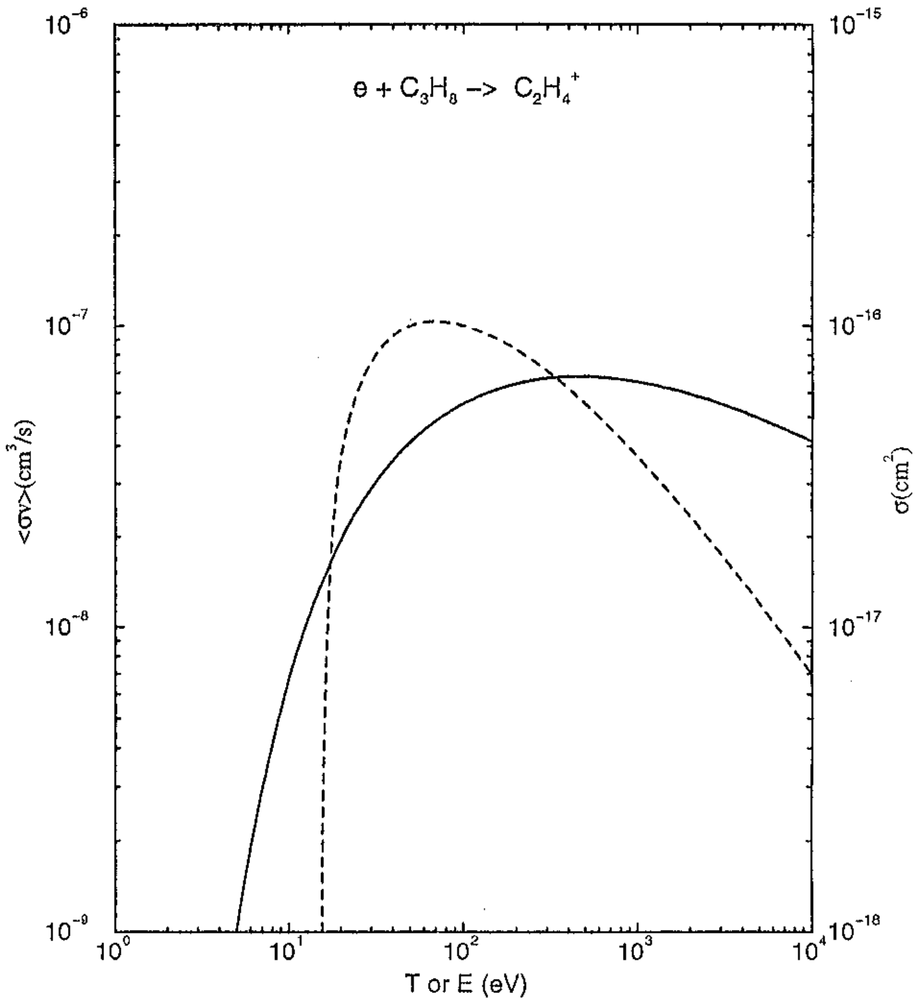

e + C3H8 -> C2H4+
<σv>(cm3/s)
σ(cm2)
T or E (eV)

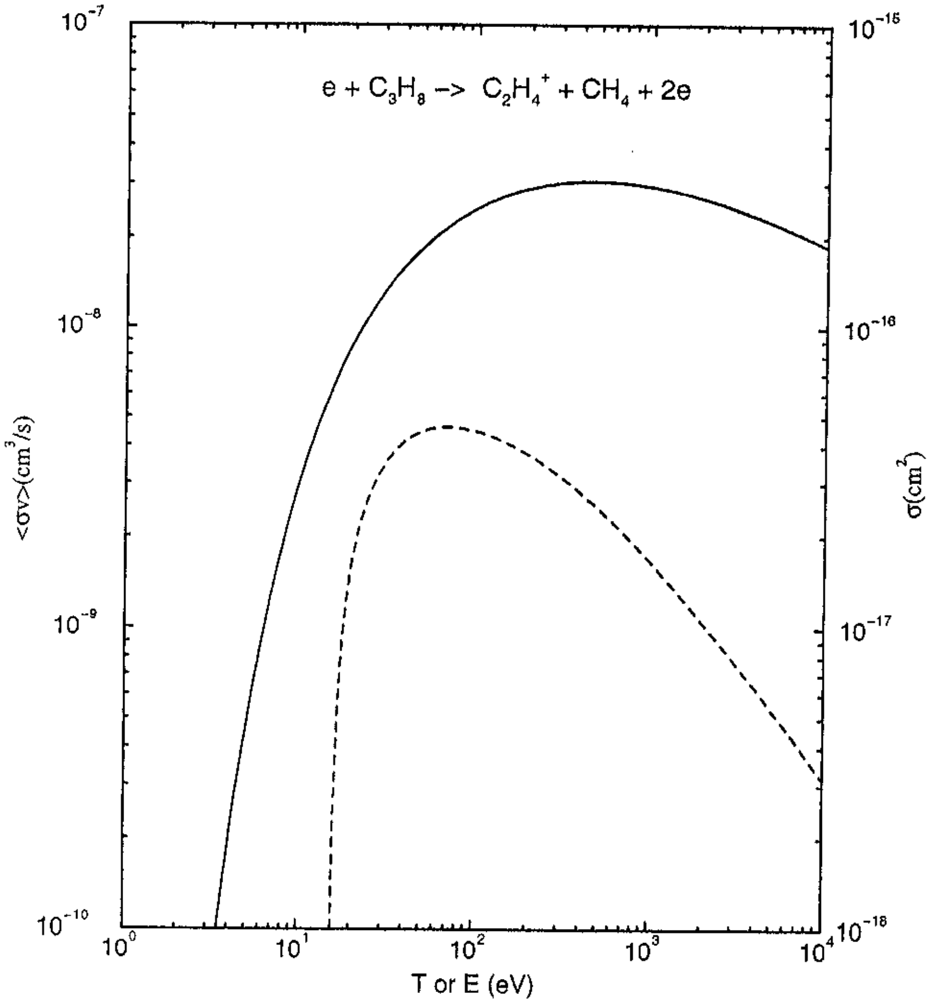
e + C3H8 -> C2H4+ + CH4 + 2e
<σv>(cm3/s)
σ(cm2)
T or E (eV)

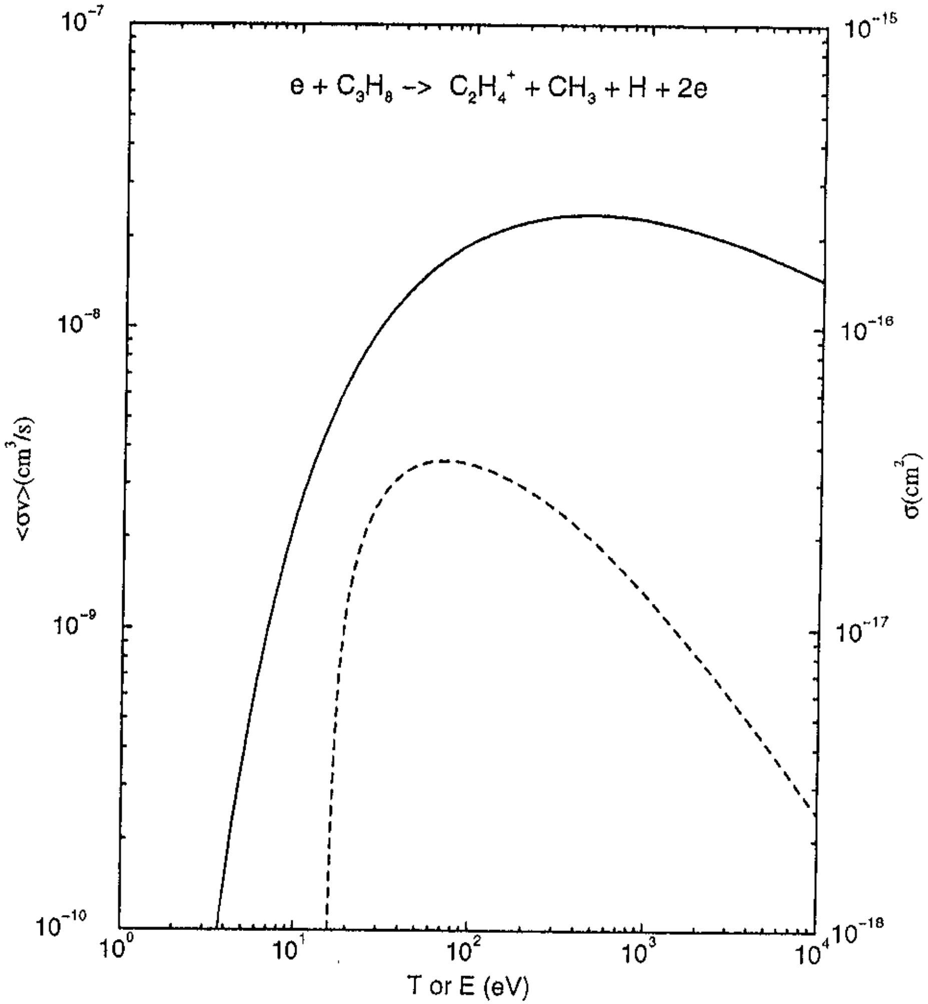
e + C3H8 -> C2H4+ + CH3 + H + 2e
<σv>(cm3/s)
σ(cm2)
T or E (eV)

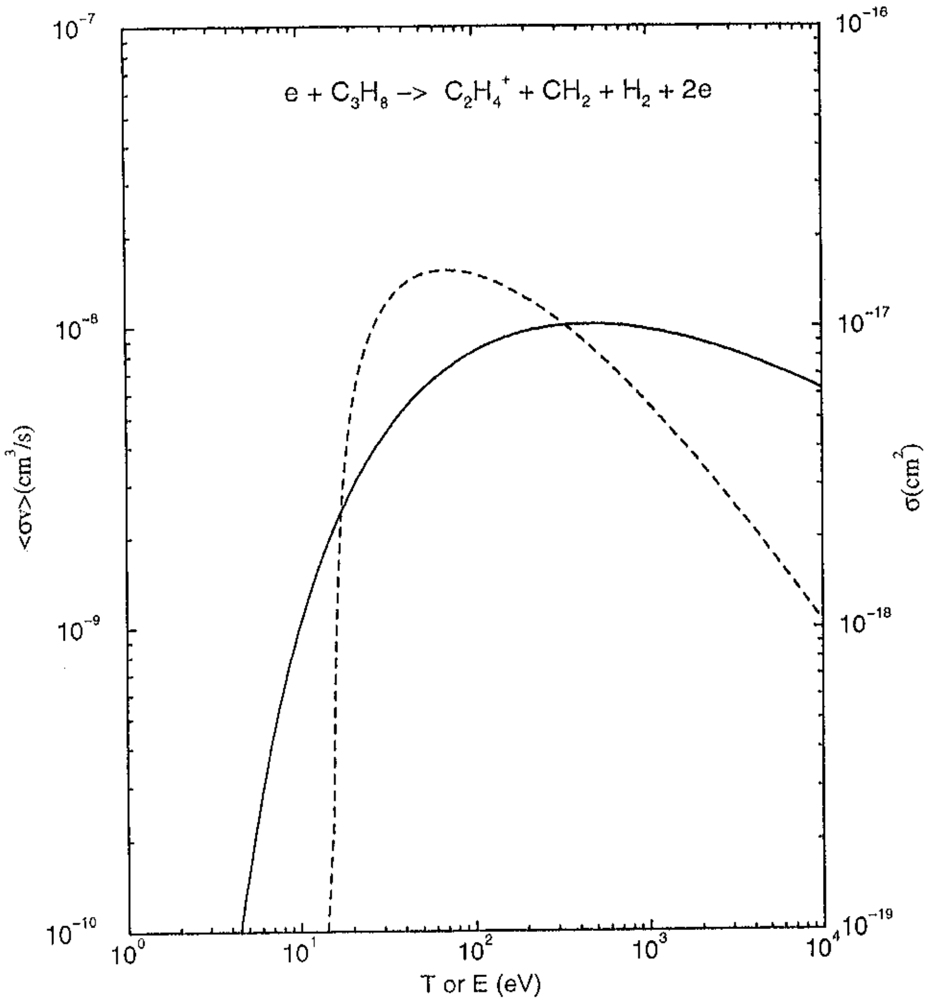
e + C3H8 -> C2H4+ + CH2 + H2 + 2e
<σv>(cm3/s)
σ(cm2)
T or E (eV)

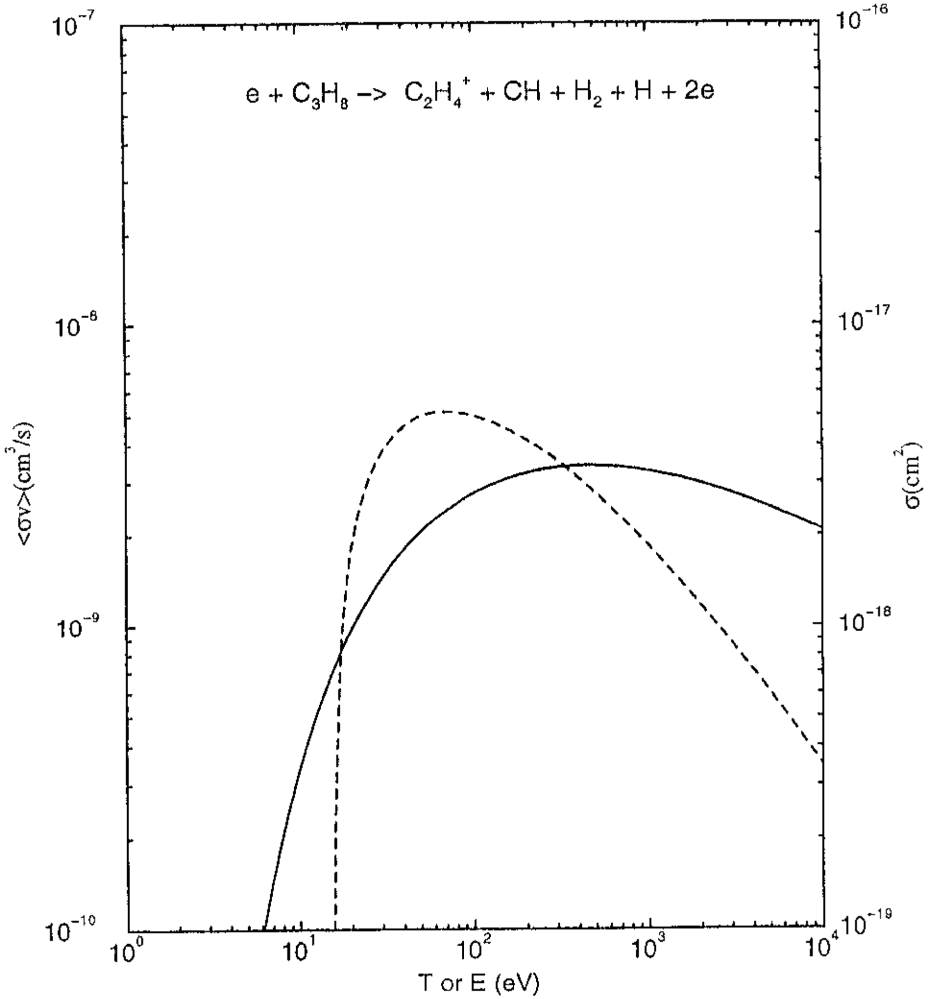
e + C3H8 -> C2H4+ + CH + H2 + H + 2e
<σv>(cm3/s)
σ(cm2)
T or E (eV)

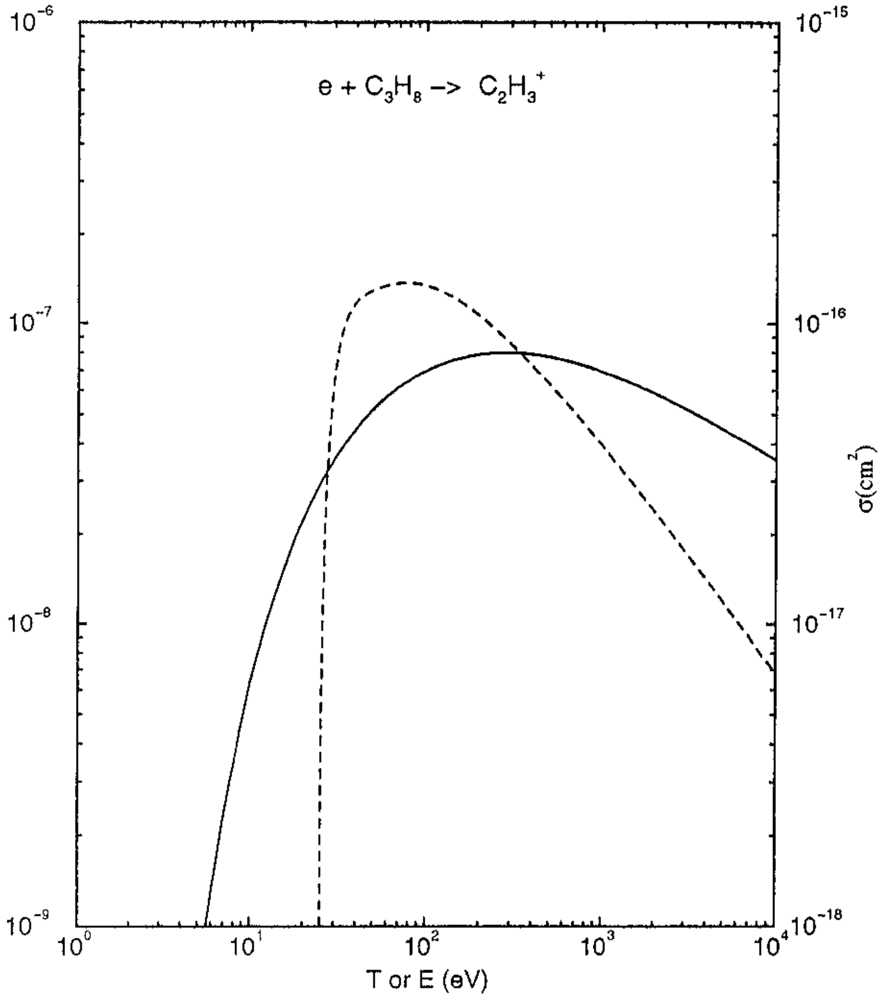
e + C3H8 -> C2H3+
<σv>(cm3/s)
σ(cm2)
T or E (eV)

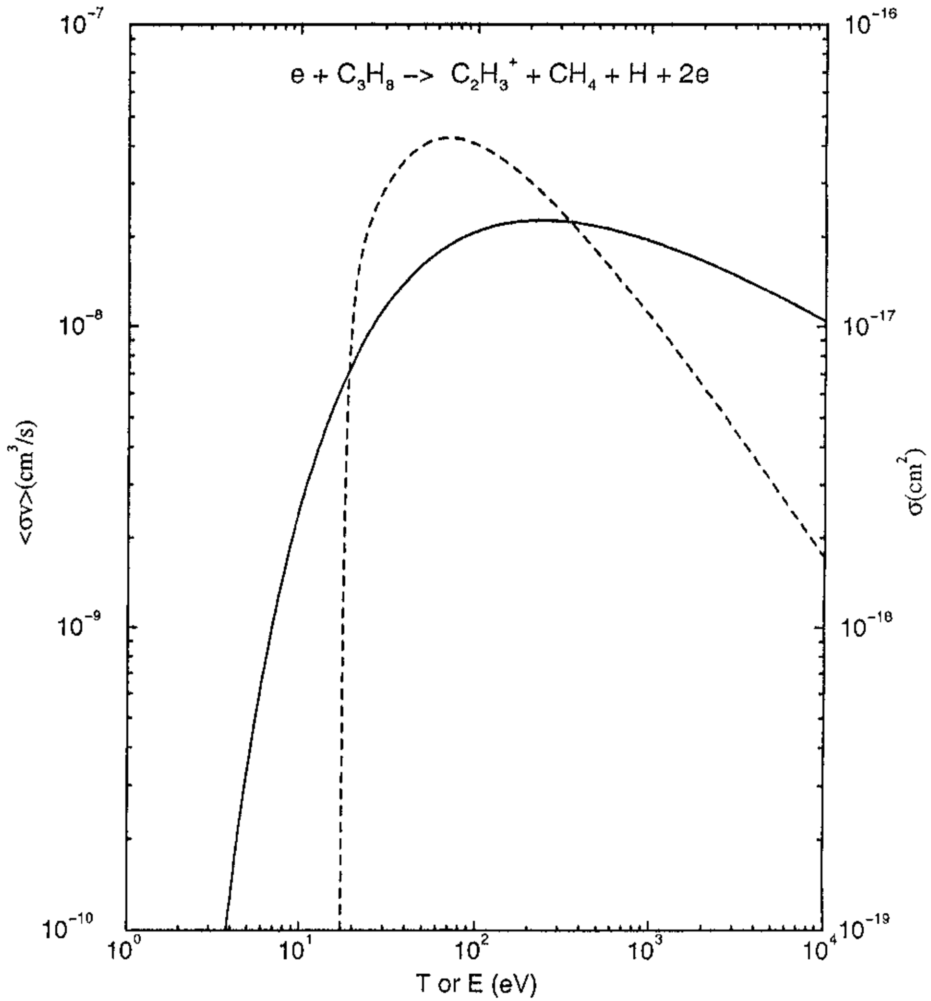
e + C3H8 -> C2H3+ + CH4 + H + 2e
<σv>(cm3/s)
σ(cm2)
T or E (eV)

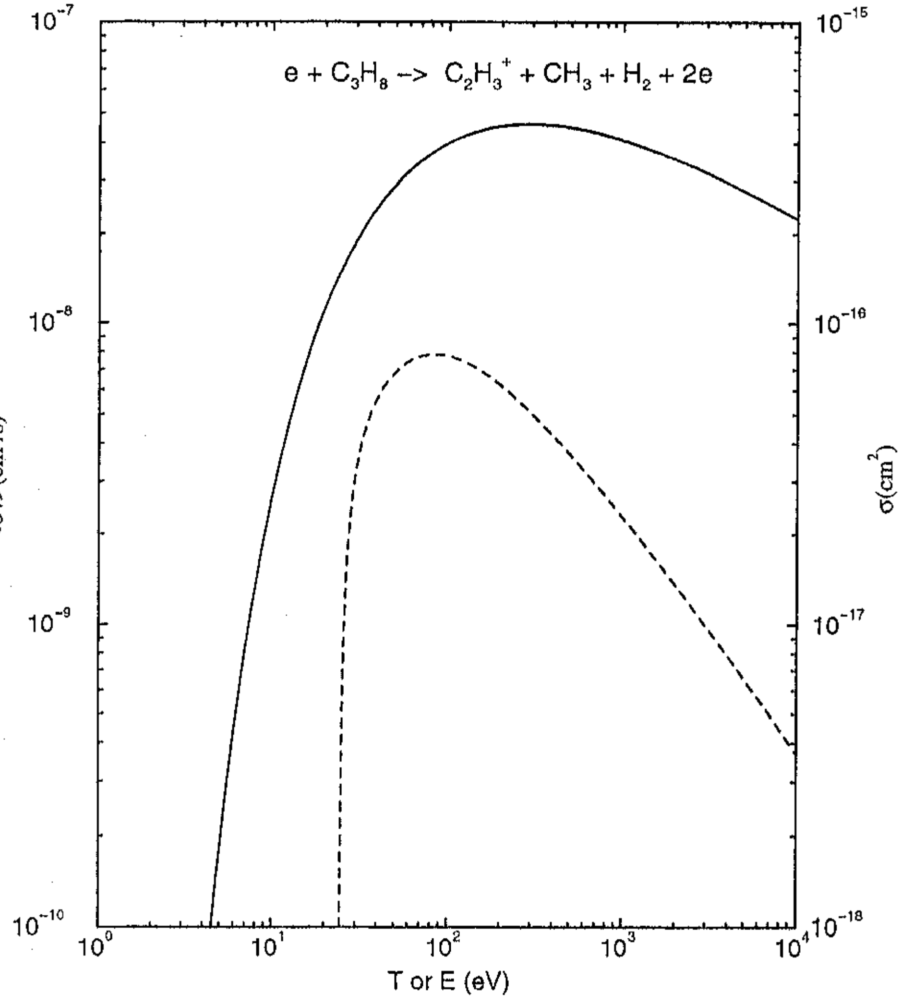
e + C3H8 -> C2H3+ + CH3 + H2 + 2e
<σv>(cm3/s)
σ(cm2)
T or E (eV)
10^-7
10^-8
10^-9
10^-10
10^-15
10^-16
10^-17
10^-18
10^0
10^1
10^2
10^3
10^4

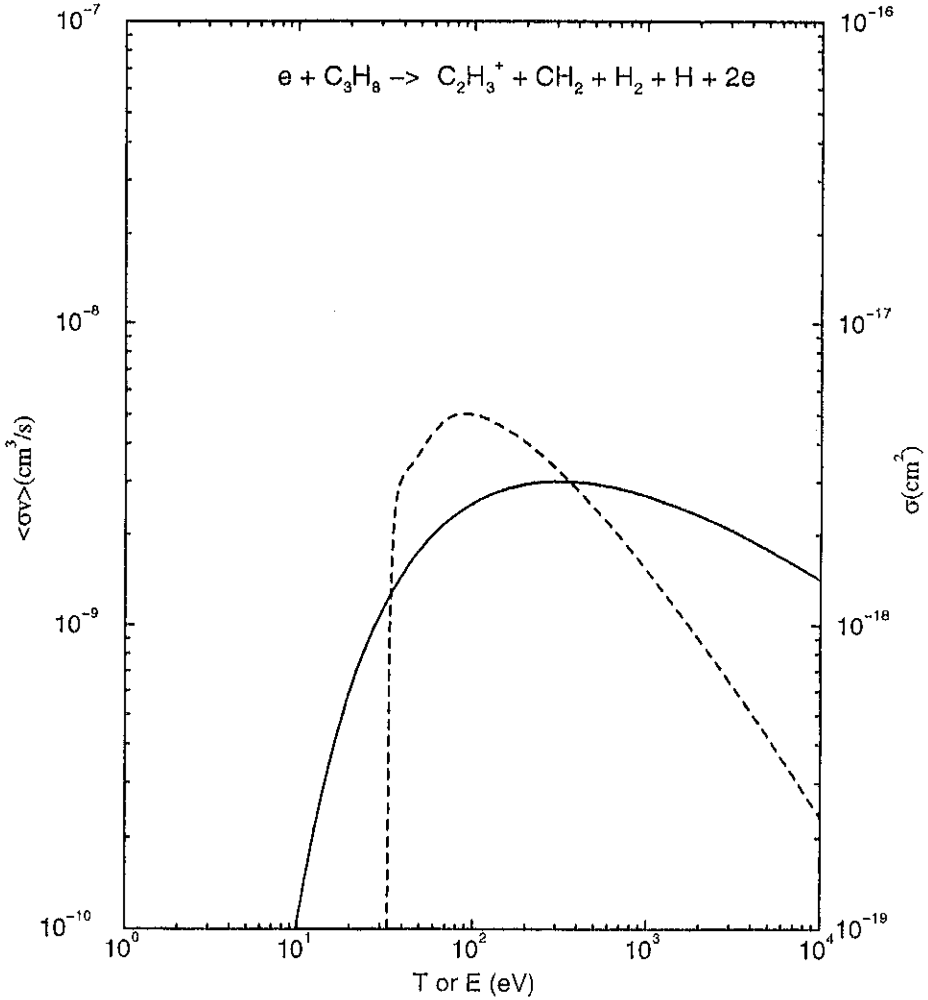
e + C3H8 -> C2H3+ + CH2 + H2 + H + 2e
<σv>(cm3/s)
σ(cm2)
T or E (eV)
10^-7
10^-8
10^-9
10^-10
10^-16
10^-17
10^-18
10^-19
10^0
10^1
10^2
10^3
10^4

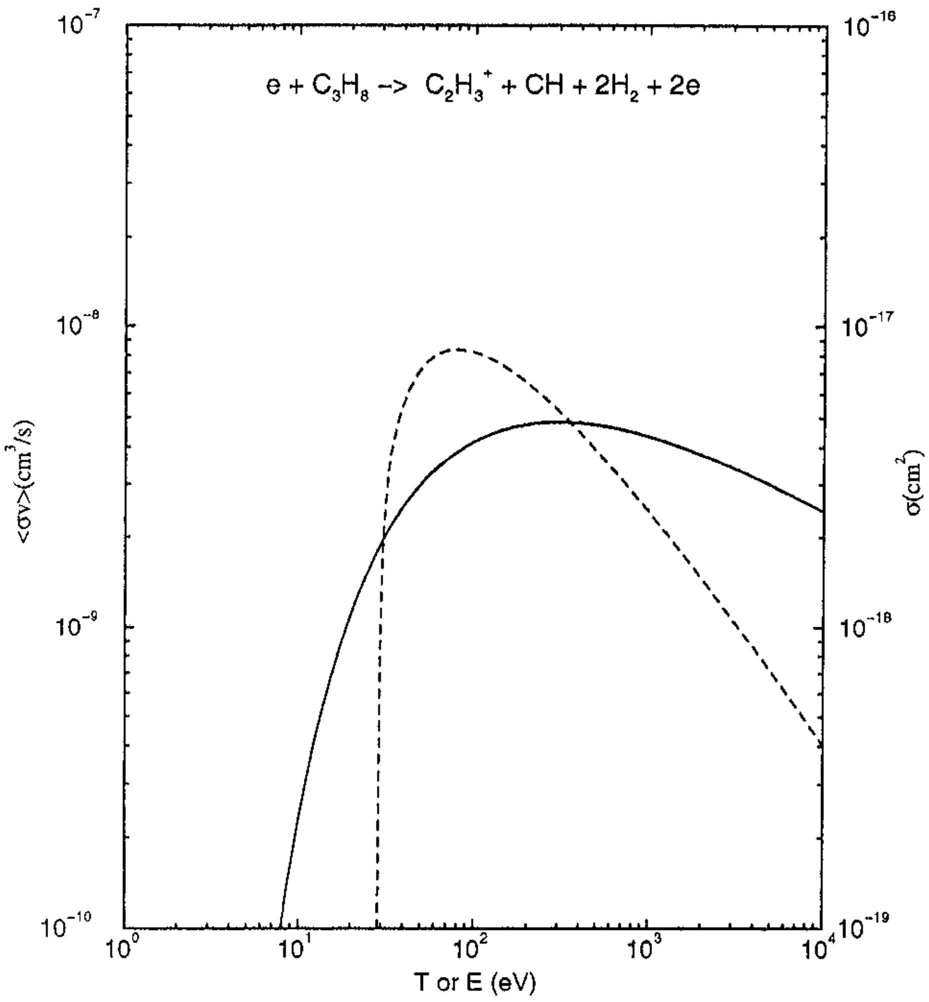
e + C3H8 -> C2H3+ + CH + 2H2 + 2e
<σv>(cm3/s)
σ(cm2)
T or E (eV)

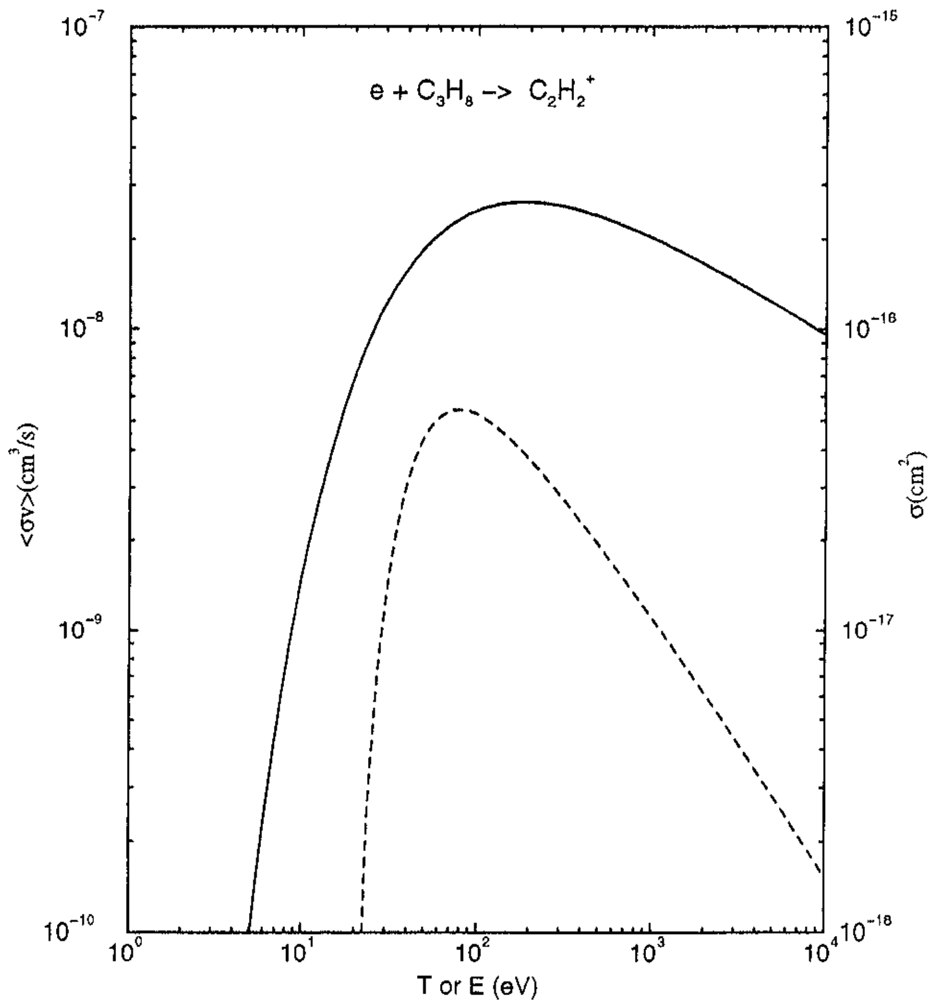
e + C3H8 -> C2H2+
<σv>(cm3/s)
σ(cm2)
T or E (eV)

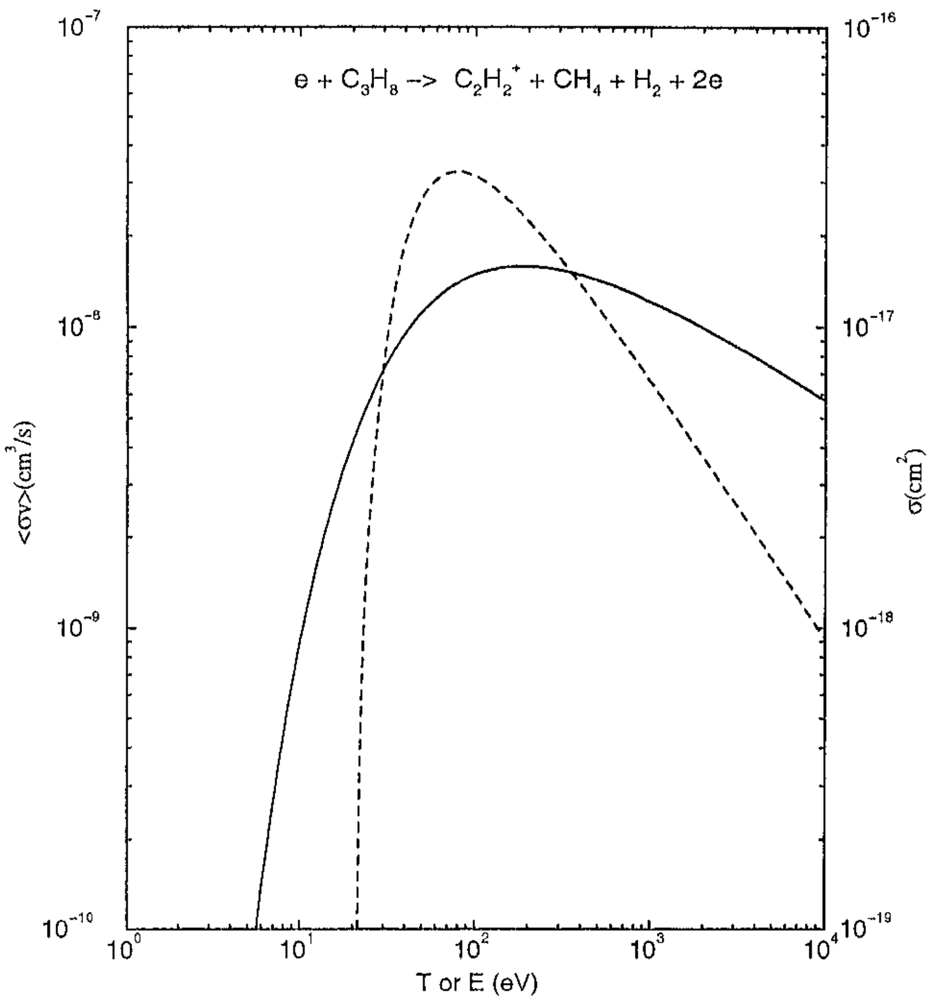
e + C3H8 -> C2H2+ + CH4 + H2 + 2e
<σv>(cm3/s)
σ(cm2)
T or E (eV)
10-7
10-8
10-9
10-10
10-16
10-17
10-18
10-19
100
101
102
103
104

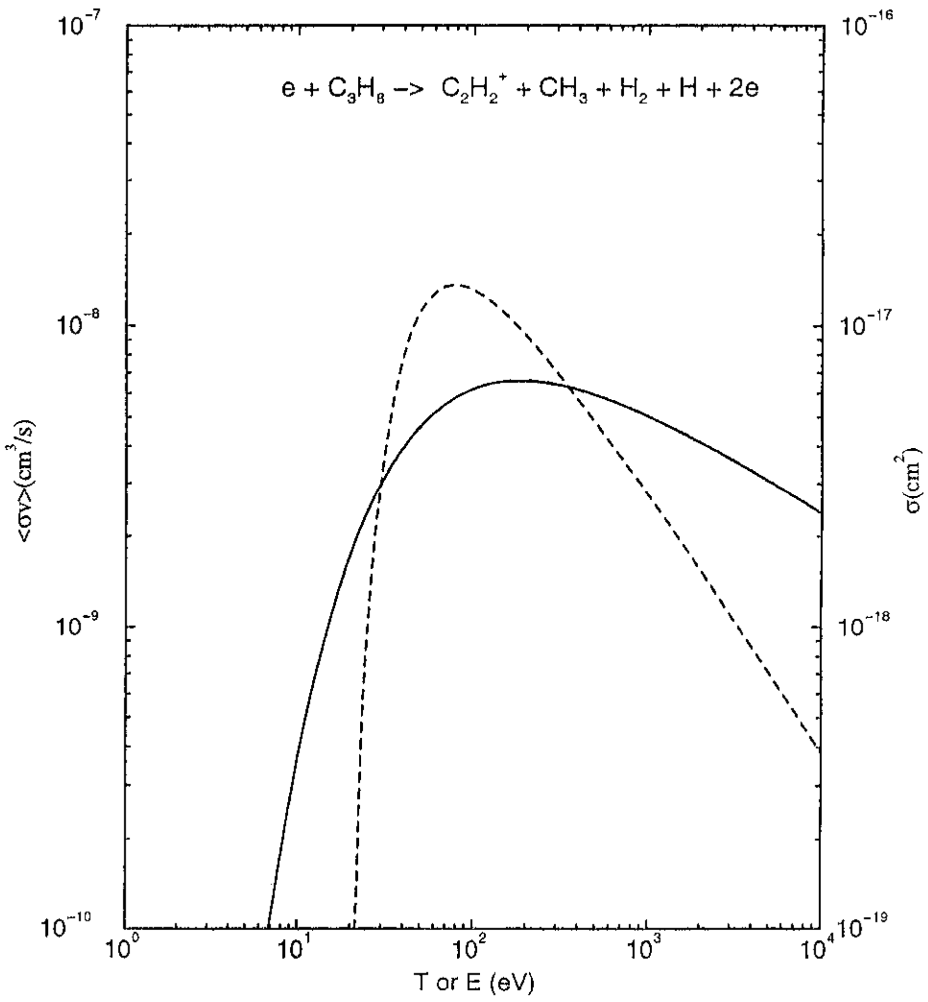
e + C3H8 -> C2H2+ + CH3 + H2 + H + 2e
<σv>(cm3/s)
σ(cm2)
T or E (eV)
10-7
10-8
10-9
10-10
10-16
10-17
10-18
10-19
100
101
102
103
104

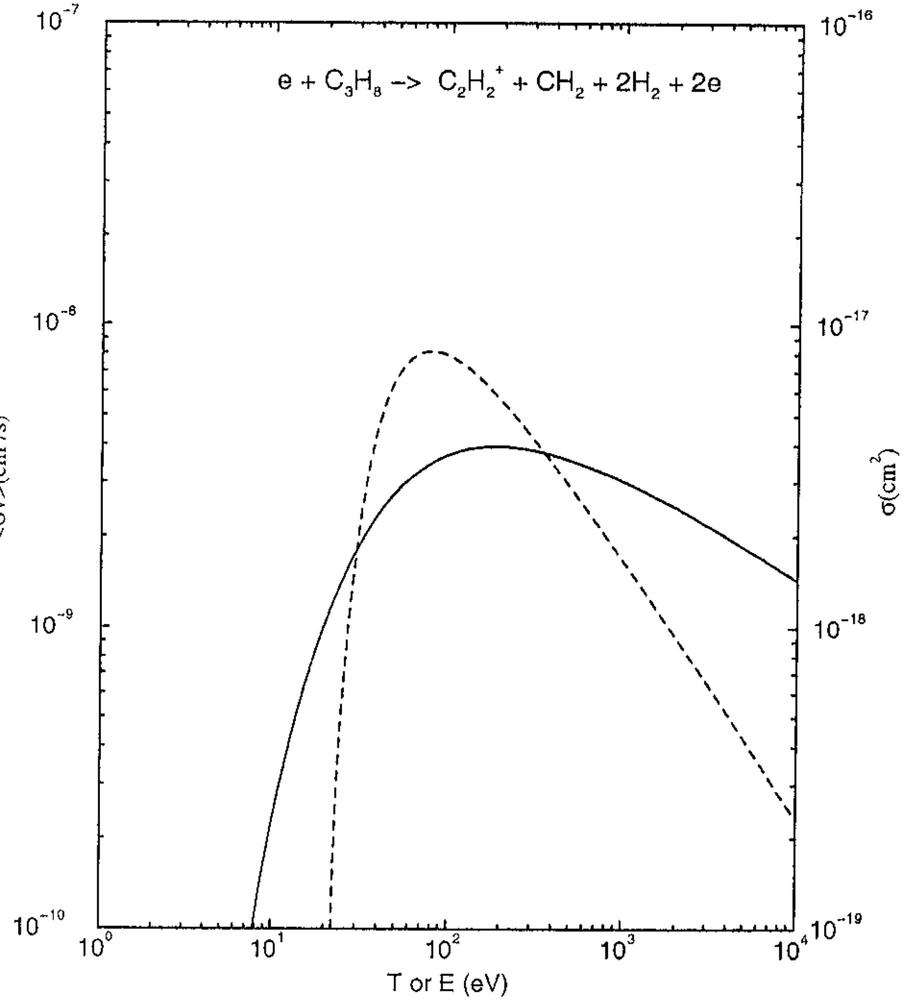
e + C3H8 -> C2H2+ + CH2 + 2H2 + 2e
<σv>(cm3/s)
σ(cm2)
T or E (eV)
10-7
10-8
10-9
10-10
10-16
10-17
10-18
10-19
100
101
102
103
104

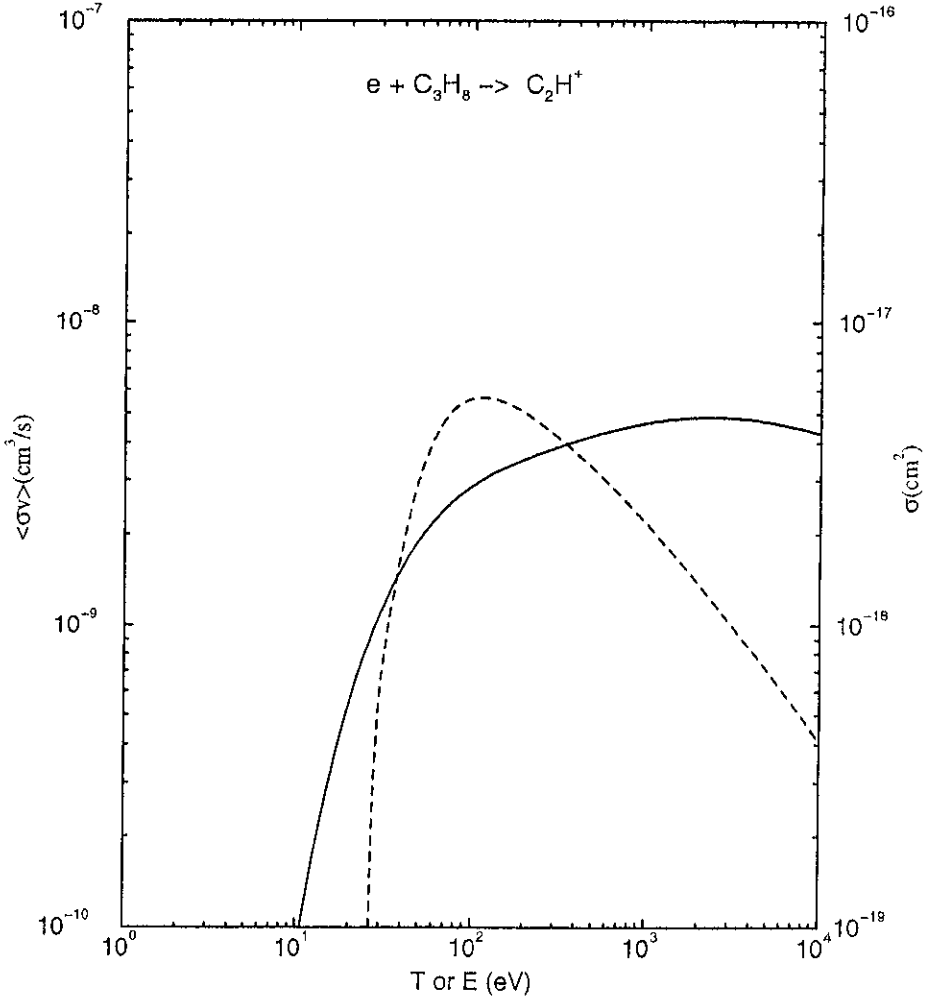
e + C3H8 -> C2H+
<σv>(cm3/s)
σ(cm2)
T or E (eV)
10-7
10-8
10-9
10-10
10-16
10-17
10-18
10-19
100
101
102
103
104

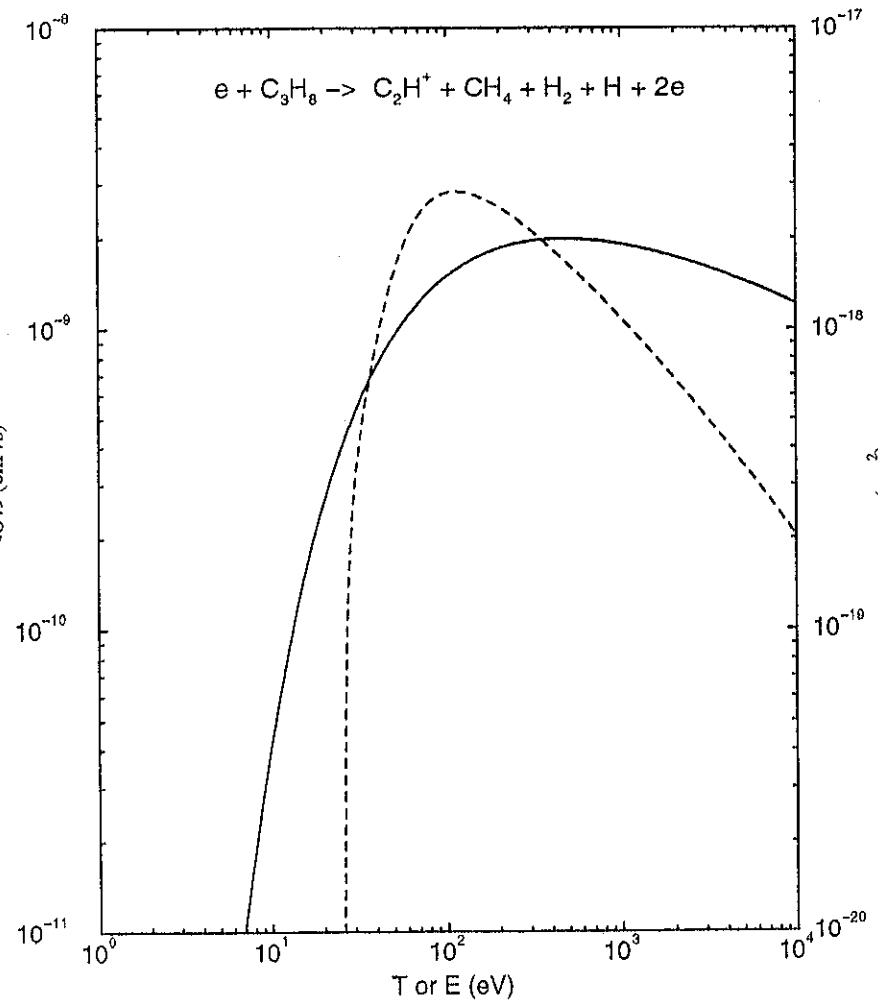
e + C_3H_8 -> C_2H^+ + CH_4 + H_2 + H + 2e
10^{-8}
10^{-9}
10^{-10}
10^{-11}
<σv>(cm^3/s)
10^{-17}
10^{-18}
10^{-19}
10^{-20}
σ(cm^2)
10^0
10^1
10^2
10^3
10^4
T or E (eV)

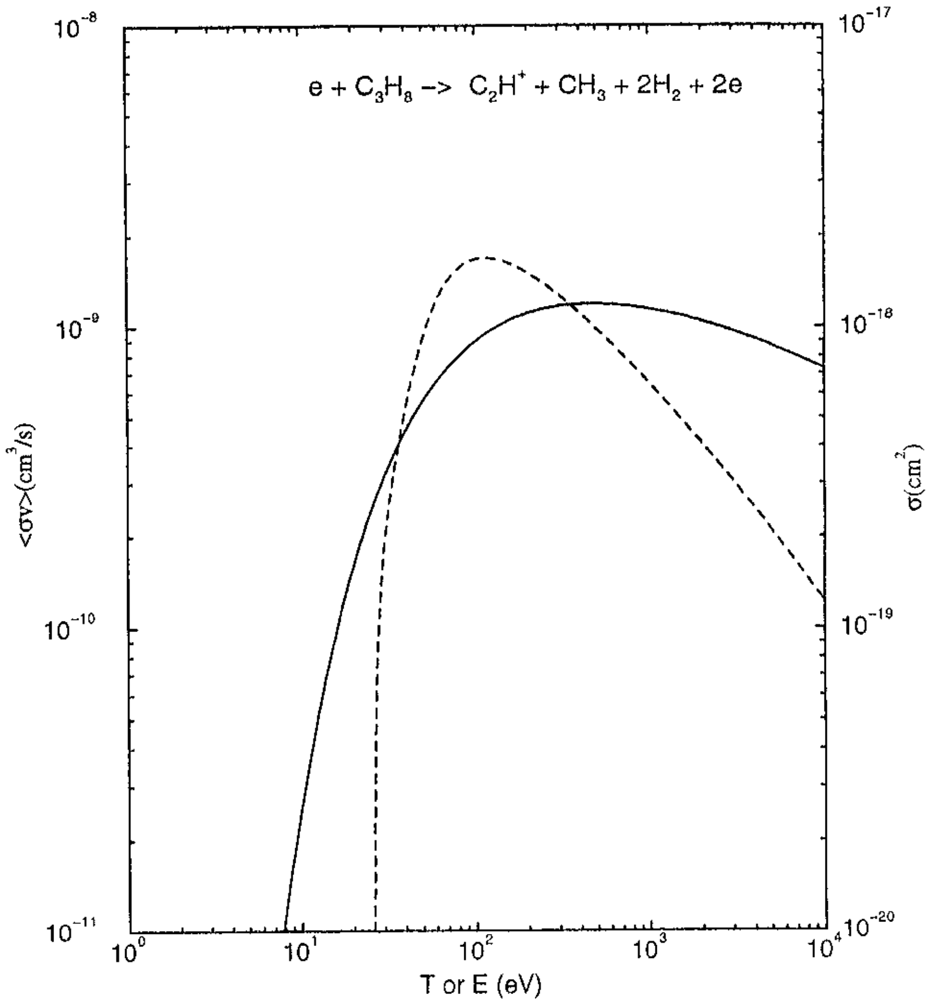
e + C_3H_8 -> C_2H^+ + CH_3 + $2H_2$ + 2e
10^{-8}
10^{-9}
10^{-10}
10^{-11}
<σv>(cm^3/s)
10^{-17}
10^{-18}
10^{-19}
10^{-20}
σ(cm^2)
10^0
10^1
10^2
10^3
10^4
T or E (eV)

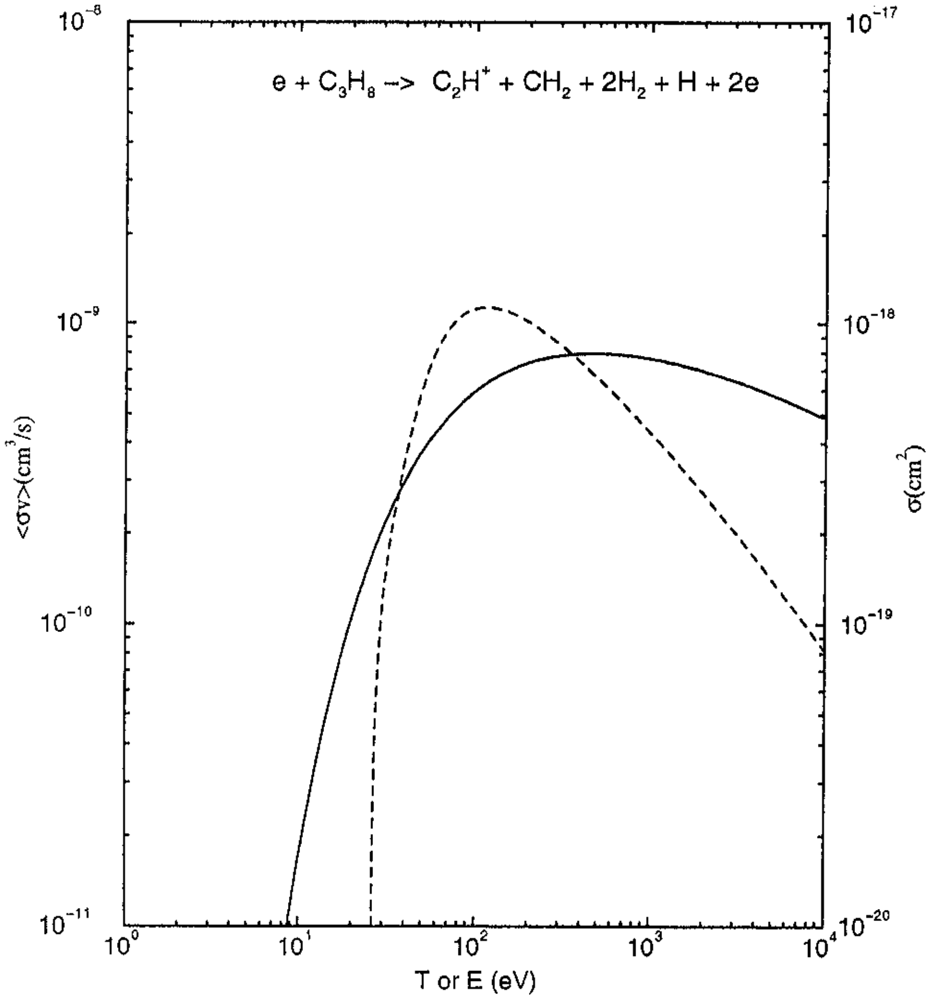

e + C3H8 -> C2H+ + CH2 + 2H2 + H + 2e
<σv>(cm3/s)
σ(cm2)
T or E (eV)

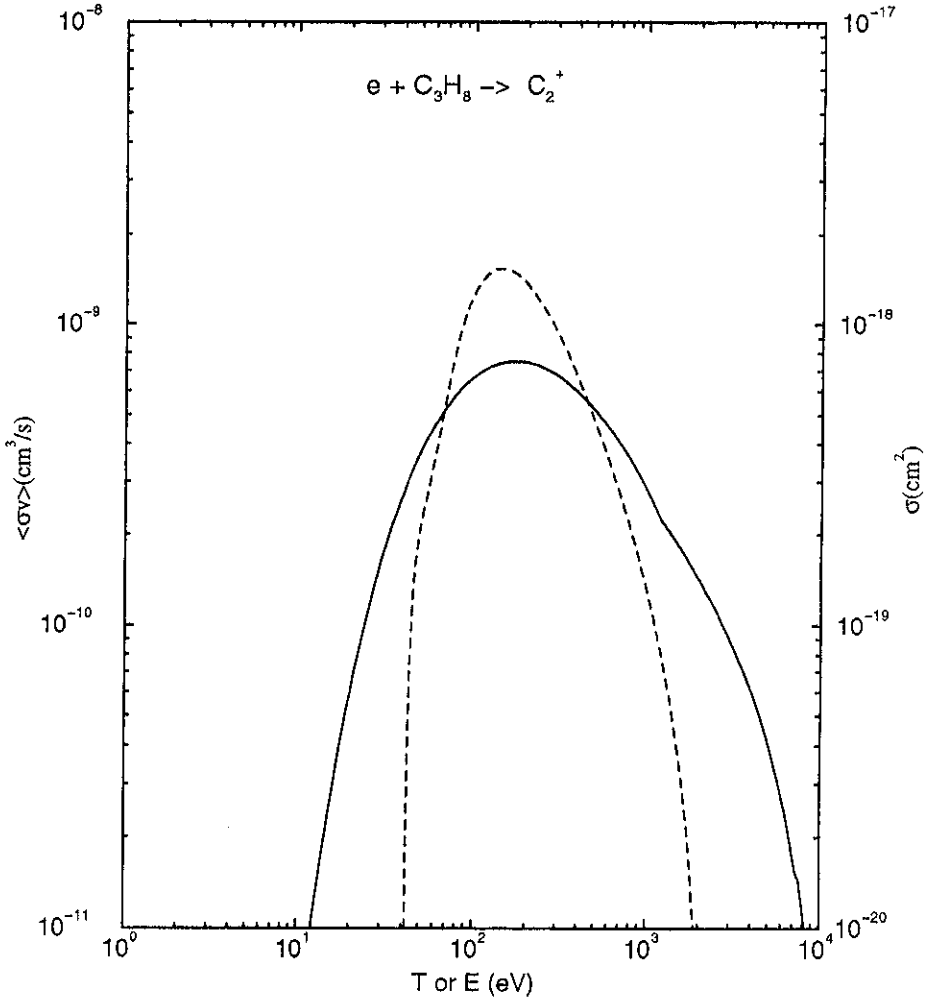

e + C3H8 -> C2+
<σv>(cm3/s)
σ(cm2)
T or E (eV)

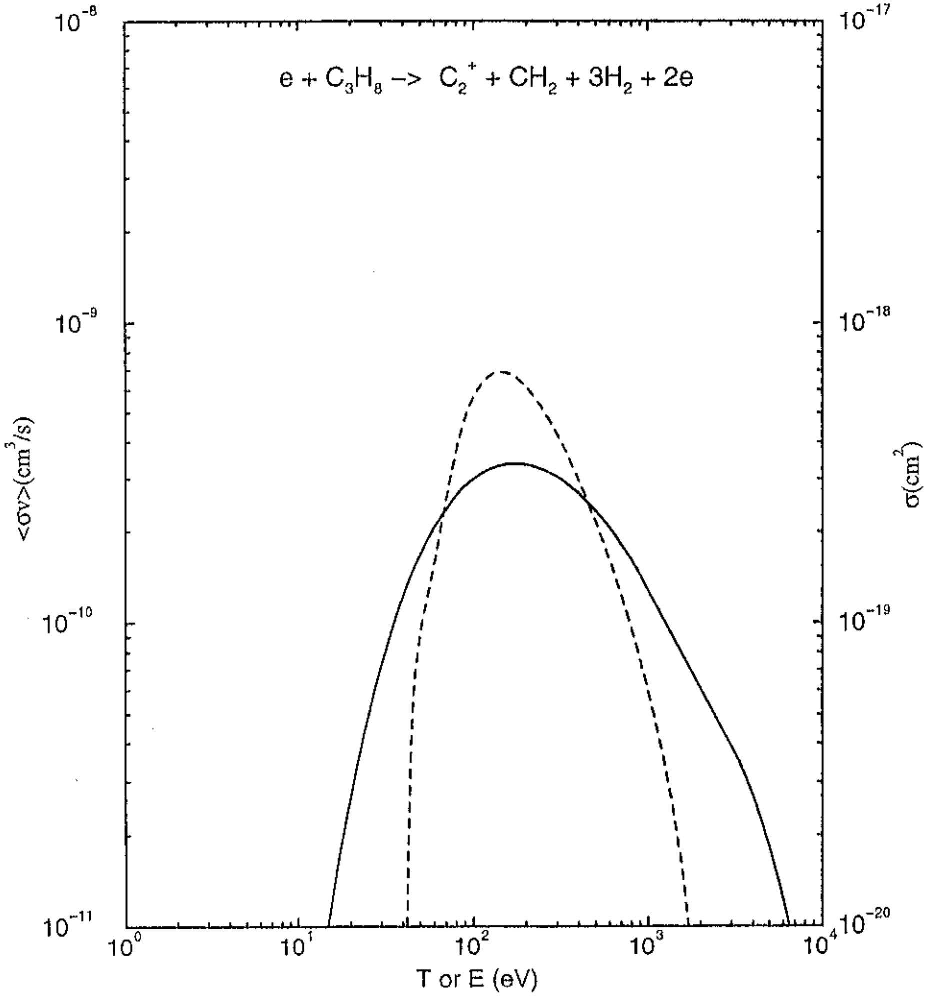
e + C3H8 -> C2+ + CH2 + 3H2 + 2e
<σv>(cm3/s)
σ(cm2)
T or E (eV)

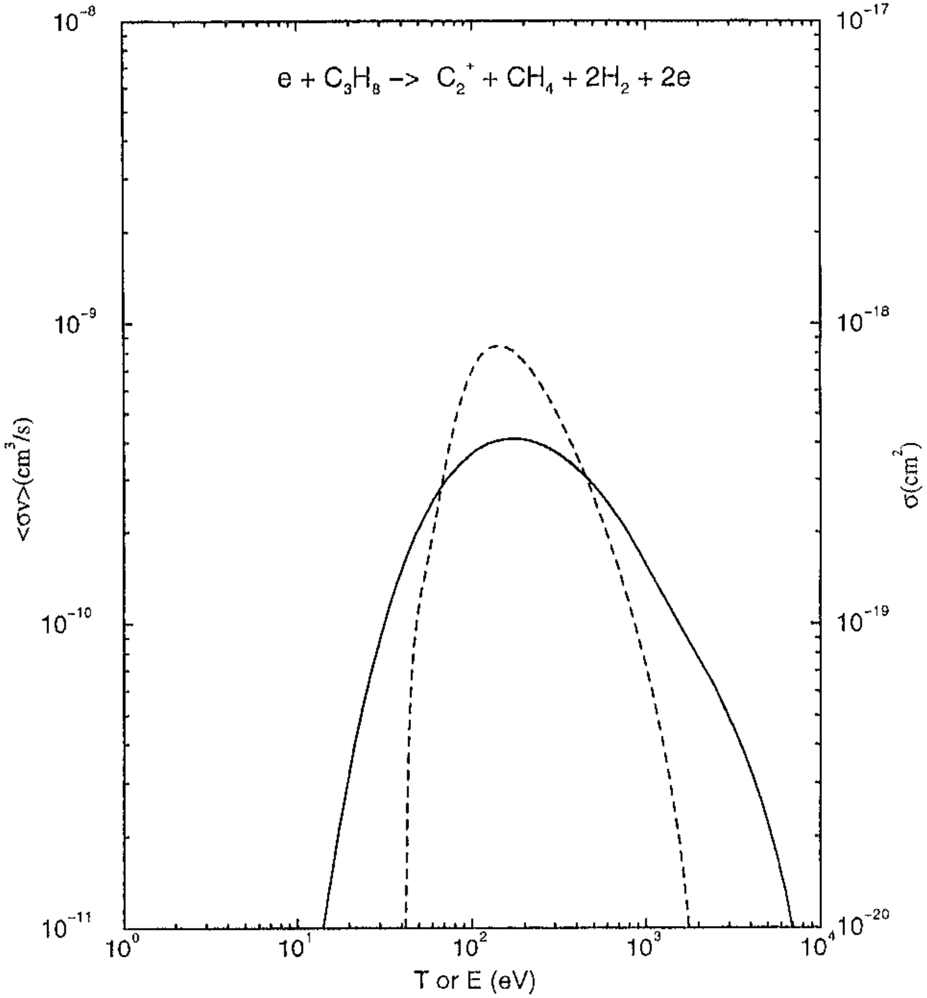
e + C3H8 -> C2+ + CH4 + 2H2 + 2e
<σv>(cm3/s)
σ(cm2)
T or E (eV)

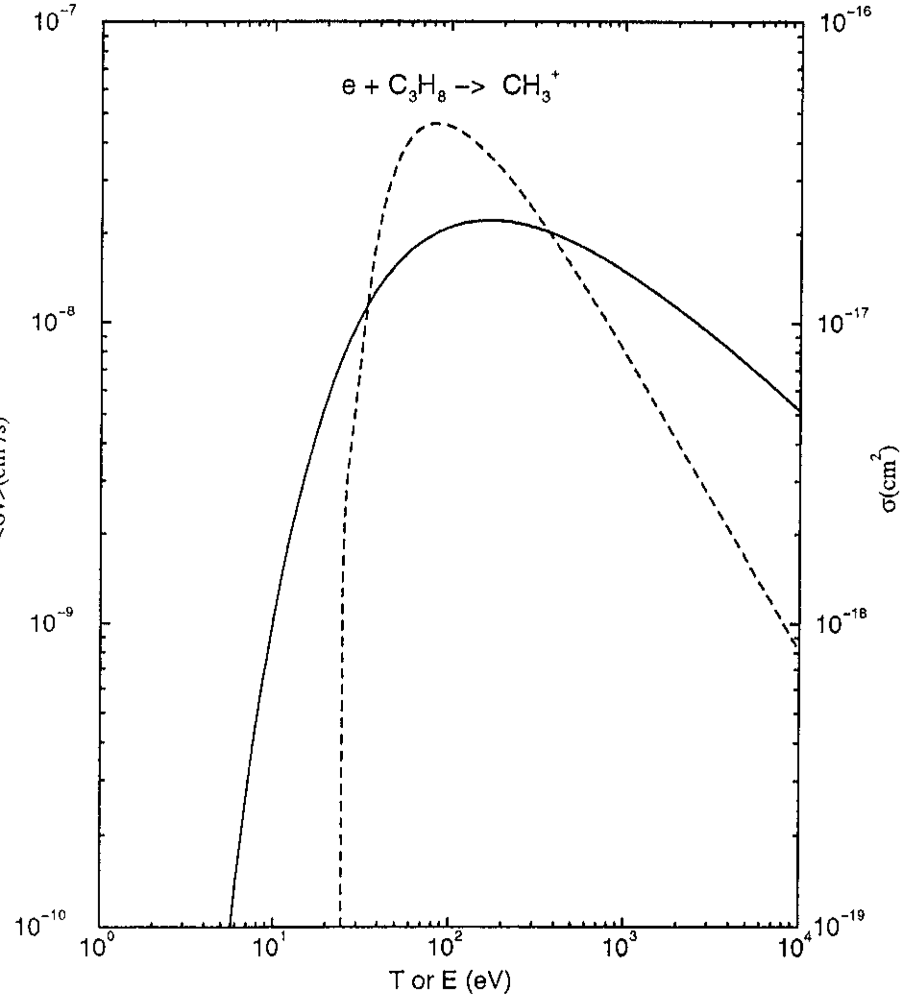

e + C3H8 -> CH3+
<σv>(cm3/s)
σ(cm2)
T or E (eV)

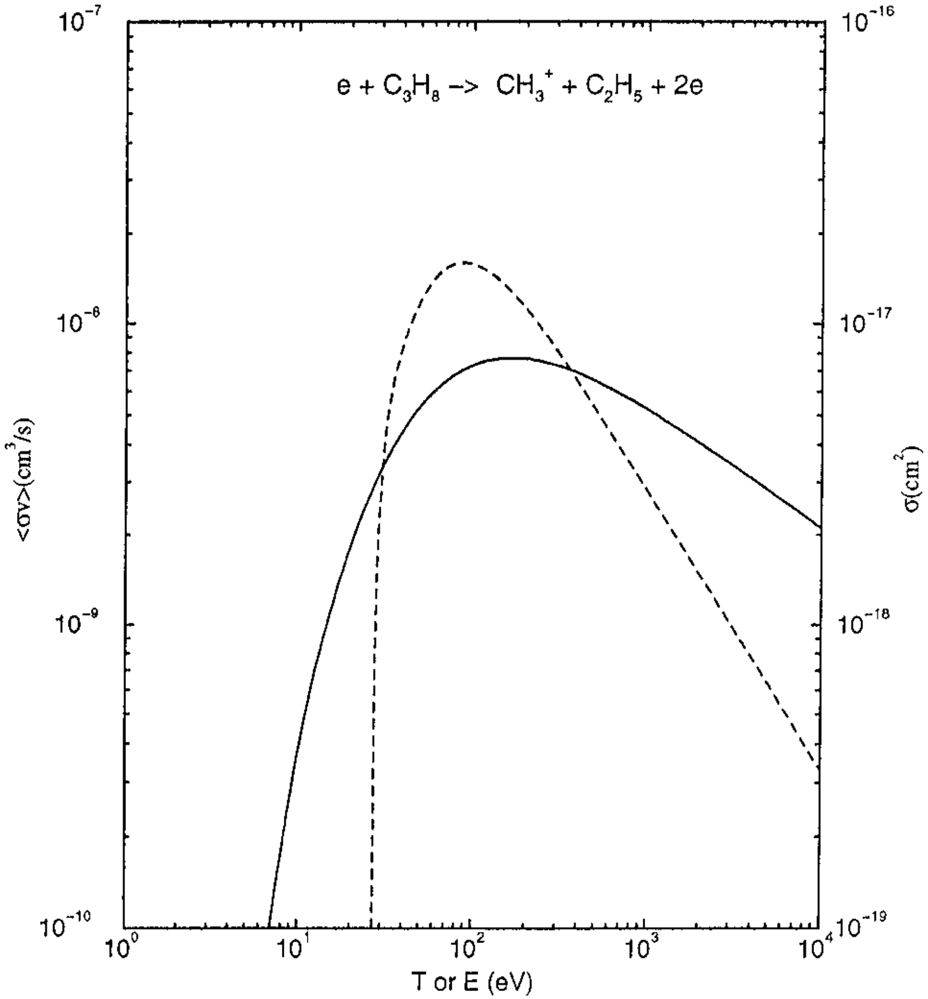

e + C3H8 -> CH3+ + C2H5 + 2e
<σv>(cm3/s)
σ(cm2)
T or E (eV)

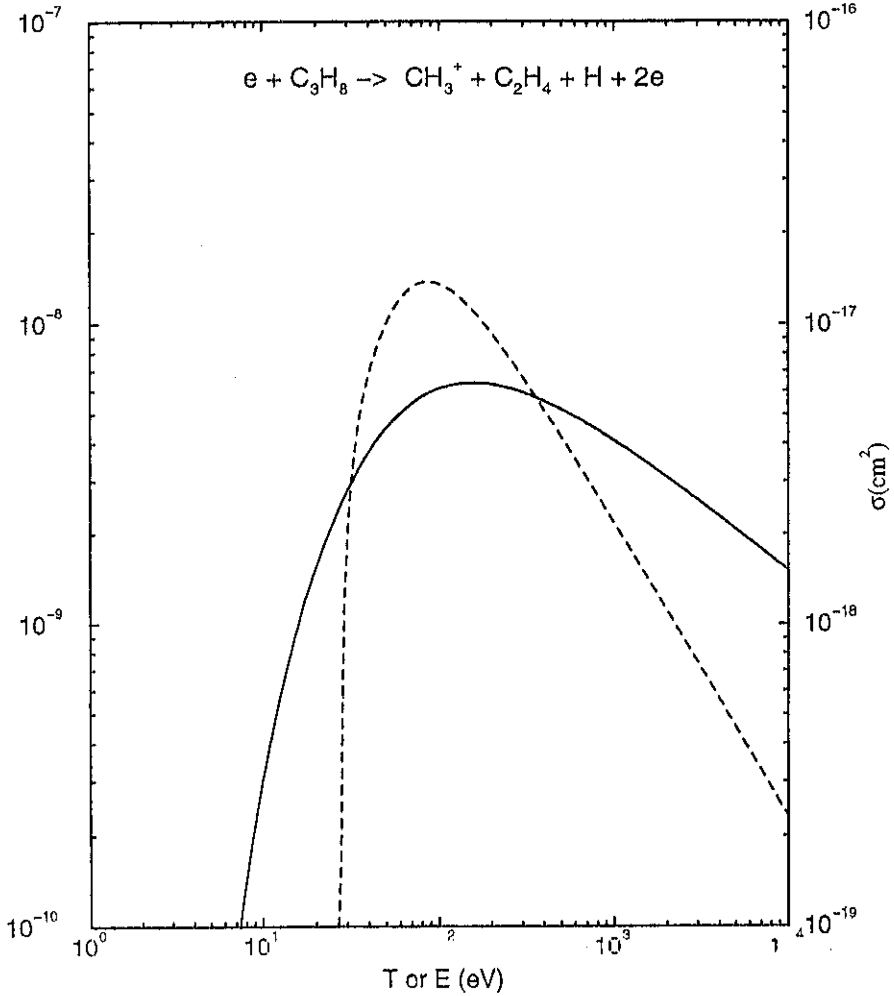

e + C_3H_8 -> CH_3^+ + C_2H_4 + H + 2e
10^{-7}
10^{-8}
10^{-9}
10^{-10}
<σv>(cm^3/s)
10^{-16}
10^{-17}
10^{-18}
10^{-19}
σ(cm^2)
10^0
10^1
10^3
T or E (eV)

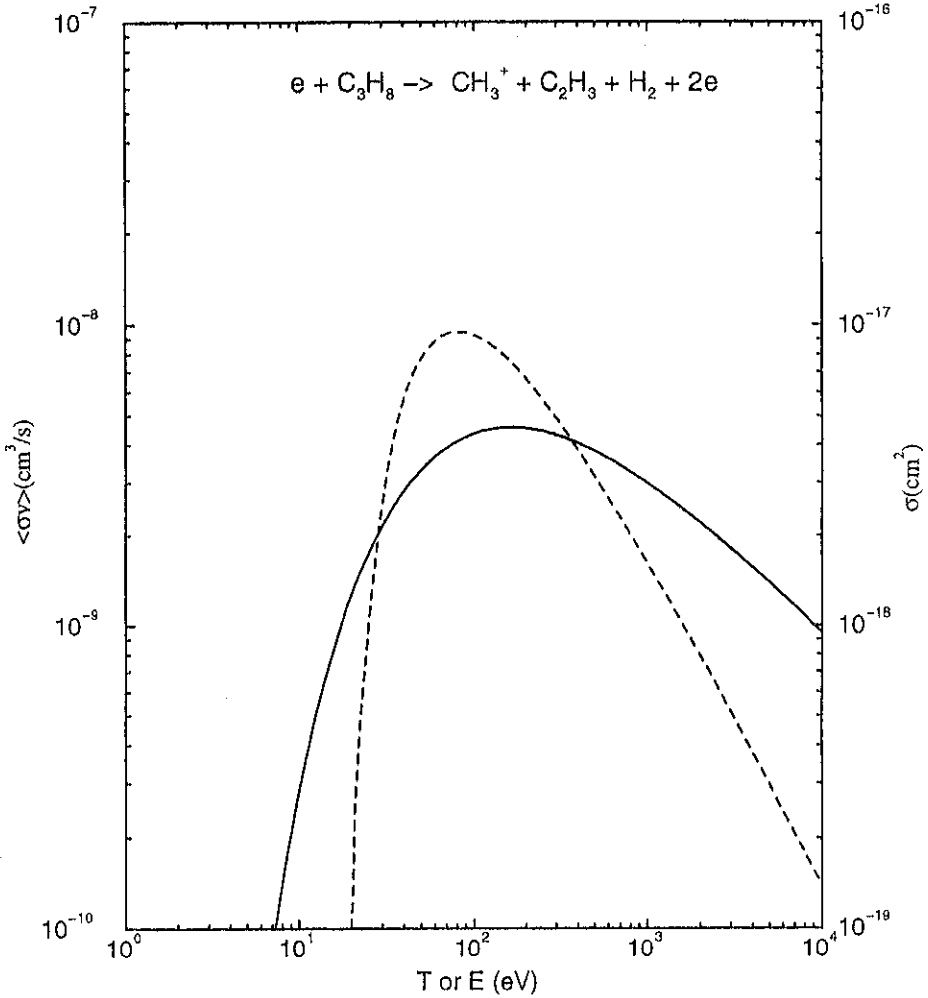

e + C_3H_8 -> CH_3^+ + C_2H_3 + H_2 + 2e
10^{-7}
10^{-8}
10^{-9}
10^{-10}
<σv>(cm^3/s)
10^{-16}
10^{-17}
10^{-18}
10^{-19}
σ(cm^2)
10^0
10^1
10^2
10^3
10^4
T or E (eV)

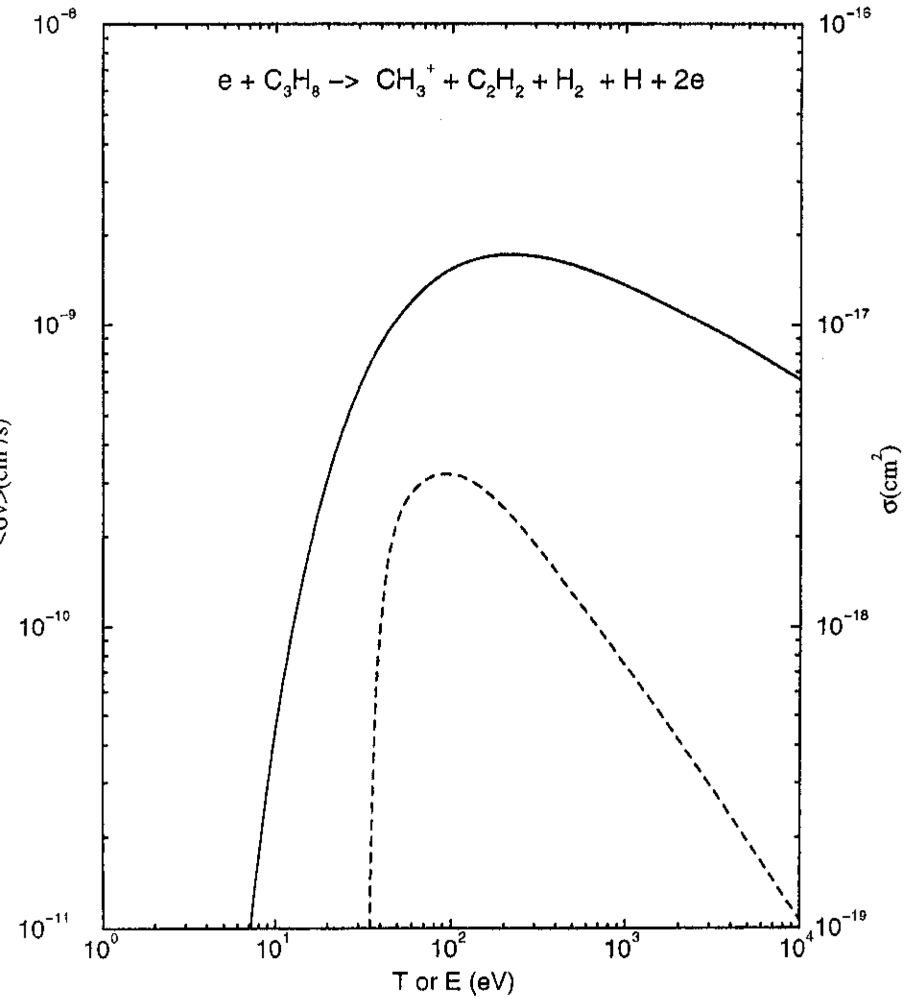
e + C3H8 -> CH3+ + C2H2 + H2 + H + 2e
<σv>(cm3/s)
σ(cm2)
T or E (eV)
10−8
10−9
10−10
10−11
10−16
10−17
10−18
10−19
100
101
102
103
104

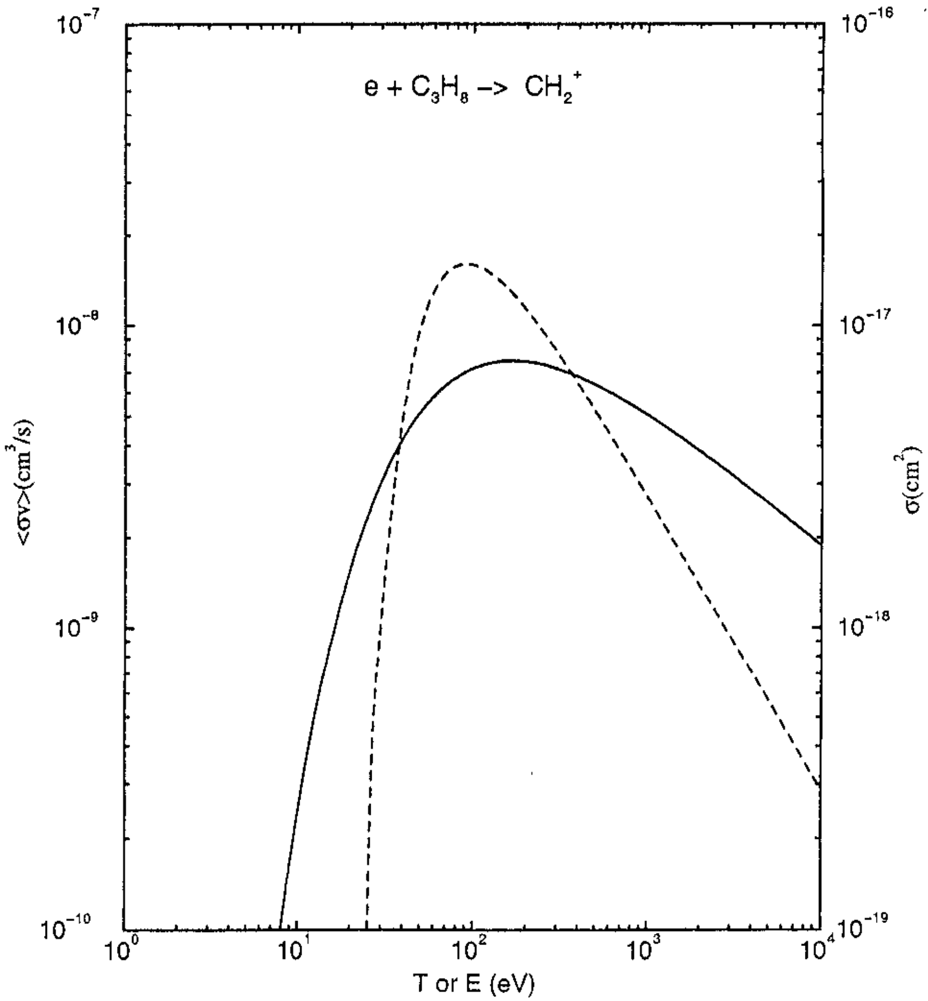
e + C3H8 -> CH2+
<σv>(cm3/s)
σ(cm2)
T or E (eV)
10−7
10−8
10−9
10−10
10−16
10−17
10−18
10−19
100
101
102
103
104

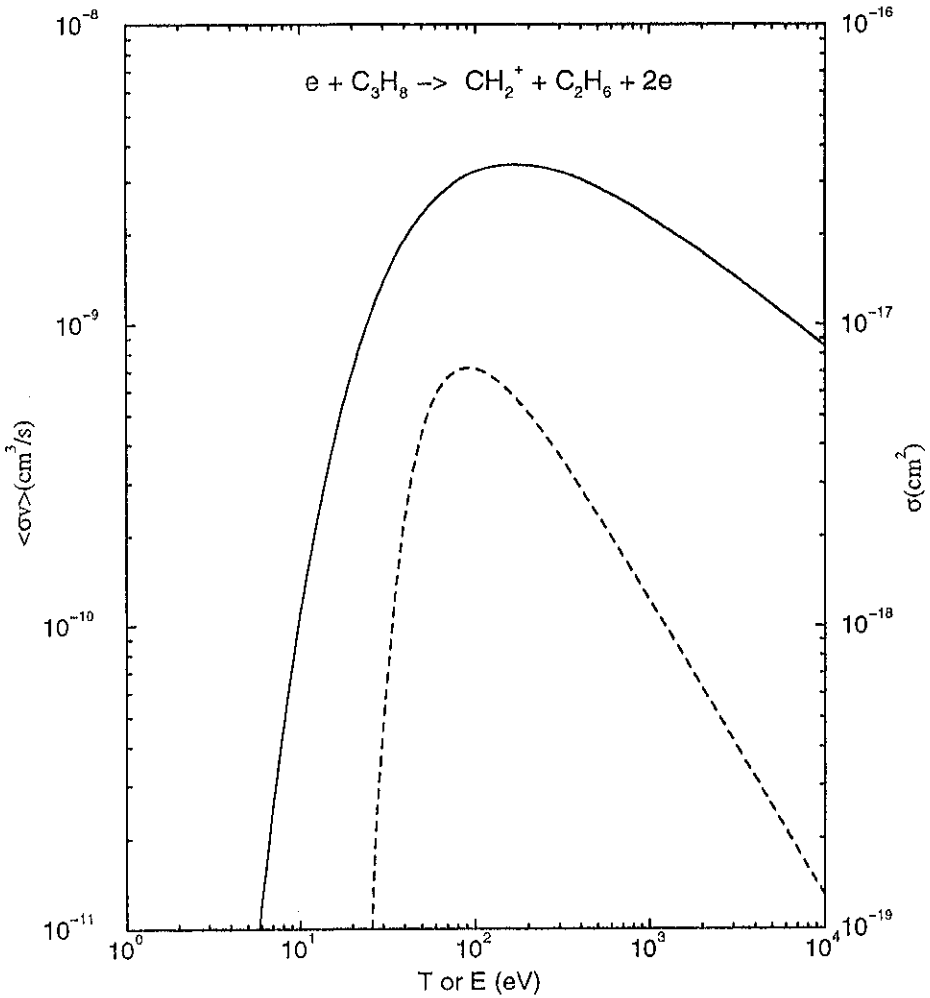
e + C3H8 -> CH2+ + C2H6 + 2e
<σv>(cm3/s)
σ(cm2)
T or E (eV)
10-8
10-9
10-10
10-11
10-16
10-17
10-18
10-19
100
101
102
103
104

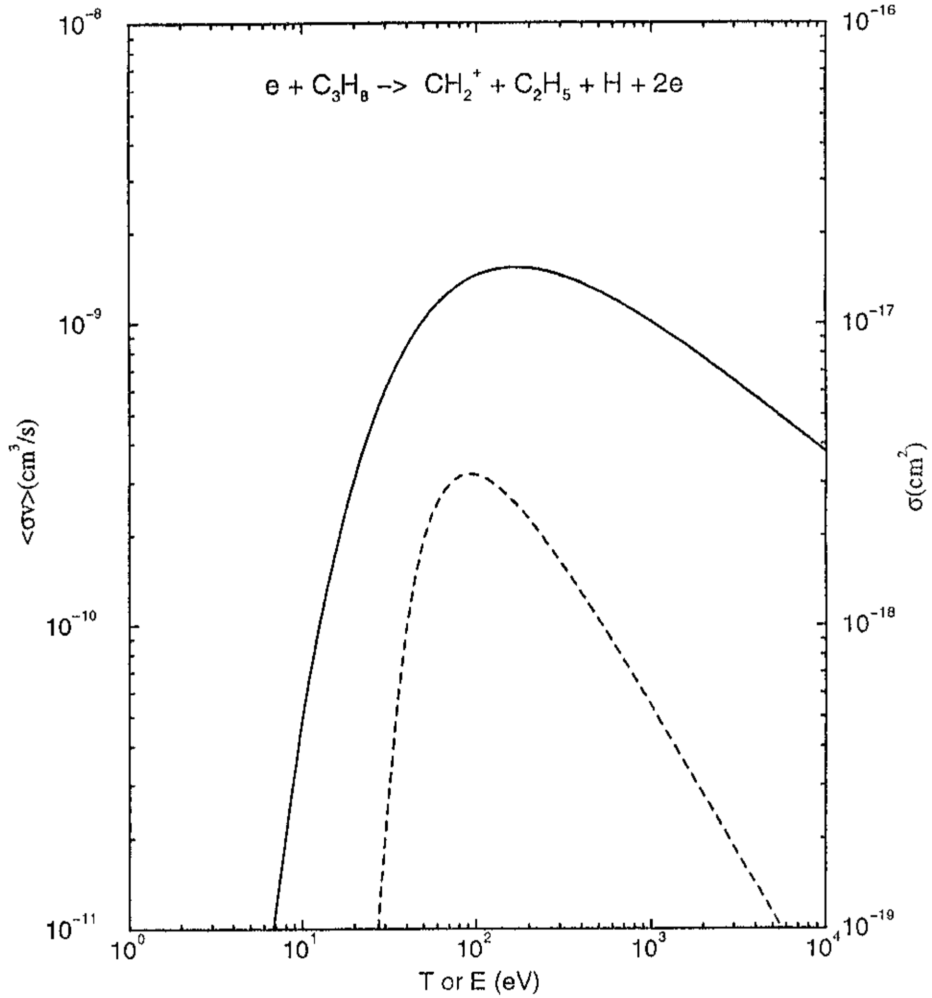
e + C3H8 -> CH2+ + C2H5 + H + 2e
<σv>(cm3/s)
σ(cm2)
T or E (eV)
10-8
10-9
10-10
10-11
10-16
10-17
10-18
10-19
100
101
102
103
104

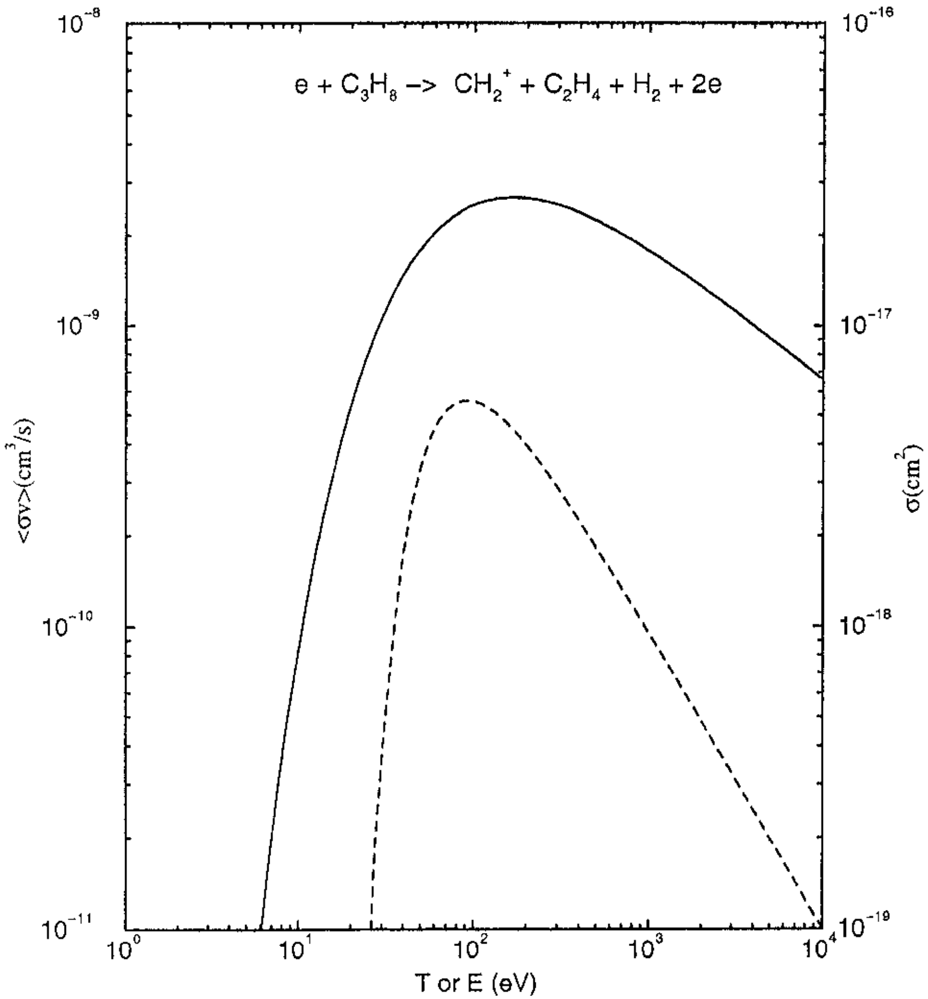
e + C3H8 -> CH2+ + C2H4 + H2 + 2e
<σv>(cm3/s)
σ(cm2)
T or E (eV)

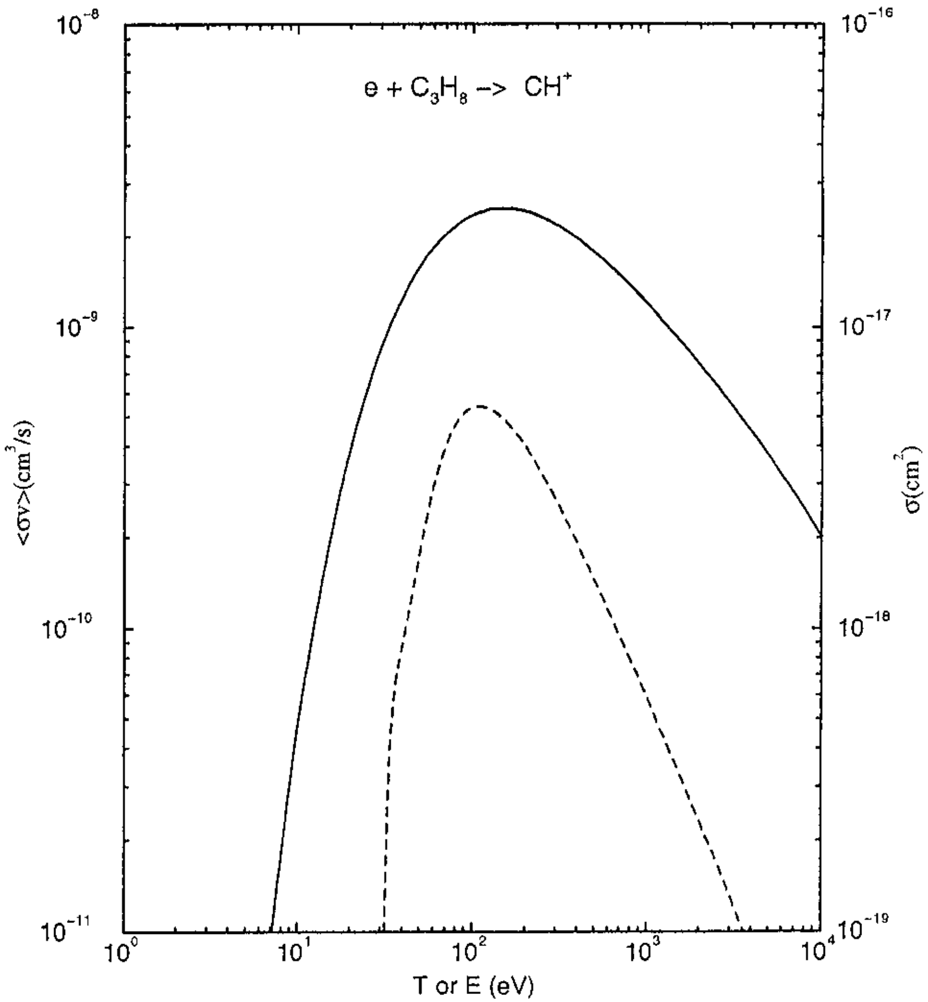
e + C3H8 -> CH+
<σv>(cm3/s)
σ(cm2)
T or E (eV)

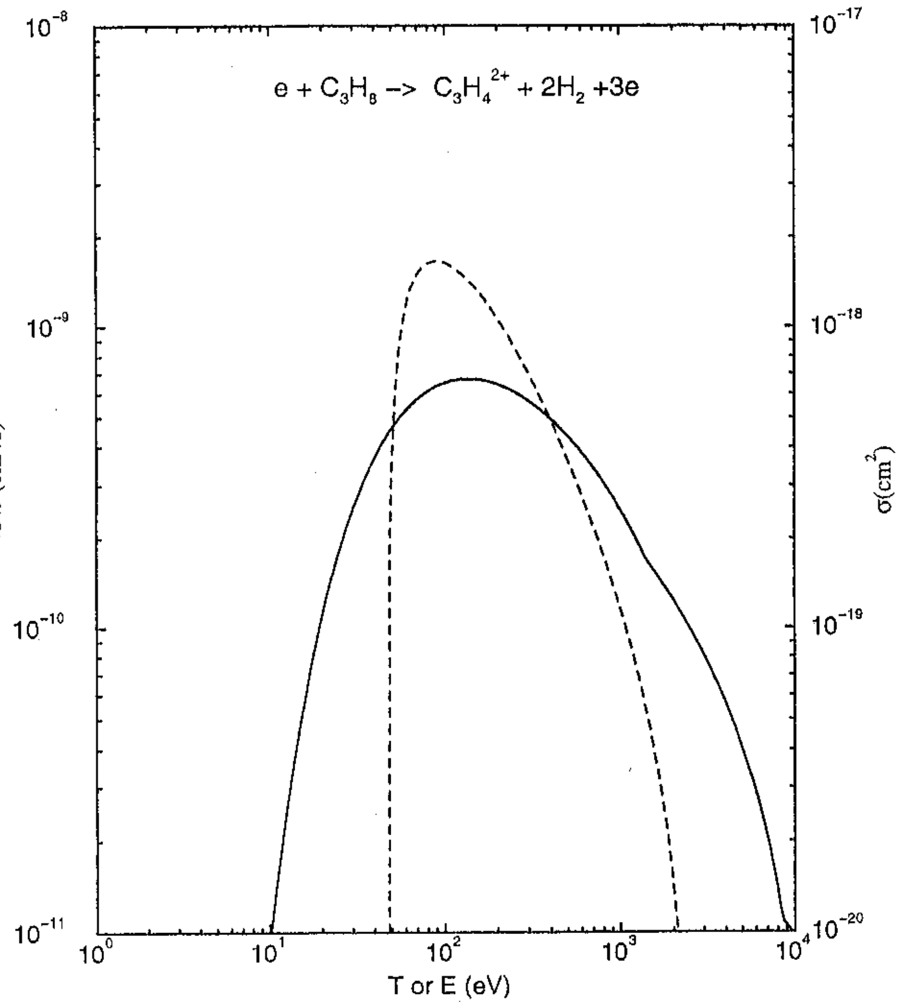
e + C3H8 -> C3H4 2+ + 2H2 +3e
<σv>(cm3/s)
σ(cm2)
T or E (eV)
10-8
10-9
10-10
10-11
10-17
10-18
10-19
10-20
10^0
10^1
10^2
10^3
10^4

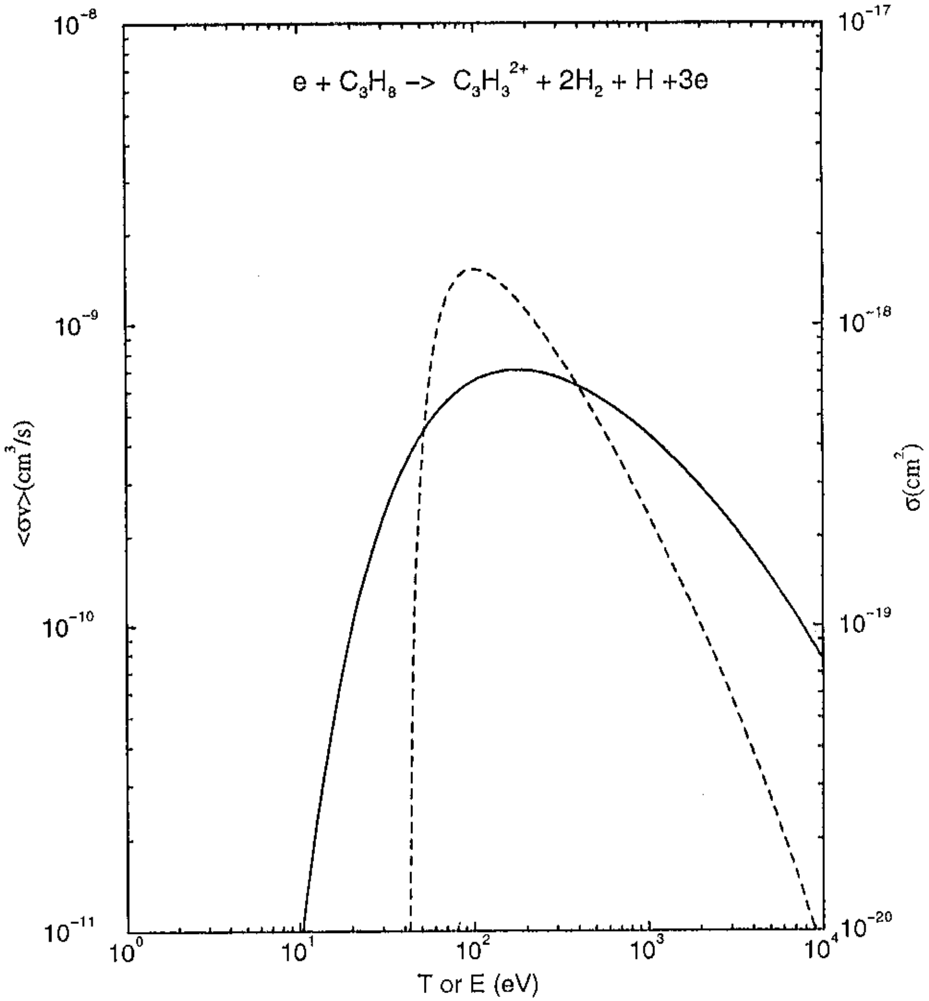
e + C3H8 -> C3H3 2+ + 2H2 + H +3e
<σv>(cm3/s)
σ(cm2)
T or E (eV)
10-8
10-9
10-10
10-11
10-17
10-18
10-19
10-20
10^0
10^1
10^2
10^3
10^4

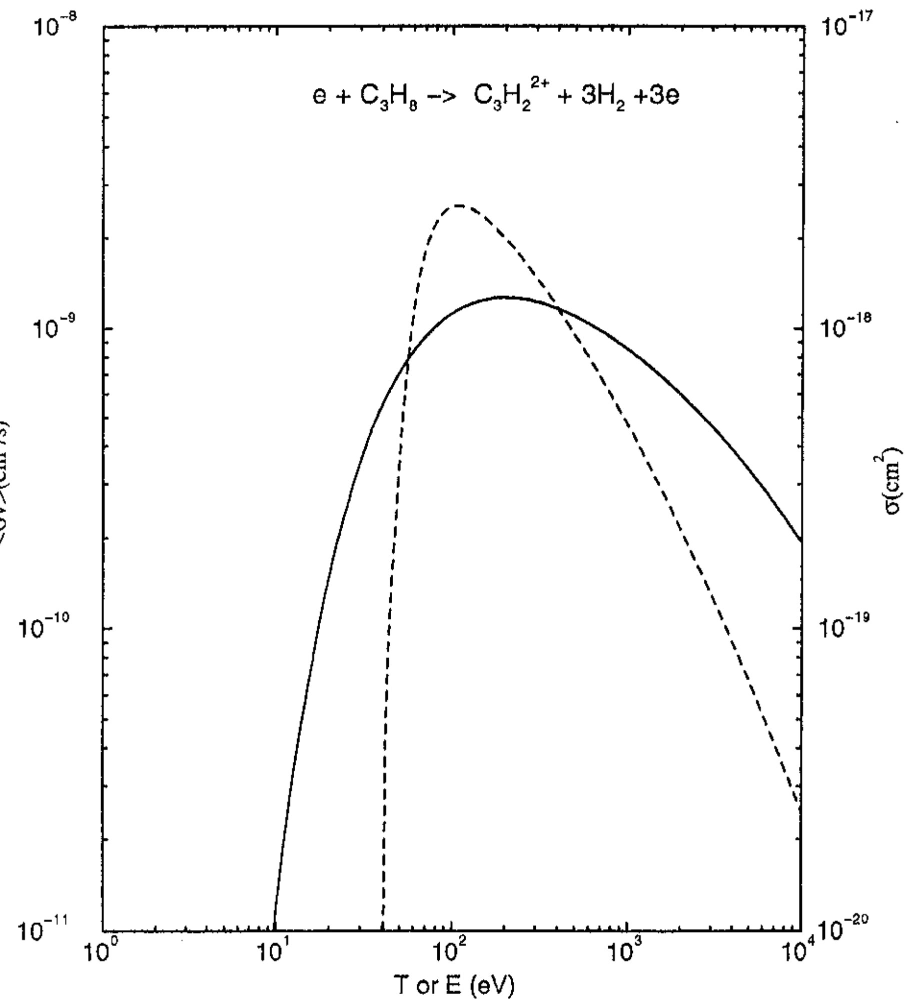
e + C3H8 -> C3H2 2+ + 3H2 +3e
<σv>(cm3/s)
σ(cm2)
T or E (eV)

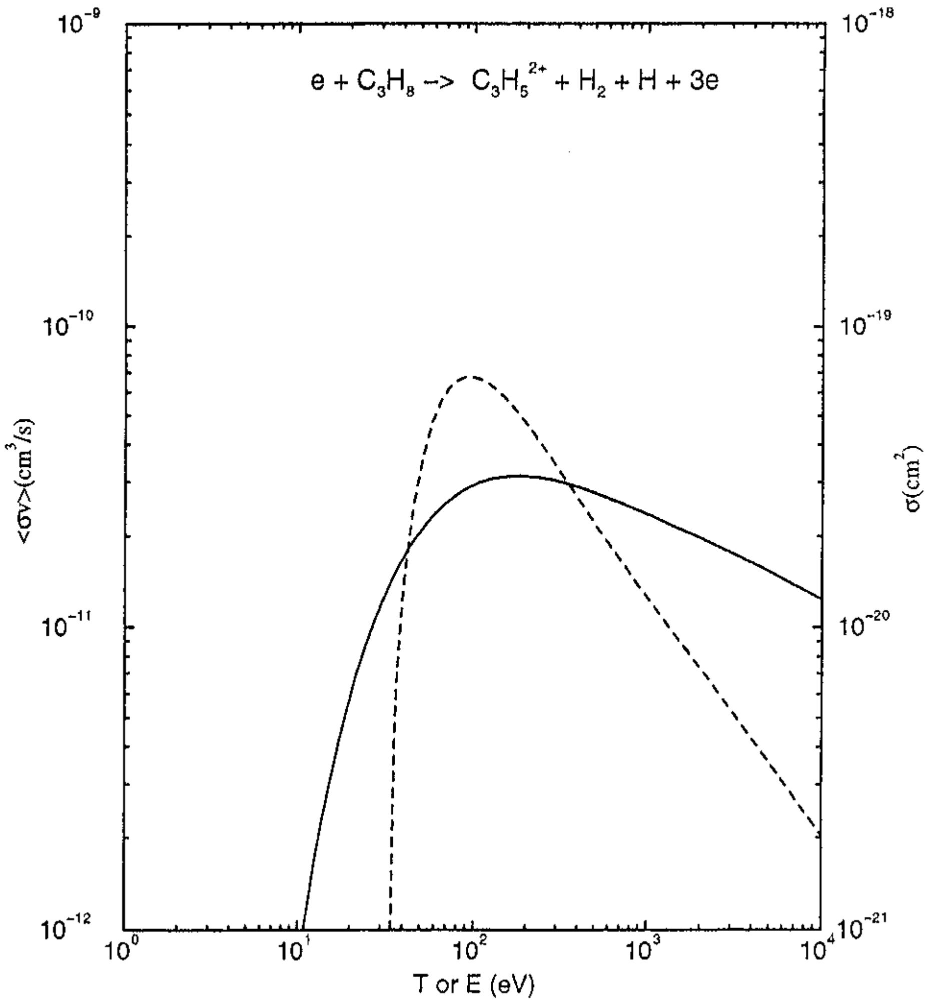
e + C3H8 -> C3H5 2+ + H2 + H + 3e
<σv>(cm3/s)
σ(cm2)
T or E (eV)

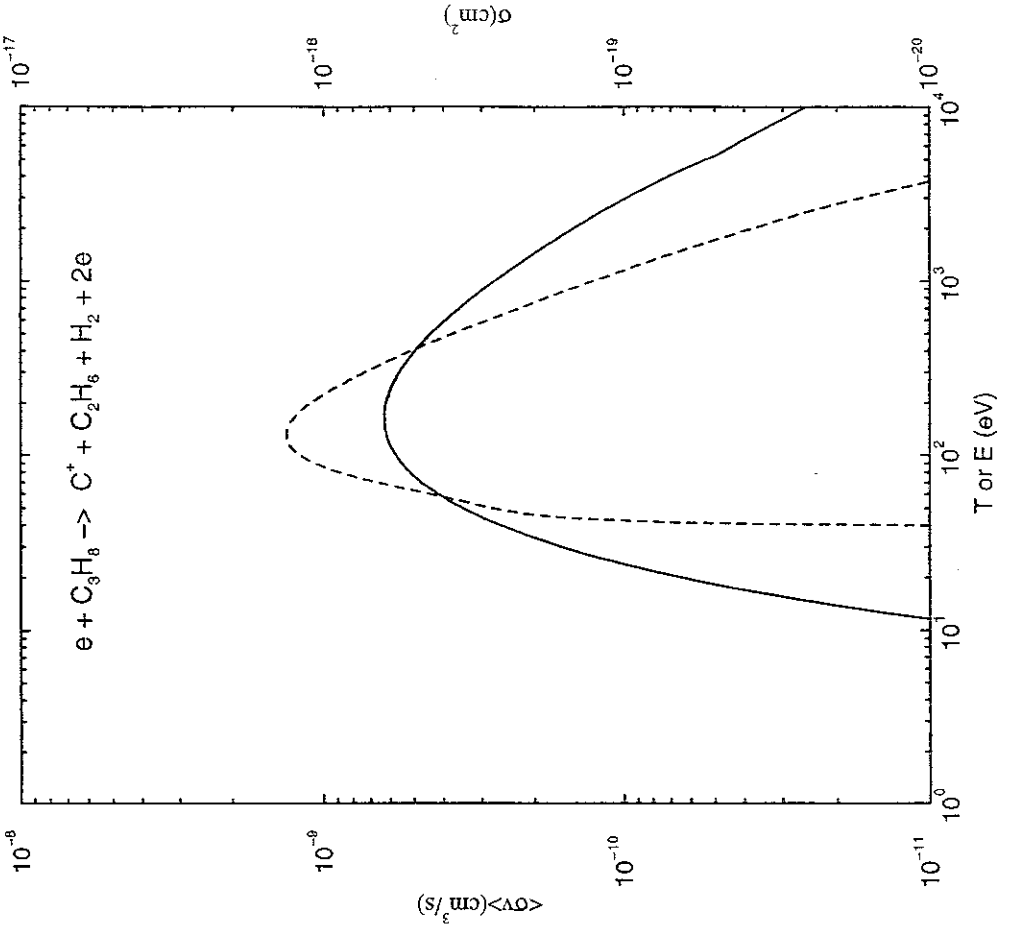

e + C_3H_8 -> C^+ + C_2H_6 + H_2 + 2e
σ(cm²)
<σv>(cm³/s)
T or E (eV)

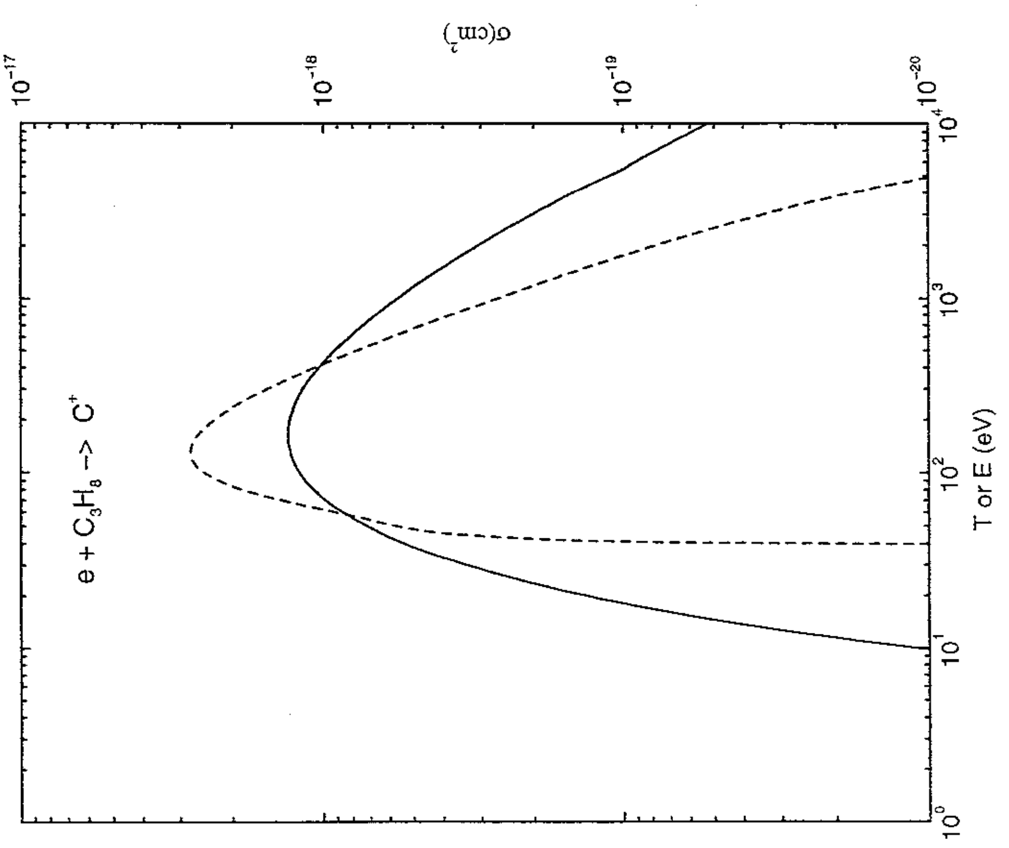

e + C_3H_8 -> C^+
σ(cm²)
<σv>(cm³/s)
T or E (eV)

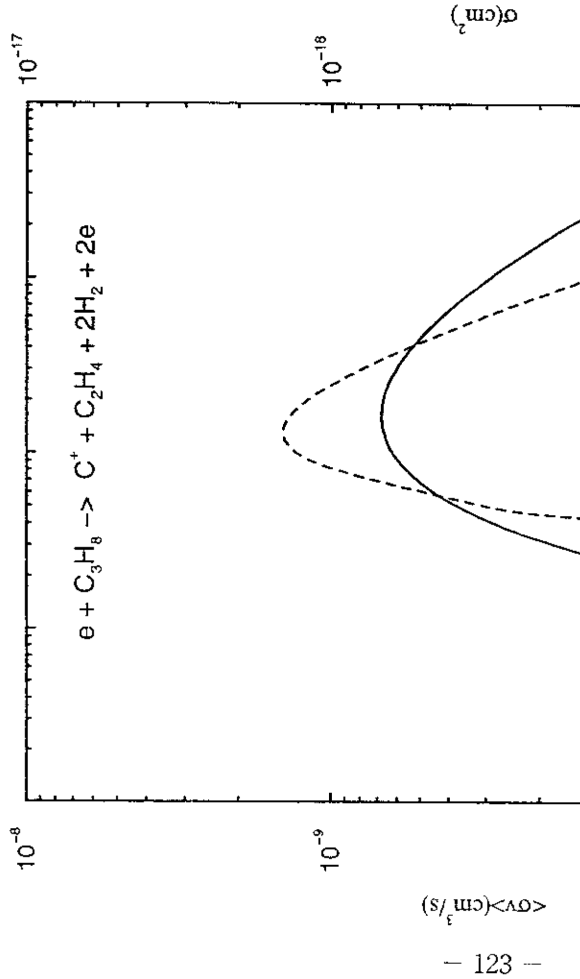

e + C3H8 -> C+ + C2H4 + 2H2 + 2e
T or E (eV)
<σv>(cm3/s)
σ(cm2)
10^0
10^1
10^2
10^3
10^4
10^-8
10^-9
10^-10
10^-11
10^-17
10^-18
10^-19
10^-20

Recent Issues of NIFS-DATA Series

Printed on 100% Recycled Paper for this Text